



**Process Regime
Classification and Modelling
of a Sequencing Batch Reactor
for Producing Polyhydroxybutyrate
with Mixed Culture using Neural Networks**

Amin Ganjian

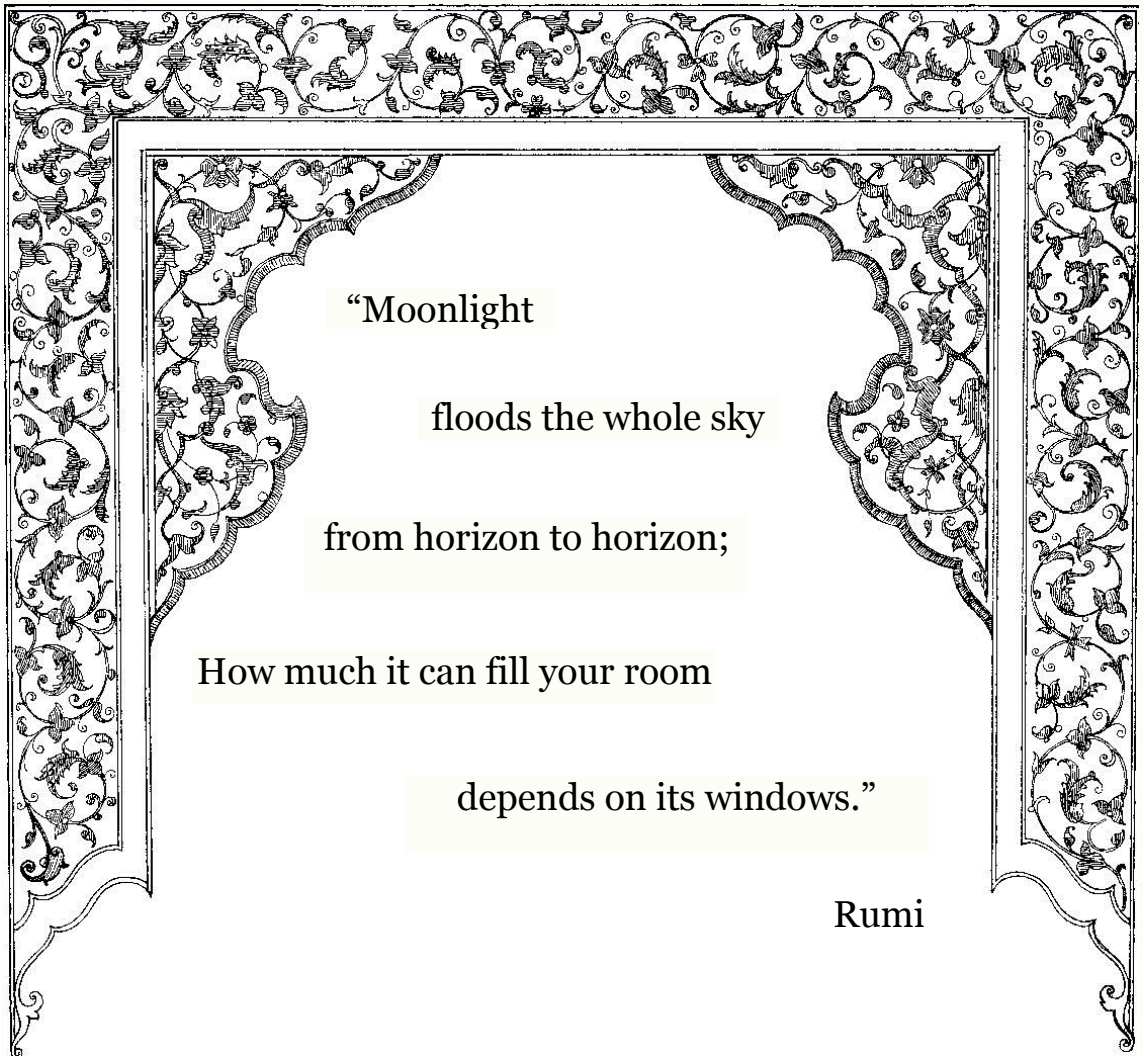
Thesis submitted for the degree of Doctor of Philosophy

Faculty of Science Agriculture and Engineering

Newcastle University

June 2015

School of Chemical Engineering and
Advanced Materials
University of Newcastle upon Tyne
NE1 7RU
UK



“Moonlight
floods the whole sky
from horizon to horizon;

How much it can fill your room

depends on its windows.”

Rumi

Acknowledgements

I would like to thank my supervisor, Dr Jie Zhang, who established the platform of my research study. His passionate, experience and guidance made this PhD possible.

I like to thank Prof Jonathan Love who has the attitude and the substance of a real gentleman. He continually and convincingly conveyed a spirit of persistence and optimism. His support and encouragements were the main research drive.

I would also like to thank my committee members, Dr Yuhong Zhou and Dr Kamelia Boodhoo for making the PhD defence session an invaluable experience.

I also like to acknowledge the help and contribution of Dr Joao ML Dias and Dr Rui Oliveira for providing the PHB process simulation program. Dr Alan Claude Ward's vision and guidance is appreciated.

I am grateful for the friendship I made with Dr Siamak Arami and his wife Sanaz. The tennis games and friendly chats were essential part of my PhD life. I also wish to thank my dearest friend, Milad Harandi and his wife, Ghazal for making the holidays more meaningful. I wish to thank my brother, Iman, his wife, Mansoureh and my younger brother, Hessam for their support during my studies in the UK.

At last but not least, I want to express my deepest gratitude and appreciation to my parents, Nazanin and Abbas, for their constant support, love and patience.

Abstract

In recent years, there has been a growing incentive towards production and application of environmentally benign materials with properties similar to those obtained from irreplaceable resources or exhibiting harmful effects on the environment. In this respect, bioplastics have gained attention in quest of materials that can be used in place of conventional petro-chemical plastics. Biocompatibility, biodegradability and compostability of bioplastics are among the most favourable characteristics of the materials mostly derived from biological systems.

Polyhydroxybutyrate (PHB) is a fully biodegradable bioplastic with similar physical properties to polyethylene and promising applications in various commercial fields including automation, aviation, medication, nutrition, fuel, packaging and many more. PHB production with Mixed Microbial Cultures (MMC) has recently gained attention as a cost effective production strategy by using bacteria that adapt with complex substrates presented in inexpensive waste materials.

The initial research motivation was to enhance PHB production operation by means of the solutions obtained from sophisticated mathematical algorithms used for process optimisation. For this aim, a computer-based program simulating PHB batch process with MMC which was successfully validated with experimental data was available. Since mechanistic models of the simulation program could not be applied in optimisation algorithms, accurate empirical models were required. In the quest for reliable and accurate empirical models that can predict product concentration at the final stage of a batch operation, a methodology was developed in this study for classification of the batch operational regions based on the PHB critical process attributes.

In the core of this research work, an innovative systematic methodology improves process understanding towards advanced process monitoring and control. This method enables operational scrutiny for generation of process knowledge regarding PHB process using MMC. The qualitative info-illustrations produced in the course of the classification method provide a sound platform for generation of considerably more accurate (quantitative) empirical models. These empirical models will be used in process optimisation studies.

In this research, PHB production occurs in a process type known as “feast and famine” or as “aerobic dynamic feeding” which is a well-known strategy applied for bacterial production with MMC. The “feast and famine” operations take place in Sequential Batch Reactors (SBR) in order to assure occurrence of the “feast” and the “famine” phases intermittently in each operational cycle. While PHB formation occurs during the “feast” phase, a “famine” phase should be followed to cause a cell physiological adaptation to maintain PHB production capability of bacteria.

Establishment of the analytical methodology developed in direction of process empirical modelling realisation enables prediction of “feast” and “famine” phase occurrences based on the batch initial state documented for the first time in this work. This mathematical equation (“Phase Differentiating Equation”) plays a significant role in development of a novel SBR recipe for production of PHB with MMC. Execution of the recipe by the PHB process simulation program demonstrates high reliability of the proposed recipe. Application of the “Phase Differentiating Equation” in the SBR recipe assures favourable occurrence of the “feast” and “famine” phases in the majority of operational cycles. Reduction of operational failure rate reduces PHB production cost to improve its market position.

The SBR recipe structure consists of six-stage cycles including (1) “feast” phase preparation stage, (2) “feast” phase operation, (3) operational quiescence, (4) product exploitation, (5) “famine” phase preparation stage and (6) “famine” phase operation. Operational reliability is investigated along with load disturbance rejection embedded in the SBR recipe. At the end, Sequential Quadratic Programming (SQP) is applied successfully as an optimisation algorithm to maximise PHB production under operational constraints.

Nomenclatures

Symbol	Description	Units
f_{PHB}	intracellular PHB content	C-mol PHB/C-mol X
$f_{PHB_{max}}$	maximum intracellular PHB content	C-mol PHB/C-mol X
k_d	kinetic constant for PHB degradation	hr ⁻¹
K_S	acetate half-saturation constant	C-mmol/L
K_τ	efficiency constant	mol ATP/mol $NADH_2$
K_{N_S}	ammonia half saturation constant in acetate uptake	N-mmol/L
K_{PHB}	intracellular PHB content half saturation constants	C-mmol/L
$K_{N_{PHB}}$	ammonia half saturation constant in PHB consumption	N-mmol/L
$K_{S_{PHB}}$	acetate half saturation constant in PHB consumption	C-mmol/L
m_{ATP}	specific ATP consumption by maintenance process	mol ATP/(C-mol.hr)
m_S	maintenance coefficient on acetate	C-mol/(C-mol.hr)
m_{PHB}	maintenance coefficient on PHB	C-mol/(C-mol.hr)
$m_{S_{max}}$	maximum maintenance coefficient on acetate	C-mol/(C-mol.hr)
N	ammonia concentration in the medium	N-mmol/L
q_S^X	specific acetate consumption rate for cell growth	C-mol/(C-mol.hr)
q_S^{PHB}	specific acetate consumption rate for PHB formation	C-mol/(C-mol.hr)
$q_{S_{max}}^X$	maximum specific acetate consumption rate for biomass growth	C-mol/(C-mol.hr)
q_{PHB}	specific PHB storage rate	C-mol/(C-mol.hr)
$q_{PHB_{max}}$	maximum specific PHB storage rate	C-mol/(C-mol.hr)
S	acetate concentration in the medium	C-mmol/L
t	the culture time	hr
X	active biomass concentration	C-mmol/L

Nomenclatures

Symbol	Description	Units
α	PHB production saturation order	1
$Y_{N/X}$	yield of ammonia on biomass	N-mol/C-mol
$Y_{PHB/S}$	yield of PHB on acetate	C-mol/C-mol
$Y_{X/S}$	yield of biomass on acetate	C-mol/C-mol
$Y_{PHB/X}$	yield of PHB on biomass	C-mol/C-mol
δ	efficiency of oxidative phosphorylation	mol ATP/mol NADH ₂
μ_S	specific growth rate on acetate	C-mol/(C-mol.hr)
μ_{PHB}	specific growth rate on PHB	C-mol/(C-mol.hr)
$\mu_{PHB_{max}}$	maximum specific growth rate on PHB	C-mol/(C-mol.hr)

Abbreviations and Acronyms

	Description
ANN	Artificial Neural Networks
BLS	Batch Least Squares
CCRD	Central Composite Rotatable Design
CDW	Cell Dry Weight
CV	Code Vector
DLS	Damped Least Squares
DNA	Deoxyribonucleic acid
DOE	Design of Experiment
EuBP	European Bioplastics
FANN	Feedforward Artificial Neural Net
GAO	Glycogen Accumulating Organism
HAME	Hydroxyalkanote Methyl Ester
HNN	Hidden Neuron Number
LMA	Levenberg Marquardt Algorithm
MIP	Molecularly Imprinted Polymers
MLR	Multiple Linear Regression
MMC	Mixed Microbial Culture
NN	Neural Networks
ODE	Ordinary Differential Equation
PA	Polyamide
PAO	Polyphosphate Accumulating Organism
PBAT	Polybutyrate
PBS	Polybutylene succinate
PCL	Polycaprolactone
PE	Polyethylene
PET	Polyethylene Terephthalate
PHA	Polyhydroxyalkanoates
PHB	Polyhydroxybutyrate
PHO	Polyhydroxy Octanoate
PLA	Polylactic acid
PP	Polypropylene

Abbreviations and Acronyms

	Description
PS	Polystyrene
PVC	Polyvinyl Chloride
RCV	Registered Code Vector
RMSE	Root Mean Squared Errors
RSM	Response Surface Methodology
RT	Regime Type
SQP	Sequential Quadratic Programming
SSE	Sum of Squared Errors
STD	Standard Deviation
TOA	Taguchi Orthogonal Array
VFA	Volatile Fatty Acids

Table of Contents

Chapter 1	
Motivation and Thesis Outline	1
1.1 The philanthropic incentive behind the research project	1
1.2 Introduction to data intensive computing and data visualisation	3
1.3 Thesis summary	4
1.3.1 Thesis structure	4
1.3.2 Brief description of the thesis chapters.....	6
1.3.3 Research contributions.....	10
Chapter 2	
Literature Review	11
2.1 Bioplastics.....	12
2.1.1 Definition of bioplastics.....	12
2.1.2 Economic and environmental incentives	13
2.2 Polyhydroxyalkanoates (PHAs): a promising group of green plastics	15
2.2.1 PHA chemical structure	15
2.2.2 PHA properties.....	17
2.2.3 PHA production companies	18
2.2.4 PHA applications	22
2.3 PHA production methods.....	26
2.3.1 PHA production by plants.....	27
2.3.2 PHA production by pure microbial cultures	27
2.3.3 PHA production by Mixed Microbial Cultures.....	28
2.3.4 PHA production by MMC in Sequential Batch Reactors	29
2.4 PHA extraction methods	30
2.5 Process optimisation	32
2.5.1 Introduction.....	32
2.5.2 Optimisation of the PHB fermentation process	33
2.5.3 Optimisation tool (Sequential Quadratic Programming)	35
2.6 Mathematical modelling	38
2.6.1. Introduction.....	38
2.6.2 MLR modelling method.....	40
2.6.3 Artificial Neural Network modelling method.....	41
2.6.4 Bootstrapping Aggregated Neural Networks	47
2.7 Summery	49

Chapter 3	
Simulation of Polyhydroxybutyrate Production Batch using Mixed Microbial Culture Cultivation in a Sequencing Batch Reactor	
	50
3.1	Introduction..... 51
3.2	Mechanistic models 52
3.2.1	Modelling assumptions 52
3.2.2	Material balance equations..... 52
3.2.3	Postulation of the kinetic model..... 54
3.2.4	Kinetic parameter estimation 57
3.3	Introduction to the simulation program 58
3.3.1	First division: simulation elements 58
3.3.2	Second division: ODE solver..... 59
3.3.3	Third division: data repository 60
3.4	Validation of the PHB simulator program by experimental data..... 61
3.5	Description of simulation results 63
3.6	Summary 66
Chapter 4	
Batch Process Characterisation Method for PHB Production with Mixed Microbial Culture Cultivation.....	
	67
4.1.	Introduction..... 68
4.2	Acquire process knowledge and selection of process significant elements 69
4.3	Process profile analysis..... 69
4.3.1	CharMeth’s first module: Ammonia profile analysis..... 70
4.3.2	CharMeth’s second module: Acetate profile analysis..... 72
4.3.3	CharMeth’s third module: Total PHB profile analysis 74
4.4	Visualisation of process profiles 76
4.5	Creation of code vectors: association of the significant process occurrences to the code values..... 77
4.6	Creation of the bank of code vectors 80
4.6.1	Application of “CharMath” module for code vector bank generation 80
4.6.2	Screening process..... 81
4.6.3	Expansion of the code vector bank by the screening process 84
4.7	Classification of the registered code vectors..... 87
4.7.1	Application of the screening plots in code vector classification..... 90
4.7.2	Definition and initial classification of Regime Types..... 91
4.7.3	Qualitative description of the RTs 92
4.7.4	Classification of the code vectors in regime type groups..... 95
4.8	Generation of characterisation plots 101
4.9	Conclusions..... 104

Chapter 5	
Identification of Regimen Boundaries on the Characterisation Plot	105
5.1 Introduction.....	106
5.2 Definition of the operational phase border curve.....	106
5.3 Identification of the border line on characterisation plots	108
5.4 Mathematical representation of the border curve equation.....	111
5.5 Validation of the border line mathematical equations	122
5.6 Conclusions.....	132
Chapter 6	
Empirical Modelling of the Most Significant Elements of PHB Batch Process using Mixed Microbial Culture Cultivation.....	134
6.1 Introduction.....	135
6.2 Empirical model development procedure	136
6.2.1 Data generation	136
6.2.2 Outlier detection.....	136
6.2.3 Data grouping.....	136
6.2.4 Data pre-processing.....	137
6.2.5 Empirical model development	137
6.2.6 Model validation	139
6.2.7 Unscaling	140
6.3 Empirical modelling for unclassified operational data	140
6.4 The “feast” phase operational modelling.....	144
6.4.1 Introduction.....	144
6.4.2 Description of the “feast” phase profile	145
6.4.3 Data generation targeting “feast” phase batch operations.....	146
6.4.4 MLR modelling targeting “feast” phase process data.....	151
6.4.5 BANN modelling targeting “feast” phase process data	153
6.4.6 Comparison of the MLR and BANN model results.....	161
6.4.7 Development of BANN models with reduced number of inputs.....	162
6.4.8 Recommendations for development of appropriate model structure targeting “feast” phase batch operations.....	165
6.5 The “famine” phase operational modelling.....	167
6.5.1 Introduction.....	167
6.5.2 Description of the “famine” phase operational profile – RT3	167
6.5.3 Description of the “famine” phase operational profile – RT5	169
6.5.4 Batch termination criterion for historic data of “famine” phase process	170
6.5.5 Data generation targeting “famine” phase batch operations	172
6.5.6 MLR modelling targeting “famine” phase process data	178
6.5.7 BANN modelling targeting “famine” phase process data.....	179

Table of Contents

6.5.8	BANN modelling targeting “famine” phase process operating under RT3	180
6.5.9	BANN modelling targeting “famine” phase process operating under RT5	182
6.5.10	Recommendations for development of appropriate model structure targeting “famine” phase batch operations	183
6.5	Conclusions	185

Chapter 7

Generation of PHB Production Recipe Using the “Phase Differentiating Equation” for Sequential Batch Reactors

187

7.1	Introduction	188
7.2	Generation of the SBR recipe	189
7.2.1	Introduction	189
7.2.2	General structure of the recipe	190
7.2.3	Implementation of the SBR recipe	191
7.2.4	Procedure of assigning values to SBR recipe parameters	194
7.2.5	Design of a typical SBR recipe	197
7.2.6	Execution of the SBR recipe	201
7.3	Capability of SBR recipe in disturbance rejection	212
7.3.1	Introduction	212
7.3.2	The effect of load disturbance on the total biomass concentration remained inside the reactor in the 3 rd step of the SBR process – RF8	215
7.3.3	The effect of load disturbance on the amount of ammonia introduced in the 4 th step of the SBR process – RF9	219
7.3.4	The effect of load disturbance to the amount of acetate introduced in the 6 th step of the SBR process – RF11	223
7.3.5	Realisation of practical SBR process execution	231
7.4	Conclusions	235

Chapter 8

Optimisation of the SBR Recipe using Sequential Quadratic Programming Algorithm for Sustainable PHB Production

237

8.1	Introduction	238
8.2	Data generation for SBR optimisation purpose	239
8.3	Empirical model development by MLR	242
8.4	Empirical model development by BANN	244
8.5	Application of SQP for optimisation of the SBR recipe	246
8.6	Conclusions	252

Chapter 9	
Conclusions and Recommendations for Future Works	253
9.1 Conclusions	253
9.2 Recommendation for future works.....	256
9.2.1 Application of PCA in the “Characterisation Method”	256
References	260
Appendix-A	274
Appendix-B	285
Appendix-C	289
Appendix-D	305

List of Figures

Chapter 1

Figure 1.1 Thesis outline.....	5
--------------------------------	---

Chapter 2

Figure 2.1 Bioplastics' material coordinate system (adopted from EuBA 2014).	13
Figure 2.2 Life cycle of bioplastics (adopted from European bioplastics, 2014)	15
Figure 2.3 PHA molecule formula.....	17
Figure 2.4 Recursive search using sequential quadratic programming.....	37
Figure 2.5 A multi-layer feedforward neural network with two hidden layers.....	41
Figure 2.6 Notation specified for inputs, neurons, synapses and the output.....	42
Figure 2.7 Procedure of the back propagation training algorithm	44
Figure 2.8 Identification of network weights using the NN training termination criterion	45
Figure 2.9 A BANN model based on three individual neural network structures	48

Chapter 3

Figure 3.1 Simulation program structure	60
Figure 3.2 Validation results	62
Figure 3.3 Programing code parameters for batch simulation in MATLAB	63
Figure 3.4 Results for batch simulation run	65

Chapter 4

Figure 4.1 Simulation program structure with the supplement of "Characterisation Method" (CharMeth) module.....	68
Figure 4.2 Identification of critical ammonia point within a batch operation period	70
Figure 4.3 Descriptive depiction of "CharMeth" ammonia module	71
Figure 4.4 "CharMeth" analytical results on different ammonia profiles.....	71
Figure 4.5 Identification of critical acetate point within a batch operation period	72
Figure 4.6 Descriptive depiction of "CharMeth" acetate module.....	73
Figure 4.7 "CharMeth" analytical results on different acetate profiles.....	73
Figure 4.8 Descriptive depiction of "CharMeth" PHB module	74
Figure 4.9 "CharMeth" analytical results on different PHB profiles (before activating the two additional analytical points).....	75
Figure 4.10 "CharMeth" analytical results on different PHB profiles (after activating the two additional analytical points).....	76
Figure 4.11 Acetate-ammonia-PHB plot for two typical simulation runs of the PHB process ..	77
Figure 4.12 Definition of code values for the sixth code vector position	79
Figure 4.13 Code vector numerating procedure and development of the bank of code vectors .	81
Figure 4.14 Illustration of code vector numbers for the first screening run on a screening plot after updating the bank of code vectors	83

List of Figures

Figure 4.15 Illustration of code vector numbers for the second screening run on a screening plot before updating the bank of code vectors (a) and after updating the bank of code vectors (b) ..	84
Figure 4.16 Demonstration of an acetate-ammonia-PHB plot for the 1 st code vector	88
Figure 4.17 Demonstration of the acetate-ammonia-PHB plot for the 18 th code vector.....	89
Figure 4.18 Screening plots for extended unrealistic biomass concentrations	90
Figure 4.19 Code vector representation for operational progression.....	91
Figure 4.20 Numeration of regime types based on the structure of Figure 4.19.....	92
Figure 4.21 Qualitative acetate-ammonia-PHB representations for the nine dominant regime types	93
Figure 4.22 Demonstration of a typical screening plot	96
Figure 4.23 Typical representations of acetate-ammonia-PHB plots from RT1 to RT9 classes	98
Figure 4.24 Progressive presentation of the screening and characterisation plots	102

Chapter 5

Figure 5.1 Progressive characterisation plot pattern in the case of PHB production process ...	107
Figure 5.2 Classification of operational regimes based on their operational pathway	108
Figure 5.3 Characterisation plots with the border curves (BIOM0=1000 C-mmol/L)	109
Figure 5.4 Characterisation plots with the border curves (BIOM0=100 C-mmol/L)	110
Figure 5.5 Qualitative pattern of the border curve area in a characterisation plot	111
Figure 5.6 Presentation of the linear equations predicting acetate _{Intercept}	121
Figure 5.7 Simulation setting No.1, validation of “Phase Differentiating Equation” - Deterministic behaviour system	123
Figure 5.8 Simulation setting No.1, validation of “Phase Differentiating Equation” - Random behaviour system	124
Figure 5.9 Simulation setting No.2, validation of “Phase Differentiating Equation” - Deterministic behaviour system	126
Figure 5.10 Simulation setting No.2, validation of “Phase Differentiating Equation” - Random behaviour system	126
Figure 5.11 Validation of PePHB0 reduction on regimen dispersion.....	127
Figure 5.12 Simulation setting No.3, validation of “Phase Differentiating Equation” - Deterministic behaviour system	128
Figure 5.13 Simulation setting No.3, validation of “Phase Differentiating Equation” - Random behaviour system	128
Figure 5.14 Simulation setting No.4, validation of “Phase Differentiating Equation” - Deterministic behaviour system	129
Figure 5.15 Simulation setting No.4, validation of “Phase Differentiating Equation” - Random behaviour system	129
Figure 5.16 Simulation setting No.5, validation of “Phase Differentiating Equation” - Deterministic behaviour system	130
Figure 5.17 Simulation setting No.5, validation of “Phase Differentiating Equation” - Random behaviour system	130
Figure 5.18 Simulation setting No.6, validation of “Phase Differentiating Equation” - Deterministic behaviour system	131

List of Figures

Figure 5.19 Simulation setting No.6, validation of “Phase Differentiating Equation” - Random behaviour system	131
Chapter 6	
Figure 6.1 Data flowchart for developing neural network models	138
Figure 6.2 Random values assigned to process parameters for data generation	141
Figure 6.3 Training data for model development.....	142
Figure 6.4 Validation data for model development	142
Figure 6.5 BANN model validation for critical process attributes at batch final operation point (Point-Z)	143
Figure 6.6 Data generation program structure separating operation phases	145
Figure 6.7 Feast phase PHB profiles (RF8) for low PePHB0 (left) and high PePHB0 (right) values	145
Figure 6.8 Random values assigned to process parameters for data generation targeting the “feast” phase	148
Figure 6.9 Identification of valid “feast” phase data set	149
Figure 6.10 Training data for the “feast” phase model development.....	150
Figure 6.11 Validation data for the “feast” phase model development	150
Figure 6.12 MLR model prediction results for the validation data	152
Figure 6.13 Development of N number of individual neural networks for a certain set of training data.....	155
Figure 6.14 SSE_{test} values obtained for NN models predicting PHB concentration at its stability point in “feast” phase profile	156
Figure 6.15 Optimal number of hidden neurons obtained for each selected single NN model.....	156
Figure 6.16 Comparison of the single NN models with the BANN model SSE values	157
Figure 6.17 Validation of the model predicting PHB concentration at Point-C	157
Figure 6.18 Number of hidden neurons for each single NN structure	158
Figure 6.19 Sum square errors of single and aggregated model predictions for “feast” phase scaled data	159
Figure 6.20 BANN model validation for significant elements of the “feast” phase profiles....	160
Figure 6.21 “Famine” phase profile with RT3.....	168
Figure 6.22 “Famine” phase profile with RT5	169
Figure 6.23 Identification of “famine” phase batch termination criterion	171
Figure 6.24 Detection of various “fPHBsumEND” points on a “famine” phase profile	171
Figure 6.25 Identification of “famine” phase batch termination point by the analytical tool...	172
Figure 6.26 Random values assigned to process parameters for data generation targeting the “famine” phase.....	173
Figure 6.27 Identification of valid “famine” phase batch data set.....	174
Figure 6.28 “Famine” phase batch durations with “fPHBsumENDratio” criterion of 20%	175
Figure 6.29 Training data for the “famine” phase model development.....	176
Figure 6.30 Validation data for the “famine” phase model development.....	177

List of Figures

Figure 6.31 MLR model validation developed for the “famine” phase data sets	178
Figure 6.32 BANN model validation for significant elements of the “famine” phase profiles.....	179
Figure 6.33 BANN model validation for significant elements of the RT3 data sets	181
Figure 6.34 BANN model validation for significant elements of the RT5 data sets	182
 Chapter 7	
Figure 7.1 General structure of the SBR configuration	190
Figure 7.2 Structure of the SBR recipe for execution.....	192
Figure 7.3 Detailed presentation of simulation results for the first cycle of PHB production under proposed SBR recipe	205
Figure 7.4 Detailed presentation of simulation results for the second cycle of PHB production under proposed SBR recipe	206
Figure 7.5 Execution of the SBR recipe in five cycles	208
Figure 7.6 Execution of the SBR recipe (demonstration of the 50 cycles).....	211
Figure 7.7 Execution of the SBR recipe using deterministic behaviour process simulator	213
Figure 7.8 Execution of the SBR recipe with load disturbances on RF8 (deterministic behaviour process simulator)	217
Figure 7.9 Execution of the SBR recipe with load disturbances on RF8.....	218
Figure 7.10 Execution of the SBR recipe with load disturbances on RF9 (deterministic behaviour process simulator)	221
Figure 7.11 Execution of the SBR recipe with load disturbances on RF9.....	222
Figure 7.12 Execution of the SBR recipe with load disturbances on RF11 (deterministic behaviour process simulator)	225
Figure 7.13 Execution of the SBR recipe with load disturbances on RF11	226
Figure 7.14 Execution of the SBR recipe with load disturbances on RF11 (deterministic behaviour process simulator)	229
Figure 7.15 Execution of the SBR recipe with load disturbances on RF11	230
Figure 7.16 Execution of the SBR recipe with maximum 25% deviation of RF8, RF9 and RF11 around their recipe specified values	232
Figure 7.17 Histogram of total PHB production for 100 SBR runs under recipe given in Table 7.4 with maximum 50% deviation of RF8, RF9 and RF11	233
Figure 7.18 Histogram of total PHB production for 100 SBR runs under recipe given in Table 7.4 with maximum 10% deviation of RF8, RF9 and RF11	234
 Chapter 8	
Figure 8.1 SBR variables randomly assigned for process modelling	240
Figure 8.2 SBR process outcome for optimisation purpose.....	241
Figure 8.3 Validation of the MLR models.....	243
Figure 8.4 Number of hidden neurons and prediction performance of the neural network models	245
Figure 8.5 Validation of BANN models (scaled date).....	245
Figure 8.6 Histogram of 100 SBR runs for the first run tabulated in Table 8.3.....	248

List of Figures

Figure 8.7 Histogram of 100 SBR runs for the second run tabulated in Table 8.3	249
Figure 8.8 Histogram of 100 SBR runs for the third run tabulated in Table 8.3	250
Figure 8.9 Histogram of 100 SBR runs for the fourth run tabulated in Table 8.3	251
Figure 8.10 Histogram of 100 SBR runs for the fifth run tabulated in Table 8.3	251

List of Tables

Chapter 2

Table 2.1 The most common PHA based on formula given in Figure 2.3	16
Table 2.2 Properties of some bio-polymers and fossil based polymers	19
Table 2.3 Worldwide PHA producing and researching companies	20

Chapter 3

Table 3.1 Metabolic model reactions for mixed cultures	54
Table 3.2 Kinetic model constants	58
Table 3.3 Acetate and ammonia concentrations in the medium after pulse feed additon in C-mmol/L and N-mmol/L respectively.....	61

Chapter 4

Table 4.1 Definition of code values and their position in the code vectors	78
Table 4.2 Identified five code vectors in the first run of the screening process.....	82
Table 4.3 Identified four code vectors in the second run of screening process	84
Table 4.4 Simulation parameters and the number of identified code vectors in each screening process (realistic parameter values).....	85
Table 4.5 Simulation parameters and the number of identified code vectors in each screening process (extended unrealistic parameter values)	86
Table 4.6 Identified 25 code vectors in the 32 screening processes	87
Table 4.7 Representation of the first CV members in RT groups.....	92
Table 4.8 Classified code vectors in the RT groups.....	97

Chapter 5

Table 5.1 Point1 and Point2 coordination and the specifications of the straight line crossing the two points (Biomass range 2-200 C-mmol/L, PePHB0=0%).....	114
Table 5.2 Point1 and Point2 coordination and the specifications of the straight line crossing the two points (Biomass range 2-200 C-mmol/L, PePHB0=100%).....	115
Table 5.3 Point1 and Point2 coordination and the specifications of the straight line crossing the two points (Biomass range 200-1000 C-mmol/L, PePHB0=0%).....	116
Table 5.4 Point1 and Point2 coordination and the specifications of the straight line crossing the two points (Biomass range 200-1000 C-mmol/L, PePHB0=100%).....	117
Table 5.5 Point1 and Point2 coordination and the specifications of the straight line crossing the two points (Biomass range 1000-1500 C-mmol/L, PePHB0=0%).....	118
Table 5.6 Point1 and Point2 coordination and the specifications of the straight line crossing the two points (Biomass range 1000-1500 C-mmol/L, PePHB0=100%).....	119
Table 5.7 The average for the LG_{α} and LG_{β} values along with their standard deviations	120
Table 5.8 Equation parameters for the Line- α and the Line- β to be applied on Equation 5.12 and Equation 5.13	121

Chapter 6

Table 6.1 Process data generation contemplating “feast” and “famine” operational phases	141
Table 6.2 Process data generation targeting “feast” phase operation	147
Table 6.3 Scaling parameters for the “feast” phase data sets.....	151
Table 6.4 MLR model parameters to predict significant occurrences in the “feast” phase operation	152
Table 6.5 Comparison of the MLR and BANN model prediction capabilities.....	161
Table 6.6 RMSE values for BANN models developed on three-input structures.....	163
Table 6.7 RMSE values for models developed on initial biomass and ammonia concentrations by BANN	164
Table 6.8 RMSE values for models developed on initial PHB and ammonia concentrations by BANN	164
Table 6.9 RMSE values for models developed on initial PHB and ammonia concentrations by BANN	165
Table 6.10 Proposition of the model structure for the significant elements of the “feast” phase operations.....	166
Table 6.11 Process data generation targeting “famine” phase operation.....	173
Table 6.12 Proposition of the model structure for the significant elements of the “famine” phase operations	180
Table 6.13 Proposition of the model structure for the significant elements of the RT3 data sets	182
Table 6.14 Proposition of the model structure for the significant elements of RT5 batch profiles	183
Table 6.15 Lowest RMSE values obtained for prediction of significant elements in “famine” phase regimes.....	184

Chapter 7

Table 7.1 SBR recipe factors	197
Table 7.2 BANN model predictions for final biomass concentration in a “famine” phase batch operation	198
Table 7.3 BANN model predictions for final biomass concentration in a “feast” phase batch operation.....	199
Table 7.4 A SBR recipe for production of PHB	201
Table 7.5 Illustrative investigations on the recipe reactions to the load disturbances	214

Chapter 8

Table 8.1 MLR model parameters	242
Table 8.2 Range of outputs from objective function for scaled data	247
Table 8.3 Optimisation results for different combinations of K values	248

Chapter 1

Research Motivations and Thesis Outline

1.1 The philanthropic incentive behind the research project

The industrial revolution initiated in the 18th and 19th centuries was supported by developments in the mining industry and application of steam power for transportation. The application of the internal combustion engine was boosted when the commercial drilling and production of petroleum began in the mid-1850s (Oliver et al., 2008). Following the industrial revolution, global economy flourished with a linear pattern of production and consumption for the past 160 years and successfully increased human welfare in many different aspects. However, this pattern is doomed to be eradicated if mankind intends to live in its cradle “the mother earth”. Earth has reached its limits as great pressure has been put by men on its resources.

The increasing rate of municipal solid waste accumulation is a significant contributor to greenhouse gas emissions and imposes disquieting threat to the earth’s ecology. The majority of these emissions are produced as a result of landfilling, which is the primary waste disposal strategy internationally. As the changing global climate has been one of the major environmental challenges facing the world today, there is an increasing need to alter waste composition or the disposal method to re-use the waste (Lou and Nair, 2009).

At the moment, the most sophisticated application of crude oil is plastic production. Around 8% of the world oil production is used to make plastics and over one third of the plastics is used to make packaging items (Thompson et al., 2009). This item consists of around 10% of the municipal waste stream by weight (Barnes et al., 2009). Unfortunately, plastic is one of the current major harmful contributors to the landfill due to its low rate of decomposition. Moreover, its presence in the landfill reduces decay rate of the biodegradable materials since they block access of microorganisms, air and water to the landfill bulk.

In the modern (sanitary) landfills, a large hole is dug in the ground and lined with a thick plastic and a layer of clay to prevent soil contamination and the refuse is covered with a layer of earth to reduce odour intermittently. With little access to air, water and sunlight, even the readily degradable waste objects such as paper and food accumulate intact for many decades (Qasim and Chiang, 1994). In addition to the terrestrial landfills, the harmful effect of fragments of plastics and glass contaminating in the

streams, rivers and ultimately the sea is another point of serious concern when plastic production issues are addressed (Thompson et al., 2005). Since plastics are buoyant in water and resistant to degradation, they comprise a considerable portion (50% to 80%) of shoreline debris (Barnes et al., 2009). Therefore, the dominant approach towards plastic disposal and linear use of hydrocarbons for short-lived applications such as packaging are far from sustainable.

In a circular economy, resources are continuously re-used or recycled in order to return materials and energy in other productive parts of the economy with the aim of maintaining sustainable growth. In a high level, the concept of circular economy is easy to understand. The natural resources such as fossil based hydrocarbons, minerals and forest products are reclaimed back to the economy instead of being disposed into the environment or forming emissions that contribute to pollution (Jones, 2013). Plastic recycling or incineration are two main approaches taken to re-use the plastics with the later producing considerable amount of CO₂ emissions which contributes to greenhouse effect (Wollny et al., 2001). However, studies suggest that greenhouse gas emissions from waste decomposition are considerably higher for landfills than composting (purposeful biodegradation of organic matters such as yard and food waste) (Lou and Nair, 2009).

An alternative approach has been taken to replace non-degradable petrochemical plastics with bioplastics that degrade readily to return harmless materials back to the environment. In addition to being environmentally benign, widespread application of bio-based plastics reduces consumption of fossil fuels as the feedstock of conventional plastics. Considerable amount of research work has been dedicated to extend the knowledge towards production cost reduction and find novel applications for bioplastics (Shah *et al.*, 2008; Accinelli *et al.*, 2012). Considering the life cycle assessment of plastics and bioplastics, some argued that environmental friendliness of bioplastics depends also on the energy supply method used to produce the materials. For example, when coal-fire was used to maintain the energy for bio-bags, the environmental impact was five times higher than the case of the conventional plastics. However, the bio-bags are reported to be 80% more environmentally friendly than plastic bags when clean and renewable energy is used throughout its life cycle production stages (Khoo and Tan, 2010).

The focus of this study is on production of polyhydroxybutyrate (PHB), a common type of polyhydroxyalkanoates (PHA) that is bio-derived and biodegradable and exhibits

similar physical properties comparable to polypropylene (Pachekoski *et al.*, 2009). The substrate used in the PHB production unit in this study is inexpensive municipal activated sludge which is associated with environmental and financial benefits (Gurieff, 2007). In the next chapter, a review on the subject of bioplastics is given.

1.2 Introduction to data intensive computing and data visualisation

The era we live in is analogous to the time when printing was invented. It took about a thousand years to develop and evolve a mechanism that can store data on papers. Using computers, it was a matter of decades to be able to store, analyse and generate knowledge in electronic format. Data is a lucrative source to form new insights for inception of niche ideas. Moreover, data management has eased data accessibility and analysis of the curated data. These new set of tools provide a platform for knowledge generation and establishment of new theories. Looking briefly at the history of science, for a thousand years knowledge was acquired by observing and describing the natural phenomena by conducting experiments (Empirical stage). For the past few hundred years models and generalisations enabled creation of hypothetical constructs (Theoretical stage). In the last few decades, the theoretical models grew too complicated to be solved analytically. With the advent of computers, development of simulation for complex phenomena escalated and increased data generation. A combination of simulation and experimental data has become the new force to extend the science boundaries (Computational stage). Extended publication and sharing of data and results between researchers in electronic knowledge networks is the latest link in this chain (eScience stage) (Hey *et al.*, 2009).

In the latest stage of science development history, knowledge is obtained through analysis and process of data using information discovery applications rather than solely simulating and generating process data and dynamically determine which data sets to process. In search for homologous structures, data-intensive applications that require the manipulation of terabytes of data aggregated across hundreds of files from comparison of numerical simulation output are used. The application may use local or remote input data sets, data stored in distributed repositories, or in archival storage systems. With increasing computational bandwidth, data-intensive computing can be coupled with the external data sets as well as the data from local sources (Moore *et al.*, 1999). Development of novel techniques that can be executed as an analytical application for mega data is one of the incentives considered in this research study.

Application of computer-based simulators can provide large amount of valuable data. It can be said that “simulation data is the new soil” to the science and engineering fields. Modern people are exposed to a world of figures, diagrams and infographics with dormant desire to observe visual aspects of high information significance. Facing a simple and descriptive graphic or a data visualisation is like coming across a clearing in a dense information jungle.

Presentation of the high volume of information obtained from the data glut is a challenge that can be resolved by expanding the observation capability. Novel techniques are required to visualise connections and patterns in simple illustrations in order to facilitate generation of a narrative to the overall picture. The inexpensive simulation source material can act as a fertile medium that feeds data visualisation like its blooming flower. Visualising information is also a form of knowledge compression. It is a way of squeezing an enormous amount of information and understanding into a small illustration.

In the core of this study, data visualisation enables pattern recognition, information encapsulation and generation of deeper insight to the chemical process being analysed.

1.3 Thesis summary

1.3.1 Thesis structure

This report concentrates on operational enhancement of polyhydroxybutyrate (PHB) production by mixed microbial cultures (MMC) with the focus on process cost reduction. Figure 1.1 shows an illustration of the thesis structure comprising of the chapter numbers and the rational linkage author made between the chapters.

The research motivation in Chapter 1 is the main driving force of the research study carried out to reduce PHB production cost. In Chapter 2 and Chapter 3 the foundations are constructed using a concise review on the literature and PHB batch process simulator respectively. These two chapters form the required frame work of the research project by other research groups and author has no claim on the results nor their level of accuracy reported in the published literatures.

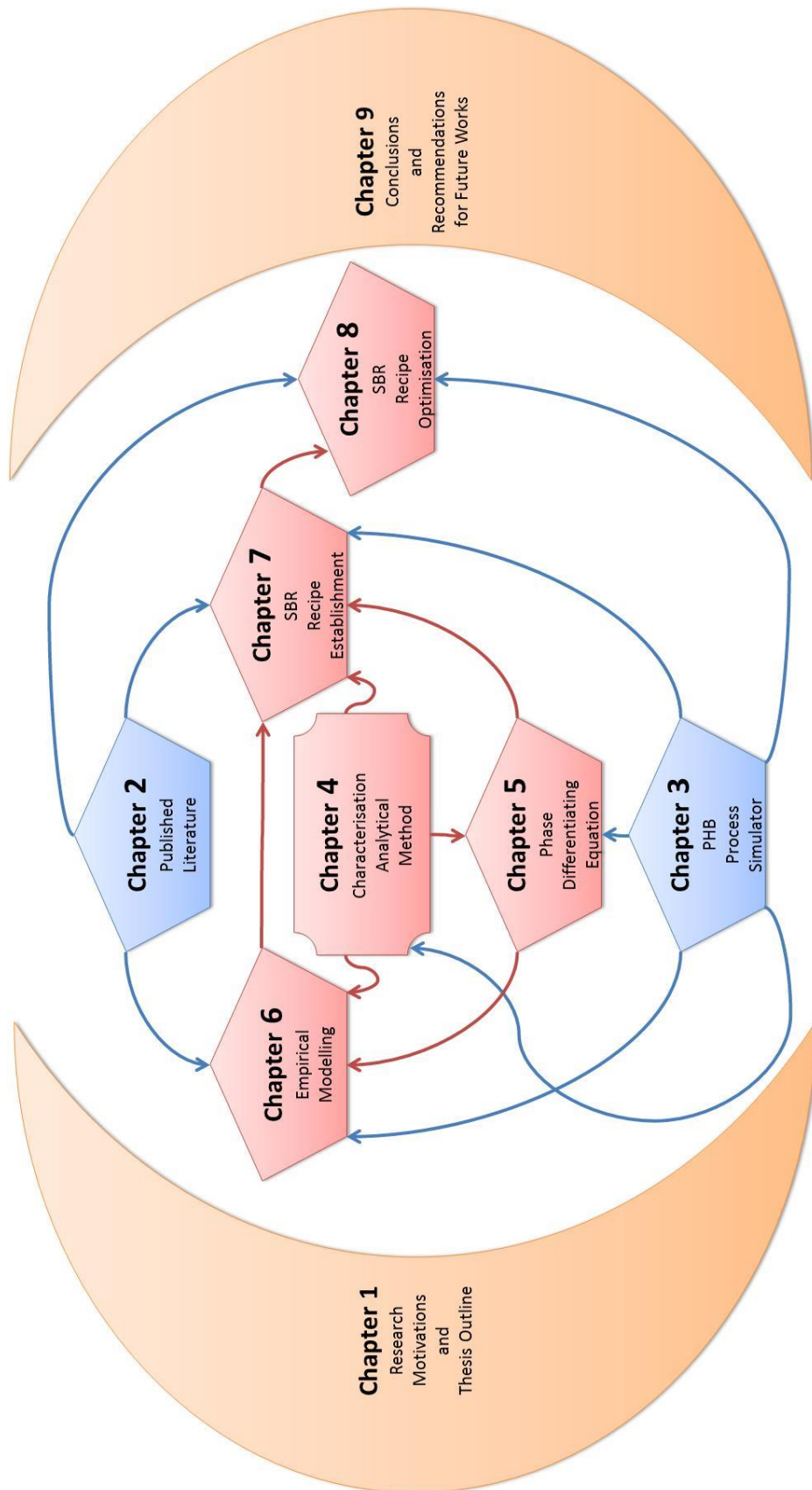


Figure 1.1 Thesis outline

The characterisation analytical method developed by the author is in the core of the research solutions addressing the complications associated with cost effective production of PHB using MMC. The “Characterisation Method” is an innovative approach developed and applied by the author to generate useful information about the process. The information obtained using the “Characterisation Method” is reported for the first time in this study and no similar results can be found in other research works. The “Characterisation Method” is developed, explained and discussed in Chapter 4. Application of the method results into generation of Chapter 5, Chapter 6 and Chapter 7 with some recommendations for extension of the method usage in Chapter 9.

In Chapter 5, mathematical representation of a border curve separating two process operational phase regimes is found using the batch simulator and the “Characterisation Method”. This mathematical model plays an important role in the analysis carried out in Chapter 6 and Chapter 7. In Chapter 6, empirical models are developed for the critical attributes of the process. The analytical tools developed in Chapter 4, Chapter 5 and Chapter 6 are used in Chapter 7 to generate operational recipe for mass production of PHB using MMC in Sequential Batch Reactors (SBR). Ultimately, a mathematical procedure to optimise a SBR process targeting maximum PHB production along with operational sustainability is discussed in Chapter 8. At the end, the research outcomes are discussed and some recommendations are given in Chapter 9 for future research works.

1.3.2 Brief description of the thesis chapters

In the current chapter, an introductory to the research project is given in addition to the motivations generating the main driving force for the research endeavour. In Chapter 2, an extended literature review is presented comprising a brief history of plastics, a thorough definition of bioplastics along with their chemical structures and physical properties. Additionally, some of the main manufacturing companies engaged in production of Polyhydroxyalkanoates (PHA) monomers as a dominant bioplastic with interesting physical and chemical properties is given.

PHA is mostly known for its application in packaging industry; however, it will be shown that packaging is not the most sophisticated approach to use the biopolymer. PHA biodegradability makes it a good candidate in search for environmentally benign replacement for the petrochemical plastics. Application of PHA in medical implant materials, cosmetics and skin care productions are mentioned in detail in Chapter 2. These materials can also be used as Nano-composite materials for textile dye

wastewater treatment, materials with therapeutic effects, drug delivery and neural tissue engineering, biofuels, production of fine chemicals, bio-surfactant and bacterial agent, carriers in agroindustry and augmentation of industrial micro-organisms survival ability which are encountered in Chapter 2. Additionally, a brief review of different PHA production and extraction methods is mentioned. The review also includes optimisation of PHB productions consisting of numerous attempts to optimise operational cultures, fermentation feeding rate and batch process duration. At the end, Sequential Quadratic Programming (SQP), the optimisation algorithm applied to find the optimal operational conditions based on the non-linear models will be formulated in Section 2.5.3. In the final sections of Chapter 2, a review of the mathematical modelling techniques including Multiple Linear Regression (MLR) and Artificial Neural Networks (ANN) as the most dominant linear and non-linear modelling methods is given respectively in Section 2.6.2 and Section 2.6.3 to be applied for optimisation purpose and production recipe generation.

In Chapter 3, mathematical equations and models reported by Dias *et al.* (2005) to envisage PHB productivity on the bases of acetate and ammonia feeding strategies are introduced. The mechanistic models are used to develop a simulation program in direction of the aims of this study. Moreover, the three divisions of the simulation program developed in MATLAB codes are encountered with experimental results published in direction of the process model development and model validations. At the end of Chapter 3, description of a typical simulation run is given with the aim of providing an overall vision about the PHB production process using Mixed Microbial Culture cultivation.

In Chapter 4, a process classification method is developed to analyse data obtained from the PHB process simulations based on results obtained from analysis of the feeding and product concentration profiles. The method will be used to generate a qualitative tool that enhances data visualisation using the PHB batch process data derived from simulation studies. With the application of the method and the visual representation of the overall behaviour of the system, general operational pathways will be identified and classified. The qualitative representations provided using the technique can be applied to predict batch process regimen along with the concentration profiles of the most important elements of the operation using process information from the batch initial state. The analytical method developed in Chapter 4 will be used in Chapter 5, Chapter 6 and Chapter 7.

In Chapter 5, a cluster of characterisation plots will be generated using the analytical tool developed in Chapter 4. Since operational pathways can be identified on each characterisation plot, a systematic method can be developed to formulate mathematical equations capable of differentiating operational pathways based on the batch initial state. By means of the PHB process simulator and the high rate of computations provided by computer machines, different operational case scenarios will be investigated to obtain co-ordination of the points forming the boundary curve that separates two dominant regions of different regime types in a characterisation plot. At the end of the chapter, the “Phase Differentiating Equation” developed in chapter 5 will be validated against a wide range of batch processes comprising different characterisation plots. This equation will be applied in Chapter 6 and Chapter 7 to segregate two most dominant operational phases for empirical modelling data generation and design of production recipes.

In Chapter 6, mathematical tools are developed to produce quantitative representations of the most significant elements of the PHB process. The empirical models can be developed using process data without the need of complex mathematical equations presenting various operational behaviour of the process. Identification of the most appropriate modelling technique and selection of the best modelling structure for prediction of the most important elements of the process will be addressed in chapter 6. Using the “Phase Differentiating Equation” developed in Chapter 5 empirical models will be built and validated to demonstrate enhanced modelling for targeted operational data sub-sets.

It will be demonstrated that accurate prediction of product concentration is not achievable if process data classification is not applied prior to model development. At first, linear MLR modelling technique will be used on the segregated data sub-sets for prediction of the most important elements of the process applying only the initial batch state condition. Furthermore, more sophisticated non-linear neural network modelling technique will be applied on the same data sets. The satisfactory non-linear models will be aggregated using bootstrapping method in quest of more accurate and more reliable models. Each model will be validated and recommendations will be made for the most effective modelling method and modelling structures for prediction of the critical process attributes. Additionally, some of the empirical models developed in Chapter 6 will be used in Chapter 7 for generation of PHB production recipe under the SBR approach.

In Chapter 7, a production recipe structure is established using the batch process simulator introduced in Chapter 3 for PHB production. This recipe is based on SBR approach to impose occurrence of the two major biological phases in each sequence of the operational process for sustainable production of PHB. The “Phase Differentiating Equation” developed in Chapter 5 will play a crucial role in the SBR recipe structure by assignment of feeding concentration to the system in different stages of the process. One SBR recipe will be designed based on the given structure and application of some of the empirical models developed in Chapter 6. The empirical models will be used to assign appropriate figures to the SBR recipe parameters.

The operability and reliability of the generated SBR recipe will be tested using the process simulator. The analytical method developed in Chapter 4 provides a sound platform to identify the types of regimen occurring during a course of simulated SBR run. Classification of the operational regimen in Chapter 4 facilitates capsulation of analytical results by associating the batch operations to a specific class of regime type operation.

Application of the “Phase Differentiating Equation” within the structure of the SBR recipe will also have significant effect on process disturbance rejection capability. In Chapter 7, investigations will be carried out to examine SBR process ability in mitigation of load and operational disturbances imposed to the production system. The SBR recipe designed in Chapter 7 will be used as the basis for optimisation studies carried out in Chapter 8.

In Chapter 8, the batch process simulator introduced in Chapter 3 will be used to generate process data for production of PHB using the SBR recipe designed in Chapter 7. Critical recipe parameters in a SBR process will be identified to enable quantification of process parameters attributed to maximum product release in a sustainable continuous operation. These SBR process elements will be modelled using the empirical modelling techniques mentioned in Chapter 2. Reliable models will be applied in an appropriate optimisation algorithm to find the optimal operational condition for a given objective function. The aim is to introduce a procedure for optimisation of real production SBR process using process data, empirical models and mathematical optimisation tools. In Chapter 8, reliability of the optimisation procedure proposed to find the optimal SBR operational recipe parameters will be investigated and discussed.

In Chapter 9, a summary of the main conclusions in this study is given along with recommendations for future research work on the subject and applications of the analytical method developed in this research study.

1.3.3 *Research contributions*

The main research contributions by the author can be divided into two divisions. In the core of the first part, an analytical method capable of classifying operational state of PHB process is developed. Application of the method enabled segregation of different operational regimen and development of a mathematical tool to estimate occurrence of the critical process attributes based on initial state of the process. Different modelling structures are investigated to suggest the most appropriate empirical models targeting each operational regimen. The classification tool developed in this study enables prediction of operational phase regimen using the process information from the initial state of the process.

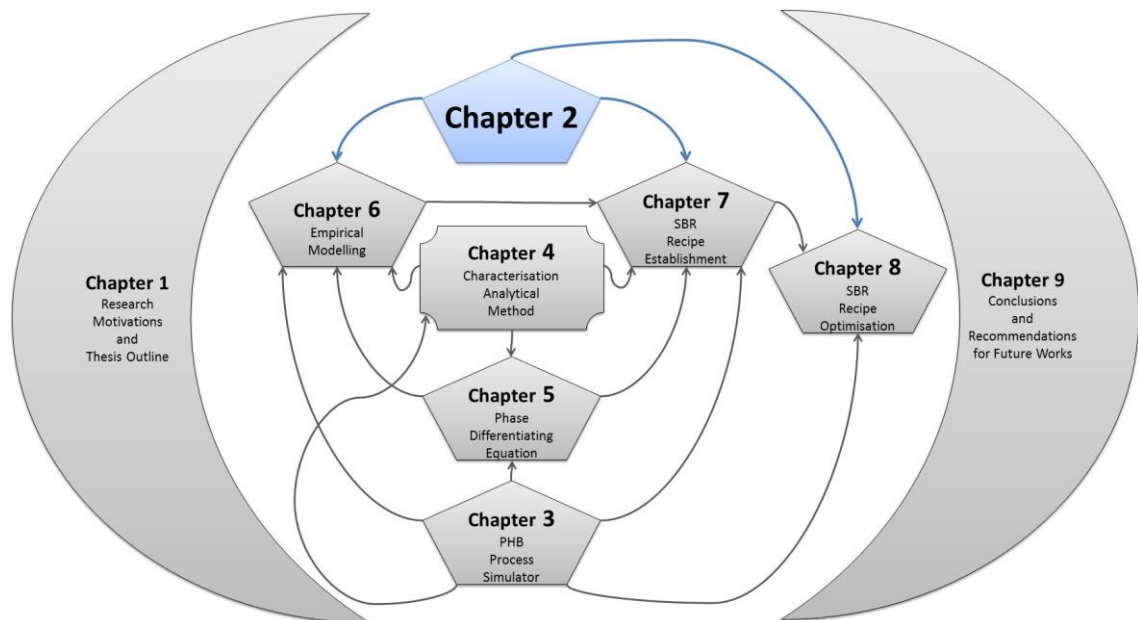
In the core of the second section of contributions, a novel operational procedure is developed by the author to address the most important process requirements for effective and sustainable production of PHB using a cluster of microbial cultures in activated sludge. In addition to the general recipe structure, a procedure is developed for assignment of appropriate recipe parameters. Stability of the proposed recipe will be examined using the PHB batch simulator. Operational variations are also studied to confirm reliability of the proposed production recipe under severe operational misconduct.

In the course of the research study, analytical results are also generated with interesting interpretations which can be used to provide significant insights into the PHB production process. Proposition of operational criteria for identification of the optimal batch termination points for different batch operational phase are among the research contributions made available in this study. The research outcomes are published in:

Ganjian, A., Zhang, J., Dias, J. M., & Oliveira, R. (2013). Modelling of a Sequencing Batch Reactor for Producing Polyhydroxybutyrate with Mixed Microbial Culture Cultivation Process Using Neural Networks and Operation Regime Classification. *CHEMICAL ENGINEERING*, 32.

Ganjian, A. Zhang, J & Oliveira, R (2014). Optimisation of a Sequencing Batch Reactor for Production of Polyhydroxybutyrate Using Process Characterisation Method and Neural Network Modelling. *ESCAPE 24*, 733-738

Chapter 2 Literature Review



2.1 Bioplastics

2.1.1 Definition of bioplastics

Bioplastics are polymers which meet the criteria defined for the biodegradability, biocompatibility or compostability characteristics. Bioplastics are produced either from renewable biological sources or made in chemical plants and can be designated as bioplastics based on the criteria defined by EU regulation EN 13432 and EN 14995 for biodegradability and compostability respectively.

While degradation is caused by enzymatic processes, chemical dissolution of materials by biological means is known as biodegradation. In general terms, a biodegradable material can be consumed by microorganisms and degraded back into water, dioxide carbon, biomass or compounds naturally found in the environment. On the other side, compostability is known as chemical degradation in compost pile forms either in presence of oxygen (aerobically) or without oxygen (anaerobically). According to the European bioplastics (EuBP), materials can be labelled as industrially compostable when they biodegrade under conditions and within a timeframe defined by the EN 13432 norm.

Chemical structure of the polymers is the key factor concerning its biodegradability rather than the origin of the materials used for their production. While most of the bio-based polymers are biodegradable, this is not an inherent characteristic of bioplastics (the term bio-based describes the part of a material or product that stems from biomass) (EuBA, 2014). Some class of bioplastic monomers lose their biodegradability through chemical reformation. Polylactic acid (PLA) and polybutylene succinate (PBS) are examples of compounds produced from renewable resources that cannot be fully biodegraded.

The majority of the conventional plastics are produced in the petrochemical industries that present minimal or none biodegradability nor compostability. For instance, polyolefins such as polypropylene (PP), polyethylene (PE), polystyrene (PS), polyvinyl chloride (PVC) and polyethylene terephthalate (PET) are the most dominant plastics produced in chemical industries.

In many cases, a combination of bio-based and chemically synthesized monomers are blended together to improve physical properties of the materials. Although the carbon feedstock is provided from renewable biological sources, chemical additives are not. In

Figure 2.1, bioplastic's material coordination system is depicted to differentiate conventional plastics from bioplastics. The majority of the bio-plastics available in market today are composed of different combination of bio-based and chemically synthesized materials such as polybutyrate (PBAT), polycaprolactone (PCL) and biobased polyamide (PA). Since some of the fossil-based plastics can also be degraded by bio-enzymes, they can be classified as bioplastics although they are not bio-derived. Among the bioplastics, polyhydroxyalkanoates (PHA) are derived from renewable sources and fully biodegradable (European bioplastics, 2014).

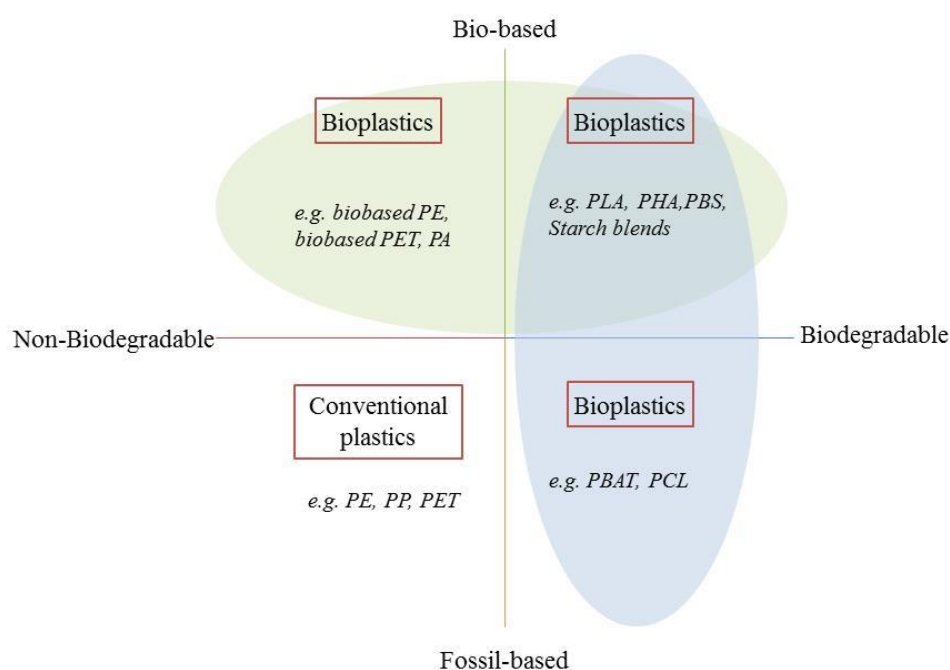


Figure 2.1 Bioplastics' material coordinate system (adopted from EuBA 2014)

2.1.2 Economic and environmental incentives

Plastics are now so commonplace in the modern life of mankind that their presence has become an inevitable factor for its life style development. Plastics come in all sizes and shapes. Production of artificial bioplastics has been known to mankind for over 150 years. The first artificial thermoplastic “celluloid” was versatile and highly inflammable material which was made of cellulose to be used in production of early films and also jewellery. Since then, numerous new compounds such as ethylene, casein, Shellac and plastics derived from soy proteins have been produced (Fiebach and Grimm, 2000; Stevens, 2002).

The early experimental production of plastics in the 1930s and 1940s remained in the laboratory phase and never made it to the commercial production. By the discovery of the low-priced crude oil in 1950s and its large scale industrial application, further investment in the field was stagnated. Production of plastics from non-petrochemical feedstock gained attention for the second time when oil price shocks took place in the 1970s. However, economic incentives towards bioplastics remained low until public attention was drawn to the increasingly amounts of waste and limited landfill capacities in the 1990s. In 2012, the share of bioplastics in the plastic market was about 1.4 million tonnes compared to the total 290 million tonnes of total plastics worldwide. Although bioplastic production is well below 1% of the total plastic production, its market growth is experiencing high growth rate between 20% and 100% annually in different divisions. The global production capacity for bioplastics increased from 1 million tonnes in 2010 to 1.4 million tonnes in 2012 and is expected to reach 6.1 million tonnes in 2017 in annual production (European bioplastics, 2014).

There are a number of incentives encouraging the growth of the bioplastic industries both within the sector and imposed by the external market. Advanced production means and methods offer cost reduction through mass production. Additionally, augmented social concerns about climate change and high acceptance of the green products by the consumers are the factors encouraging investment in the field. Moreover, political instability in the oil production contraries especially in the Middle East presents high potential for sudden increase in the price of fossil resources which favours investment in the replacing industries using bio-based resources.

Market penetration of the bioplastics is just beginning. Some leaders in the automotive market such as Toyota, Volkswagen, Ford and Mercedes have already launched or integrated bioplastics into their products. Bioplastics have gained attention for food and drug packaging by some of the big brand names including Danone, Coca-Cola, PepsiCo, Heinz, Tetra Pak and L'occitane (European bioplastics, 2014).

Figure 2.2 illustrates an idealised life cycle of a bioplastic product that can be either recycled or converted into natural elements and extracted to obtain bio-polymer structures (European bioplastics, 2014).

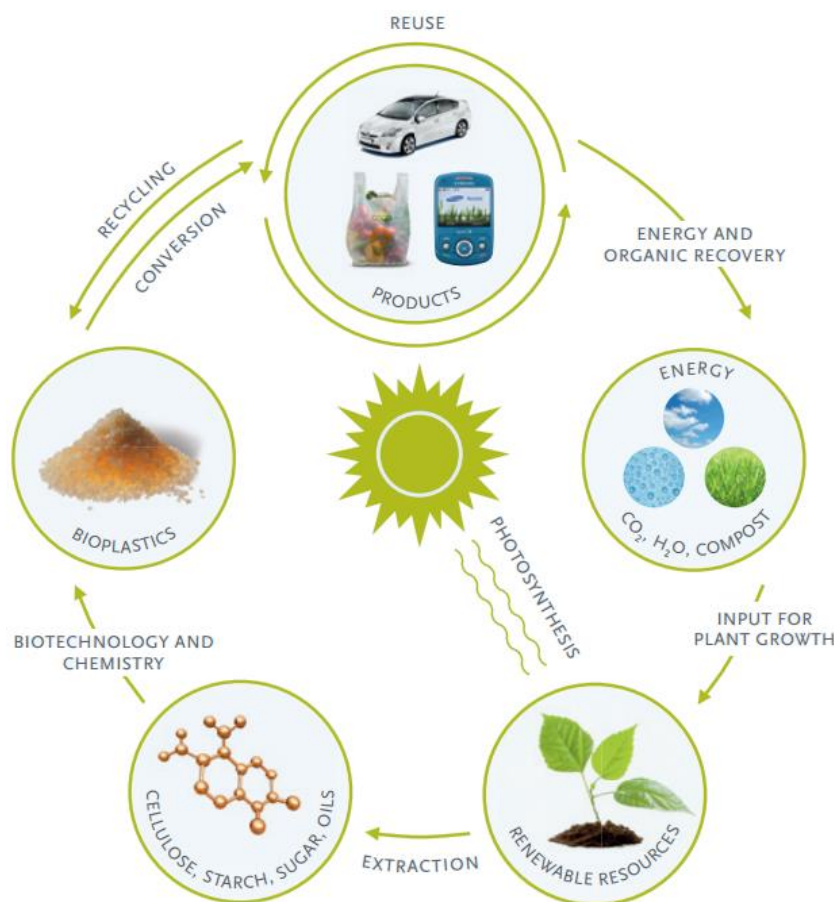


Figure 2.2 Life cycle of bioplastics (adopted from European bioplastics, 2014).

The bioplastic products used in a circular economy follow one of the two main pathways for energy/organic recovery or recycling. In the former pathway, used products are degraded to compost, CO₂ and water that form the feedstock to fecundate plants or living organisms. The biopolymers are produced and processed to obtain bioplastics with a physical properties required for specific applications. The raw bioplastics are converted to usable products and released to markets. Bioplastic recycling is the second pathway that requires development of logistics and infrastructure to collect, separate, process and return of the waste bio-based products.

2.2 Polyhydroxyalkanoates (PHAs): a promising group of green plastics

2.2.1 PHA chemical structure

PHA is a family of diverse biopolyesters (Hazer and Steinbüchel, 2007) with similar mechanical properties to those of polypropylene. The advantage of PHA is related to its biodegradability, biocompatibility and production from renewable resources (Serafim *et al.*, 2004). Discovery of the first PHA dates back to the 1920s with identification of poly(3-hydroxybutyrate) or PHB at the Pasteur Institute (Lemoigne, 1926). Since then,

more than 300 bacteria species have been identified to produce over 150 different types of hydroxyalkanoates (Steinbüchel and Valentin, 1995).

Bioplastics in the form of PHA are stored as granules in the cytoplasm of almost all genera of the bacteria kingdom under stress conditions imposed by lack of nutrient, electron donor or acceptor (Valentin *et al.*, 1999; Reddy *et al.*, 2003). These polymers are in fact intracellular carbon and energy reserves for the bacteria that can take up to 90% CDW (cell dry weight) (Madison and Huisman, 1999). PHA in the form of Poly(3HB) that is produced in the cytoplasmic membrane and cytoplasm of *Escherichia coli* is reported to be a non-storage part of the cell that can be found in yeasts, plants and animals (Dawes and Senior, 1973).

The generic formula for PHAs is shown in Figure 2.3. The members of the PHA family vary by the structure of the side chains of parent compounds. The short chain length monomers consist of three to five carbon atoms while the long chain length monomers have more than fourteen carbon atoms. The medium chain length monomers are classified in between those two groups. The most common types of PHA are tabulated in Table 2.1 (Lee, 1996b; Liu *et al.*, 2011).

Table 2.1 The most common PHA based on formula given in Figure 2.3

X	R	Chemical name	PHA full name
1	hydrogen	poly(3-hydroxypropionate)	P(3HP)
1	methyl	poly(3-hydroxybutyrate)	P(3HB)
1	ethyl	poly(3-hydroxyvalerate)	P(3HV)
1	propyl	poly(3-hydroxyhexanoate)	P(3HHx)
1	pentyl	poly(3-hydroxyoctanoate)	P(3HO)
1	nonyl	poly(3-hydroxydodecanoate)	P(3HDD)
2	hydrogen	poly(4-hydroxybutyrate)	P(4HB)
2	methyl	poly(4-hydroxyvalerate)	P(4HV)
3	hydrogen	poly(5-hydroxyvalerate)	P(5HV)
3	methyl	poly(5-hydroxyhexanoate)	P(5HHx)
4	hexyl	poly(6-hydroxydodecanoate)	P(6HDD)

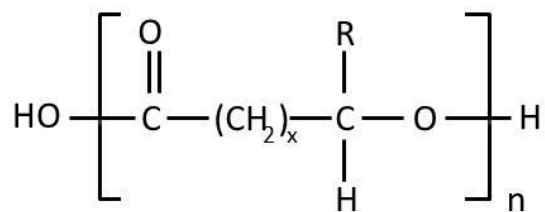


Figure 2.3 PHA molecule formula

The average number of repeating units (n) can alter in between 100 to 30,000 times (Lee, 1996b). Other arrangements of monomers exist in copolymers of PHAs. For example, poly(3-hydroxybutyrate-co-3-hydroxyvalerate), P(3HB-co-3HV), is a medium chain length produced by *Bacillus circulans* from cheap carbon sources like dextrose. This PHA consists of a random arrangement of methyl and ethyl monomers (Phukon *et al.*, 2012). The copolymer poly(3-hydroxybutyrate-co-3-hydroxyhexanoate), P(3HB-co-3HHx), is made up of methyl and propyl monomers and can be produced by recombinant bacterium *Cupriavidus necator* harbouring plasmid DNA (Anis *et al.*, 2012). High purity of the latter copolymer has biomedical applications (Anis *et al.*, 2013).

2.2.2 PHA properties

The composition of the monomers, their microstructure and their molecular weights have dominant role on the PHA properties. Some of the general properties are listed in Table 2.2 for three PHAs, PLA as other type of bioplastic and fossil based plastics for comparison. Since the focus of this research project is on industrial production of P(3HB) (or as commonly referred to as PHB), further information is provided with focus on the PHB properties.

The molecular weight of PHB produced from wild type bacteria is usually in the range of $1 \times 10^4 - 3 \times 10^6$ g/mol with a polydispersity of around two (Doi, 1990). The glass transition temperature is around 4°C while the melting temperature is about 180°C . The densities of crystalline and amorphous PHB are 1.26 and 1.18 g/cm³ respectively. PHB is reported to be a stiffer and more brittle plastic material when compared to polypropylene. PHB is water insoluble and relatively resistant to hydrolytic degradation (Sudesh *et al.*, 2000).

Crystallisation kinetics, morphology of melt and solution crystallised PHB, the variation of lamellar thickness with crystallisation temperature, and the assessment of some

thermodynamic quantities are reported in (Barham *et al.*, 1984). Films of PHB show gas barrier properties comparable to PVC and PET (Avella and Martuscelli, 1988). Pure PHB bioplastic suffers from a very narrow window of processability and low impact resistance. For this reason, different polymers are mixed with PHB to obtain new PHB-based materials with improved processability and impact resistance (Avella and Martuscelli, 1988). The crystalline structure of PHB is also very well studied in (Sudesh *et al.*, 2000).

There are a number of different species of bacteria and fungi recognised that can degrade PHA into components naturally found in nature, both aerobically and anaerobically. For instance for biodegradation of PHA, *Comamonas testosterone* and *Pseudomonas stutzeri* are two types of bacteria found in the sea water sources, *Acidovorax faecalis*, *Aspergillus fumigatus*, *Pseudomonas lemoigne*, and *Variovorax paradoxus* are found in the soil, and *Alcaligenes faecalis*, *Pseudomonas sp.*, and *Illyobacter delafieldi* are found in the anaerobic sludge (Tokiwa *et al.*, 2009; Banerjee *et al.*, 2014).

2.2.3 PHA production companies

Commercial production of PHA has been exploited for four short chain length structures known as poly(3-hydroxybutyrate), poly(3-hydroxybutyrate-co-3-hydroxyvalerate), poly(3-hydroxybutyrate-co-4-hydroxybutyrate) and poly(3-hydroxybutyrate-co-3-hydroxyhexanoate) with short names PHB, PHBV, P3HB4HB and PHBHHx respectively (Chen, 2009).

By 2010, more than 14 active research and producing companies were reported to engage in PHA production as tabulated in Table 2.3. About 50% of these companies were established after the gold rush of oil price increase to over \$100 USD per barrel in 2003. The majority of the companies initiated large scale production of PHA but did not manage to endure the competitive market of late 1990s with low oil price. Chemie Linz AG Austria was the first company to commercialise PHB production in 1980s to the scale of 60 tons per year. The company produced PHB in a 15 m³ fermentor using *Alcaligenens latus* strain. The bioplastics produced in this unit was used to make sample bottles, cups and syringes (Hrabak, 1992). The technology was later bought by Biomer in Germany for production of PHB for making of combs, pens and plastic bullets (Chen, 2010).

Table 2.2 Properties of some bio-polymers and fossil based polymers (adapted from (Albuquerque, 2009)).

Physical properties	Relevance for plastic applications	PHA			Other biobased plastic	Fossil based polyolefins					
		P(3HB) ^{1,2,3,4}	P(HB-co-HV) ^{4,5}	P(HB-co-HHx) ⁶	PLA ²	HDPE ^{2,7}	LDPE ^{2,7}	PS ^{2,7}	PP ^{2,7}	PET ^{2,7}	PVC ^{2,7}
Molecular weight, M_w	Strength, Processability	$10^4 - 3 \times 10^6$	$10^4 - 3 \times 10^6$	$10^4 - 3 \times 10^6$	$10^5 - 3 \times 10^5$	$10^5 - 5 \times 10^5$	9×10^4				
Melt flow rate (g/10 min)	Processability	5 – 25	15 – 25	0.1 – 100	3 – 6	0.1 – 3.5	0.2 – 3.5				
Density (g/cm ³)		1.20 – 1.26	1.20 – 1.40	1.07 – 1.25	1.25	0.94 – 0.97	0.92 – 0.93	1.05	0.95	1.37 – 1.46	1.39
Crystallinity (%)	Transparency Stiffness Brittleness	55 – 80	40 – 50	< 55	Often amorphous	Semi-crystalline					
Mechanical properties											
Tensile strength at yield (MPa)	Resistance to permanent deformation	15 – 45	25 – 30	10 – 20	53 – 70	25 – 32	15 – 20	42 – 60	12 – 43	55 – 75	50 – 80
Elongation to break (%)	Flexibility	2 – 10	20 – 30	10 – 25	0.1 – 2.4	600 – 900	600	2 – 4	150 – 400	50 – 150	20 – 40
Young's modulus (GPa)	Elasticity/ Stiffness	0.9 – 3.5	1.2 – 3.2		0.35 – 3.6	0.7 – 1.2	0.15 – 0.45	3 – 3.5	0.6 – 1.2	2.8 – 3.1	2.9 – 3.3
Thermal properties											
Melting temperature T_m (°C)	Processability	175 – 185	155 – 170	< 175	85 – 170	120 – 130	105 – 115	240	170	265	100 – 260
Glass transition temperature T_g (°C)	Temperature below which presents rigid structure	4	< 4	< 4	55 – 65		-30	95	0	69 – 75	82
In use temperature range (°C)		-30 – 120	-30 – 120	-30 – 120	< 60	0 – 100					
Other properties											
Water resistance		Yes			No	Yes					
O ₂ permeability		Very low			High	Low					
Water vapour permeability		Lower than other bio-based plastics but higher than most polyolefins			High	Low					
Biodegradability		Yes			No	No					

¹(Lee, 1996b), ²(Crank and Patel, 2005), ³(www.biomer.com), ⁴(www.biocycle.com.br), ⁵(www.bio-plastics.org), ⁶(www.pg.com), ⁷(Brandrup *et al.*, 1999)

Imperial Chemical Industries (ICI) was a UK company that initiated mass production of PHBV to the scale of 300 tons per year during the 1980s and 1990s. The PHA copolymer PHBHHx was produced by Procter & Gamble (P&G) from 1980s to 2005 based on manufacture contracts (Chen, 2010).

Table 2.3 Worldwide PHA producing and researching companies

Company	PHA type	Production scale (tons/year)	Production initiation
Biomers, Germany	PHB	Unknown	1990s
Metabolix, USA	Several PHA	Unknown	1990s
Tepha, USA	Several PHA	Pilot scale	1990s
ADM, USA	Several PHA	50,000	2005
Meridian, USA	Several PHA	10,000	2007
Kaneka, Japan	Several PHA	Unknown	1990s
Biocycles, Brazil	PHB	100	1990s
Bio-On, Italy	Unclear	10,000	2008
Zhejiang TianAn, China	PHBV	2,000	1990s
Yikeman, Shandong, China	Unclear	3,000	2008
Jiangsu Nan Tian, China	PHB	Pilot scale	1990s
Shenzhen O'Bioer, China	Several PHA	Unknown	2004
Tianjin Green Bioscience, China	P3HB4HB	10,000	2004
Shandong Lukang, China	Several PHA	Pilot scale	2005

The Brazilian sugar mill, Copersucar, built a pilot plant for PHB production using biomass as the energy supplier in 1995. The advantage of the production technique was that the polymer could be produced at low cost. Prospect of future development is promising considering the annual production of sugar and ethanol is considerably high in the south and central region of Brazil (Chen, 2010). Production cost could be significantly decreased when large scale production under sugarcane is accomplished (Nonato *et al.*, 2001).

The European section of Metabolix, a bioscience engineering company, has recently launched a new PHA production program with more than thirty platforms allocated for production of novel materials. PHB production is maximised by the multi-gene expression technique using different carbon sources such as switchgrass (*Panicum virgatum*), camelia and sugarcane (Bernard, 2014).

In China, NingBo TianAn developed a high efficiency PHBV model unit in collaboration with the Chinese Institute of Microbiology. This pilot plant was able to grow *Ralstonia eutropha* in glucose medium with density of 160 g/L CDW within 48 hours (Chen, 2010). PHBV has also been identified as a biodegradable and biocompatible polymer that can be used for drug delivery (Vilos and Velasquez, 2012).

Copolymers of P3HB4HB with various thermal and mechanical properties are produced by Tianjin Green Bioscience, China, and Metabolix, USA, using recombinant *E.coli* and *R. eutropha* (Chen, 2010; Metabolix, 2014; TianjinGreenBio, 2014). Chen reported that the Chinese and the American companies were developing sites to increase P3HB4HB production to the capacity of 10 kilotons and 50 kilotons per year respectively by 2010 (Chen, 2010). In addition to the general characteristics exhibited by the PHA family, P3HB4HB can be designed to demonstrate different mechanical properties by varying the ratio of 4HB and 3HB (Li *et al.*, 2010). P3HB4HB can be used for composite fabrication with enhanced thermal and dynamic mechanical properties (Chen *et al.*, 2014).

A collaborated work by P&G, KAIST and Jiangmen led to production of PHBHHx in a 20 m³ fermentor by *Aeromonas hydrophila* (Chen *et al.*, 2001). The crucial process that increased the cost of production was the application of ethyl acetate and hexane in the extraction. The product was exploited in China to be applied in films, binders, flexible packaging, coated paper, coating systems and medical devices (Chen, 2010).

The main drawback has always been the PHA production cost which was about five to ten times more than their equivalent petroleum based polymers (Suriyamongkol *et al.*, 2007). This is the case even though the prices of several degradable polymers have decreased greatly as a result of recent efforts to develop the manufacturing technology; for instance, the price of PHB was more than \$25 USD per pound in 2008 but is now around \$4 USD per pound when purchased in massive quantities (Biby, 2013). In order to sustain economically beneficial PHB products, target markets should be aimed for large scale production with a realistic production scenario. When PHB is available in large amounts, more specialised companies and research groups are expected to increase investment on projects related to the bioplastics. This is an interdisciplinary field comprising joint efforts of microbiologists, geneticists, botanists, chemists, polymer scientists, chemical engineers, biotechnologists and medical scientists.

2.2.4 PHA applications

The initial application of PHA was production of everyday articles such as shampoo bottles or shopping bags. It has also been used as paper coatings, carpets, containers and disposable items such as razors, utensils, diapers and feminine hygiene products (Chen, 2009). PHA in the form of PHB is bacterial energy storage compound and is postulated as animal feed or feed additives with nutritional value (Boon *et al.*, 2013). PHA has also been reported to have applications in printing and photographic materials (Chen, 2009). Additionally, some forms of PHA can be used as heat sensitive adhesives, or smart gels with biodegradable and biocompatible properties (Chen, 2009).

- *Food packaging*

The most frequently used materials for food packaging applications are polypropylene (PP), polyethylene terephthalate (PET) and polystyrene (PS). In the quest of biodegradable alternatives to mitigate the plastic waste disposal problems, biopolymers are being investigated. Apart from the economic barriers, one of the main challenges of biopolymers is to adapt their oxygen and water permeability to the food product requirements (Fabra *et al.*, 2014). In a recent study, physical properties of PHBV polymers were enhanced to reach permeability levels similar to those of PET by adding a zein interlayer. The use of PHA based compounds for food packaging applications has also been documented (Fabra *et al.*, 2013b). Starch and PLA polymers are also two families of biopolymers that present interesting properties for food packaging applications. They are commercially made available in large scale by companies such as Novamont (www.novamont.com) and Natureworks (www.natureworkslc.com) respectively (Fabra *et al.*, 2013a).

- *Medical implant materials*

It has been documented that different monomers of PHA can be used for various medical applications with various physiological functionalities. Toxicity of PHB, P4HB, PHBV, PHO and their degradation products are refuted and even some therapeutical or nutritional benefits are counted for these PHAs (Reusch, 1995; Williams and Martin, 2003; Chen, 2009). The first successful demonstration of a tri-leaflet heart valve was performed in a sheep model using poly(4-hydroxybutyrate) (P4HB) (Martin and Williams, 2003). Application of implanted PHB patches on the defected cranium of adult male rats confirmed good biocompatibility and

osteoconductive character of the implants (Gredes *et al.*, 2014). PHA including PHB, PHBV, P4HB, P3HB4HB are frequently investigated for various medical applications such as wound dressings, tendon repair devices, orthopaedic pins, slings, sutures (Chen, 2009).

- *Cosmetics and skin care*

Three copolymers of P(3HB), P(3HB3HV) and P(3HB3HHx) exhibit suitable level of oil absorbability, retention and oil-indication as potential facial oil blotting material. All three films revealed similar effects for sebum absorption (Sudesh *et al.*, 2007). The premium advantage of PHB components over other materials is that no lipophilic additive is required for sebum absorption while commercial facial oil usually add zinc stearate to enhance absorption level. The PHA films provided effective oil absorption even after being washed with detergent; whereas, the commercial counterparts loss their ability to absorb oil upon washing with detergents (Sudesh *et al.*, 2011).

- *Nanocomposite materials for textile dye wastewater treatment*

Novel applications of PHA films for absorption of oily substances were encountered based on their hydrophobic properties discovered for cosmetic applications. Solvent-cast P(3HB) films were able to remove over 35% of colour from textile dye wastewater. The film was enhanced to form electrospun P(3HB) - 50 CDW% TiO₂ which also can be used as an intelligent packaging material with self-cleaning properties to ensure the safety and quality of food products (Sudesh, 2013).

- *Therapeutic effect*

Evidence has been accumulated for ketone bodies including 3-hydroxybutyrate (3-HB) (most common degradation product of PHB) to have therapeutic role in treatment of neural diseases. It has be shown that 3-hydroxybutyrate methyl ester (3-HBME) improves intracellular communication between neurons that enhance learning and memory capabilities (Zou *et al.*, 2009). Additionally, application of other hydroxybutyrate ketones (especially β -hydroxybutyrate, β -OHB) for neural protection against Alzheimer and Parkinson diseases has been confirmed (Kashiwaya *et al.*, 2000; Dedkova and Blatter, 2014).

- *Drug delivery and neural tissue engineering*

Application of non-toxic, biodegradable and biocompatible PHA has recently gained enormous attention by the researchers. The low cost of PHA production make it a good candidate to replace some of the conventional compounds for controlled drug delivery in future. Controlled release of antibiotic and paclitaxel for effective treatment of periodontal diseases and ovarian cancer respectively has been reported (Sendil *et al.*, 1999; Vilos *et al.*, 2013a; Vilos *et al.*, 2013b).

PHBV has also exhibited properties to have important benefits for neural tissue engineering (Chen and Tong, 2012). In regeneration therapies, scaffolds are essential for cell viability (Hutmacher, 2000). PHBV is an established drug delivery system providing a sustained and controlled release (Chen and Davis, 2002). Moreover, its biodegradable and can disappear from implant site to leave space for the regenerated tissue (Hankermeyer and Tjeerdema, 1999). Drugs can be entrapped or microencapsulated in an engineered PHA structures (film, porous, matric, microcapsule, microsphere and nanoparticle) (Shrivastav *et al.*, 2013). PHA in the form of poly(3-hydroxybutyrate-co-3-hydroxyvalerate) (PHB-HV) has distinctive thermoplasticity and piezoelectricity properties presenting a suitable nominee for regeneration of injured spinal cord. Studies showed that PHB-HV scaffolds are well tolerated by the host tissue and do not have negative impact on the recovery procedure (Samy *et al.*, 2013).

Among natural and synthetic biodegradable polymers, PHB is found to be remarkable for its application in drug delivery (Tian *et al.*, 2008). Application of PHB for drug delivery is a recent innovation with further investigations on polymeric capsule formation (Mora-Huertas *et al.*, 2010).

- *Biofuels*

Development of renewable fuels including bioethanol, biomethanol, biodiesel, biogas, bio-oil and biochar has attracted attention of many research centres (Demirbas, 2008). Conversion of some short and medium chain length PHA led to production of hydroxyalkanote methyl ester (3HAME) by acid catalysed hydrolysis (Zhang *et al.*, 2009). One of the most important criteria used to evaluate the quality of a fuel is its combustion heat. The combustion heat of 3HAME is 30 kJ/g which is 3 kJ/g higher than that of ethanol. Although the quality of this biofuel is considerably lower than the 0[#] diesel and 90[#] gasoline (50 kJ/g and 52 kJ/g respectively), its application is

environmentally friendly which is produced from common biomass sources (Zhang *et al.*, 2009).

- *Fine chemical industry*

Pure (R)-3-hydroxyalkanoic acids are conveniently prepared by depolymerizing the biosynthesized PHA (Seebach *et al.*, 1992). The RHA monomers have two functional groups (-OH and -COOH) that can be modified. Additionally, the chiral center available in the structure of the RHA monomer provide flexibility to perform as synthons and to act as starting material for the synthesis of fine chemicals such as pheromones, aromatics, vitamins and antibiotics (Ruth *et al.*, 2007).

- *Increasing survival ability of industrial microorganisms*

Physiological functionalities of PHA have proved to be beneficial for extending survival threshold of bacteria and their stress tolerance under adverse conditions such as starvation, desiccation, radiation and high pressure. This effect can also be observed in competitive environmental settings where carbon or energy sources may be limited (as observed in “feast” and “famine” cycles in activated sludge waste water treatment systems (Kadouri *et al.*, 2005; Goh *et al.*, 2014)).

- *Bio-surfactant and bacterial agent*

The term surfactant refers to “surface active agents” (Clint, 1975). Bio-surfactants are compounds synthesized by some microorganisms with hydrophilic and hydrophobic ends (Makkar and Cameotra, 2002; Marchant and Banat, 2012). Application of bio-surfactants has recently gain attention in food (Nitschke and Costa, 2007), beverage, pharmaceutical (Gharaei-Fathabad, 2011), cosmetics, detergents (Bafghi and Fazelipour, 2012), oil and mining exploitations (Shubhrasekhar *et al.*, 2013). In addition to biodegradability and production from renewable resources (Müller *et al.*, 2012), bio-surfactants consist of a very promising and interesting substance class that can play the role of emulsifiers, demulsifiers, wetting agent, penetrant and bubble agents (Rosen and Kunjappu, 2012).

- *Carriers in agroindustry*

For many years, application of different chemicals to eliminate pests, weeds, and pathogens from cultivated plant species have been known as one of the most important factors effecting both the agriculture industry and ecology of the environment.

Unfortunately, large scale application of these chemicals has resulted into significant accumulation of these mostly toxic materials in the biosphere while plant protection could not be assured. Pesticides exhibiting mutagenic and carcinogenic effects are ingested by humans with food and thus they pose threats on human health. To resolve this issue, researches have been carried out in direction of replacing uncontrolled distribution of xenobiotics in the environment with controlled delivery of pesticides and nutrients to plants. Application of ethyl cellulose (Pérez-Martínez *et al.*, 2001), polyurethane (Shukla *et al.*, 2002), sodium alginate (Kulkarni *et al.*, 2000), and molecularly imprinted polymers (MIPs) (Piletska *et al.*, 2005) are examples of materials reported for delivery of a number of weed and pest killer chemicals. (Voinova *et al.*, 2009)

The key property of PHA materials for application in delivery systems is their biodegradability in relatively prolonged time period that is important for pesticides formulation design. The copolymer of PHB-PHV has been reported as an appropriate candidate for embedding pesticides to be released on a controlled manner. The rate of pesticide release to the soil can be regulated by varying the polymer-pesticide ratio. (Sudesh *et al.*, 2000; Voinova *et al.*, 2009).

In this review, numerous applications were encountered for PHA in different formation. Mass production of new products requires appropriate facilities enabling utilisation of the product in an efficient and economic manner. Currently, there is a huge insufficiency in utilisation of facilities, even though bioplastics have already come into the market (Bernard, 2014).

2.3 PHA production methods

Industrial production of PHA is a two-step process: formation and accumulation of PHA followed by its extraction (Snell and Peoples, 2009). With over 300 bacteria producing PHA naturally, there is a wide range of options to start from. The most interesting case is fermentation using microbial aerobic sourced from cellulosic material, sugar, or even vegetable oil. Transgenic plants can also accumulate PHA in their leaves or seeds in very efficient manner (Bernard, 2014). In this section, PHA production methods are introduced briefly.

2.3.1 PHA production by plants

As early as 1930, one third of industrial organic chemicals were derived from plants. With the advent of petroleum industries, low cost materials were made available with properties that could not be duplicated by abundantly available natural materials. Production of high value technical materials in crop plants have recently gain attention using genetically engineered plants. This approach serves the widely held social goal of developing more sustainable and environmentally benign methods of maintaining market needs. The idea remains a research project until economic incentives justify execution of the plant mass production projects (Somerville and Bonetta, 2001).

PHA can also be produced by genetically engineered plants. Since fermentation process is avoided, the overall production cost of PHA product is expected to reduce significantly. The transgenic plants require fixed CO₂, water and soil nutrients to produce biopolymers through photosynthesis which can degrade back to CO₂ and water again after disposal. Three forms of PHA synthesis mechanisms are reported by Suriyamongkol *et al.* (2007).

In one of the earliest attempts, PHB was produced using *Arabidopsis thaliana*, a model plant with a relatively small genome and short life cycle that could be easily transformed with *Agrobacterium tumefaciens* (Poirier *et al.*, 1992). Other PHA polymers were also produced in plant leaves containing saturated and unsaturated 3-hydroxyalkanoic acids ranging from 6 to 16 carbons with 41% monomers being 3-hydroxyoctanoic acid and 3-hydroxyoctenoic acid (Mittendorf *et al.*, 1998). Later, it was demonstrated that PHB formation in the oilseeds of *Brassica napus* is more efficient with 7.7% CDW accumulated PHA content, yet commercial production require twice the amount of PHA accumulation achieved (Houmiel *et al.*, 1999). Plants containing up to 3.72% CDW of PHB in leaf tissues and 1.23% CDW of PHB in whole tillers is reported for *Panicum vigatum* (Somleva *et al.*, 2008). Recently, accumulation of 14% CDW of PHA is reported for *Arabidopsis thaliana* (NewsRX, 2013). Application of agricultural systems to produce bioplastics in sustainable and economically beneficial plants has a promising prospect not only to replace non-degradable petrochemical plastics, but to sequester CO₂.

2.3.2 PHA production by pure microbial cultures

PHA accumulation has been reported for many bacteria, but only a few of them have the capacity of producing these polymers in high volumetric productivity (Steinbüchel,

1992). On the other side, the lactic acid bacteria or the methanogenic bacteria were classified as the bacteria groups with no PHA synthesis. PHA accumulation with *Pseudomonas* (Escapa *et al.*, 2012; Acuña *et al.*, 2014), *Cupriavidus necator* (former *Ralstonia eutropha*) (Passanha *et al.*, 2013), *Methylobacterium organophilum* (Zuñiga *et al.*, 2013), recombinant *Escherichia coli* (Wang *et al.*, 2012b; Salamanca-Cardona *et al.*, 2014), and *Alcaligenes latus* (Wang *et al.*, 2013) has been reported more than other bacterium species. High PHA production (more than 80% CDW) was achieved using mutant species under nutrient limitation of essential elements such as carbon, nitrogen, phosphorus, sulphur, oxygen or manganese (Anderson and Dawes, 1990; Lee, 1996a; Steinbüchel and Fuchtenbusch, 1998).

The optimal operation systems were identified with growth limitation to drive more carbon for PHB storage in the case of *Cupriavidus necator* and *Alcaligenes*; whereas, PHB formation is associated with cell growth when recombinant *Escherichia coli* and *Alcaligenes latus* is considered. The enzymes identified for PHB synthesis and degradation can also be associated with the substrate and the bacteria used in the production process (Sudesh *et al.*, 2000).

2.3.3 PHA production by Mixed Microbial Cultures

In order to escalate market penetration, volumetric production capacity of fermentor systems should be capitalised to decrease cost price of PHA products. With the aim of reducing production cost, one option is to use inexpensive, low quality substrate which accounts for one of the main cost factors (Kim, 2000). Additionally, mixed substrates can be utilised to harvest mixed microbial cultures in an open environment. The mixed population is able to adapt continuously with the changes in substrate conditions (Van Loosdrecht *et al.*, 1997). Moreover, the production cost is reduced using sterile-free fermentations (Reis *et al.*, 2003). The combination of these factors allow saving equipment costs, minimises the need for enhanced process control and energy saving (Serafim *et al.*, 2008). However, the mixed culture PHA production process requires optimisation in direction of providing cultures with higher intracellular PHA contents so that they can compete with pure culture production processes.

In wastewater treatment, when organic load rate is not significant the biomass is not very active, meaning that the PHA storage rate is low (Dircks *et al.*, 2001). In order to produce PHA at high rate, activated sludge is enriched with microorganisms that

produce and store more PHA in the presence of excessive organic load rate (Dionisi *et al.*, 2004).

PHA formation can occur in two metabolism pathways based on the type of the operating systems. In the first type, electron donor (reducing agent) and electron acceptor (oxidizing agent) availability are separated with anaerobic/aerobic dynamics. In the second type, microorganisms are subjected to periodic substrate availability (dynamic feeding) (Reis *et al.*, 2003). The polyphosphate accumulating organisms (PAOs) and glycogen accumulating organisms (GAOs) are the two groups of bacteria operating mainly under anaerobic/aerobic dynamics. In the both groups (PAO and GAO), PHA synthesis plays a crucial role in their metabolism (Serafim *et al.*, 2008). In the literature, comprehensive studies on different aspects of PAO-GAO operations are available. Metabolic analysis for acetate uptake (Yagci *et al.*, 2003), the effects of carbon source, pH and temperature on PAO-GAO competition (Lopez-Vazquez *et al.*, 2009), and the salinity of the medium on the organisms (Welles *et al.*, 2014). The amount of PHA accumulated by these groups of microorganisms is generally less than 20% CDW (Sato *et al.*, 1996). In different attempts, productivity on PHA storage was enhanced to up to 62% CDW; however, experimental results were not reliably repeatable. Comparing operational outcome with the pure cultures producing PHA for more than 88% CDW, utilisation of mixed cultures can be justified in the favour of an enhanced economy, an improved use of waste, a simpler process control and a monoseptic free production process (Salehizadeh and Van Loosdrecht, 2004).

2.3.4 PHA production by MMC in Sequential Batch Reactors

PHA production by mixed microbial cultures (MMC) is most commonly operated in sequential batch reactor (SBR) configuration (Dionisi *et al.*, 2005; Albuquerque *et al.*, 2007). The SBR is a batch (as opposed to continuous) operation generally performed on biological waste treatment plants. An SBR system may be composed of one or many reactors (tanks) to execute periodic operations. For a standard SBR operation, each cycle or sequence of operation has five modes or periods, each of which is named according to its primary function. The periods are fill (the receiving of raw material), react (the occurrence of desired reactions), settle (the separation of operational phases), draw (the discharge of reacted effluent) and idle (the period between discharge and recharge of the reactor) (Irvine and Busch, 1979).

In the dynamic feed system, a two-step process consisting of (1) a culture replication and growth step with presence of the carbon substrate (“feast” phase) and (2) a PHA consumption step in absence of the carbon substrate (“famine” phase) is considered. In a “feast”-“famine” system, PHA storing bacteria normally outcompete other bacteria since they can maintain their metabolic balance throughout the feeding alteration conditions and also they have very high substrate uptake rate (Reis *et al.*, 2003). A stable PHA production of about 70% CDW was achieved with carbon limitation in a fed-batch SBR system under dynamic feeding (Reis *et al.*, 2003). This is a very promising result considering the economic and environmental merits offered in production under mixed microbial cultures.

By definition, an operation in nutrition shortage state is said to run in the “famine” phase and “feast” phase occurs when nutrition abundance results in cell replication and intracellular growth. As mentioned, PHB production in SBR operations by mixed cultures consists of both “feast” and “famine” phases. Although PHB is formed only under “feast” phase, occurrence of “famine” phase is very important for the process feasibility. The cell physiological adaptation to nutrient limitation results in higher PHB formation rates once nutrition is in excess (Dias *et al.*, 2005). It is proposed in the literature that the best operating strategy consists of three consecutive phases with (1) a cell growth phase with acetate and ammonia excess, (2) followed by a “famine” phase with carbon limitation and (3) PHB production with acetate excess in absence of ammonia supply (Dias *et al.*, 2005). In Chapter 7, a different approach to SBR operation is constructed to assure occurrence of both “feast” and “famine” phase in each sequence of SBR process.

Presence and relative properties of the type of PHA stored in the process depend on the type of carbon substrate, limiting factors and the microorganism producing the PHA. The most common form of PHA occurrence is PHB structure; however, other PHA copolymers have also been reported to be produced by a mixture of microbial cultures (Reis *et al.*, 2003; Lemos *et al.*, 2006).

2.4 PHA extraction methods

Extraction and purification of PHA produced in various production units is essential. In addition to fermentation, extraction is one of the most costly production stages in PHA manufacturing. Development of novel inexpensive extraction processes that can purify

PHA with minimal or none harmful effect on the environment is always highly favourable.

In the case of PHA production by plants, there are some other useful byproducts that should be harvested from the transgenic plants along with the PHA components. On the laboratory scale, solvent extraction is applied using methanol and chloroform to purify PHA. However, this method is not suitable for mass production of PHA since chloroform is highly toxic and it demolishes other useful byproducts in the crops. There are some other extraction methods based on the solvent and non-solvent procedures; however, no scientific publication is found for large scale PHA extraction (Poirier, 2001).

There are two common protocols used for PHA extraction from bacteria. In the conventional method, the lipophilic components in the cells are removed in hot methanol. Since PHA is insoluble in methanol, the lipid phase separates from the PHA product. On the other side, PHA solves in chloroform and highly purified PHA can be recovered by solvent evaporation and precipitation of the PHA by methanol. This method is not suitable for PHA mass production due to utilisation of large amount of hazardous solvents and their harmful effect on the environment (Byrom, 1987; Suriyamongkol *et al.*, 2007). In the second method, a cocktail of harmless enzymes (including proteases, nucleases and lysozymes) and detergents are used to extract PHA from the proteins, nucleic acids and other components in the cell (Byrom, 1987; Bernard, 2014). Similar to non-solvent PHA extraction from bacteria, the use of a cocktail of enzymes has been suggested for extraction of PHA from plant tissue. However, it is not clear if this protocol is realistic and cost effective for industrial scale PHA production (Macdonald, 1997; Yu and Chen, 2006; Furrer *et al.*, 2007; Bernard, 2014).

In this study, process optimisation will be carried out in direction of sustainable production of PHB using a cost effective manufacturing approach in Chapter 8. In the next section a brief review on the optimisation concept and the optimisation method applied in this study is presented.

2.5 Process optimisation

2.5.1 Introduction

In chemical processes, optimisation is the use of specific tools to determine the most efficient approach to design a process by means of qualitative methods. Through optimisation, many industrial decisions are made in direction of profit increase with maximising the use of resources with minimum effort or cost. While a typical chemical engineering design problem has many solutions, the optimised solution is concerned with the best solution among the entire set of possible outcomes. Numerous mathematical methods and techniques are made available today for specific optimisation problems and application fields in the format of computer-based packages or associated software (Sahinidis, 1996; Gill *et al.*, 2002; Lofberg, 2004; Pintér *et al.*, 2006; Grötschel and Mathematiker-Vereinigung, 2012; Masood *et al.*, 2012; Mason, 2013; Vaezipour *et al.*, 2013; Carriglio *et al.*, 2014). However, they all require (1) critical analysis of the process or design, (2) insight about the appropriate performance objectives and (3) sufficient knowledge and experience about the process in order to obtain useful information using optimisation tools (Edgar *et al.*, 2001).

Optimisation problems can be found in many levels in a company, ranging from complex combination of plants, units, individual pieces of equipment, subsystems in a piece of equipment, or even smaller entities. The areas in which optimisation are broadly applicable can be segregated in three levels comprising of (1) management, (2) process design and equipment specification, and (3) plant operations.

In the management level, high level decisions concerning the time and place of plants construction, project evaluation, corporate budget, product selection, and investment approaches are made. In the second level, decisions are made to specify the size and the type of process and its nominal operating conditions. For instance, the number of production units and their arrangements to yield maximum operating efficiency, or selection of specific heat exchangers from more than ten different types are the sort of questions addressed in the process design and equipment specification. Once decisions are made and implemented in these two levels, further modifications are usually very costly and time demanding. On the other side, considering the third constituency employing optimisation, modification of operating conditions can be a monthly, weekly, daily, hourly, or at the extreme, every minute task. Change of the feedstock, temperature or pressure of the ambiance may have influence on the optimised setpoint values of the

operating control systems. An optimal solution is a set of values of the variables that satisfy problem constraints while providing proper solution to the objective function (Edgar *et al.*, 2001).

2.5.2 Optimisation of the PHB fermentation process

A review of fermentation modelling methods for pure and mixed cultures producing PHB is written by Patnaik (2005). Three types of mechanistic, cybernetic and empirical modelling approaches were encountered either as unstructured or structured models. Mechanistic models are built on chemical kinetics derived from postulated mechanism in each metabolic step. Cybernetic models are employed to provide a more natural description of cellular behaviour. It has been pointed out that internal regulatory controls in metabolic processes have influential effect on biological behaviour of PHB fermentation. In cybernetic methodology, biological manner is formalised with evolutionary concept to improve the chance of survival based on cells past experiences. Empirical modelling of process data provides faithful representation of specific observations. Therefore, hybrid models consisting of a combination of mechanistic, cybernetic and neural networks offers powerful tools to capture process representations (Patnaik, 2005).

In a different study, optimisation of the culture conditions for production of PHB using *Bacillus megaterium* SW1-2 isolated from activated sewage sludge has been conducted using Box-Behnken design. The four parameters including ammonium sulphate, glucose, KH_2PO_4 and Na_2HPO_4 concentrations were optimised using an appropriate mathematical tool and validated experimentally to reveal maximum PHB production of 1.8-folds the basal medium (Berekaa and Al Thawadi, 2012).

Khanna and Srivastava (2005) applied statistical media optimisation to design a cheap growth medium for production of *Ralstonia eutropha* reserving PHB as granule. Ammonium sulphate was substituted by ammonium nitrate, urea and ammonium chloride as cheaper alternatives. Additionally, yeast extract were replaced by corn steep liquor as a cheaper source of minerals and vitamins. The experimental results demonstrated a better and cheaper production of PHB using the alternative approach as a successful case of medium optimisation study (Khanna and Srivastava, 2005).

More recently, sucrose and urea were found to produce maximum biomass and PHB by bacterial strain *Azohydromonas lata* MTCC 2311 among three carbon source candidates of sucrose, fructose and glucose and four nitrogen source candidates of $(\text{NH}_4)_2\text{SO}_4$,

NH₄Cl, urea and NH₄NO₃. Response surface methodology (RSM) and artificial neural network models (ANN) were applied to navigate the optimal combination of sucrose, urea and TE solution concentrations. Simulation results were validated with shake flask experiments with less than 4% prediction errors (Zafar *et al.*, 2012).

In PHB production using mixed culture, optimisation of eight important medium factors including iron, glucose, volatile fatty acids (VFA), nitrogen, phosphorus concentrations, VFA composition, pH, and microenvironment on the bioplastic production were investigated. Design of experiment (DOE) methodology using Taguchi orthogonal array (TOA) was applied to navigate influence of microenvironment, pH and glucose concentration with contributing percentage of 81, 11 and 2.5 respectively. Validation experiments demonstrated performance improvement with optimum conditions (Venkata Mohan and Venkateswar Reddy, 2013).

Three physical process variables; pH, temperature and agitation speed were optimised in batch production of PHB using *Alcaligenes* sp. Central composite rotatable design (CCRD) was the optimisation technique employed to obtain the optimal values. The shake flask experiments represented 98% resemblance with the predicted percentage yield. The scale up study on bioreactor also demonstrated higher productivity and PHB yield than previous reports under similar conditions (Tripathi *et al.*, 2013).

Shahhosseini (2004) employed dynamic optimisation program to determine optimal feeding rates for carbon and nitrogen sources in a fed-batch culture of *Ralstonia eutropha* producing PHB. The optimised feeding rates obtained from simulation were applied experimentally to present PHB productivity increase of around 100% compared with the results of other fed-batch culture experiments using bioreactor engineering to determine feeding rates.

For the case of mixed microbial cultures operating under sequencing batch reactor for PHB production, the influence of carbon and nitrogen concentration on the PHB accumulation yield was investigated in a range of 15 to 180 C-mmol/L for acetate and 0 to 2.8 N-mmol/L for ammonia. Maximum PHB content was achieved with induction of 180 C-mmol/L acetate into the operational system. Since injection of 180 C-mmol/L acetate in one shot impose substrate inhibition, two feeding strategies of two pulses of 90 C-mmol/L or three pulses of 60 C-mmol/L acetate were compared experimentally. The PHB content obtained were reported to be 56.2% and 78.5% respectively. The PHB content of above 70% CDW is similar to that obtained by pure cultures and never had been reported for mixed cultures (Serafim *et al.*, 2004).

The upstream process time has also been the focus of research studies for a two-stage batch and fed-batch fermentations with *Alcaligenes latus* ATCC 29714 for PHB production. In this study, nitrogen limited media (“famine” phase) was imposed at different operational time in the batch and fed-batch modes. The optimal points for switching to nitrogen limited media and returning to nitrogen abundance were obtained and experimented. This optimal strategy improved PHB production by approximately 7% CDW comparing with the best results reported prior to this study (Wang *et al.*, 2012a).

As mentioned, research studies have been carried out in order to optimise production of PHB using various production approaches. In this study, PHB production process will be optimised in Chapter 8 using a novel production recipe developed in Chapter 7. The optimisation algorithm applied in this study will be described in the next section as formulated in Love (2007).

2.5.3 Optimisation tool (Sequential Quadratic Programming)

Application of Sequential Quadratic Programming (SQP) in complex optimisation problems is common especially for non-linear objective functions. Let the cost function be $f(\underline{x})$. The optimisation is cast in the form:

$$\text{minimise } f(\underline{x}) \quad (2.1)$$

$$\text{subject to: } g_i(\underline{x}) = 0 \quad (2.2)$$

where $i = 1, 2, \dots, m$

$$\text{and: } h_i(\underline{x}) \leq 0 \quad (2.3)$$

where $i = m + 1, \dots, p$ and $\underline{x} = [x_1 \ x_2 \ \dots \ x_n]^T$. In these equations, n is the dimension of the optimisation problem (decision variables), m is the number of equality constraints and p is the number of equality constraints plus the number of inequalities that are at their constraints. The solution of the optimisation problem is based on the assumption that any function may be adequately approximated by a quadratic function on a local basis. Therefore, a merit function $\Phi(\Delta \underline{x})$ is defined on a recursive basis for Taylor’s series expansion of the cost function introducing the ∇ notation ($\nabla = d/d\underline{x}$)

$$\Phi(\Delta \underline{x}) = \frac{1}{2} \cdot \Delta \underline{x}^T \cdot \nabla^2 f(\underline{x}(k)) \cdot \Delta \underline{x} + \Delta \underline{x}^T \cdot \nabla f(\underline{x}(k)) \quad (2.4)$$

where

$$\Delta \underline{x} = \begin{bmatrix} \Delta \underline{x}_1 \\ \Delta \underline{x}_2 \\ \vdots \\ \Delta \underline{x}_n \end{bmatrix} = \begin{bmatrix} x_1(k+1) - x_1(k) \\ x_2(k+1) - x_2(k) \\ \vdots \\ x_n(k+1) - x_n(k) \end{bmatrix} \quad (2.5)$$

Defining the search direction $\underline{s}(k) = \Delta \underline{x}$ gives:

$$\Phi(\underline{s}(k)) = \frac{1}{2} \cdot \underline{s}(k)^T \cdot \nabla^2 f(\underline{x}(k)) \cdot \underline{s}(k) + \underline{s}(k)^T \cdot \nabla f(\underline{x}(k)) \quad (2.6)$$

The $\underline{s}(k)$ is a step in the search direction towards the minimum of the cost equation.

The minimisation problem finds the following recursive formation:

$$\text{minimise } \Phi(\underline{s}(k)) \quad (2.7)$$

$$\text{subject to: } g_i(\underline{x}(k)) = 0 \quad (2.8)$$

where $i = 1, 2, \dots, m$

$$\text{and: } h_i(\underline{x}(k)) \leq 0 \quad (2.9)$$

where $i = m + 1, \dots, p$. The Lagrangian of the optimisation problem is formed by combination of the cost function and constraints to be minimised. The Lagrangian function of the optimisation problem is formed and differentiated with respect to $\underline{s}(k)$ in order to obtain the gradient of the Lagrangian. It can be shown that the cost function is minimised when gradient of the Lagrangian is set to zero. The following equation should be satisfied for a minimum:

$$\nabla^2 f(\underline{x}(k)) \cdot \underline{s}(k) + \nabla f(\underline{x}(k)) + G(k) \cdot \underline{\lambda}(k) = 0 \quad (2.10)$$

The set of positive $\underline{x}(k)$ and $\underline{\lambda}(k)$ which satisfies the aforementioned criteria corresponds to the solution of the quadratic approximation provided that the Hessian $\nabla^2 f(\underline{x}(k))$ is positive. In Figure 2.4, general SQP recursion method is depicted.

As shown in this depiction, the merit function $\Phi(\underline{s})$ which is a quadratic approximation of the problem for the slope $f(\underline{x})$ in a local interval is calculated in the fourth stage. In the iteration loop, the position of the $\underline{x}(k)$ in the search space is taken in the direction of $\underline{s}(k)$ such that quadratic approximation is minimised. The step size taken towards the local minimum is determined by the factor α . The position $\underline{x}(k+1)$ is the initial position of the consecutive iteration where the merit function $\Phi(\underline{s})$ is redefined. The

criteria for iteration termination is depicted in the sixth stage of the SQP algorithm in which position alteration of the \underline{x} in two consecutive iterations is less than the value specified by factor ϵ .

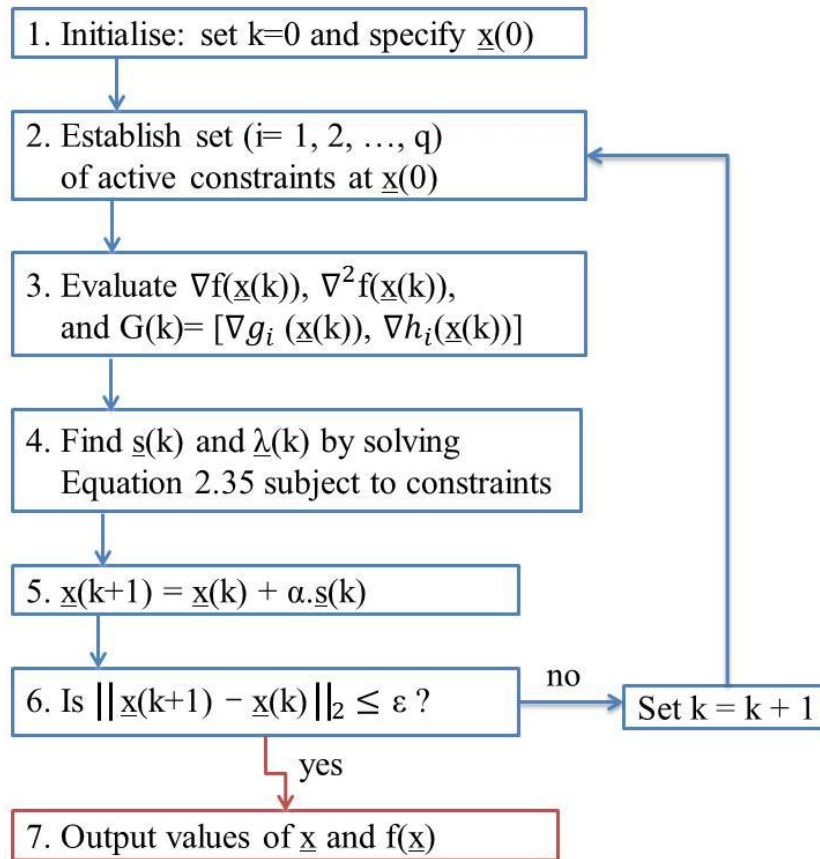


Figure 2.4 Recursive search using sequential quadratic programming

MATLAB optimisation function *fmincon* applies the SQP algorithm to solve optimisation problems. In order to optimise SBR recipe parameters, empirical models are developed and appropriate cost functions of the optimisation problems are established in Chapter 8.

Since optimisation methods and algorithms employ mathematical features, optimisation problem must be presented in form of mathematical expressions (models). An optimisation problem consists of at least one objective function to be optimised under a set of equality and/or inequality constraints imposed by the process or equipment limitations. In the next section, two of the most dominant linear and non-linear mathematical modelling techniques are reviewed.

2.6 Mathematical modelling

2.6.1 Introduction

A mathematical model is a representation of a particular part or feature of the world which is easier to understand, define, quantify, visualise or simulate than the original phenomena. Different types of models are formulated for different aims; for instance, the conceptual models developed to provide insight about a particular phenomenon, mathematical models to quantify the input output relationship and graphical models to improve visualisation of subjects. Modelling has always been an essential and inseparable part of humane scientific activities and many scientific fields have their own idea and specific types of modelling (Hacking, 1983). A mathematical model seeks to represent empirical objects, phenomena and physical processes in a logical and objective manner. An empirical object is known to be a source of knowledge acquired by means of observation or experimentation (Bird, 2004). Developing and validating empirical models is fundamental to the analysis carried out in direction of generating production recipe in Chapter 7. Although it is impossible to build a complete and true representation of a real phenomenon, the aim is to construct a sound system that produces the most accurate interpretation of the reality.

Amplification of thought processes and knowledge in models enable scientists to perform enhanced analysis on the phenomena being modelled (Ulrich, 1988). Scientific models can also be characterised based on the model origins. (1) *In vivo* models are living organisms such as laboratory rats, (2) *in vitro* models are developed in laboratory glassware such as tissue culture and (3) *in silico* models are mathematical structures rendered in computer-based software. In the field of cellular biology, simulation of biological systems (*in silico* models) to be paired with experiments are being successfully and routinely used by computational biologists. These models can be used as complementary tools to unravel the principles and operation of complex biological systems (Di Ventura *et al.*, 2006).

In this study, mechanistic and empirical modelling approaches are considered for PHB process analysis. In terms of the mechanistic methods, it is believed that deterministic mathematical equations based on established scientific laws are capable of describing physical systems at least to an acceptable extent. The mechanistic models are in fact extensions to the understanding of a real phenomenon rather than an accurate representation of the phenomenon. Although mathematical representations of a

phenomenon provide valuable insight about the phenomenon itself, prediction precision is frequently dismissed due to uncertainties or lack of knowledge associated with the real phenomenon. On the other side, empirical models are trained based on actual observations rather than theoretical statements. Uncertainties embedded within the mechanistic models are overcome using data-based empirical models. Since an empirical model has a general structure consisting of model parameters trained for a specific phenomenon, it lacks valuable mathematical representation of the phenomenon (Yamashita and Hashida, 2003).

In case of availability of complex accurate mechanistic models describing a phenomenon, development of empirical models is justified in light of the simplicity and straightforward calculations to provide predictions. This is one of the most important advantages of empirical models over mechanistic ones when model predictions are embedded within mathematical optimisation algorithms in particular. Additionally, empirical models are known to be less effort demanding in the development stage; and hence, they are inexpensive in comparison with the mechanistic counterparts. When the phenomenon under investigation is scientifically established and there is a lack of experimental data for empirical modelling, development of mechanistic models is the rational solution. In general, training an empirical model requires considerably more experimental data in comparison with a mechanistic counterpart (Leonidou and Katsikeas, 1996).

The mechanistic models developed by Dias *et al.* (2005) for PHB batch production will be explained in detail in Chapter 3. In this study, application of different empirical modelling strategies is investigated for prediction of PHB critical process attributes in Chapter 6. Additionally, operational data obtained from simulation runs of a novel production recipe developed in Chapter 7 will be used in Chapter 8 for empirical modelling to be used in optimisation algorithms.

The empirical modelling techniques applied in this study include multiple linear regression (MLR) and artificial neural network (ANN) commonly used for linear and non-linear data sets respectively. The mathematical methods described in Love (2007) are applied in this study to develop MLR and ANN models. A more sophisticated version of the latter approach is the bootstrapping aggregated neural network (BANN) in which a number of individual neural network models are aggregated for overall prediction improvement (Zhang, 1999). In this section, MLR, ANN and BANN applied in this study are described in detail.

2.6.2 MLR modelling method

Since several independent variables are involved in prediction of the dependant variable, multiple linear regression (MLR) is applied to fit linear equation to a set of observed data. In this study, “least squares” approach is applied to minimise the error involved in curve fitting. For p number of independent variables, the following equation is considered.

$$y = \theta_0 + \theta_1 \cdot x_1 + \theta_2 \cdot x_2 + \cdots + \theta_p \cdot x_p + \varepsilon \quad (2.11)$$

where y is the dependant variable, model output or response, x_i are the independent variables, model inputs, regressor or predictor, θ_i are the coefficient values and ε is the error value between the measured data and the model prediction. The regression analysis results θ_p coefficients for which n sets of experimental data are best fitted to the fitting curve. This data can be collated in matrix form as follows:

$$\begin{bmatrix} y_1 \\ y_2 \\ \vdots \\ y_n \end{bmatrix} = \begin{bmatrix} 1 & x_{11} & x_{21} & \cdots & x_{1p} \\ 1 & x_{21} & x_{22} & \cdots & x_{2p} \\ \vdots & \vdots & \vdots & \ddots & \vdots \\ 1 & x_{n1} & x_{n2} & \cdots & x_{np} \end{bmatrix} \begin{bmatrix} \theta_0 \\ \theta_1 \\ \theta_2 \\ \vdots \\ \theta_p \end{bmatrix} + \begin{bmatrix} \varepsilon_1 \\ \varepsilon_2 \\ \vdots \\ \varepsilon_n \end{bmatrix}$$

which is of the general form:

$$Y = X \cdot \theta + \gamma \quad (2.12)$$

where Y and γ are $(n \times 1)$ vectors, X is an $(n \times (p + 1))$ matrix and θ is a $((p + 1) \times 1)$ vector. The sum of the squared errors is formulated as:

$$\begin{aligned} Q &= \sum_{j=1}^n \varepsilon_j^2 = \gamma^T \cdot \gamma & (2.13) \\ &= (Y - X \cdot \theta)^T \cdot (Y - X \cdot \theta) \\ &= Y^T Y - \theta^T X^T Y - Y^T X \theta + \theta^T X^T X \theta \end{aligned}$$

Noting that $(\theta^T X^T Y)^T = Y^T X \theta$ and that both $\theta^T X^T Y$ and $Y^T X \theta$ are scalar quantities:

$$Q = Y^T Y - 2\theta^T X^T Y + \theta^T X^T X \theta$$

The regression equation that best fits the data corresponds to the vector θ that minimises Q . The derivative of Q with respect to θ is given by:

$$\frac{\delta Q}{\delta \theta} = -2X^T Y + 2X^T X \theta \quad (2.14)$$

Setting the derivative to zero yields the optimal estimation of the vector $\hat{\theta}$:

$$-2X^T Y + 2X^T X \hat{\theta} = 0 \quad (2.15)$$

Therefore the so-called batch least squares (BLS) solution is obtained as:

$$\hat{\theta} = (X^T X)^{-1} X^T Y \quad (2.16)$$

The solution exists provided that the independent variables are linearly independent of each other or in other words; no column of the X is a linear combination of the other columns. Vector $\hat{\theta}$ contains coefficients of the multiple linear equation best fitting to the curve with minimal residual to the measured data (Love, 2007).

2.6.3 Artificial Neural Network modelling method

Artificial neural networks are often referred to as Neural Nets (NN), is essentially a means of prediction inspired from the human process of thought and reasoning. Application of this method is mostly significant when no mathematical structure can be identified to establish relationships between the variables. This is a very powerful and sophisticated tool to capture non-linearity in rapport development between variables of interest. This technique should not be used in the case of linear problems since regression methods are more appropriate and simpler to be applied.

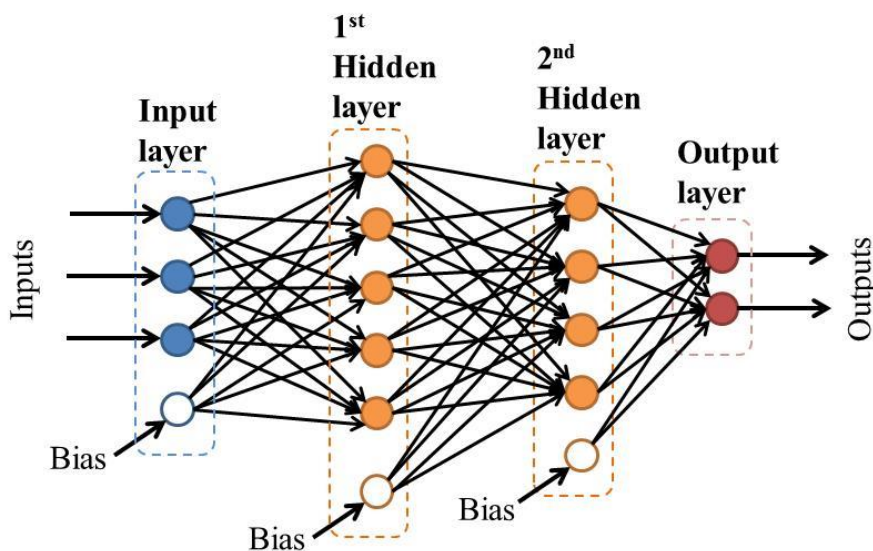


Figure 2.5 A multi-layer feedforward neural network with two hidden layers

In 1990s, with emergence of the powerful computational tools, application of NN gained enormous attention in different scientific and especially engineering fields. The NN technique is based on a structure known as Multi-Layer Perceptron (MLP) where each independent and dependant variable is referred to as a neuron. These neurons are connected and these connections are referred to as synapses. The prediction properties of the NN can be improved by introducing additional intermediary neurons in between the independent and dependent variables as referred to the hidden neurons. The independent, dependant and hidden neurons form input, output and hidden layers respectively when considering the overall structure of a NN. Depending on the number of hidden neurons considered in between the input and output layers, the number of hidden layers is defined. In Figure 2.5, an illustration of a neural network structure with two hidden layers is depicted. As shown, each of the neurons is connected to every neuron in the subsequent layer.

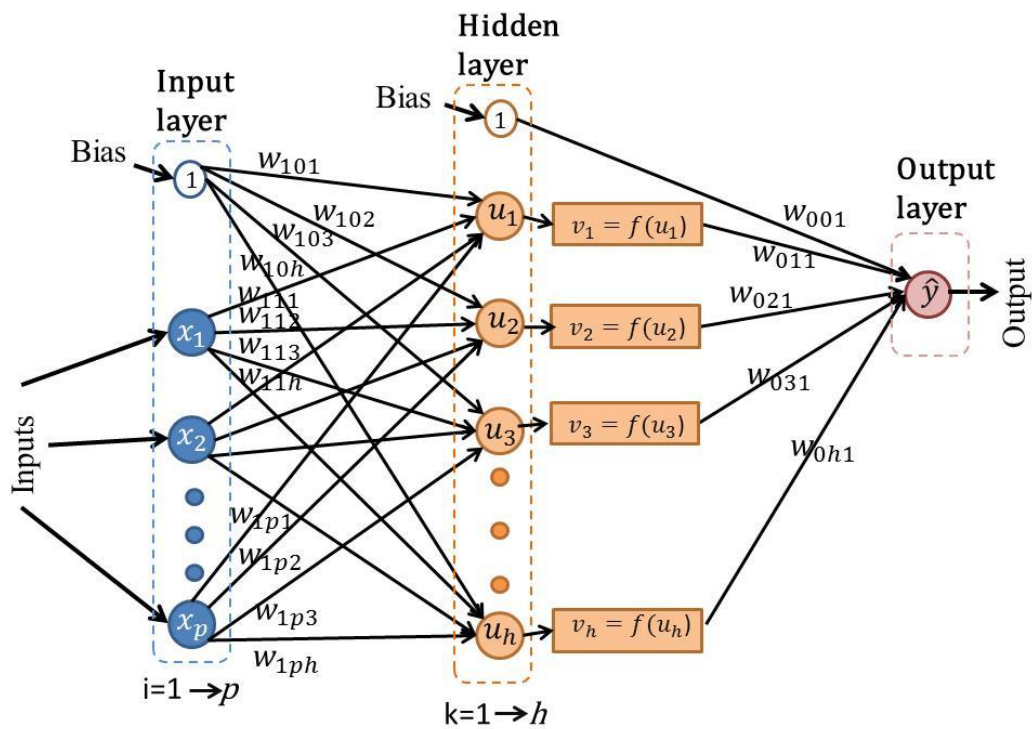


Figure 2.6 Notation specified for inputs, neurons, synapses and the output

The neural network shown in this figure relates two dependant variables in the output layer to three independent variables in the input layer via nine hidden neurons in the two hidden layers. It is normal practice to include one bias neuron in each input and hidden layers in order to improve network's prediction capability as shown in the illustration. This structure is referred to as a back propagation net or as a feedforward artificial

neural net (FANN) and it is the dominant form of neural network due to its simplicity and effectiveness.

The structure of the neural network developed in this study consists of a single hidden layer with p inputs neurons ($i = 1 \rightarrow p$), h neurons in the hidden layer ($k = 1 \rightarrow h$) and a single output neuron. The model tuning parameters are the weightings associated with each synapses connecting the neurons. In Figure 2.6, notations applied for weighting synapses is shown. The objective is to predict the output by any valid combination of the inputs.

The weightings w are identified by three subscripts for a network with single hidden layer. The first subscript denotes the target layer of the synapse. If synapse ends at the output layer, the first subscript is 0 and if it ends at the hidden layer, the subscript is 1. The second subscript indicates the neuron in the layer from which the synapse originates. And the third subscript indicates the neuron in the layer to which the synapse is directed. For the second and the third subscripts, 0 indicates the bias node.

The first set of operations is taken to calculate the magnitude of the hidden layer neurons by the summation of the input neurons multiplied to their synapses weightings. For p number of inputs with magnitude of x_i , the hidden layer neuron u_k is calculated using the following equation.

$$u_k = w_{10k} + \sum_{i=1}^p w_{1ik} \cdot x_i \quad (2.17)$$

The hidden layer neurons are transformed using a function which has bounded derivative. This function is referred to as an activated function or a squashing function. The two most commonly implemented functions are the sigmoid and hyperbolic tangent. In this study, the sigmoid function is used as the activated function to handle non-linearities by squashing the summation between limits of 0 and 1. The following equation is used to calculate the output from the k^{th} neuron in the hidden layer.

$$v_k = f(u_k) = \frac{1}{1 + e^{-u_k}} \quad (2.18)$$

The prediction output is the summation of the h weighted outputs from the hidden layer and the bias as given by the following equation.

$$\hat{y} = w_{001} + \sum_{k=1}^h w_{0k1} \cdot v_k \quad (2.19)$$

With the overall structure designed, training of the model can be carried out using n sets of input data of process variables for each of which the correct value of the output is known. A back propagation algorithm is applied to minimise a quadratic error function by adjusting the model parameters (weighting values). The prediction error is defined as the difference between the true and predicted values of the output as follows:

$$E = \sum_{j=1}^n (y_j - \hat{y}_j)^2 \quad (2.20)$$

Figure 2.7 provides a schematic depiction of the back propagation algorithm used in NN model training by adjusting the weightings assigned to the synapses. The algorithm starts with assigning initial weights as small random values. Additionally, some completion criterion must be specified to be used as an evaluation measure applied in the procedure. In the NN training procedure applied in this study, one fifth of the training data is used to test model performance. The sum of the squared errors (SSE) for the testing data is the evaluation measure implemented in the coding program applied in this study.

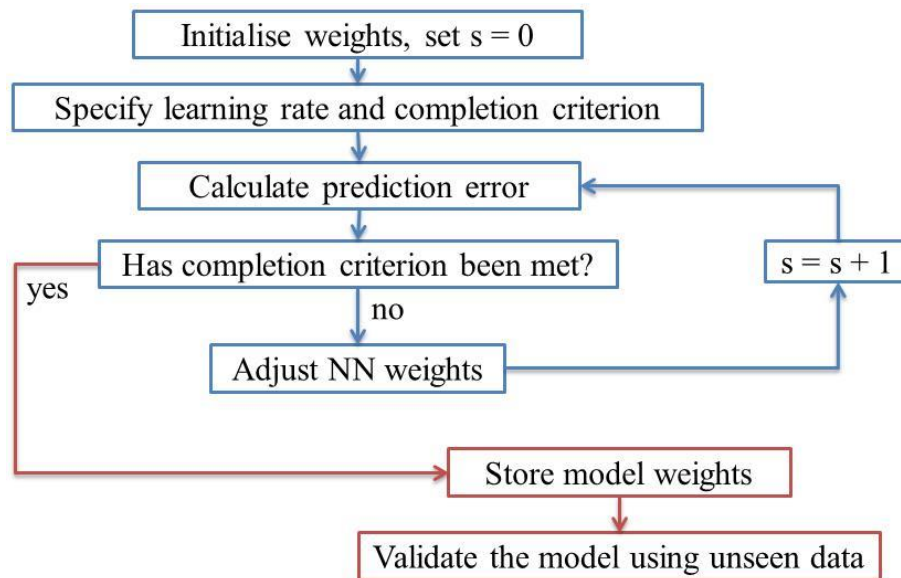


Figure 2.7 Procedure of the back propagation training algorithm

As shown in Figure 2.7, the back propagation training method is an iterative procedure in which the model parameters (w) are replaced by a new estimate with the aim of minimising the error function. Each iteration of the procedure is referred to as an epoch.

One of the model training termination criterion used in this study is the occurrence of SSE increments for testing data set in ten consecutive iteration loops. In Figure 2.8, an illustration is shown to describe two of the criteria used to identify the optimal epoch in which model weightings are the most appropriate to be established in the model structure.

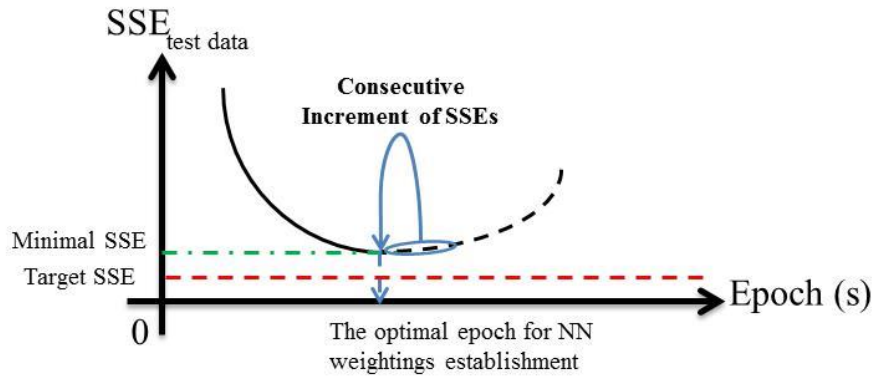


Figure 2.8 Identification of network weights using the NN training termination criterion

In the first few epochs, model accuracy improves as SSEs obtained for the testing data decreases when appropriate NN weighting adjustment technique is applied. The minimal SSE value is identified when a number of consecutive SSE values (10, in this case) increases with epoch number increment. Another criterion used for weighting adjustment iteration termination is achievement of the target SSE value. This target value is low enough to assure appropriate prediction performance of the NN model with the established weightings. In addition to these two criteria, other measuring tools can be used to avoid open-ended iteration procedure such as limiting the total permissible number of epochs.

In the core of the back propagation training algorithm a mathematical algorithm is considered to change NN model weightings in the direction of prediction improvement. The weighting adjustment procedure used in this study is the well-known Levenberg-Marquardt algorithm (LMA) which is also referred to as the damped least squares (DLS) method. This numeric minimisation algorithm is used in iteration loops as a least squares curve fitting solver for non-linear problems. The objective function has already been defined by Equation (2.20) where \hat{y} is a function of model inputs and NN weightings. Therefore, the minimisation problem can be defined as:

$$\min_w E = \sum_{r=1}^m (y_r - f(x_r, w))^2 \quad (2.21)$$

where m is the number of training data (testing data excluded) available for weight adjustment procedure. The model parameter vector (w) is replaced by a new estimate ($w + \phi$) in each iteration step. In LMA method, a linear approximation of the function representing the model is applied to determine weighting alteration vector (ϕ).

$$f(x_r, w + \phi) \approx f(x_r, w) + J_r \cdot \phi \quad (2.22)$$

where J is the row-vector gradient of f with respect to w as follows:

$$J_r = \frac{\partial f(x_r, w)}{\partial w} \quad (2.23)$$

The minimisation problem takes the following formation when model function is replaced by its linear approximation.

$$\min_w E \approx \sum_{r=1}^m (y_r - f(x_r, w) - J_r \cdot \phi)^2 \quad (2.24)$$

At the extremum, gradient of E with respect to ϕ should be infinitesimal; therefore, the first derivative of the Equation (2.24) with respect to ϕ is set to zero with the aim of specifying the weighting alteration vector (ϕ) that optimises E . In vector notation Equation (2.24) takes the following formation:

$$E = \|y - f(w) - J \cdot \phi\|^2 \quad (2.25)$$

where J is the Jacobian matrix whose r^{th} row equals J_r , f and y are vectors with r^{th} component of $f(x_r, w)$ and y_r respectively. The first derivative of the aforementioned equation with respect to ϕ is:

$$\frac{\partial E}{\partial \phi} = -2J^T \cdot (y - f(w) - J \cdot \phi) \quad (2.26)$$

Setting the derivative function to zero gives:

$$J^T J \cdot \phi = J^T \cdot (y - f(w)) \quad (2.27)$$

In order to solve the linear equations obtained to determine the elements of ϕ vector, Levenberg replaced the equation by a “damped version”.

$$(J^T J + \lambda I) \cdot \phi = J^T \cdot (y - f(w)) \quad (2.28)$$

or

$$\phi = (J^T J + \lambda I)^{-1} \cdot J^T \cdot (y - f(w)) \quad (2.29)$$

where I is the identity matrix and λ is a non-negative damping factor also referred to as the regularisation parameter. For a large value of the damping factor, the Levenberg's "damped term" $(J^T J + \lambda I)$ paralyses the algorithm in ϕ solution. Marquardt contribution is in replacement of the identity matrix with a diagonal matrix consisting of the diagonal elements of $J^T J$, resulting in the Levenberg-Marquardt algorithm:

$$\phi = (J^T J + \lambda \cdot \text{diag}(J^T J))^{-1} \cdot J^T \cdot (y - f(w)) \quad (2.30)$$

Marquardt recommended starting the iteration procedure with an initial damping factor λ_0 and modification of the factor with a tuning factor (ρ) in the consecutive iterations. Model residual is obtained using the testing data and damping factor is modified accordingly if the residual deteriorates. It is common to modify the damping factor by the following equation

$$\lambda = \lambda_0 / \rho^\varphi \quad (2.31)$$

where φ is specified depending on the iteration number (s).

For one specific set of data, appropriate tuning parameters should be identified to present the most accurate prediction of a neural network model (Love, 2007). In this study the aforementioned technique was implemented to build NN models.

2.6.4 *Bootstrapping Aggregated Neural Networks*

A neural network model is developed for a set of train-test data under a certain initial constants randomly assigned to the model weightings. These limitations impose a deficiency in model generalisation when unseen data is engaged in model validation. Among a number of techniques developed to improve neural network generalisation capability, combining multiple networks is the method applied in this study. In this approach, the same principle of neural network modelling is applied to build a number of networks using various train-test data organisation and initial weighting values in model development procedure. Each individual NN model may consist of a different hidden layer structure; and most definitely, different weighting values when compared to the other networks. Figure 2.9 shows a diagram of a bootstrap aggregated neural network (BANN) implementing individual NNs with different structures modelling the same relationship.

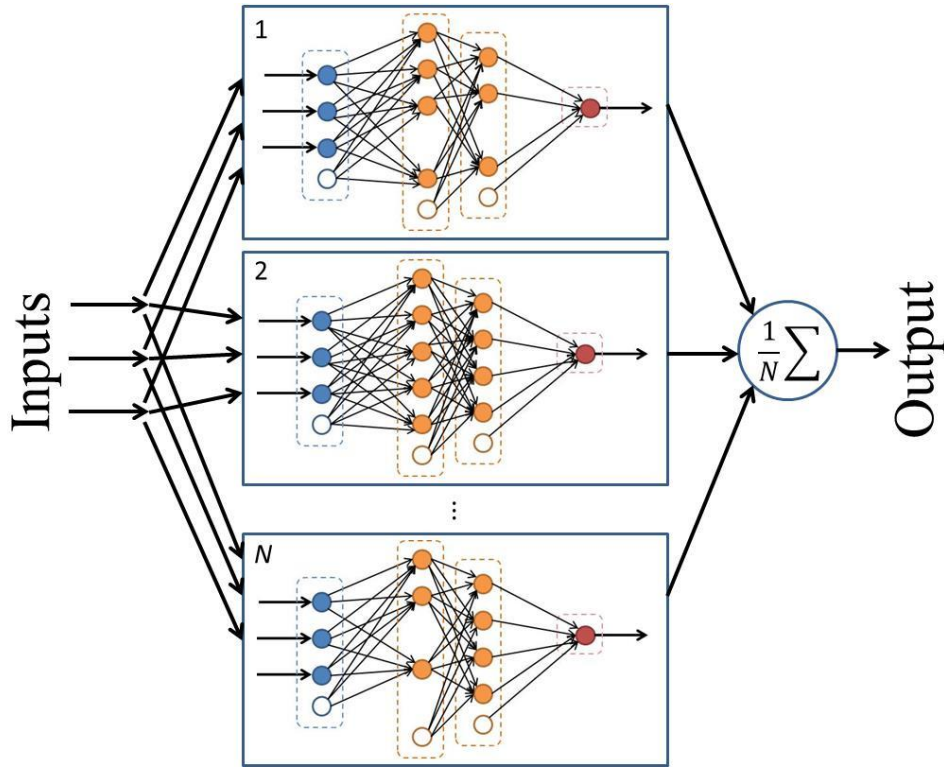


Figure 2.9 A BANN model based on three individual neural network structures

It is a documented practice that network aggregation improves both accuracy and robustness of the model prediction capability (Zhang, 1999). Among a number of aggregation methods, the most straight forward approach is to obtain the average of the individual neural network outputs which is implemented in this study. This can be represented as:

$$\hat{y} = \frac{1}{N} \sum_{l=1}^N \hat{y}_l \quad (2.32)$$

where N is the number of individual neural networks. Another advantage in application of a series of networks is that model prediction confidence bounds are calculated using the residual obtained from each individual model. The standard error of the predicted value is estimated as

$$\sigma_e = \left\{ \frac{1}{N-1} \sum_{l=1}^N [\hat{y} - \hat{y}_l]^2 \right\}^{0.5} \quad (2.33)$$

The 95% prediction confidence bounds can be calculated as

$$y_{UB} = \hat{y} + 1.96 \sigma_e \quad (2.34)$$

$$y_{LB} = \hat{y} - 1.96 \sigma_e \quad (2.35)$$

where y_{UB} and y_{LB} are upper and lower confidence bounds respectively assuming that residuals are normally distributed (Mukherjee and Zhang, 2008). A narrow confidence bound associates with more reliable prediction capability for the model.

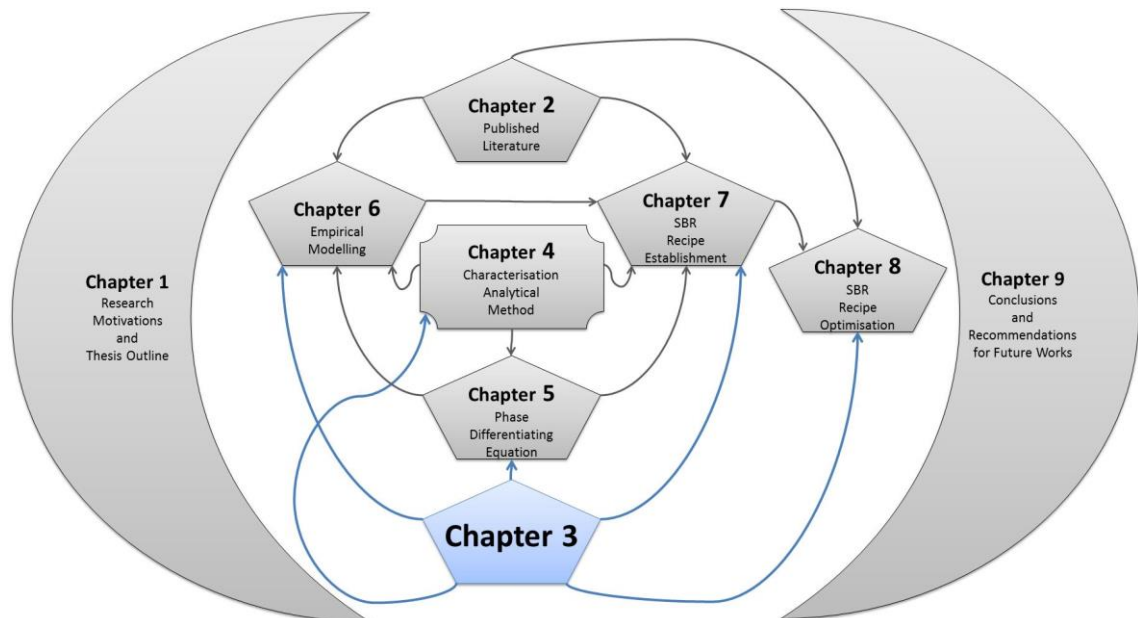
2.7 Summary

In the quest of sustainable alternatives for petrochemical plastics, PHA has been nominated as an appropriate candidate with a number of promising current and potential applications in different monomer combinations. PHB production process by mixed microbial cultures has recently gained attention due to cost effective high yield of PHB production. PHB production by means of SBR is expected to be comprising of a “feast” and a “famine” phase operation occurring intermittently in each production sequence. The literature survey demonstrates significance of operational phase identification and the capability of manipulating process pathway towards “feast” and “famine” phase operations. Based on these studies, an analytical module is developed in Chapter 4 for classification of PHB operational regimens. The analytical outcome generated in Chapter 4 plays an essential role for differentiation of “feast” and “famine” phases using batch initial conditions in Chapter 5. Additionally, an SBR production recipe structure is constructed in Chapter 7 to increase possibility of “feast” and “famine” phase operation occurrence in each sequence of the process.

A series of optimisation studies were carried out to improve PHB production procedure by different research groups which were partially reviewed in this Chapter. Sequential Quadratic Programming was introduced as a mathematical optimisation tool applied in direction of identification of optimal process conditions. Empirical modelling techniques such as linear Multiple Linear Regression and non-linear Bootstrapping Aggregated Neural Networks were introduced as mathematical adjunct to quantitative analysis of the PHB process and optimisation studies. Empirical models are developed in Chapter 6 and Chapter 8 as quantitative representations of PHB production processes and mathematical adjunct to the optimisation endeavours. The SBR recipe developed in this study will also be optimised by Sequential Quadratic Programming in Chapter 8.

Chapter 3

Simulation of Polyhydroxybutyrate Production Batch using Mixed Microbial Culture Cultivation in a Sequencing Batch Reactor



3.1 Introduction

Mathematical modelling of bio-processes with mixed cultures has been subject of many research studies. Activated Sludge Model No.3 (ASM3) has become a reference in activated sludge processes analysis (Gujer *et al.*, 1999). This model attempts to describe storage of organic substrates, sludge production, nitrification and denitrification processes for heterotrophic (that cannot synthesize their own food) and autotrophic (that synthesize their own food from inorganic substances) organisms (Gujer *et al.*, 1999). The ASM3 was later modified to enhance description of heterotrophic conversion, enabling simultaneous adaptation of cell growth and PHB formation (Carucci *et al.*, 2001). This change increased the accuracy of the process description significantly by modifications implied in the process kinetics and stoichiometry.

Other more complex metabolic models were developed to describe intracellular PHB production by activated sludge. However, most of these works lack adequate experimental validation. Among those, Beun *et al.* (2002) investigated calculation of theoretical yields and maintenance coefficients using a model based on seven metabolic reactions adapted from the previous work of Van Aalst *et al.* (1997). In another attempt, a model of six metabolic reactions is considered with a focus on the effect of dissolved oxygen on PHB accumulation (Third *et al.*, 2003).

In Dias *et al.* (2005), a process model is developed to envisage PHB productivity on the bases of acetate and ammonia feeding strategies. The main objective of developing this model was to support model-based optimisation studies aiming to enhance both volumetric productivity and PHB formation ratio over biomass. This model was an adaptation of Beun *et al.* (2002) to describe process states i.e. concentrations of acetate, ammonia, active biomass and intracellular PHB (Beun *et al.*, 2002). Validation of the model with experimental results confirms its accuracy and reliability for optimisation applications. The experimental validation tests were performed similar to the description reported by Serafim *et al.* (2004) in optimisation of PHB production by mixed cultures under aerobic dynamic feeding conditions (Serafim *et al.*, 2004).

A simulation programme based on this model was developed in MATLAB and is used as a case study in this research. This chapter presents the model and simulation programme developed by Dias *et al.* (2005) and author has no claim on model development, its accuracy nor its validation method.

This chapter is organised as follows. Section 3.2 presents the mechanistic model of PHB production in a sequencing batch reactor. Section 3.3 describes the software program developed to simulate the process. In Section 3.4, a report of experimental validation of the PHB simulator is given. At the end, a typical simulation run is described in Section 3.5.

3.2 Mechanistic models

3.2.1 Modelling assumptions

The complex nature of a mixed culture with different types of microorganisms competing for the nutrients in the medium requires a level of simplification in order to facilitate process description by mathematical expressions. In Dias *et al.* (2005), a number of assumptions were made:

1. The active microorganisms are those requiring organic compounds of carbon and nitrogen for nourishment. In other words, organisms in the operating system are all heterotrophic.
2. The metabolic behaviour of the microorganisms does not change in time and their PHB storage capacity remains the same. In Serafim *et al.* (2004) it is shown that the PHB storage capacity remained stable in a SBR operated in period of 2 years of the study (Serafim *et al.*, 2004).
3. Dominant PHB storage process is aerobic acetate storage while dissolved oxygen is always in excess.
4. Perfect mixing was assumed throughout the process with no formation of flocs and therefore, negligible external or internal mass transfer resistance is assumed.
5. Other than acetate and ammonia, all nutrients are in excess in the medium. Therefore, these two are the only limiting substrates that can be used for process control.
6. The mass of cells is divided between the active biomass and the stored PHB and no further intracellular structure is considered.

3.2.2 Material balance equations

With the assumptions mentioned, the following mass balance equations are considered for acetate and ammonia uptake, biomass growth and intracellular PHB formations.

Acetate uptake:

$$\frac{dS}{dt} = -(q_S^X + q_S^{PHB} + m_S) \cdot X \quad (3.1)$$

where S is acetate concentration in the medium (C-mmol/L), t is the culture time (hr), X is the active biomass concentration (C-mmol/L), q_S^X is the specific acetate consumption rate for cell growth (C-mol/(C-mol.hr)), q_S^{PHB} is the specific acetate consumption rate for PHB formation (C-mol/(C-mol.hr)) and m_S is the maintenance coefficient on acetate (C-mol/(C-mol.hr)).

Ammonia uptake:

$$\frac{dN}{dt} = -Y_{N/X} \cdot (\mu_S + \mu_{PHB}) \cdot X \quad (3.2)$$

where N is ammonia concentration in the medium (N-mmol/L), $Y_{N/X}$ is the yield of ammonia on biomass (N-mol/C-mol), μ_S is the specific growth rate on acetate (C-mol/(C-mol.hr)) and μ_{PHB} is the specific growth rate on PHB (C-mol/(C-mol.hr)).

Biomass growth:

$$\frac{dX}{dt} = (\mu_S + \mu_{PHB}) \cdot X \quad (3.3)$$

In the presence of both acetate and ammonia in the medium, dominant biomass growth is under acetate consumption rate (μ_S). On the other side, intracellular PHB is consumed to supply carbon for growth when acetate is absent (μ_{PHB}).

PHB formation:

The material balance for intracellular PHB content is based on the f_{PHB} value which is defined by the ratio of PHB concentration per active biomass.

$$\frac{d(f_{PHB} \cdot X)}{dt} = (q_{PHB} - Y_{PHB/X} \cdot \mu_{PHB} - m_{PHB}) \cdot X \quad (3.4)$$

where q_{PHB} is the specific PHB storage rate (C-mol/(C-mol.hr)), $Y_{PHB/X}$ is the yield of PHB on biomass (C-mol/C-mol) and m_{PHB} is the maintenance coefficient on PHB (C-mol/(C-mol.hr)). The active biomass factor can be taken from this equation by decomposing the derivative term of the equation and implementation of Equation (3.3).

$$\frac{d(f_{PHB})}{dt} = (q_{PHB} - Y_{PHB/X} \cdot \mu_{PHB} - m_{PHB}) - (\mu_S + \mu_{PHB}) \cdot f_{PHB} \quad (3.5)$$

3.2.3 Postulation of the kinetic model

Kinetic model equations are used to specify parameters defined in the material balance equations. In the acetate uptake Equation (3.1), three terms are considered for consumption of acetate in biomass growth (q_S^X), PHB formation (q_S^{PHB}) and to maintain carbon source for metabolic activities of cells (m_S). The latter is limited by acetate concentration in the medium and is calculated from the following equation.

$$m_S = m_{S_{max}} \cdot \frac{S}{K_S + S} \quad (3.6)$$

where $m_{S_{max}}$ is the maximum maintenance coefficient on acetate (C-mol/(C-mol.hr)) and K_S is the acetate half-saturation constant (C-mmol/L). The metabolic model reported in (Beun *et al.*, 2002) allows derivation of expressions for theoretical yields and maintenance coefficients in Van Aalst-van Leeuwen *et al.* (1997). Table 3.1 contains metabolic model reactions for biomass empirical formula.

Table 3.1 Metabolic model reactions for mixed cultures (adapted from van Aalst-van Leeuwen *et al.* (1997))

Acetate uptake
$0.5 \cdot HAc + 0.5 \cdot CoA + 1 \cdot ATP \rightarrow 0.5 \cdot AcCoA + 0.5 \cdot H_2O$
Biomass precursors synthesis
$0.6335 \cdot AcCoA + 0.2 \cdot NH_3 + 0.66 \cdot ATP + 0.102 \cdot H_2O \rightarrow 1 \cdot CH_{1.4}N_{0.2}O_{0.4} + 0.267 \cdot CO_2 + 0.534 \cdot NADH_2$
Biomass precursors polymerization
$1 \cdot CH_{1.4}N_{0.2}O_{0.4} + (1.5 + \frac{m_{ATP}}{\mu}) \cdot ATP \rightarrow \frac{1}{n} \cdot (CH_{1.4}N_{0.2}O_{0.4})_n$
Respiration
$0.25 \cdot AcCoA + 0.75 \cdot H_2O \rightarrow 0.5 \cdot CO_2 + 1 \cdot NADH_2$
Oxidative phosphorylation
$1 \cdot NADH_2 + 0.5 \cdot O_2 \rightarrow 1 \cdot H_2O + \delta \cdot ATP$
Aerobic PHB storage
$0.5 \cdot AcCoA + 0.25 \cdot NADH_2 \rightarrow 1 \cdot CH_{1.5}O_{0.5}$
Aerobic PHB consumption
$1 \cdot CH_{1.5}O_{0.5} + 0.25 \cdot ATP \rightarrow 0.5 \cdot AcCoA + 0.25 \cdot NADH_2$

Dias *et al.* (2005) formulated the following equations for calculation of yields and maintenance coefficients based on the metabolic reactions.

$$Y_{X/S} = \frac{4 \cdot \delta - 2}{4 \cdot \delta + 4.32} \quad (3.7)$$

$$Y_{PHB/S} = \frac{4 \cdot \delta - 2}{4.5 \cdot \delta} \quad (3.8)$$

$$Y_{PHB/X} = \frac{4 \cdot \delta + 4.32}{4.5 \cdot \delta + 0.5} \quad (3.9)$$

$$m_{S_{max}} = \frac{m_{ATP}}{2 \cdot \delta - 1} \quad (3.10)$$

$$m_{PHB} = \frac{m_{ATP}}{4.5 \cdot \delta - 0.5} \quad (3.11)$$

where $Y_{X/S}$ is the yield of biomass on acetate (C-mol/C-mol), δ is the efficiency of oxidative phosphorylation (mol ATP/mol NADH₂) and m_{ATP} is the specific ATP consumption by maintenance process (mol ATP/(C-mol.hr)). According to Beun *et al.* (2002) for mixed cultures under aerobic conditions, δ is 2 (mol ATP/mol NADH₂) and m_{ATP} is 0.02 (mol ATP/(C-mol.hr)) (Dias *et al.*, 2005).

The flux of acetate consumption for cell growth in Equation (3.1) is mainly limited by acetate and ammonia concentrations (Van Aalst-van Leeuwen *et al.*, 1997; Gujer *et al.*, 1999; Serafim *et al.*, 2004). Therefore, this term is defined as

$$q_S^X = q_{S_{max}}^X \cdot \frac{S}{K_S + S} \cdot \frac{N}{K_{N_S} + N} \quad (3.12)$$

where $q_{S_{max}}^X$ is the maximum specific acetate consumption rate for biomass growth (C-mol/(C-mol.hr)) and K_{N_S} is the ammonia half saturation constant in acetate uptake (N-mmol/L). The specific growth rate on acetate is defined as

$$\mu_S = Y_{X/S} \cdot q_S^X \quad (3.13)$$

thus

$$\mu_{S_{max}} = Y_{X/S} \cdot q_{S_{max}}^X \quad (3.14)$$

and Equation (3.12) take the following form

$$q_S^X = \frac{\mu_{S_{max}}}{Y_{X/S}} \cdot \frac{S}{K_S + S} \cdot \frac{N}{K_{N_S} + N} \quad (3.15)$$

By definition specific acetate consumption rate for PHB formation is

$$q_S^{PHB} = \frac{q_{PHB}}{Y_{PHB/S}} \quad (3.16)$$

where $Y_{PHB/S}$ is the yield of PHB on acetate (C-mol/C-mol). It was observed that q_{PHB} is limited by the acetate concentration and the intracellular PHB content. Therefore, the following equation is adapted from (Kato *et al.*, 1999), (vanLoosdrecht and Heijnen, 2002) and (Third *et al.*, 2003) with a power coefficient modification from (Kato *et al.*, 1999).

$$q_{PHB} = q_{PHB_{max}} \cdot \frac{S}{K_S + S} \left[1 - \left(\frac{f_{PHB}}{f_{PHB_{max}}} \right)^\alpha \right] \quad (3.17)$$

where $q_{PHB_{max}}$ is the maximum specific PHB storage rate (C-mol/(C-mol.hr)), f_{PHB} is the intracellular PHB content (C-mol PHB/C-mol X), $f_{PHB_{max}}$ is the maximum intracellular PHB content (C-mol PHB/C-mol X) and α is a dimensionless constant describing PHB production saturation order. These values are determined by experimental results carried out by Dias *et al.* (2005). Based on this information, material balance for acetate uptake given in Equation (3.1) can be established.

The ammonia uptake rate is directly proportional to the rate of biomass growth in the “feast” phase operation as described in Equation (3.2). Therefore, the specific biomass growth rate on acetate (μ_S) and the specific biomass growth rate on PHB (μ_{PHB}) are used in the ammonia uptake material balance. In order to identify the specific biomass growth rate, Equation (3.13) and Equation (3.15) are used to form the following equation.

$$\mu_S = \mu_{S_{max}} \cdot \frac{S}{K_S + S} \cdot \frac{N}{K_{N_S} + N} \quad (3.18)$$

(μ_S) is the dominant term when biomass growth is under “feast” phase operation in abundance of both acetate and ammonia. The following equation defines the dominant term of biomass growth in the “famine” phase operation in absence of acetate.

$$\mu_{PHB} = \mu_{PHB_{max}} \cdot \frac{f_{PHB}}{K_{PHB} + f_{PHB}} \cdot \frac{N}{K_{N_{PHB}} + N} \quad (3.19)$$

where $\mu_{PHB_{max}}$ is the maximum specific growth rate on PHB (C-mol/(C-mol.hr)), K_{PHB} is the intracellular PHB content half saturation constants (C-mmol/L), and $K_{N_{PHB}}$ is the ammonia half saturation constant in PHB consumption (N-mmol/L).

When ammonia material balance is identified, it is possible to model biomass concentration based on Equation (3.3) since all terms have already been calculated. Intracellular PHB content defined in material balance Equation (3.5) can be calculated

with q_{PHB} , μ_S , μ_{PHB} and m_{PHB} from Equation (3.17), Equation (3.18), Equation (3.19) and the following equation respectively:

$$m_{PHB} = k_d \cdot f_{PHB}^n \quad (3.20)$$

where k_d is the kinetic constant for PHB degradation (/hr). The maintenance on PHB (m_{PHB}) was shown to follow first order kinetics on PHB intracellular content (Murnleitner *et al.*, 1997; Carta *et al.*, 2001; Beun *et al.*, 2002; Third *et al.*, 2003; Serafim *et al.*, 2004). A kinetic order of “ n ” was adopted by (Beun *et al.*, 2000) and (Dircks *et al.*, 2001) yielding more accurate results. An adaptation of Equation (3.7), Equation (3.19) and Equation (3.20) are used in the simulation program to produce more accurate results by (Dias *et al.*, 2005).

$$Y_{X/S} = \frac{4 \cdot \delta - 1}{4 \cdot \delta + 2 \cdot K_\tau + 1.267} \quad (3.21)$$

$$\mu_{PHB} = \mu_{PHB_{max}} \cdot \frac{f_{PHB}}{K_{PHB} + f_{PHB}} \cdot \frac{N}{K_{N_{PHB}} + N} \cdot \frac{K_{S_{PHB}}}{K_{S_{PHB}} + S} \quad (3.22)$$

$$m_{PHB} = k_d \cdot f_{PHB}^n \cdot \frac{K_{S_{PHB}}}{K_{S_{PHB}} + S} \quad (3.23)$$

where K_τ is the efficiency constant (mol ATP/mol $NADH_2$) and $K_{S_{PHB}}$ is the acetate half saturation constant in PHB consumption (C-mmol/L).

3.2.4 Kinetic parameter estimation

(Dias *et al.*, 2005) specified kinetic parameters by applying simultaneous parameter estimation strategy to minimise the sum of squared errors (SSE) employing the Levenberg-Marquardt algorithm. The simulation program implements the material balance and the postulated kinetic equations in MATLAB using a 4th/5th order Runge-Kutta solver. Table 3.2 contains simulation parameters as reported in (Dias *et al.*, 2005) and applied in the simulation program to provide the best prediction results.

Table 3.2 Kinetic model constants (adapted from Dias *et al.* (2005))

Constants	Values	Constants	Values
K_S	0.0625 (C_mmol/L)	δ	2.96 ± 0.06 (mol ATP/molNADH ₂)
K_{SPHB}	0.01 (C_mmol/L)	$f_{PHB_{max}}$	2.71 ± 0.64 (C_molPHB/C_molX)
K_{N_S}	0.5776 (N_mmol/L)	$q_{PHB_{max}}$	0.44 ± 0.1 (C_mol/(C_mol.hr))
$K_{N_{PHB}}$	0.5776 (N_mmol/L)	$\mu_{S_{max}}$	0.4 ± 0.08 (C_mol/(C_mol.h))
K_{PHB}	0.001 (N_mmol/L)	$\mu_{PHB_{max}}$	0.083 (C_mol/(C_mol.h))
K_τ	1.7 (mol ATP/molNADH ₂)	$Y_{PHB/X}$	1.83 (C_mol/C_mol)
K_d	0.067 (/h)	m_{ATP}	0.02 (mol ATP/(C_mol.h))
α	3.85	n	1.94

In the next section, the structure of the simulation program is described.

3.3 Introduction to the simulation program

The simulation program developed by Dias *et al.* (2005) is called (BIOSIM) which consists of three main divisions. In the first division, initial process parameters are defined to be implemented in the second division which contains kinetic parameters and material balance equations. An ordinary differential equation is solved to obtain simulation results for the given initial values. These results are stored in an organised manner for further data analysis applications in the third division of the program.

3.3.1 First division: simulation elements

In the first division, process parameters and process initial values are defined to be applied in the mechanistic model. These include mathematical description of the bacteria and the operational medium which set up the building block of the program that simulates PHB production under mixed microbial culture of 32 different genotypes. The PHB simulation model constants are assigned based on experimental results carried out using a mixed microbial culture of 32 genotypes as reported in Dias *et al.* (2005). For each genotype, one specific value is associated for their efficiency of oxidation phosphorylation (δ), maximum intracellular PHB content ($f_{PHB_{max}}$), maximum specific PHB storage rate ($q_{PHB_{max}}$) and maximum specific growth rate on acetate ($\mu_{S_{max}}$). Additionally, process parameters describing the initial state of the process such as initial biomass concentration “*BIOM0*” and initial PHB content “*fPHB0*” is specified in this division for each population.

In the simulation runs reported in this study, an assumption is taken to facilitate description of PHB content within the population of cells. Based on this assumption, the ratio of initial PHB content of different population to their maximum PHB content capacity is considered to be the same ratio. Equation (3.24) shows how initial PHB content of different population is defined in the simulation.

$$f_{PHB0} = f_{PHB_{max}} \times Pe_{PHB0} \quad (3.24)$$

where $f_{PHB_{max}}$ is a vector containing maximum intracellular PHB content values (C-mol PHB/C-mol X) and Pe_{PHB0} is a decimal number between 0 and 1 which specifies PHB content ratio from no PHB content ($Pe_{PHB0} = 0$) to PHB saturation ($Pe_{PHB0} = 1$). Each batch operation is divided into a number of process time units where feed injections and product exploitation may occur. The number of these time units is specified by “*CycleTimes*” and the duration of batch operation within each time unit is specified by “*Tcycle*”. In simulations, each time unit is divided into a number of segments to indicate time step size when solving the Ordinary Differential Equation (ODE). The number of divisions is specified by “*Time_intervals*” in the beginning of the simulation program.

Injections of feeding materials are specified by “*ADDHA*” and “*ADDN*” for acetate augmentation concentration and ammonia augmentation concentration respectively. Figure 3.1 shows general structure of the program with the eight process parameters illustrated in the left hand side of the box.

3.3.2 Second division: ODE solver

In the second division of the simulation program, ODE parameters are identified based on the process values specified in the first division of the program, kinetic and material balance equations mentioned in the previous section. MATLAB finds the solution of the ODE for the independent step size dictated by “*Time_intervals*” using 4th/5th order Runge-Kutta (ode45). In order to simulate a complete batch, simulation program calculates ODE solutions for all batch unit times specified by “*CycleTimes*” in an iteration loop. In Figure 3.1, second division of the batch simulation program is shown in the middle of the box.

3.3.3 Third division: data repository

Solution of the material balance differential equation provides simulation data for material concentrations over the course of the simulated batch. In this case, concentration profiles of activated biomass, PHB content that yields to the PHB product, acetate and ammonia are available at the end of the simulation. In the third division of the program, in line with the operational time, concentration profiles are stored in an organised manner to enable further analysis of data. In Figure 3.1, third division of the simulation program is shown in the right side of the box.

“BIOSIM” is a MATLAB code developed by Dias *et al.* (2005) to simulate PHB production under MMC using two sub-programs called “MatBal” and Kinetics. In the BIOSIM, MATLAB random generator assigns random values to the kinetic parameters for the 32 populations in their pre-specified range. The aim is to capture natural alteration of bacterial behaviour which may alter from one batch to another batch.

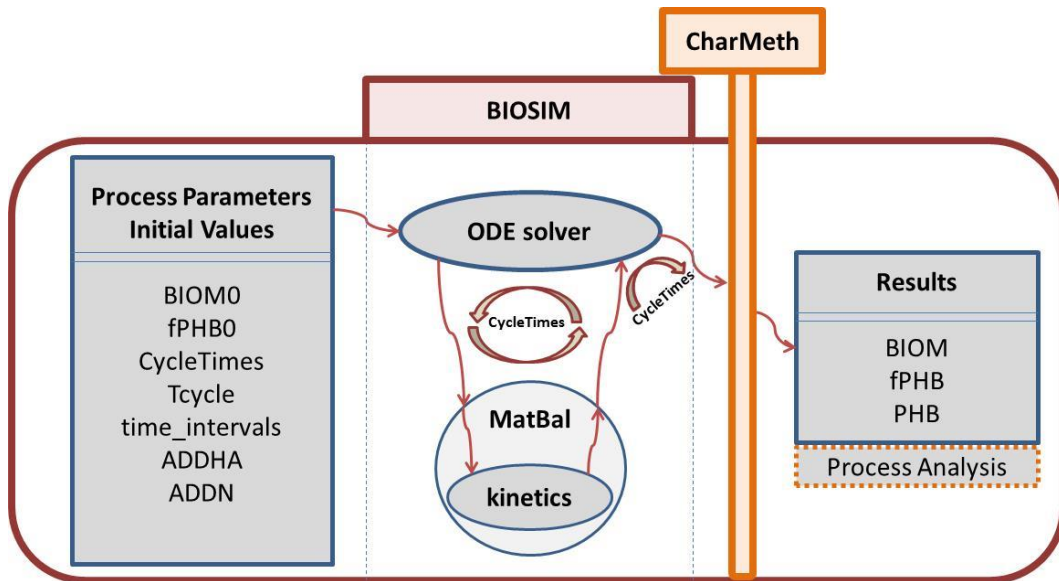


Figure 3.1 Simulation program structure

Since biological processes are carried out by living organisms, their behaviour characteristics may vary despite maintaining same process conditions. Dias *et al.* (2005) altered biological behaviour of the populations by associating random values to the efficiency of oxidation phosphorylation (δ), maximum intracellular PHB content ($f_{PHB_{max}}$), maximum specific PHB storage rate ($q_{PHB_{max}}$) and maximum specific growth rate on acetate ($\mu_{S_{max}}$) for each genotypes.

Although introduction of random behaviour biological simulations increases the analogy between the experimental and the simulation results, this is unfavourable when repeatable simulation results is addressed to carry out studies based on comparisons. Therefore, in a modified version of the BIOSIM program, biological randomness behaviour is cancelled out by assigning constant values to δ , $f_{PHB_{max}}$, $q_{PHB_{max}}$ and $\mu_{S_{max}}$ simulation parameters. This facilitates analysis of the batch process when simulations are repeated with the same initial process parameters. The modified version of the simulation program is referred to as the “deterministic behaviour process simulator” in this study. In the next section, experimental data used for model development and validation conducted by Dias *et al.* (2005) are reported.

3.4 Validation of the PHB simulator program by experimental data

The mathematical modelling of a mixed culture cultivation process for the production of PHB formulated by Dias *et al.* (2005) has also been validated with data of batch experiments performed in reactors with volume of 600 mL. The validation tests were carried out by varying the amount of acetate and ammonia injected to the reactor. Eight experiments are designed with acetate and ammonia fed pulse wise and tabulated in Table 3.3 for estimation of modelling parameters and validation of the process simulator.

Table 3.3 Acetate and ammonia concentrations in the medium after pulse feed addition in C-mmol/L and N-mmol/L respectively(adapted from Dias *et al.* (2005)).

Substrates	Experiments	1 st pulse	2 nd pulse	3 rd pulse	4 th pulse
Acetate	I	30	---	---	---
Ammonia		---	1.29	---	---
Acetate	II	60	---	---	---
Ammonia		0.73	---	---	---
Acetate	III	61	61	69	---
Ammonia		0.61	---	---	---
Acetate	IV	58	64	64	---
Ammonia		0.7	---	---	---
Acetate	V	60	62	63	63
Ammonia		0.68	---	---	---
Acetate	VI	30	---	---	---
Ammonia		0.76	---	---	---
Acetate	VII	24	---	---	---
Ammonia		1.1	---	---	---
Acetate	VIII	63	61	63	---
Ammonia		0.66	---	---	---

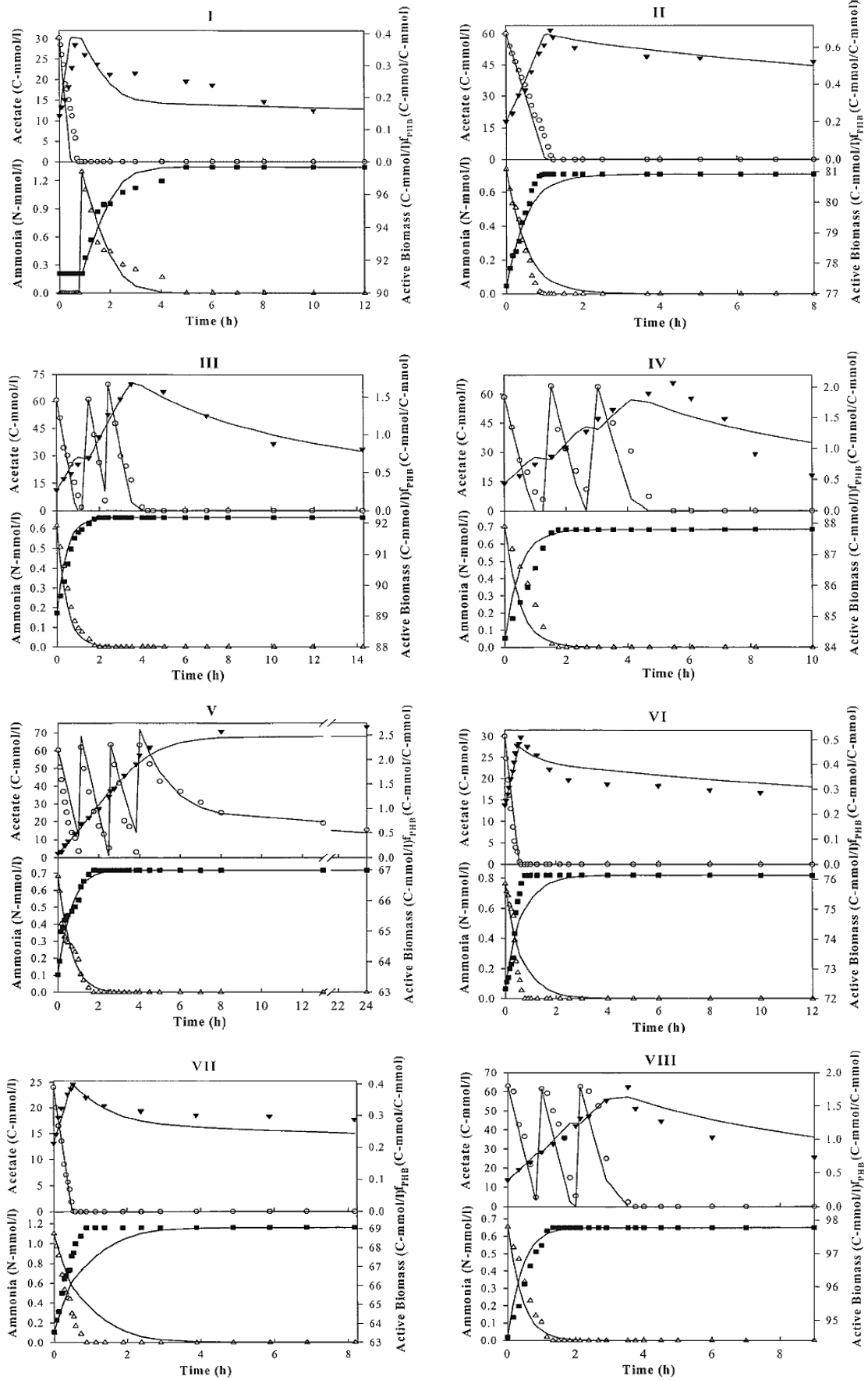


Figure 3.2 Validation results. Symbols represent measured data (\blacktriangledown -intracellular PHB content; \circ - acetate concentration; \triangle - ammonia concentration; \blacksquare -active biomass) full lines represent model predictions (adapted from Dias *et al.* (2005)).

Figure 3.2 shows model simulations and measured data for the experiments used for parameter estimation (the first five experiments) and model validation (the last three experiments). Model predictions and experimental data show an excellent agreement in most cases. The reported average absolute error was 6.20 C-mmol/L, 0.059 N-mmol/L, 0.30 C-mmol/L and 0.12 C-mmol/L for acetate, ammonia, active biomass and intracellular PHB content respectively for model estimation experiments. The average absolute error obtained was 5.81 C-mmol/L, 0.13 N-mmol/L, 0.65 C-mmol/L and 0.080 C-mmol/L for acetate, ammonia, active biomass and intracellular PHB content respectively for validation experiments. The accuracy of the predictions is promising and it strengthens the generalisation potential of the model for model-based optimisation studies (Dias *et al.*, 2005).

In the next section, a typical simulation run is described to provide a general view about the PHB production process by the MATLAB simulator program.

3.5 Description of simulation results

In the a simulation run, a batch process initiating with total activated biomass concentration of 13 C-mmol/L which is normally distributed between the 32 populations is considered. The initial PHB content is considered to be only 10% of the maximum PHB capacity of populations ($Pe_{PHB0} = 0.1$). The batch duration of 30 hours is simulated in three time units of 10 hours with acetate augmentation of 60 C-mmol/L, 20 C-mmol/L and 50 C-mmol/L and ammonia augmentation of 0.6 N-mmol/L, 1 N-mmol/L and 0.2 N-mmol/L respectively in the beginning of each batch time unit. Figure 3.3 shows code parameters specified to simulate the aforementioned batch process in MATLAB code program.

```
BIOM0=13;           % Initial Biomass Concentration (C-mmol/L)
PePHB0=0.1;        % Initial PePHB0 value
CycleTimes=3;      % Number of Cycles
Tcycle=10;         % Duration of one batch (hr)
Time_intervals=500; % Divisions in batch unit time
ADDHA=[60 ; 20 ; 50]; % Induction of Acetate (C-mmol/L)
ADDN=[0.6 ; 1 ; 0.2]; % Induction of Ammonia (N-mmol/L)
```

Figure 3.3 Programing code parameters for batch simulation in MATLAB

In Figure 3.4, simulation results are shown for acetate, ammonia, active biomass and intracellular PHB profiles in three 10-hour operational segments. In Figure 3.4.a, acetate profile is depicted to demonstrate acetate consumption from its initial point of 60 C-mmol/L to 4 C-mmol/L in the first 10 hours of batch operation. The second

injection of feed substrate to the system increases acetate concentration by 20 units to reach to 24 C-mmol/L in the second segment of the batch operation. In the second batch segment, acetate is completely exhausted. Acetate augmentation of 50 C-mmol/L at 20 hours of batch operation time, maintains carbon source in the medium during the third segment of the batch operation time. At the end, acetate concentration is about 20 C-mmol/L in the medium.

Similar to acetate profile, ammonia concentration subplot shown in Figure 3.4.b illustrates complete exhaustion of ammonia in each batch time segment after introduction of the substrate at the beginning of each segment. In Figure 3.4.c and Figure 3.4.d, biomass concentration profiles are depicted for each 32 active populations and the total biomass respectively. Gradual biomass growth can be observed in presence of acetate and ammonia in the system.

In Figure 3.4.e, Figure 3.4.f and Figure 3.4.g, fPHB and PHB profiles are depicted. In the first 10 hours of the batch operation, intracellular PHB content increases along with biomass growth in presence of both acetate and ammonia in the medium. Figure 3.4.e shows two drops in fPHB profile during the batch operation. The first fPHB drop occurs when feed substrates are added to the system at the beginning of the second batch time segment. At this point, PHB saturated cells are exposed to a nutrient rich medium where they start to grow in a significant rate. Therefore, fPHB drops in reflection of higher biomass growth rate as oppose to the lower PHB formation rate. Since PHB concentration is maintained during this period, no PHB drop is observed in the PHB profiles at this point of operation. However, in the second fPHB drop observed at about 15 hours of batch operation, PHB profile drops as well. This occurs when acetate completely exhausts during the operation and bacteria change their pathway from PHB reservation to PHB consumption in order to provide their metabolic activates in absence of carbon source of the medium. Deduction of PHB concentration continues until acetate injection takes place at the 20 hours of batch operation time. In presence of both acetate and ammonia in the third 10 hours of the batch operation, PHB storage takes place to retain PHB consecration at about 58 C-mmol/L by the end of the process.

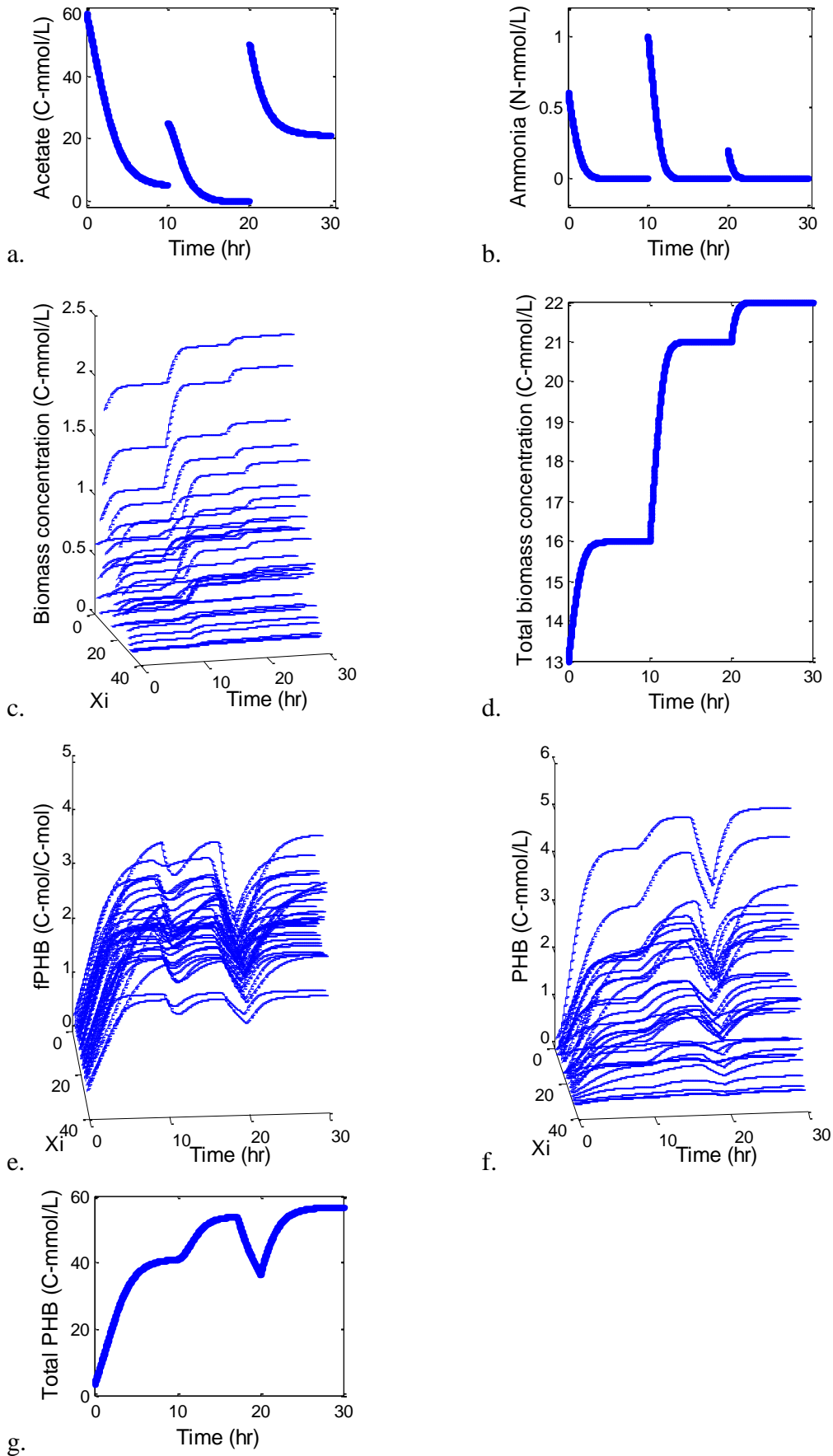


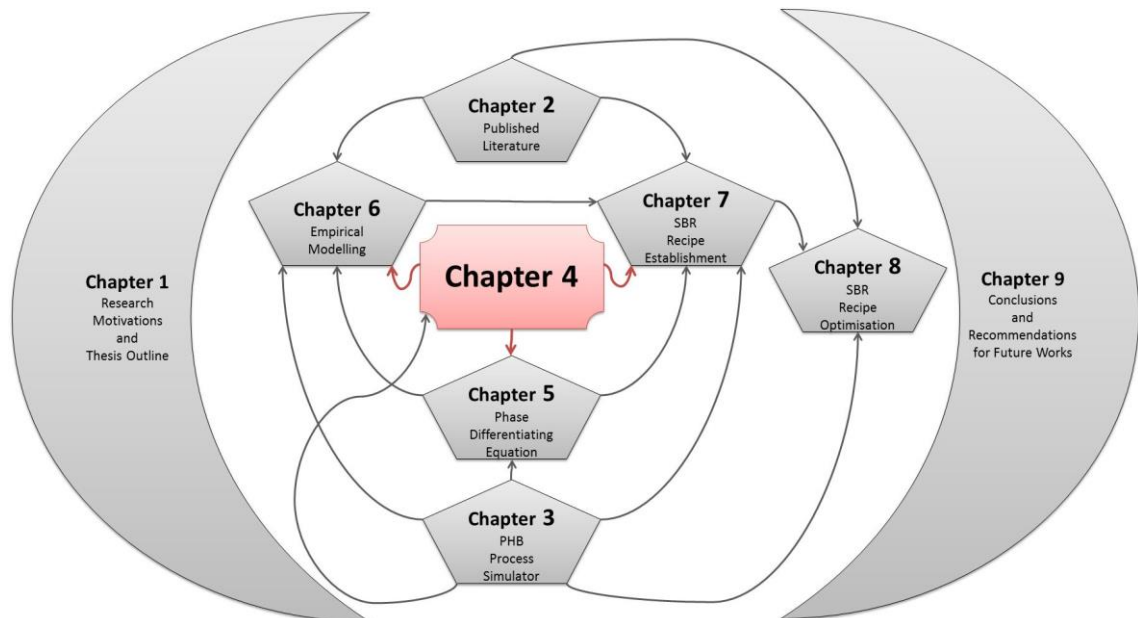
Figure 3.4 Results for the batch simulation run

3.6 Summary

In this chapter, mechanistic model assumptions, material balances and kinetic parameters implemented by Dias *et al.* (2005) to simulate PHB batch production with mixed microbial cultures are given. The model is developed under a main simplifying hypothesis that organisms presented in the medium are heterotrophic with a metabolism that does not change significantly in time. The model was successfully validated with promising accuracy to conclude that a two-compartment model is able to describe the state variables.

The simulation model introduced in this chapter is applied in the consecutive chapters as process data generator for PHB batch production with mixed microbial cultures.

Chapter 4
Batch Process Characterisation Method for PHB Production
with Mixed Microbial Culture Cultivation



4.1 Introduction

Nowadays with the advent of advanced computational tools, application of analytical methods has become an essential adjunct to the experimental techniques developed with the aim of operational enhancement of complex behaviour systems. The analytical method developed in this chapter will be referred to as the “Characterisation Method” which occurs in a module code called “CharMeth” added on to the main process simulation program. Simulated process results are evaluated with a series of analytical modules to generate analytical results for each simulated batch process prior to storing simulation and analytical data. Figure 4.1 shows the structure of the simulation program when the analytical module code is placed in the process simulator depicted in Figure 3.1.

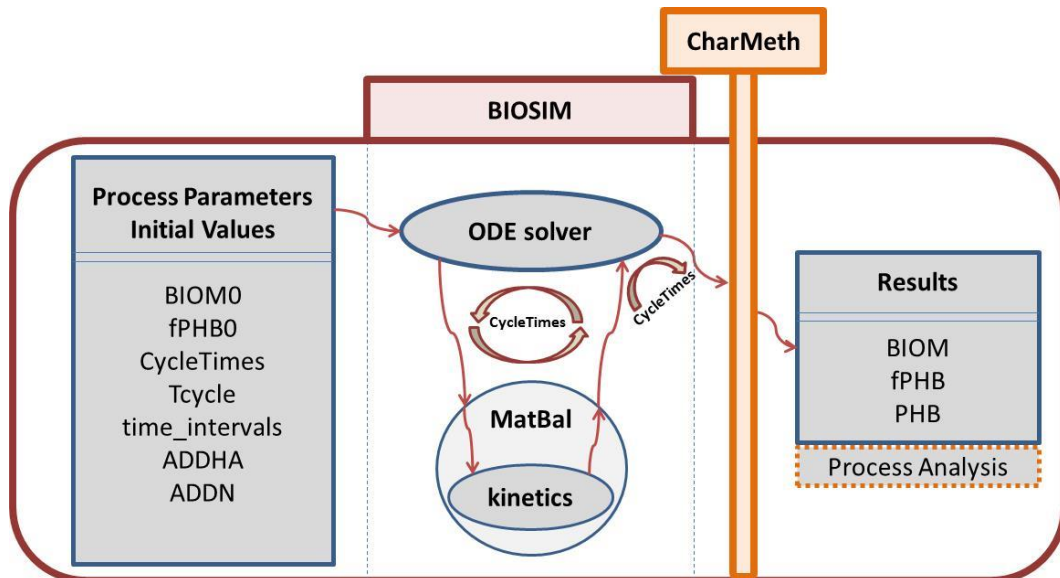


Figure 4.1 Simulation program structure with the supplement of “Characterisation Method” (CharMeth) module

The “Characterisation Method” procedure is followed to generate characterisation plots for the simulation program. This method is divided into 7 divisions, each providing useful information about the PHB batch process behaviour. In the first division (Section 4.2), PHB process is analysed to find the most significant elements of the process. In the second division (Section 4.3), the identified process profiles are investigated to create analysis modules to be applied on process profiles. In the third division (Section 4.4), process profiles are visualised along with the analysis results obtained from the modules. In the fourth division (Section 4.5), code values are defined to be associated with significant process occurrences. In the fifth division (Section 4.6), a bank of code vectors is created by screening various operational scenarios. The code

vectors will be classified in the sixth division (Section 4.7) and characterisation plots are drawn using the classified code vectors (Section 4.8). At the end, the capability of the developed procedure to differentiate major process regimen will be investigated.

4.2 Acquire process knowledge and selection of process significant elements (Critical Process Attributes)

Good process understanding is crucial in process control and optimisation. The first step to gain knowledge about a particular unknown process is associated with measuring process variables (e. g. measurement of temperature, pressure, concentration of various dilutes, spectroscopic data and etc.). In a particular chemical process, a number of correlated and uncorrelated variables are measured to map relationships between different process elements and to provide mathematical representations of these relationships. The “Characterisation Method” developed in this study makes use of the process variables with the most dominant effect on the process element of high importance (normally the amount of process product). The observations associated with each process variable are generated using computer-based simulations. However, the role of variables remains the same in simulations with high level of accuracy. Therefore, initial step in the “Characterisation Method” is to identify the most important process variables.

The simulation program discussed in Chapter 3 is applied in this chapter for “Characterisation Method” development targeting PHB production process with mixed microbial cultures. As mentioned in Chapter 3, two feeding substrates of acetate and ammonia play dominant role on PHB formation rate. Process profiles comprising of the feeding substrates and product concentration are scrutinised in the “Characterisation Method”.

4.3 Process profile analysis

In this step of the “Characterisation Method”, the two main process profiles (acetate and ammonia concentration) are scrutinised along with the process product profile. A fair understanding of the nature of the process facilitates identification of the high significance profile occurrences.

A combination of mathematical and logical algorithms coded in adjunct to the simulation program enables detection of this type of significant occurrences in the process profiles. For a specific simulated process, a specified code is required to be

develop and tuned to detect these operational points in a profile. The three profiles of acetate, ammonia and total PHB concentrations are considered for analysis in this stage. The analytical modules developed for each of these three profiles are discussed in the following sections. These modules are developed and established by the author.

4.3.1 CharMeth's first module: Ammonia profile analysis

The first process profile analysed in the “CharMeth” module code is the ammonia profile for a simulated batch process. The most significant occurrence in the ammonia profile is when its concentration stabilises at a certain point with either a zero or a positive value. In order to develop a code module to detect such point in the ammonia profile, a vector called “AmmoniaFactor” is defined as a factor of the first order derivative values of progressive ammonia concentrations in respect to the operational time. This vector is defined when a complete ammonia concentration profile is available for one batch process. One of the first few values in the “AmmoniaFactor” vector (which can be associated with the initial process point in the analytical batch) is stored in the “AmmoniaCons” and is used as the basis for identification of the ammonia critical point during a batch process. The “AmmoniaFactor” values are compared with the “AmmoniaCons” constant value in an iteration loop. Since absolute value stored as “AmmoniaCons” is much larger than the absolute values stored in the “AmmoniaFactor” vector, a tuning factor, “F1”, is multiplied to the “AmmoniaCons” value so that comparisons can be made between the absolute value of “AmmoniaCons” and the absolute values in the “AmmoniaFactor” vector. As it is shown in Figure 4.2, the ammonia critical point is identified when absolute value of “AmmoniaFactor” is bigger than the multiplication of “F1” and the absolute value of “AmmoniaCons”.

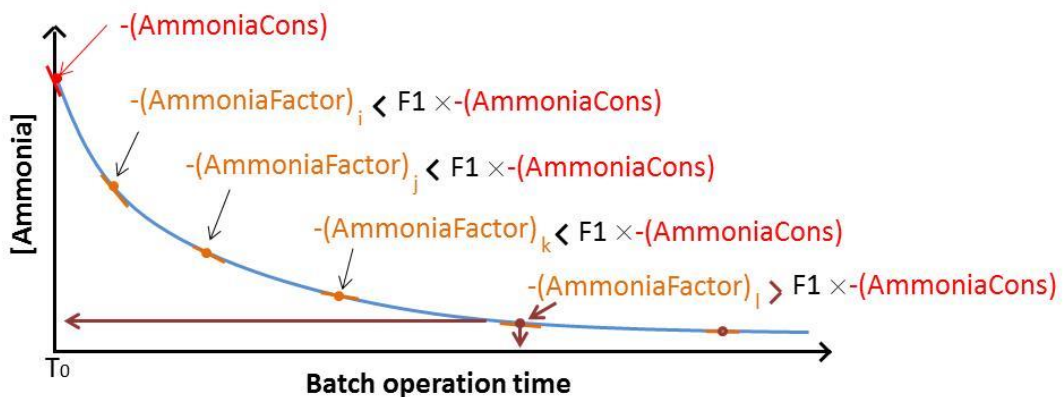


Figure 4.2 Identification of critical ammonia point within a batch operation period

The tuning parameter is assigned to have a value of (0.05) for the case of critical ammonia module in this particular process. This value was assigned using trial and error. If “F1” is altered to a larger value, the critical ammonia point is identified in an operational time earlier than the one assigned with the current setting. In an iteration loop considered in the module program, the values of “AmmoniaFactor” vector are compared with the multiplication of “F1” and “AmmoniaCons” in an ascending order of batch process operational time in order to find the operational time in which ammonia critical point is identified. This operational time is one of the simulation observations specified as the “time_intervals” and stored in “IK001”. Figure 4.3 shows an illustration of the MATLAB coding embedded in the “CharMeth” module in which ammonia critical point is identified.

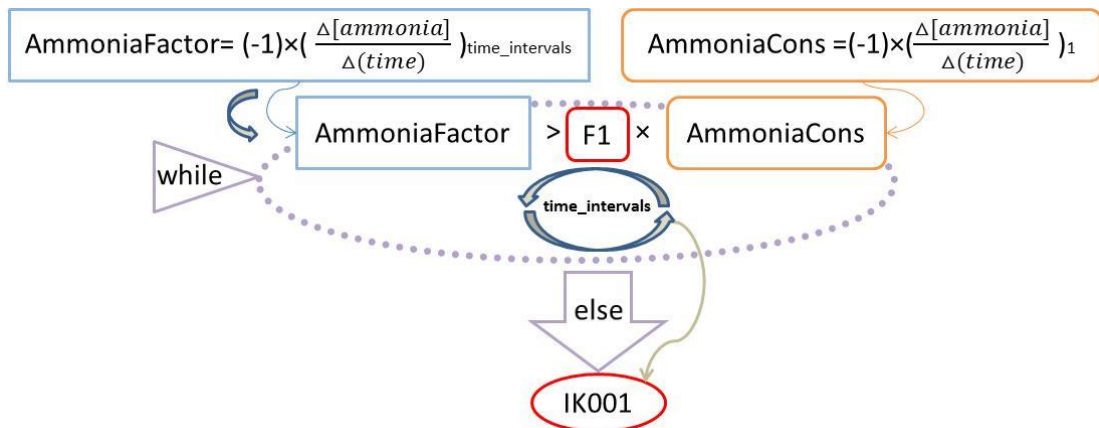


Figure 4.3 Descriptive depiction of “CharMeth” ammonia module

Figure 4.4 shows analytical results obtained from the “CharMeth” module for four arbitrary ammonia test profiles in four different batch operations. In this figure, the ammonia critical point on each profile is depicted by (▲) sign indicators.

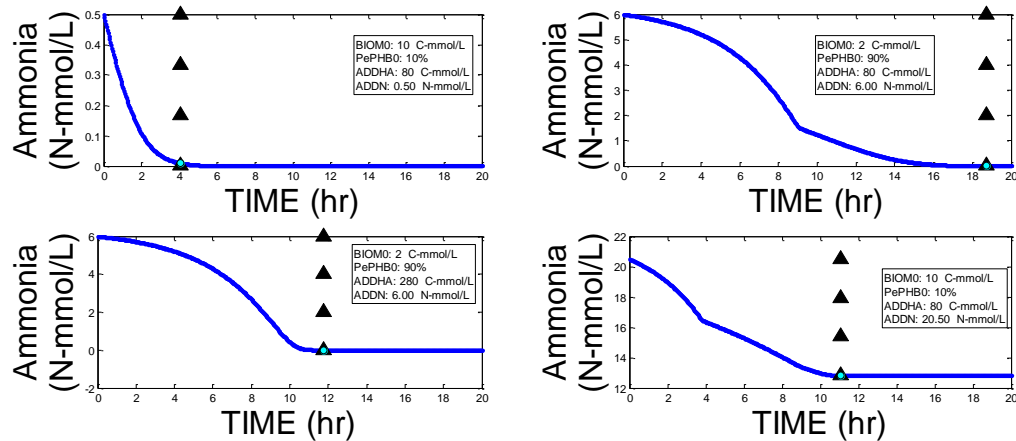


Figure 4.4 “CharMeth” analytical results on different ammonia profiles

As shown in the four profiles, the algorithm designed to identify the critical point of ammonia concentration profile is capable of producing reliable and accurate estimations.

In the next section, description of a similar procedure is given to identify the acetate concentration critical point within a batch of PHB production using MMC.

4.3.2 CharMeth's second module: Acetate profile analysis

In the second section of the "CharMeth" module, a profile of acetate concentration for one process batch is considered. Like the ammonia concentration profile, the most significant occurrence in the acetate profile is acetate stability point. Therefore, the structure of the module code in this section is similar to that of ammonia section with a small modification.

The vector containing the first order derivative values of the acetate concentrations in respect to the batch operational time is called "AcetateFactor". Similar to the previous algorithm, one of the first few values in the "AcetateFactor" is stored in "AcetateCons" as the constant for comparison in the iteration loop. The tuning parameter for acetate critical point identification, "F2", is assigned to be equal to 0.035 by trial and error. In addition to the simple structure of the iteration loop, an update procedure is considered for "AcetateCons" within the comparison practice. The purpose of this supplement is to assign the steepest gradient as the basis for comparison in the algorithm. An illustration of the acetate concentration profile in which the supplement algorithm plays an effective role is given in Figure 4.5.

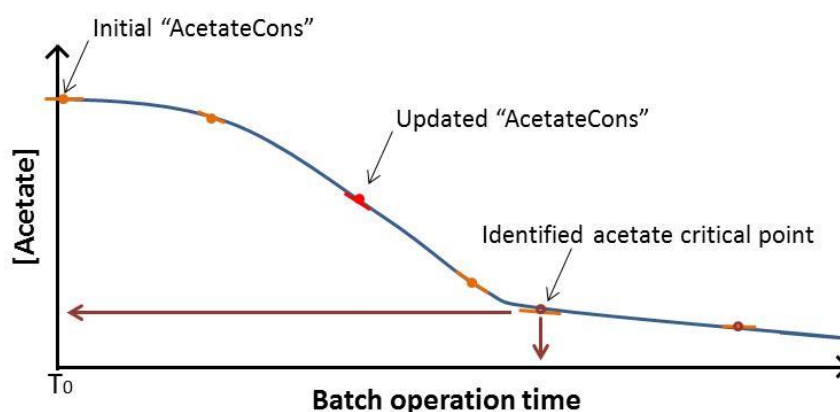


Figure 4.5 Identification of critical acetate point within a batch operation period

In Figure 4.6, a descriptive demonstration of the acetate analysis module is depicted including the constant updating algorithm.

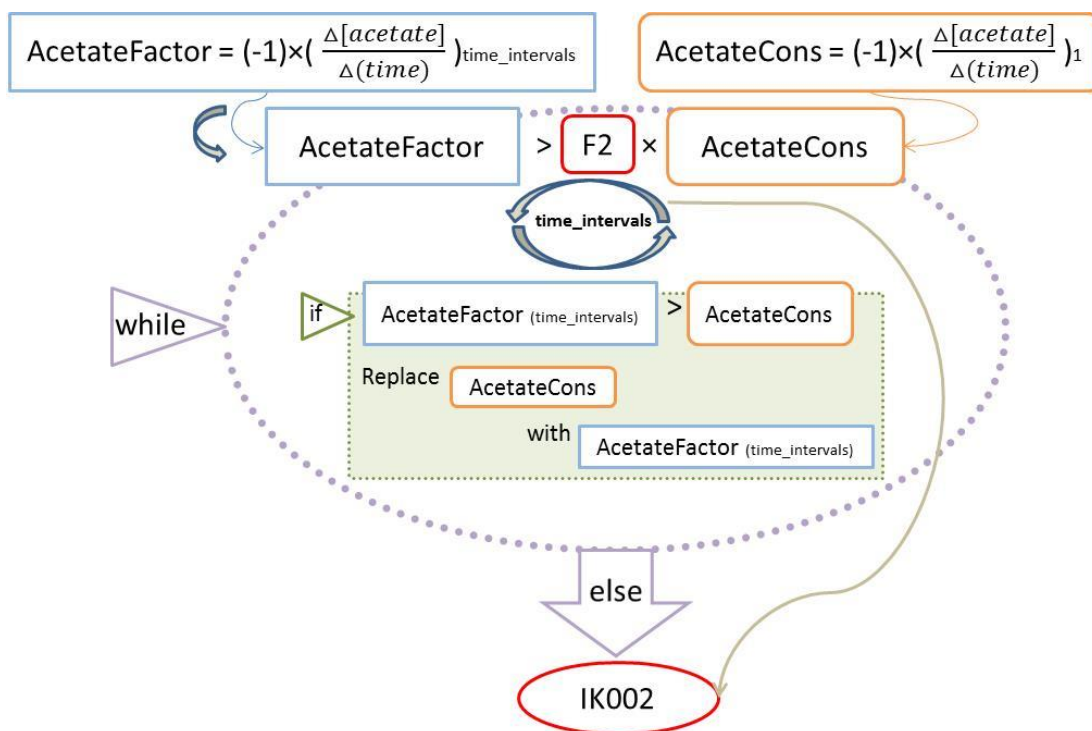


Figure 4.6 Descriptive depiction of “CharMeth” acetate module

The analysis outcome is stored as “IK002” which is the observation number (time_intervals) of the critical point detected within the acetate profile of a batch process. Figure 4.7 shows analytical test results obtained from the “CharMeth” module for four arbitrary acetate profiles obtained from four different batch processes. In this figure, the acetate critical point on each profile is depicted by (▼) sign indicators.

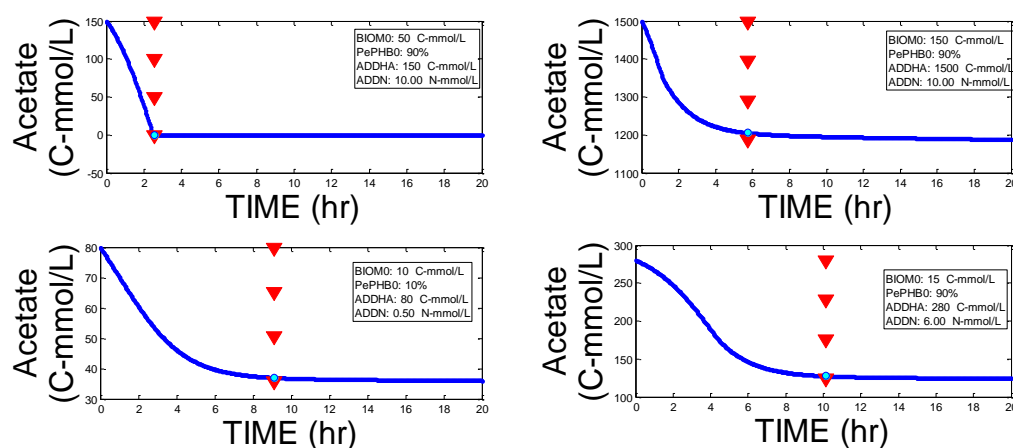


Figure 4.7 “CharMeth” analytical results on different acetate profiles

As shown in Figure 4.7, although the scale and the consumption trend of the four acetate profiles are different from each other, the module code designed to identify the

acetate critical point is capable of making accurate estimations. In the third section of the “CharMeth” module, total PHB concentration profile is considered.

4.3.3 CharMeth’s third module: Total PHB profile analysis

In the third section of the “CharMeth” module, analysis of the process product profile (total PHB concentration) is carried out. Investigations on the total PHB concentration profile show that a number of different case scenarios may exist representing beneficial or detrimental product profile for lucrative or a sustainable production system. For this reason, a relatively more complex strategy is considered in comparison to the two previous profile analysis procedures in order to differentiate various batch PHB profiles. This procedure consists of two additional test points on the PHB profile at a certain operational point after detection of profile critical point. First, the algorithm for detection of the PHB critical point is described and then the role of these two test points will be explained.

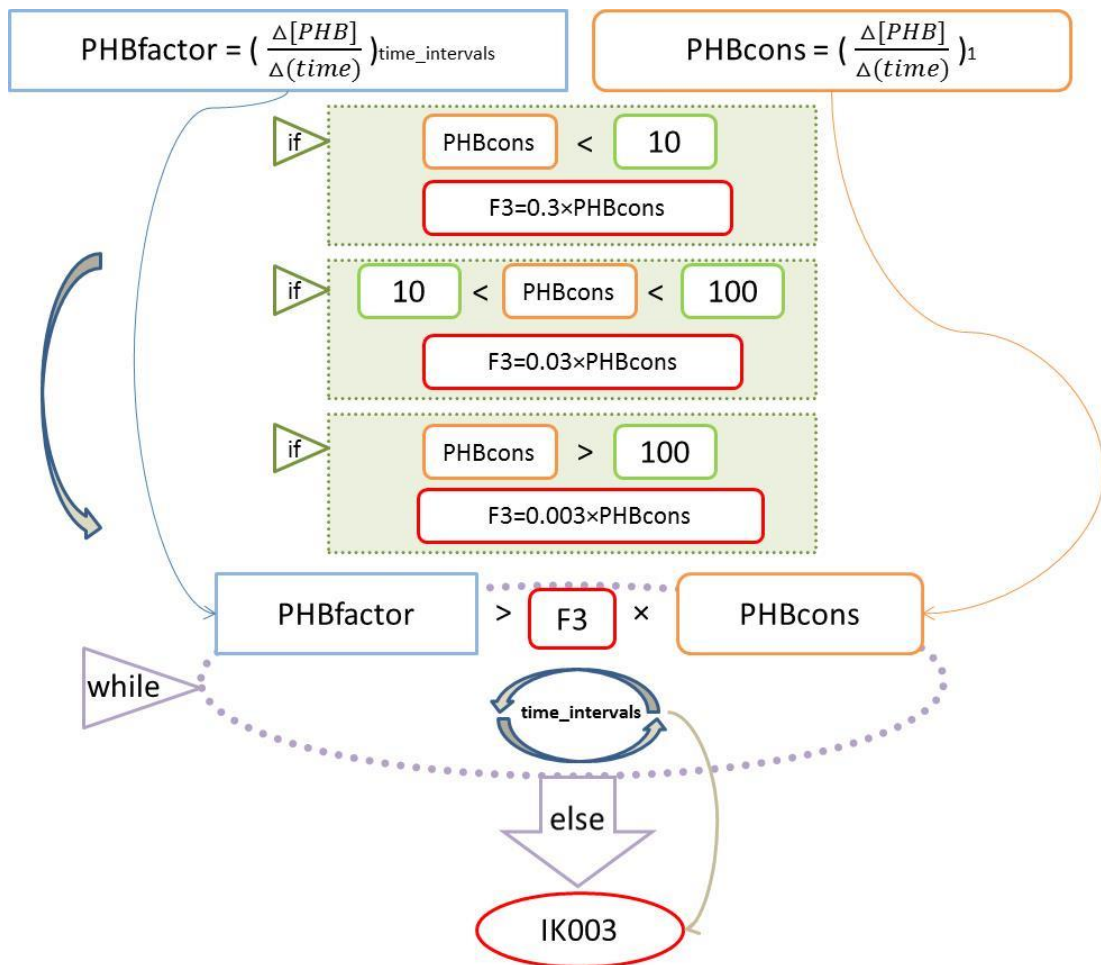


Figure 4.8 Descriptive depiction of “CharMeth” PHB module

In addition to the total PHB stability point in the profile, any sudden change in the profile curvature is required to be detected by the main analytical algorithm. Similar to

the previous algorithms, a vector of absolute first order total PHB values in respect to the operational time is defined as “PHBfactor” and its first value for the initial point of the simulation process is stored in “PHBcons”. The major modification in this algorithm is in definition of the multiplication factor, “F3”, in the structure of the iteration loop comparing derivative values. This factor is assigned to be 0.3, 0.03 and 0.003 times the “PHBcons” value when “PHBcons” is less than 10 C-mmol/L, between 10 C-mmol/L and 100 C-mmol/L and more than 100 C-mmol/L respectively. These coefficients are specified based on trial and error tests to tune the factor value for the scale of PHB profile when investigating best algorithm for detection of the PHB profile critical point. Figure 4.8 shows a depiction of the analytical algorithm embedded in the “CharMeth” module for detection of the critical point in the total PHB concentration profile.

At the end of the PHB profile analysis by the “CharMeth” module, the critical observation point is detected and stored in “IK003” as shown in Figure 4.8. Four different PHB profiles for four different batch operations are shown in Figure 4.9 along with their critical points illustrated with (●) sign indicators. These plots show that the proposed algorithm is able to detect both stability and curvature alteration in the total PHB concentration profiles.

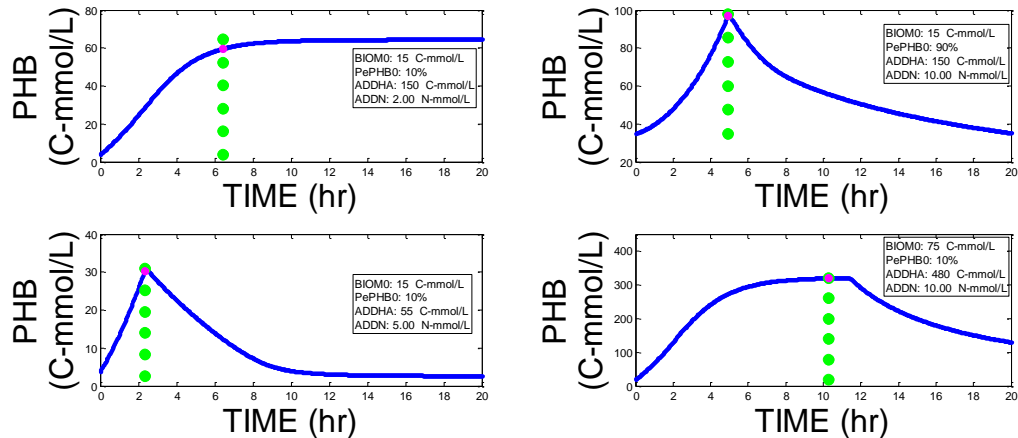


Figure 4.9 “CharMeth” analytical results on different PHB profiles (before activating the two additional analytical points)

As mentioned, two additional analytical points are considered to enhance profile analysis. The first additional point examines the PHB profile at a certain time step ahead of the main analytical point (the critical point). In this study, the time step for this analytical point is considered to be 10% of the total batch operation duration. The aim is to investigate if total PHB concentration is retained after the detection of the critical point or PHB is consumed within the 10% of total time period after detection of critical point.

The second additional analytical point is the last simulated operational data from a batch process. This test point is embedded in the algorithm to check the status of the final total PHB concentration in comparison with the total PHB concentration at the detected critical point. Figure 4.10 shows four different PHB profiles for four different batch operations with the addition of the first analytical point shown by (★) sign indicators when total PHB concentration does not drop within the 10% time period of detection of the critical point. It can also be noted that PHB concentration drops in three out of the four cases after detection of the critical point at the end of batch process.

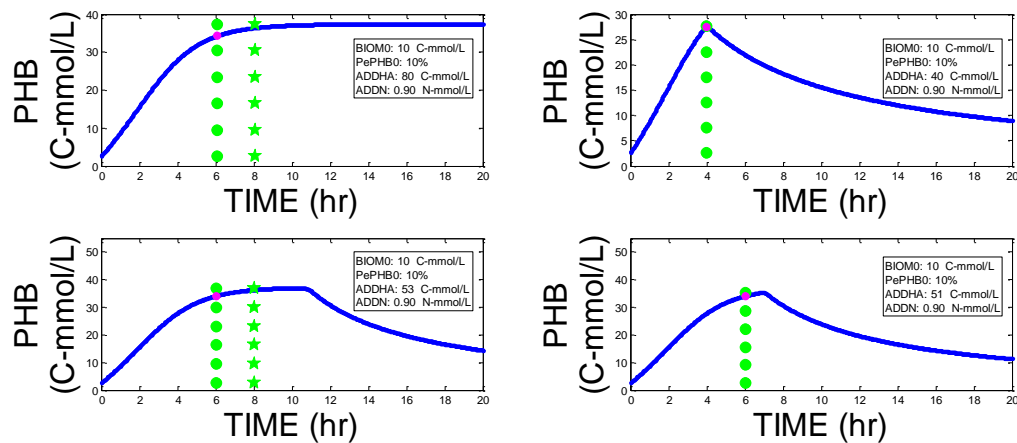


Figure 4.10 “CharMeth” analytical results on different PHB profiles (after activating the two additional analytical points)

The three analytical sections of the “CharMeth” module would store useful information about the three process profiles. In the following section of the study, the information obtained from this module will be combined and used to form acetate-ammonia-PHB plots for PHB production process under mixed microbial cultures.

4.4 Visualisation of process profiles

In this stage, acetate-ammonia-PHB plots are generated to provide better insight about process variables and their effect on the PHB profile. Figure 4.11 shows two acetate-ammonia-PHB plots for two typical PHB production batch runs. The acetate and ammonia detected critical points are also noted in the PHB profiles in order to provide better insight about the effect of these two critical points on the PHB profile.

As shown, in the two batch operations acetate, ammonia and PHB critical points in their profiles are correctly detected and noted. In the batch operation shown in Figure 4.11.a, ammonia depletion occurs prior to acetate stability point; whereas, in Figure 4.11.b, acetate depletion detected prior to ammonia exhaustion. These different feeding profiles have different effect on the PHB profiles that results into continues augmentation of

PHB for the first batch (Figure 4.11.a) and a PHB increase followed by a PHB drop in the second batch operation (Figure 4.11.b).

The “CharMeth” module contains the three analytical segments described in this section to detect ammonia, acetate and PHB profiles significant occurrences. With generation of the acetate-ammonia-PHB plot graphs, foundations are available to assign code values in code vectors as will be discussed in the next section.

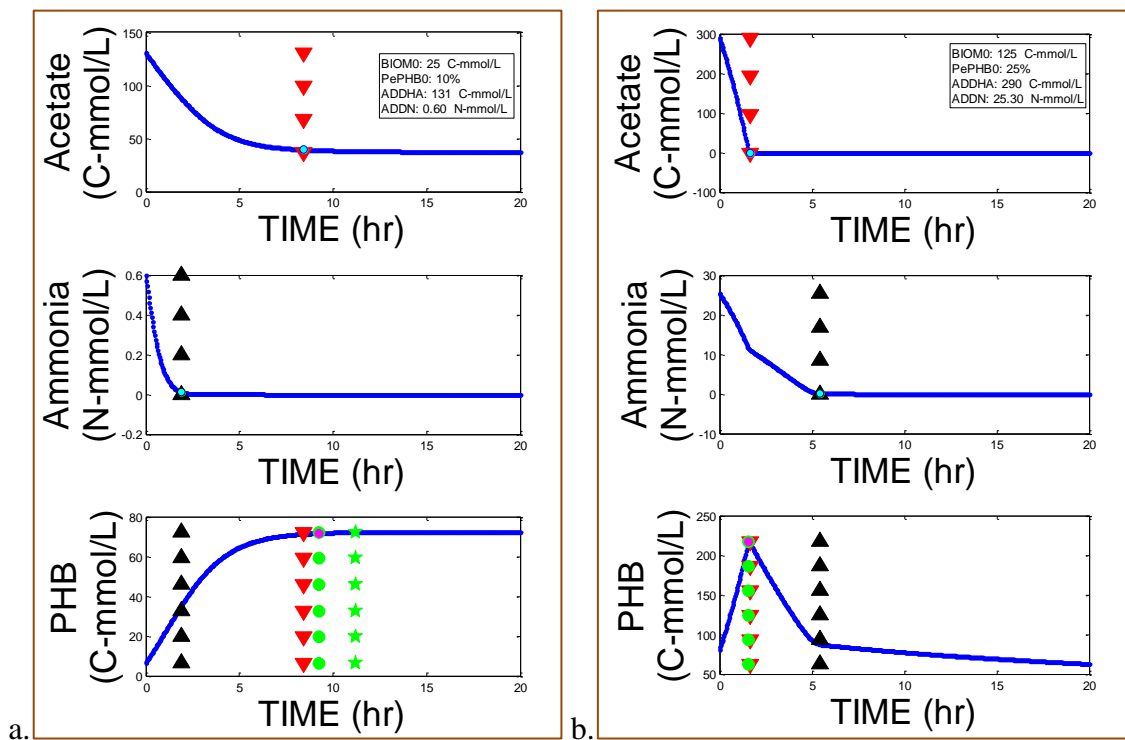


Figure 4.11 Acetate-ammonia-PHB plot for two typical simulation runs of the PHB process

4.5 Creation of code vectors: association of the significant process occurrences to the code values

With robust and reliable algorithms to detect significant occurrence points of the process profiles, the aim is to assign code values to each type of the significant occurrences. These code values will be used in the classification step in the subsequent stages. At the end of this step, a code vector is generated containing code values that enable qualitative interpretation of the acetate-ammonia-PHB plot obtained from process simulations. In fact, a certain set of code values can provide a rapport between process profiles that present similar qualitative characteristics. This property of identical code vectors builds up the foundation of the “Characterisation Method” in order to find clusters of process profiles with the same qualitative descriptions. These clusters will be used in direction of characterisation plot generation.

The code values are defined to reflect the analytical results obtained from the third step of the procedure. These code values are stored in an organized arrangement to form a Code Vector (CV) at the end of this stage. It is evident that both code values and their positions in the CV should be carefully considered to avoid any misinterpretation or information lost in deciphering stage.

In the case of the PHB production process, a series of acetate-ammonia-PHB plots were generated and scrutinised with the aim of generating appropriate coding mechanism that fits to the process specifications. Table 4.1 associates code values in the specified code vector (CV) with qualitative descriptions that can be obtained by analysing various acetate-ammonia-PHB plots.

Table 4.1 Definition of code values and their position in the code vectors

CV position	Assigned value	Description
CV(1)	1	Acetate and ammonia are both present in the system at the initial point
CV(1)	0	Acetate or ammonia is absent in the system at the initial point
CV(2)	1	Stability of ammonia profile is detected
CV(2)	0	Stability of ammonia profile is not detected
CV(3)	1	Stability of acetate profile is detected
CV(3)	0	Stability of acetate profile is not detected
CV(4)	1	Acetate complete depletion is detected
CV(4)	0	Acetate is present at the end of the process
CV(5)	2	Acetate depletion is detected prior to ammonia depletion
CV(5)	1	Ammonia depletion detected prior to acetate stability point/depletion
CV(5)	0	Acetate or ammonia stability point is not detected or both occur simultaneously
CV(6)	3	PHB growth rate decreases before PHB drop
CV(6)	2	PHB grows to its saturation point
CV(6)	1	PHB drop detected with no prior PHB stability detection
CV(6)	0	Immature augmentation of PHB
CV(7)	1	PHB profile maintains its saturated concentration at least up to the first additional analytical point
CV(7)	0	PHB profile does not maintain its saturated concentration

This table is formed based on a series of observations carried out on acetate-ammonia-PHB plots of different batch operations. It should be mentioned that the setting defined in this study is not unalterable and different arrangement of coding can be considered to map PHB batch process behaviour. The code vector consists of seven elements with the first five focusing on the two feeding concentration profiles of acetate and ammonia and the last two elements comprising information about the PHB profile.

In the first position, existence or absence of acetate and ammonia in the medium at the initial point of the process is investigated. In the second code vector position, the focus is on the ammonia profile independent of any other process profiles. Two code values

are considered to demonstrate detection or concealment of ammonia stability point in the profile. Due to the nature of the PHB batch process, biomass replication continuous until nitrogen source (ammonia) is completely exhausted in presence of the carbon sources (acetate or PHB). Since carbon is available in either the PHB form or acetate, and no limitation is considered for biomass growth, ammonia is completely consumed in the majority of mature production batches.

The acetate profile analysis determines code values for the third and the fourth vector positions independent of the other two profiles (ammonia and PHB). In the third vector position, detection of acetate stability point is coded while in the fourth vector position existence or complete exhaustion of acetate by the end of the batch profile is recorded.

The fifth element of the code vector is mainly associated with the order of significant sequences in the acetate and ammonia profiles. Absence of either acetate or ammonia stability point detection or occurrence of both points at the same time is assigned with code value 0 while code values 1 and 2 are assigned to demonstrate sequence of appearance of the acetate and ammonia stability points.

In the sixth vector position, a code value is assigned based on the PHB profile analysis independent of the feeding profiles. Four examples of PHB profiles for four different batch simulation runs are shown for each of the code values assigned to the sixth vector position in Figure 4.12.a, Figure 4.12.b, Figure 4.12.c, and Figure 4.12.d for the code values 0, 1, 2 and 3 respectively. In this figure, ammonia, acetate, PHB stability points are indicated along with the first additional analytical point with (\blacktriangle), (\blacktriangledown), (\bullet), and (\star) sign indicators respectively.

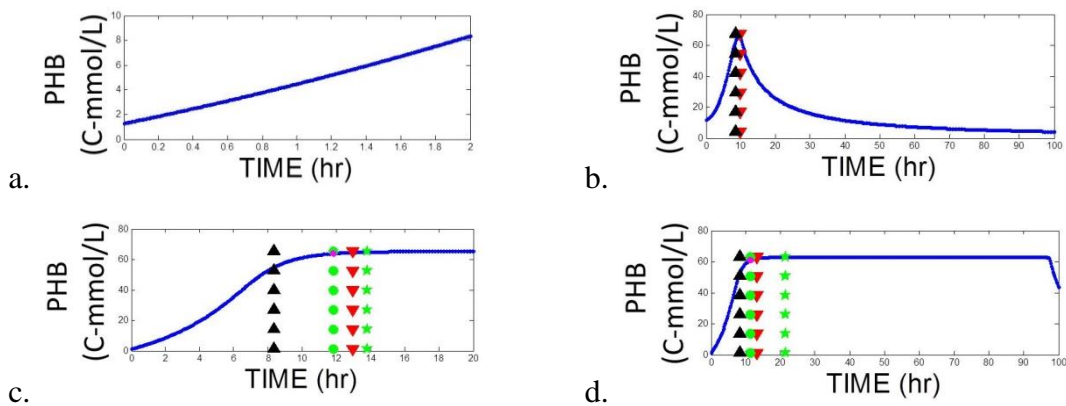


Figure 4.12 Definition of code values for the sixth code vector position

In the seventh vector position, maintenance of the PHB saturation concentration is coded considering the first additional analytical point defined in the “CharMeth” third module in Section 4.3.3.

By the end of this stage, foundations are prepared in order to assign appropriate code vectors to a simulated PHB batch process. In the next step of the “Characterisation Method” development procedure, a bank of code vectors is created to form the basis of the analysis in the subsequent steps of the method.

4.6 Creation of the bank of code vectors

4.6.1 Application of “CharMath” module for code vector bank generation

With the advent of high speed computation machines, it is possible to perform several hundreds of simulated processes with varying initial parameters in a relatively short period of time. The “Characterisation Method” takes good advantage of the computer-based simulators in high speed process screening with the aim of generating a list of major code vectors appearing in simulations.

Assuming that a robust and reliable algorithm to detect points of significant occurrences in the process profile is available and that a structure has successfully developed to assign appropriate code values to the code vectors. In this step, the code vectors containing code values that represent a particular batch profile are identified and stored as the bank of code vectors. In other words, code vector bank consists of the code vectors that appear in process simulations in the case of different combinations of process variables.

In this stage, code vectors that appear in simulated batch operations are first numerated and then stored in an organised manner. Figure 4.13 shows general description of the fourth division of “CharMeth” module designed by the author to assign a code number to new code vectors or report the code number of the code vector previously registered in the code vector repository.

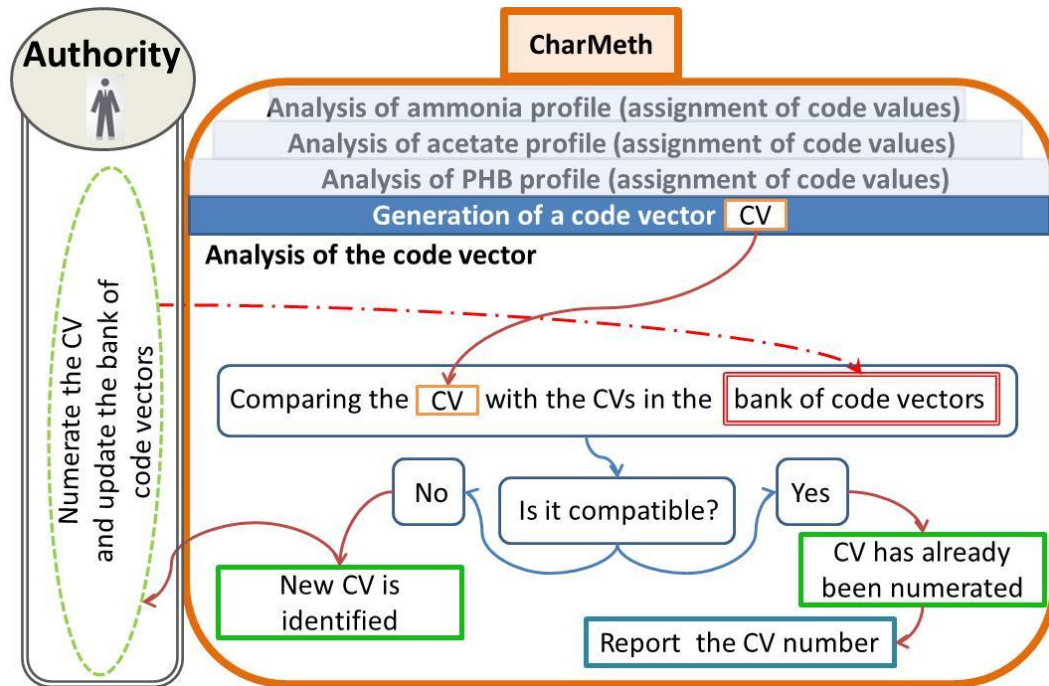


Figure 4.13 Code vector numerating procedure and development of the bank of code vectors

As shown in Figure 4.13, in the first three segments of the module, ammonia, acetate and PHB process profiles are analysed by the algorithm previously mentioned. The appropriate code values are assigned to the code vector associated with a batch process in the “CharMeth” module. This code vector is then compared with a set of code vectors previously stored in the code vector repository. If no match could be found for the generated code vector, an identical code number is assigned to this code vector and they are stored in the bank of code vectors. If an identical pair of the code vector exists in the bank, the code number of the code vector in the bank is reported for the batch process being analysed. There are numerous possibilities for the code vectors. However, only a few numbers of these possible cases occurs when codes are assigned to the actual process profiles in simulated batches. The bank of code vectors contains code vectors appeared in the analysis of different process profiles and therefore it is limited to the combinations occurred in simulations for code values.

4.6.2 Screening process

With the aim of identifying the possible code vector combinations, batch profiles are generated using the simulation program introduced in Chapter 3 and then analysed by the “CharMeth” analytical tool. The practice of assigning different feeding concentration pairs to the simulator is carried out in an organised manner in order to screen possible profile occurrences on different pairs of acetate and ammonia

introduced into batch operations. The screening process applied in this section initiates with minimal feeding concentration values and finishes on maximum values of the pair by covering the acetate range initially and then augmenting ammonia concentrations subsequently. In each screening procedure, process parameters such as initial total biomass concentration, initial PHB content of the bacteria cells and batch operational duration are recorded as the operational variables.

A screening plot for a specific process is a two dimensional graph illustrating the code vector number of the process profiles for each pairing of the two process variables forming the graph axes. A screening plot can provide a general insight to the process behaviour regarding the two dominant variables effacing the process. Visualisation of the process qualitative behaviour can potentially lead to obtaining valuable information about the process and can open a window to improve the process monitoring and control scheme.

In this report, first few screening runs are described in this section and the results for the remaining screening plots are given in Appendix-A. In the beginning, no code vector is recognised and the bank of code vectors is empty. Therefore, all the code vectors generated in the first screening process are unknown to the analytical module. The first screening parameters are 5 C-mmol/L for initial biomass concentration, cells contain 10% of their maximum PHB content and batch operation continues for 2 hours. After the first screening execution, five code vectors are identified and registered in the code vector bank repository.

As the result of the first screening process, five new code vectors are identified and numerated. Table 4.2 tabulates the seven code values assigned to each of the five code vectors generated by “CharMeth” module in the first screening run process. These code vectors are stored in the bank of code vectors with an identical number. For instant, vectors $\begin{bmatrix} 1 & 0 & 1 & 1 & 0 & 3 & 0 \end{bmatrix}$ and $\begin{bmatrix} 1 & 0 & 0 & 0 & 0 & 0 & 0 \end{bmatrix}$ are labelled by CV1 and CV2, respectively.

Table 4.2 Identified five code vectors in the first run of the screening process

	CV(1)	CV(2)	CV(3)	CV(4)	CV(5)	CV(6)	CV(7)
CV1	1	0	1	1	0	3	0
CV2	1	0	0	0	0	0	0
CV3	1	0	1	1	0	1	0
CV4	1	0	0	0	0	2	0
CV5	1	0	1	1	0	3	1

Figure 4.14 shows the screening plot generated when the five code vectors are defined in the “CharMath” module after execution of the first screening run. In this figure, code vector numbers are depicted for 25×25 batch operations initiating with different combinations of ammonia and acetate concentrations. On the X-axis, acetate concentration range is from around 0 to about 250 C-mmol/L and on the Y-axis ammonia range is from 0 to 5 N-mmol/L. The operational parameters are assigned based on the experimental results carried out to validate the batch simulator with the real experimental outcomes and other practical ranges given in the literatures (Serafim *et al.*, 2004; Dias *et al.*, 2005; Dias *et al.*, 2006).

In Figure 4.14, the five classified code vectors are depicted by “*”, “✖”, “●”, “✕”, and “○” iconic symbols to demonstrate occurrence of the first (CV1), the second (CV2), the third (CV3), the fourth (CV4) and the fifth (CV5) code vectors respectively. In addition to the iconic symbols, code vector numbers are also shown in black boxes for the bottom, middle, top iconic rows and the right edge of the screening plot.

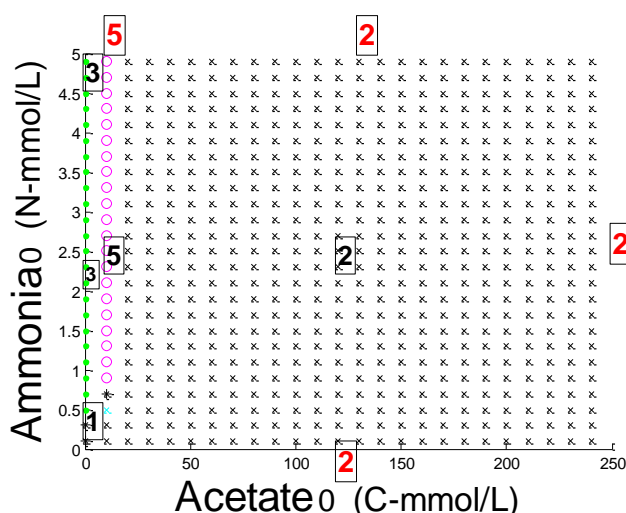


Figure 4.14 Illustration of code vector numbers for the first screening run on a screening plot after updating the bank of code vectors

In the second run of the screening process, batch operation duration is increased from 2 hours to 10 hours when other settings remained the same as the first screening process. Figure 4.15.a shows the screening plot for the screening outcome. As shown, only code vector number 1 (CV1) and code vector number 3 (CV3) were recognised by the “CharMath” module and the rest of the generated code vectors were unidentified. Some of the unidentified code vectors are noted with negative figures in the black boxes in the same subplot. In the second screening process, 11 new code vectors were identified, numerated and then stored in the “CharMath” module. The content of these code vectors and their identical numbers are tabulated in Table 4.3.

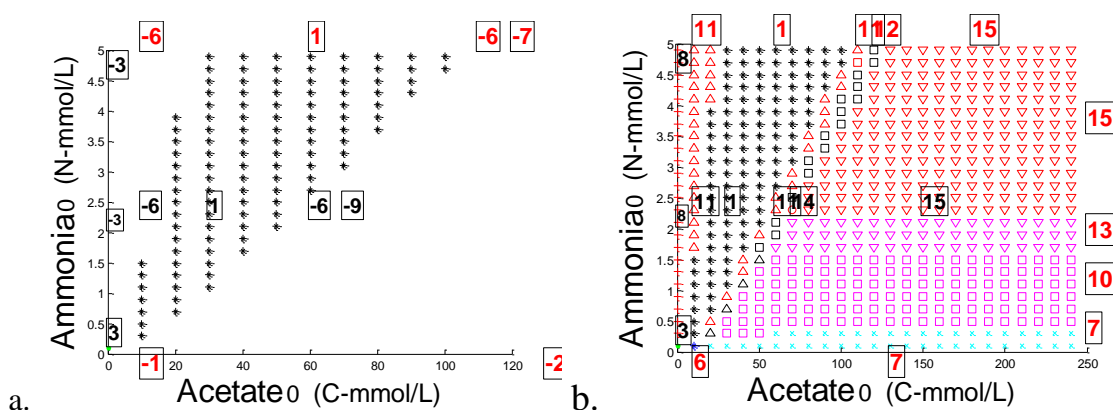


Figure 4.15 Illustration of code vector numbers for the second screening run on a screening plot before updating the bank of code vectors (a) and after updating the bank of code vectors (b)

When screening process is re-run with an updated “CharMeth” module, the screening plot of Figure 4.15.b is generated with the iconic symbols to demonstrate occurrence of different code vectors in different batches.

Table 4.3 Identified four code vectors in the second run of screening process

	CV(1)	CV(2)	CV(3)	CV(4)	CV(5)	CV(6)	CV(7)
CV6	1	1	1	1	2	3	1
CV7	1	1	1	0	1	2	1
CV8	1	1	1	1	2	1	0
CV9	1	1	1	1	1	3	1
CV10	1	1	0	0	0	2	1
CV11	1	1	1	1	2	3	0
CV12	1	1	1	1	1	3	0
CV13	1	1	0	0	0	2	0
CV14	1	1	1	0	1	3	0
CV15	1	1	0	0	0	0	0
CV16	1	1	1	1	0	3	0

The procedure mentioned in this section will be applied to execute various screening processes in order to develop a code vector bank containing the majority of the code vectors that can potentially occur during batch process analysis in the next section.

4.6.3 Expansion of the code vector bank by the screening process

In this section, in addition to the two screening runs mentioned in the previous section, a report of 32 screening runs for the purpose of developing a code vector bank that can represent majority of the batch operation profiles are tabulated in two tables. In Table 4.4, information obtained from 16 screening runs including the two screening runs mentioned in the previous section is tabulated. At the end of the 16 runs, total of 24 different code vectors are identified and stored in the “CharMeth” module as Registered

Code Vectors (RCVs). The screening plots related to this section can be found in Appendix A.

Table 4.4 Simulation parameters and the number of identified code vectors in each screening process (realistic parameter values)

Screening run number	Simulation parameters					Number of new CVs identified	Total number of RCVs
	BIOM0 (C-mmol/L)	PePHB0 (%)	Tcycle (hr)	ADDHA range (C-mmol/L)	ADDN range (N-mmol/L)		
1	5	10	2	0.1-5	0.1-250	5	5
2	5	10	10	0.1-5	0.1-250	11	16
3	5	10	20	0.1-5	0.1-250	0	16
4	5	10	100	0.1-5	0.1-250	2	18
5	5	90	2	0.1-5	0.1-250	1	19
6	5	90	10	0.1-5	0.1-250	0	19
7	5	90	20	0.1-5	0.1-250	0	19
8	5	90	100	0.1-5	0.1-250	2	21
9	70	10	2	0.1-5	0.1-250	1	22
10	70	10	10	0.1-5	0.1-250	0	22
11	70	10	20	0.1-5	0.1-250	0	22
12	70	10	100	0.1-5	0.1-250	0	22
13	70	90	2	0.1-5	0.1-250	1	23
14	70	90	10	0.1-5	0.1-250	0	23
15	70	90	20	0.1-5	0.1-250	1	24
16	70	90	100	0.1-5	0.1-250	0	24

In order to provide a more comprehensive set of RCVs in the code vector bank, 16 screening runs are executed with unrealistic extended simulation parameters. The screening plots obtained from this process provide a wider insight about general behaviour of the batch operation. Table 4.5 tabulates a summary of the simulation parameters and the number of code vectors identified in each screening process.

Table 4.5 Simulation parameters and the number of identified code vectors in each screening process (extended unrealistic parameter values)

Screening run number	Simulation parameters					Number of new CVs identified	Total number of RCVs
	BIOM0 (C-mmol/L)	PePHB0 (%)	Tcycle (hr)	ADDHA range (C-mmol/L)	ADDN range (N-mmol/L)		
17	150	0.1	2	0.1-10	0.1-500	0	24
18	150	0.1	10	0.1-10	0.1-500	0	24
19	150	0.1	20	0.1-10	0.1-500	0	24
20	150	0.1	100	0.1-10	0.1-500	0	24
21	150	0.9	2	0.1-10	0.1-500	0	24
22	150	0.9	10	0.1-10	0.1-500	0	24
23	150	0.9	20	0.1-10	0.1-500	0	24
24	150	0.9	100	0.1-10	0.1-500	0	24
25	1,000	0.1	2	0.1-3,000	0.1-70,000	0	24
26	1,000	0.1	10	0.1-3,000	0.1-70,000	1	25
27	1,000	0.1	20	0.1-3,000	0.1-70,000	0	25
28	1,000	0.1	100	0.1-3,000	0.1-70,000	0	25
29	1,000	0.9	2	0.1-3,000	0.1-70,000	0	25
30	1,000	0.9	10	0.1-3,000	0.1-70,000	0	25
31	1,000	0.9	20	0.1-3,000	0.1-70,000	0	25
32	1,000	0.9	100	0.1-3,000	0.1-70,000	0	25

It should be noted that only one more code vector was identified in the overall 16 screening process runs. This result demonstrates that the code vector bank comprising of the 25 registered code vectors capable of representing the general behaviour of the PHB operational batches. A complete set of the 25 code vectors registered in the code vector bank is tabulated in Table 4.6.

Table 4.6 Identified 25 code vectors in the 32 screening processes

	CV(1)	CV(2)	CV(3)	CV(4)	CV(5)	CV(6)	CV(7)
CV1	1	0	1	1	0	3	0
CV2	1	0	0	0	0	0	0
CV3	1	0	1	1	0	1	0
CV4	1	0	0	0	0	2	0
CV5	1	0	1	1	0	3	1
CV6	1	1	1	1	2	3	1
CV7	1	1	1	0	1	2	1
CV8	1	1	1	1	2	1	0
CV9	1	1	1	1	1	3	1
CV10	1	1	0	0	0	2	1
CV11	1	1	1	1	2	3	0
CV12	1	1	1	1	1	3	0
CV13	1	1	0	0	0	2	0
CV14	1	1	1	0	1	3	0
CV15	1	1	0	0	0	0	0
CV16	1	1	1	1	0	3	0
CV17	1	1	1	0	1	2	0
CV18	1	1	1	0	1	3	1
CV19	1	0	0	1	0	3	0
CV20	1	1	1	1	1	1	0
CV21	1	1	1	1	0	1	0
CV22	1	1	1	1	0	3	1
CV23	1	1	0	1	0	3	0
CV24	1	1	1	0	1	1	0
CV25	1	1	1	0	1	0	0

It is clear that the dominant code vectors with frequent presence in the screening procedure should gain more attention as they represent the more dominant process behaviour. On the other side, the less frequent code vectors exhibit combinations of code values that appear only in simulation runs. This is due to high precision and sensitivity of the mathematical calculations carried out in the simulation program. In any case, each code vector and their position on the screening graph should be closely studied to gain insight about the process operational behaviour. In this regard, code vector classification will be carried out in the next section.

4.7 Classification of the registered code vectors

The registered code vectors should be studied in line with the batch profiles with the aim of detecting similarities and dissimilarities between batch profiles of different set of code vectors. Since process data generation and execution of the “Characterisation Method” are both carried out by mathematical computations, the precision of the calculations is considerably high. The high precision imposes non-necessary complexity to the code vector analysis when different code vectors are assigned to batch profiles which are inherently alike. Additionally, some different combinations of the code values

in the code vectors might refer to the same type of process profile with an identical qualitative description. Hence, investigations should be carried out to classify code vectors based on their qualitative descriptions. The code vectors that present similar batch profiles should be classified as a group with identical qualitative description.

For this purpose, both the acetate-ammonia-PHB plot of the batch profiles and the screening plots demonstrating the code vectors obtained from the screening process should be utilised. The acetate-ammonia-PHB plots of process profiles are highly valuable especially when recognition of similarities and dissimilarities between different sets of code vectors is favourable. Figure 4.16, acetate-ammonia-PHB plots are shown for a batch process initiating with 5 C-mmol/L biomass (BIOM0), 10% initial PHB content (PePHB0), 0.1 C-mmol/L acetate (ADDHA), 0.1 N-mmol/L ammonia (ADDN) for duration of 2 hours (Tcycle). The analytical result obtained by the “CharMeth” module represents the code values as

1	0	1	1	0	3	0
---	---	---	---	---	---	---

 which indicates occurrence of the 1st code vector (CV1). In this figure, illustrative indicators are also depicted on each of the acetate-ammonia-PHB plots when required.

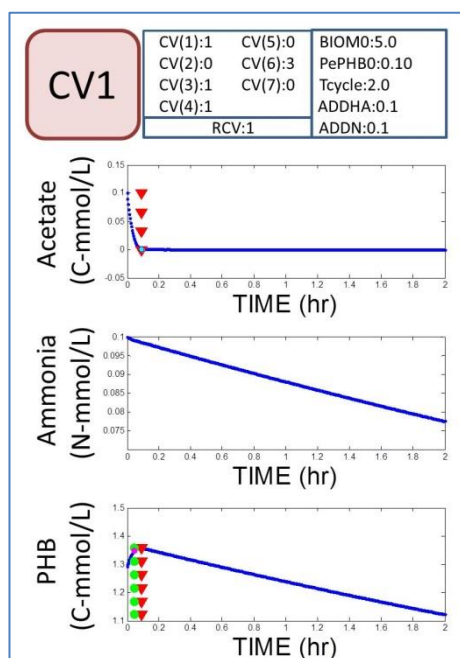


Figure 4.16 Demonstration of an acetate-ammonia-PHB plot for the 1st code vector

In a rare situation, the algorithm designed to identify a significant occurrence by means of the “CharMeth” module fails to operate correctly. For instance, in the 18th code vector acetate-ammonia-PHB plot shown in Figure 4.17, the code value assigned to the fourth code vector position is 0 which indicates existence of acetate at the end point of the batch process. However, looking at the PHB profile, it is evident that PHB

concentration drops at about 96 hours from the batch initial operation point due to acetate complete exhaustion. This failure is compensated by the “CharMeth” PHB submodule which indicates PHB drop at the late stage of the batch process with the sixth code position assigned to 3. Therefore, a reflection of the acetate exhaustion can be observed in the set of code values assigned by the “CharMeth” module which results into identification of correct regime type at the end of the analytical process. These rare occurrences do not reduce the reliability of the method especially when their registered code vectors are captured for a specific regime type number as explained in Section 4.7.2.

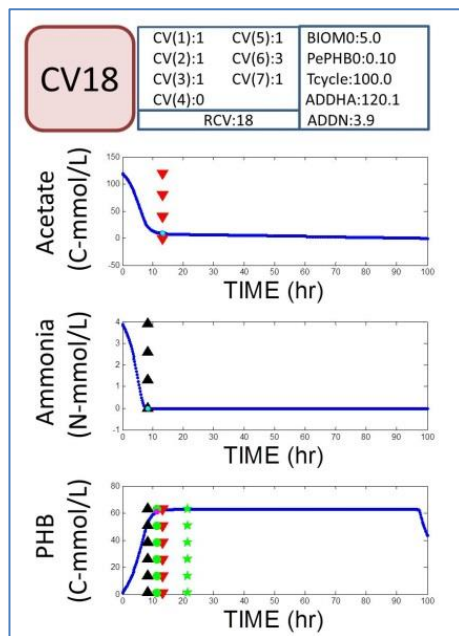


Figure 4.17 Demonstration of the acetate-ammonia-PHB plot for the 18th code vector

A series of acetate-ammonia-PHB plots are given in Appendix B as typical examples of batch profiles for each combination of the 25 registered code vectors. Moreover, the screening plots generated in the screening process provide general insight about PHB process operational progression using the code vectors. This enables the process investigator to observe the sequence of code vector appearance in an operating batch process. In the following section, application of the screening plots for extended unrealistic biomass concentrations is discussed.

4.7.1 Application of the screening plots in code vector classification

In order to observe general behaviour of the batch operations, amplified concentration of acetate, ammonia and biomass is considered in batch simulations. These simulation parameters are chosen to be extremely high (practically unrealistic) so that small fluctuations of variables have insignificant effect on the screening plots. In Figure 4.18, six screening plots show operational progression batch simulations for 2, 7, 12, 18, 23 and 300 hours after process initiation. In these plots, the colour bars associate the registered code vector numbers with the areas on the screening plots that represent batches with the same code vector number. The dominant code vector areas are also numerated on each plot.

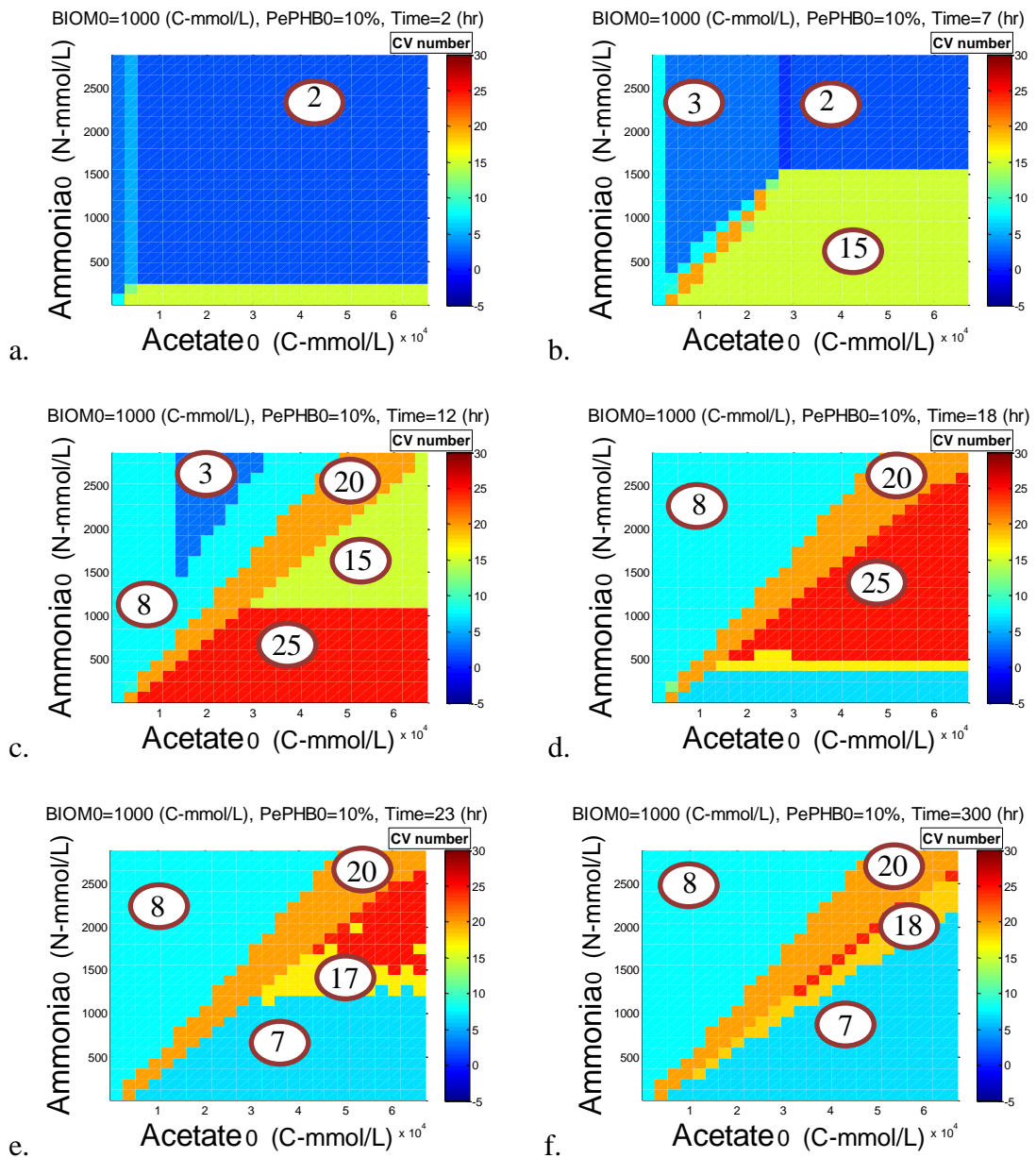


Figure 4.18 Screening plots for extended unrealistic biomass concentrations

After 2 hours of process operation, the majority of batch operations with initial biomass concentration of 1,000 C-mmol/L, PePHB0 of 10% and various combinations of feeding acetate and ammonia concentrations present code vector number 2 as a qualitative profile representation in Figure 4.18.a. Further progression of these batch processes up to 7 hours of process operation led to code vector presentation depicted in Figure 4.18.b with emergence of code vector numbers 3 and 15. Additional progression of the batch processes shown in the plots of Figure 4.18.c, Figure 4.18.d, Figure 4.18.e, and Figure 4.18.f demonstrate appearance of CV8, CV15, CV17, CV18, CV20 and CV25 in addition to CV2, CV3 and CV15.

CV2 is the code vector that represents the batch operation at its initial stage. As shown in Figure 4.18.b, CV2 is altered to either CV3 or CV15. The batch operations under CV3 eventually terminated in CV8 to form the first operational pathway. The batch operations under CV15 grew into either CV20 or CV25 as shown in Figure 4.18.c and Figure 4.18.d. The batches labelled with CV25 grew into CV17, CV7 and eventually CV18 as shown in Figure 4.18.e and Figure 4.18.f.

Looking at the six plots in Figure 4.18 three operational pathways can be observed for a batch process to grow into. These three pathways are depicted in Figure 4.19 with the first pathway consisting of CV2-CV3-CV8, the second pathway comprising CV2-CV15-CV20 and the third pathway residing on CV2-CV15-CV25-CV17-CV7-CV18.

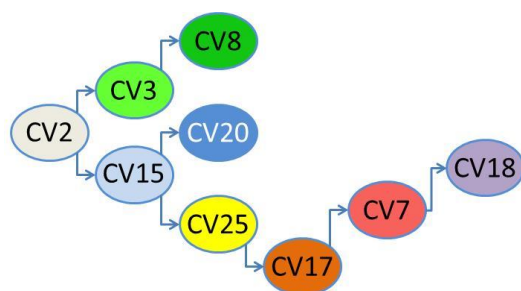


Figure 4.19 Code vector representation for operational progression

These nine registered code vectors will be used to define operational regime types in the next section.

4.7.2 Definition and initial classification of Regime Types

Regime Types (RTs) consist of one or a number of CVs that represent inherently similar batch profiles. Since nine dominant code vectors were identified in the previous section, nine regime type groups are defined for the PHB production process. In order to

numerate these nine regime type groups, the structure of Figure 4.19 is applied. Figure 4.20 shows the nine RTs numerated in the ascending order.

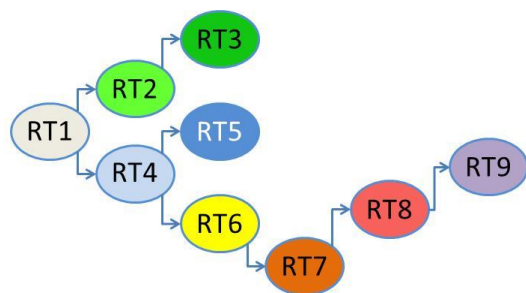


Figure 4.20 Numeration of regime types based on the structure of Figure 4.19

It is clear that the suggested arrangement is not the only manner of setting the numbers to the classification groups; however, it facilitates application of RT numbers. The arrangement showed in Figure 4.20 will be used throughout this study.

Up to this point, each RT group contains one CV member as obtained from the representations of the screening plots for unrealistically extended simulation process parameters shown in Figure 4.18. The first CV members in RT groups are tabulated in Table 4.7.

Table 4.7 Representation of the first CV members in RT groups

RT1	RT2	RT3	RT4	RT5	RT6	RT7	RT8	RT9
CV2	CV3	CV8	CV15	CV20	CV25	CV17	CV7	CV18

In order to classify other CVs into the nine RT groups, qualitative presentation of these nine regime types are given in the next subsection.

4.7.3 Qualitative description of the RTs

The qualitative acetate-ammonia-PHB plots representing each one of these nine regime types are shown in Figure 4.21. These plots were obtained using the acetate-ammonia-PHB plots of CVs associated with the regime types. This figure can be used as a reference tool for classification of other CVs in the RT groups. In this figure, ammonia, acetate, PHB stability points are indicated along with the first additional analytical point with (▲), (▼), (●), and (★) sign indicators respectively.

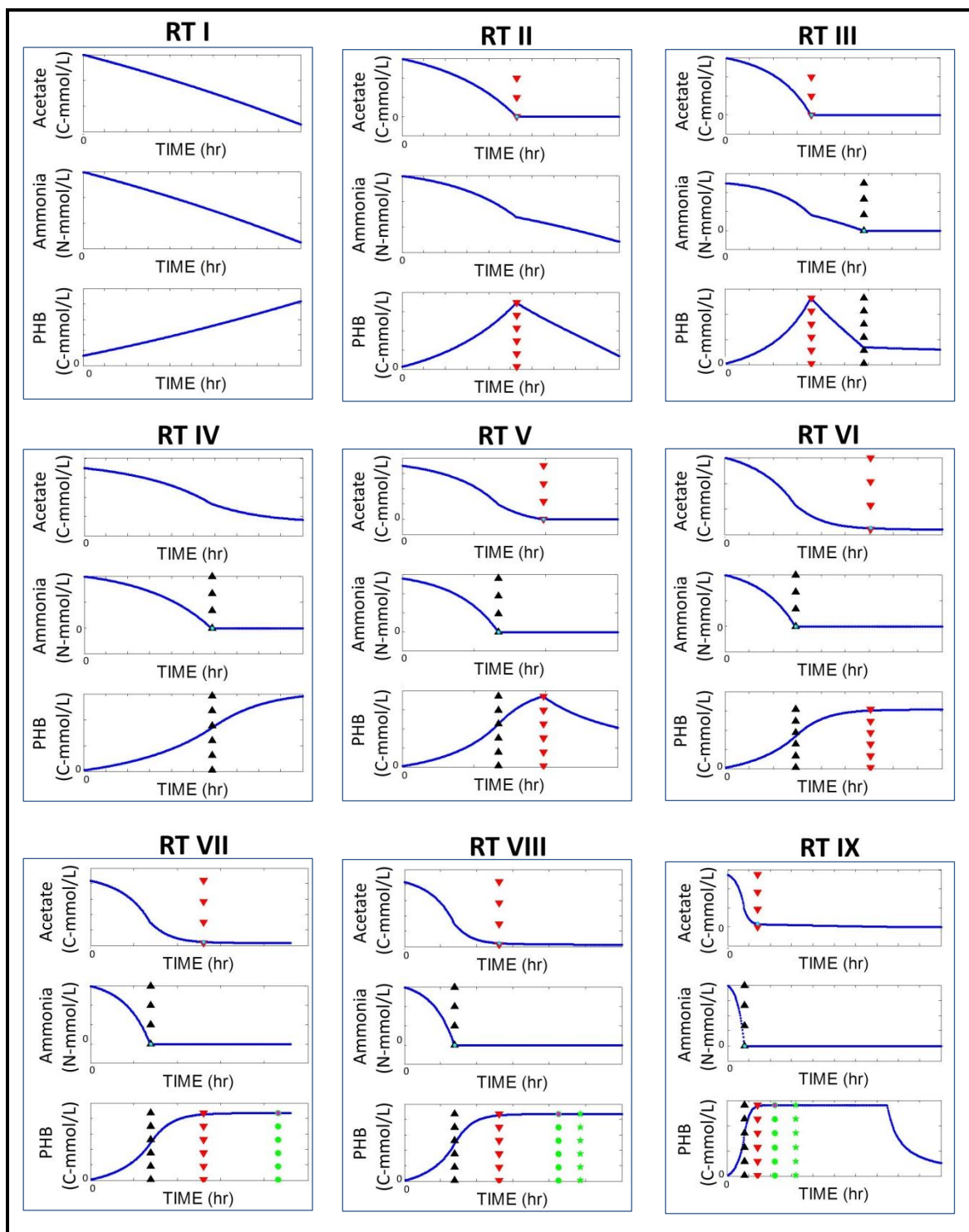


Figure 4.21 Qualitative acetate-ammonia-PHB representations for the nine dominant regime types

Qualitative description of the nine regime types are as follow:

RT1. The two feeding substrates of acetate and ammonia are continuously consumed throughout the operation resulting in continues biomass growth and PHB formation inside the cells.

RT2. Acetate complete exhaustion occurs within the operational time resulting in total PHB drop. After acetate scarcity, cells change their metabolic pathway from storing to consuming PHB as a carbon source inside them. In presence of ammonia and consumption of the carbon source in the PHB, biomass growth continues throughout this regime type operation.

RT3. Ammonia complete exhaustion follows acetate complete depletion within the operational time. Biomass growth halts with ammonia scarcity when PHB consumption rate decreases in reflection of biomass inactivity. RT2 is always followed by RT3 as depicted in Figure 4.20 (when enough operational time is allocated to complete the batch under analysis).

RT4. The main occurrence in this regime type is detection of ammonia complete depletion during the course of batch operation. After ammonia scarcity, PHB formation continues with acetate consumption; however, biomass replication is negligible.

RT5. Acetate complete exhaustion occurs after ammonia depletion during the batch operation resulting in total PHB drop. RT5 appears after RT4 in an operational batch process and terminates the second operational pathway with its appearance.

RT6. Acetate stability point is detected after ammonia depletion during the batch operation. The major differentiating factor between this regime type and RT5 is that acetate is present in the medium throughout an operation under RT6 whereas it completely exhausts in the case of RT5.

RT7. Similar to RT6, acetate stabilises with ammonia depletion. PHB stability point is also detected suggesting saturation of the product in the batch operation. From an operational viewpoint, RT7 represents the optimal operation time to terminate a production batch. Further progression of RT7 is associated with additional running cost while no significant improvement is made in PHB production.

RT8. At the initial point of the batch, both acetate and ammonia are present in the medium. Similar to RT6 and RT7, acetate stability point is detected with ammonia complete depletion. In addition to detection of the PHB saturation point, PHB profile

maintains its saturated concentration for at least 10% of the operational time (as defined for the seventh element of the code vectors in Table 4.1) after detection of the PHB stability point. In this regime type, batch operation runs longer than it is required but it is still acceptable when PHB production is addressed.

RT9. Similar to RT6, RT7 and RT8, acetate stability along with ammonia depletion is followed by detection of PHB saturation point in addition to its maintenance after 10% of the total batch operation. The main characteristic of this regime type is occurrence of a PHB drop after a period of PHB stabilisation due to acetate scarcity. This regime type appears when PHB production batch operates for a prolonged period. This regime type operation is not favourable when PHB production is the aim of the batch process.

From the regime type descriptions provided for RT6, RT7 and RT8 it can be noted that the process profiles are qualitatively similar and the single characterisation difference between them is the operational time factor. In case of RT6, PHB production is immature. In RT7, production batch is in its optimal point for termination. For the case of RT8, production process has stayed operational longer than it is required but not too long to fail the “feast” phase operation as in RT9.

The qualitative descriptions given above and the acetate-ammonia-PHB plot references provided in Figure 4.21 are used as the basis for classification of code vectors.

4.7.4 Classification of the code vectors in regime type groups

Up to this point, registered code vectors 2, 3, 8, 15, 20, 25, 17, 7 and 18 are assigned to regime types 1 to 9 respectively. In this section, the remaining registered code vectors found in the screening process are classified in the RT groups. In order to draw a rapport between each of the remained code vectors to a RT group, a combination of the process profiles and descriptive comparison analysis should be made. In effect, screening plots obtained in the code vector identification process can be very useful in code vector classification as well.

For instance, one of the screening plots in Appendix A (Run No.26) is shown in Figure 4.22.

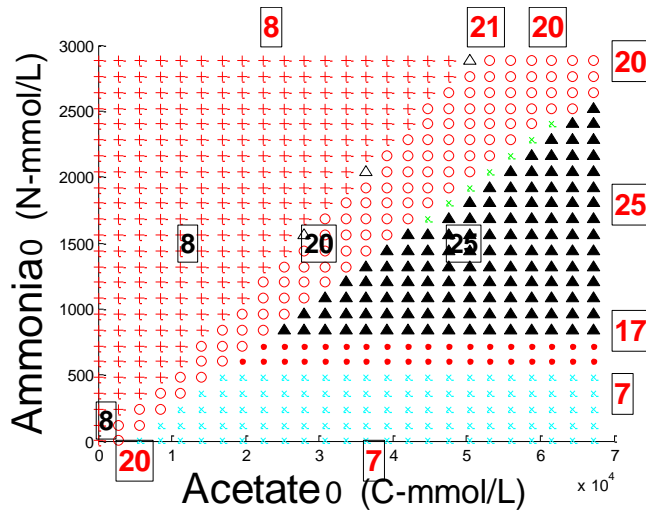


Figure 4.22 Demonstration of a typical screening plot

As mentioned before, the numbers in the boxes represent the code vector number of the batch process depicted with iconic symbols on the plot. In this case, iconic symbols “ \times ”, “+”, “●”, “○”, “ \triangle ”, “ \times ”, and “ \blacktriangle ” represent code vector numbers 7, 8, 17, 20, 21, 24, and 25 respectively. For the batches shown on the top row of the plot, CV21 is a rare occurrence placed in between CV8 and CV20. Since CV8 and CV20 are classified as RT3 and RT5 respectively (Table 4.7), CV21 should be classified as either one of the two regime types. Looking at the code values for CV21 in Appendix-A, it can be seen that the fifth element in its code vector which differentiates RT3 from RT5 has zero value stating that both feed stability points are detected for the same operational time. Therefore, CV21 can be classified as either of the two regime types by definition. However, since RT5 occurrence is less favourable than RT3 as will be explained in Chapter 6, CV21 is classified as RT5 to increase confidence bounds of RT3 estimation using the mathematical models predicting the regime types in Chapter 5.

In similar manner, each acetate-ammonia-PHB plot of the code vectors that is not classified in RT groups are investigated along with its code values in order to assign each registered code vector to an identical regime type group. In Table 4.8 all 25 registered code vectors are tabulated in the nine RT groups so that the members of the same group represent similar characterisations in their process profiles.

Table 4.8 Classified code vectors in the RT groups

RT1	RT2	RT3	RT4	RT5	RT6	RT7	RT8	RT9
CV2	CV1	CV6	CV15	CV9	CV25	CV13	CV7	CV14
	CV3	CV8	CV23	CV12		CV17	CV10	CV18
	CV4	CV11		CV16				
	CV5			CV20				
	CV19			CV21				
				CV22				
				CV24				

Based on regime type classifications, the representative acetate-ammonia-PHB plots depicted for registered code vectors in Appendix B are assigned to their regime type classes and illustrated in Figure 4.23.

The bank of registered code vectors have 25 members with the simulation runs carried out in this chapter. However, this number may increase if unrecognised code vectors are found. Since screening plots generated in this chapter includes wide range of process variability, it can be claimed that majority of the possible cases has been captured in the current set of RCVs. When a new code vector is identified and registered, the same procedure can be applied to classify the new RCV in a RT group.

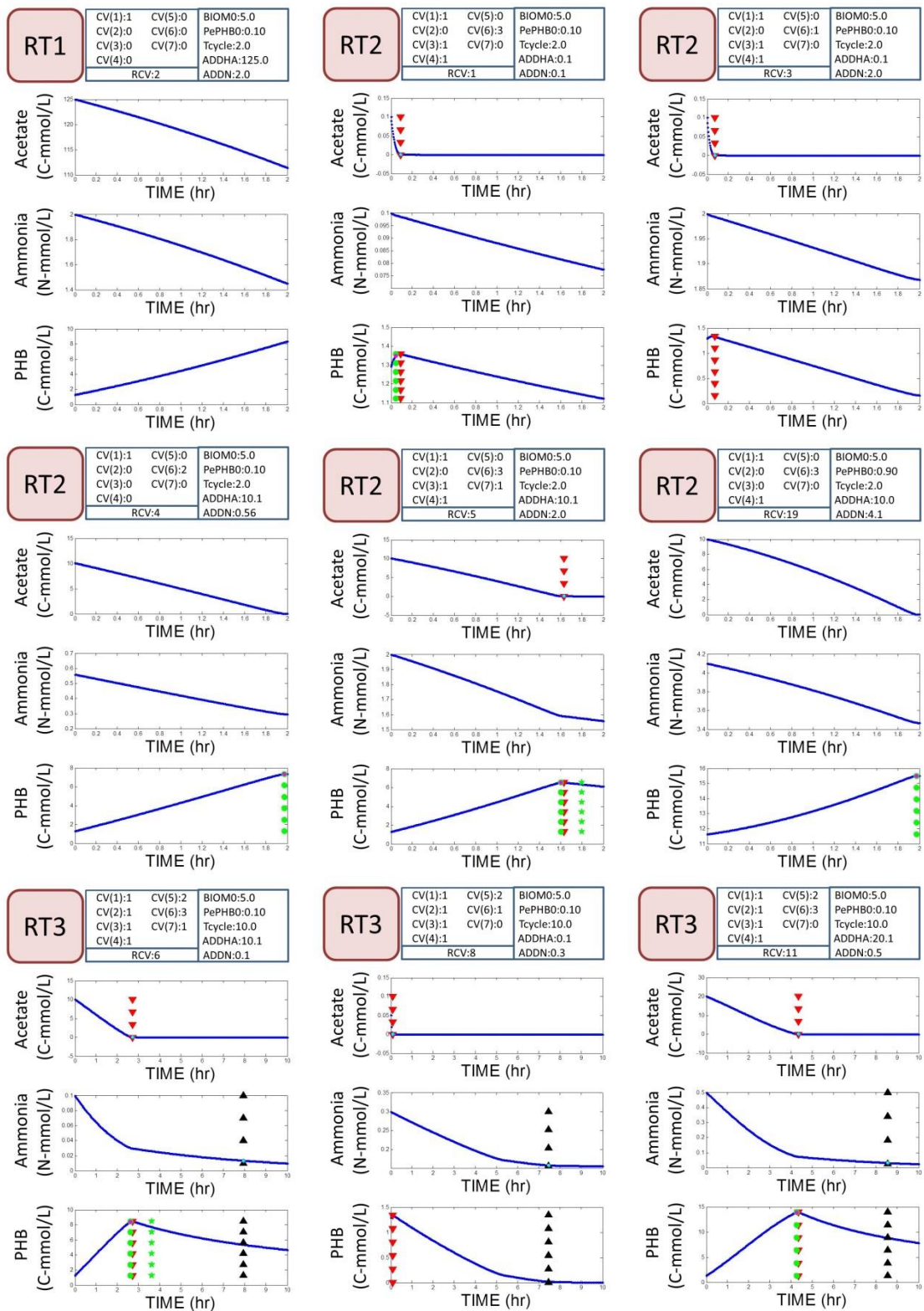


Figure 4.23 Typical representations of acetate-ammonia-PHB plots from RT1 to RT9 classes (continued)

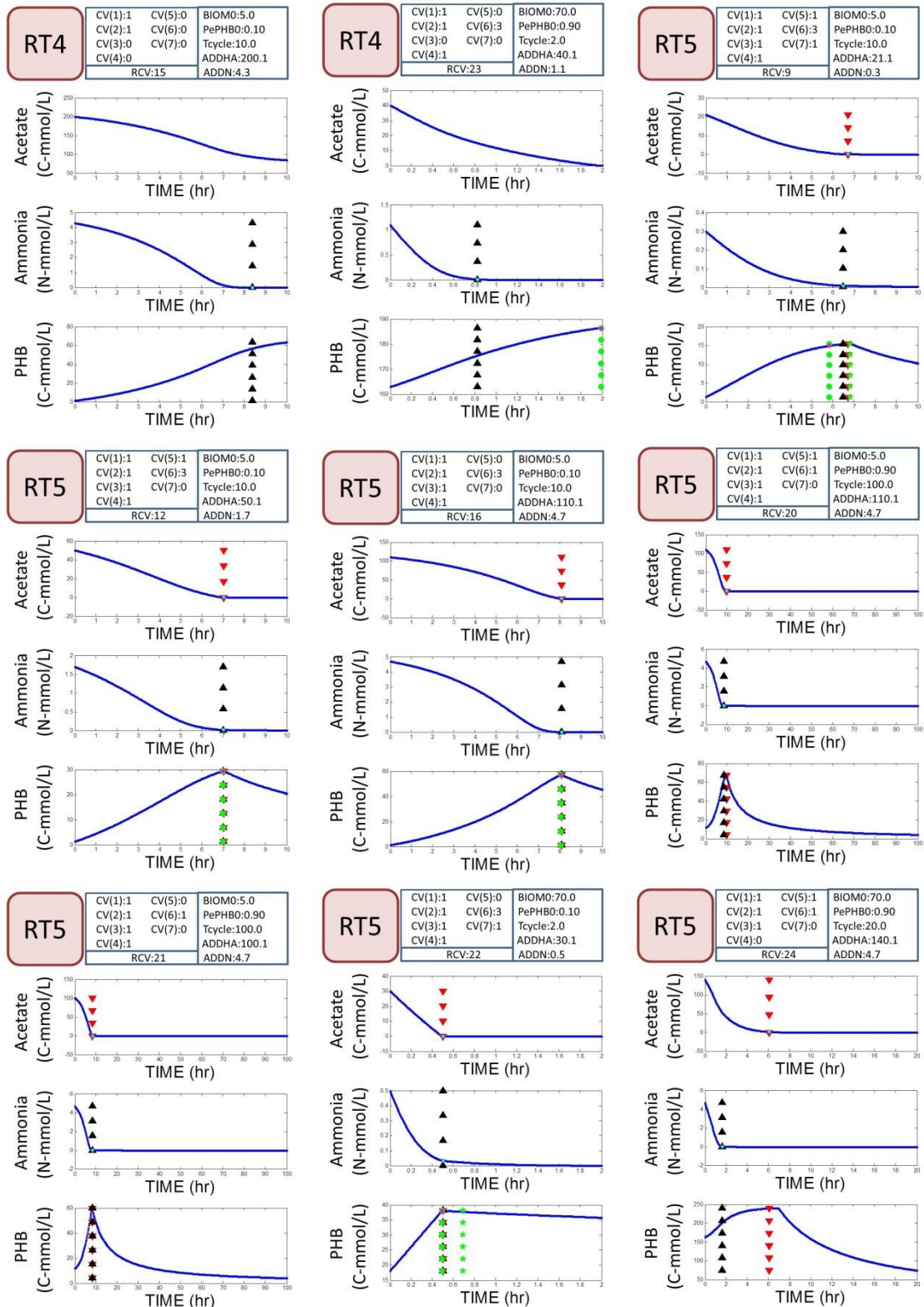


Figure 4.23 Typical representations of acetate-ammonia-PHB plots from RT1 to RT9 classes (continued)

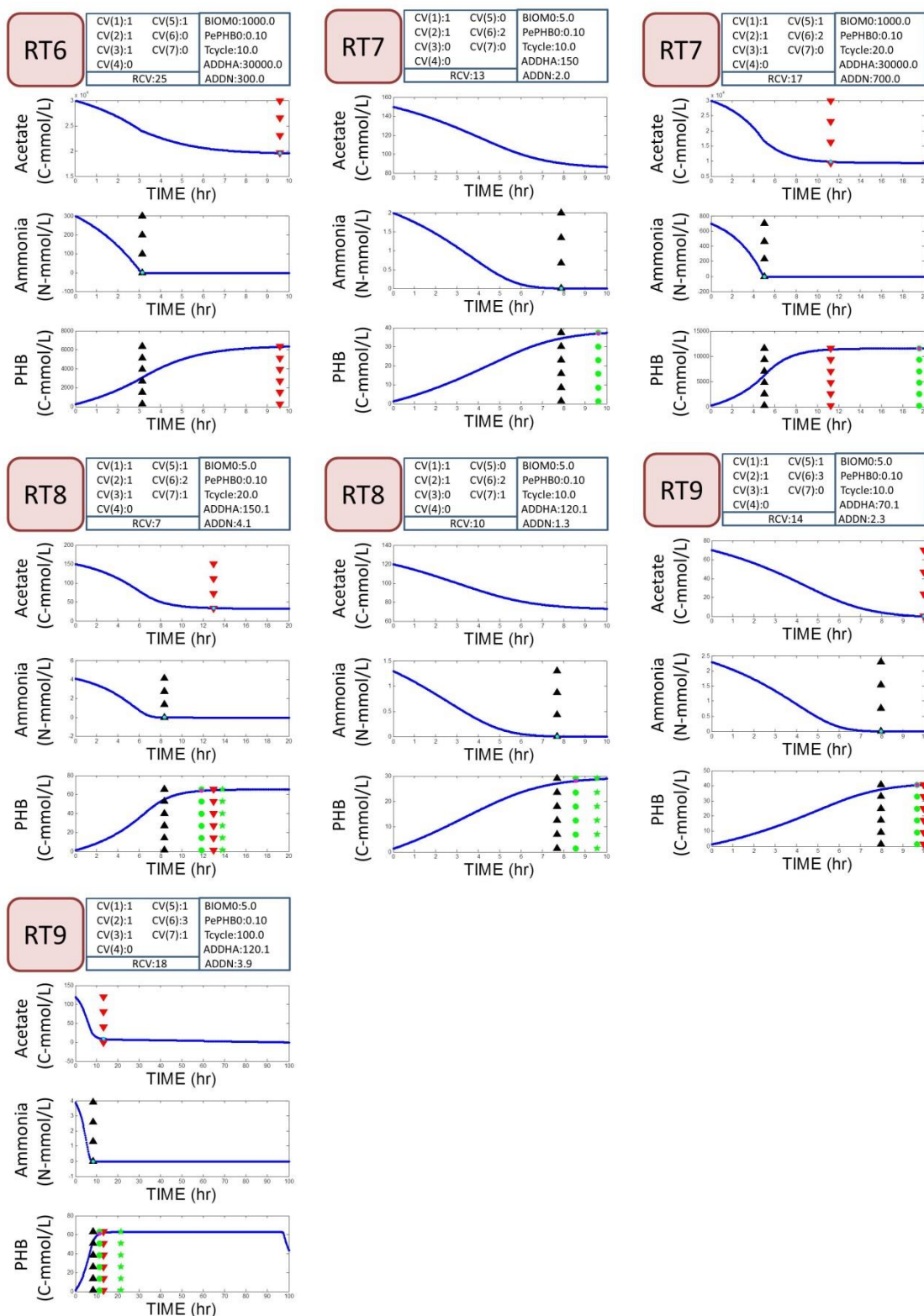


Figure 4.23 Typical representations of acetate-ammonia-PHB plots from RT1 to RT9 classes

With the proper classification of the code vectors, foundations are established to generate characterisation plots in the next division of the “Characterisation Method” development procedure.

4.8 Generation of characterisation plots

Based on the simulation studies, a characterisation plot for PHB production process is a two dimensional graph illustrating the regime types for each pairing of the acetate and ammonia variables. These plots are generated applying the same procedure mentioned in formation of the screening plots. However, in the case of characterisation plots, the classified RT numbers are used in place of the CV numbers in the illustrations. Figure 4.24 shows a progressive presentation of the screening plots along with their equivalent characterisation plots for a PHB batch process initiating with 90 C-mmol/L of biomass concentration containing intracellular PHB in the level of 15% of cells maximum PHB storage capacity. The progressive plots are depicted for 1, 2, 5, 9, 10, 15, 25 and 150 hours of batch operation from its initial operational point.

In Figure 4.24, CV numbers are depicted in the boxes of the screening plots; whereas, RT group numbers are given in the boxes shown on the characterisation plots. For the nine RT groups, iconic symbols “+”, “★”, “◆”, “▼”, “●”, “●”, “★”, “★” and “▲” are used to demonstrate RT1 to RT9 respectively.

Comparing the screening plots with the characterisation plots shown on the left and right sides of the Figure 4.24 demonstrates one of the advantages gained from classification of code vectors into regime types. As shown, a characterisation plot is a neat version of a screening plot with more apparent regimen region boundaries. Additionally, Figure 4.24 confirms validity of the procedural steps taken for classification of the code vectors by observing the results of the amplified simulation results (using extended unrealistically large parameter values) prior to the analysis of the simulation results under its practical range of the simulation variables. The initial biomass concentration applied in generation of Figure 4.18 was 1,000 C-mmol/L whereas in generation of Figure 4.24, this value is decreased to 90 C-mmol/L which is within the practical range of the variable (Serafim *et al.*, 2004; Dias *et al.*, 2005; Dias *et al.*, 2006). Despite the significant change in the scale of simulations, validity of the general operational pathways depicted in Figure 4.20 can be confirmed by the results obtained from the characterisation plots shown in Figure 4.24.

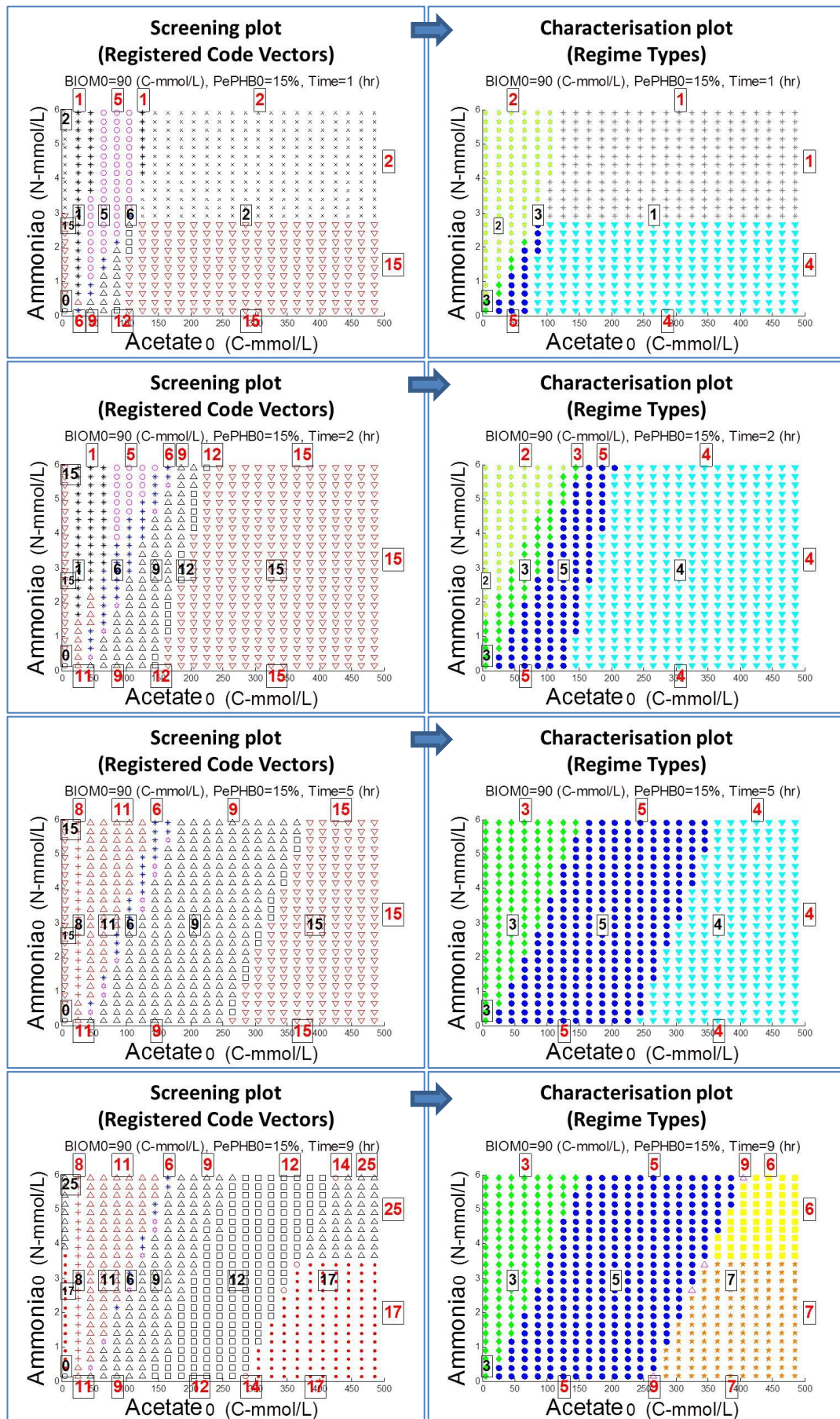


Figure 4.24 Progressive presentation of the screening and characterisation plots (continued)

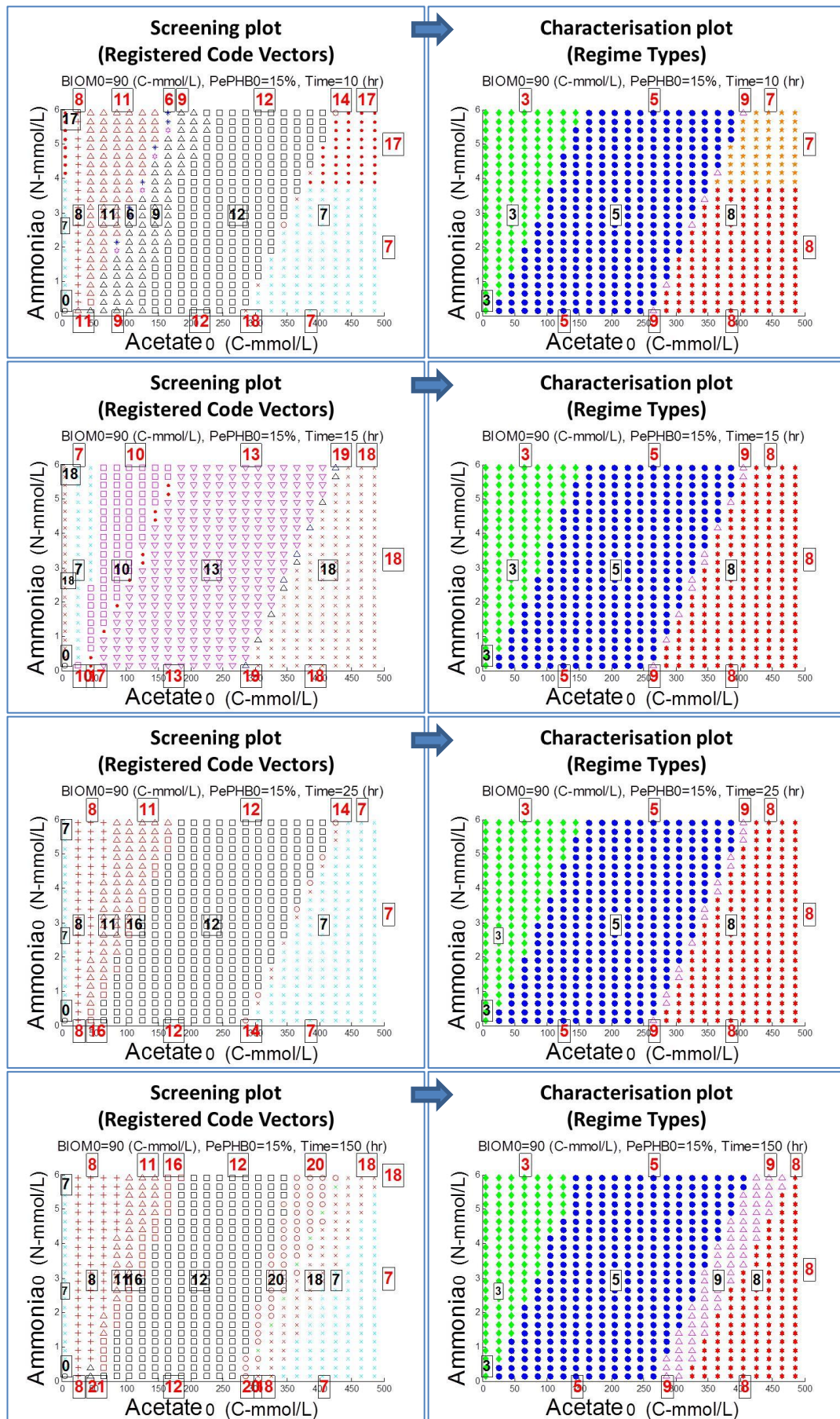


Figure 4.24 Progressive presentation of the screening and characterisation plots

In the next chapter, characterisation plots developed using the procedure mentioned in this chapter will be used to navigate different operational regions.

4.9 Conclusions

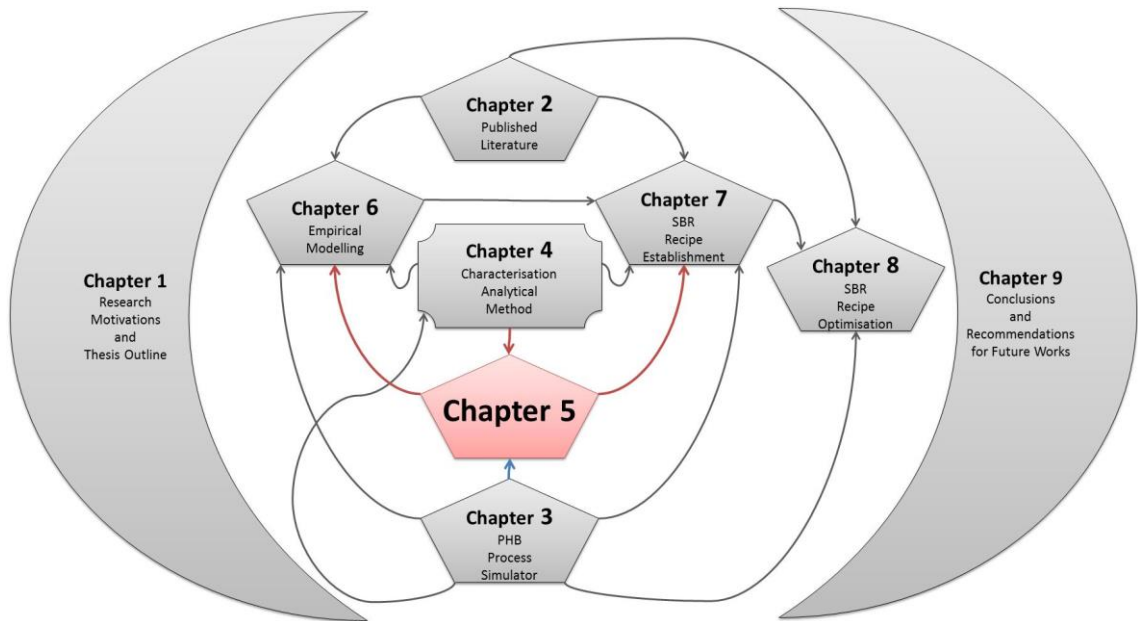
An analytical technique called “Characterisation Method” was developed by the author in this chapter. This technique is the main achievement of the research work in terms of novelty and originality. It plays a crucial role in generation of a mathematical model for prediction of a batch operational pathway based on process initial state in Chapter 5. Combination of the research outcomes in this chapter and Chapter 5 results into generation of a novel operational recipe for PHB production using MMC.

For the first time, prediction of classification of process regimens and batch operational pathways are made possible by the application of the “Characterisation Method” developed in this work which is a significant contribution to the field.

Complex biological behaviour of the process leading to PHB production with mixed microbial cultures acquires detailed analytical method for classification of various operational routes. Based on the observations obtained from the simulated PHB process, the feeding rate of acetate and ammonia demonstrated major effect on PHB formation. Therefore, batch profiles associated with the feeding and product concentrations were studied to create mathematical algorithm capable of identifying occurrences of high significance in the profiles. Successful release of the algorithms enabled systematic examination of various operational scenarios with the aim of generating meaningful codes enabling classification of operational regimen. The classified regimes were arranged in three operational pathways to exhibit process progression course from a batch initial state to its maturity point. The analytical results present a more vibrant demonstration of operational progression.

In the next chapter, application of the “Characterisation Method” for navigation of different operational regimen will be investigated. The mathematical equation obtained in the next chapter enables prediction of the operational phase in its maturity point using process data at the initial point of a batch.

Chapter 5 Identification of Regimen Boundaries on the Characterisation Plot



5.1 Introduction

In Chapter 4, a module code capable of analysing acetate, ammonia and PHB profiles was established for generation of code vectors associated with specific batch profiles for production of PHB under mixed microbial culture cultivation. These code vectors were classified into nine regime type groups with the aim of presenting more clear demonstration of operational progression and identification of operational regions associated with a specific regimen on characterisation plots.

In this chapter, analysis is carried out on the characterisation plots generated by the analytical module to identify operational regimen in characterisation plots generated for mature batch operations. Additionally, mathematical equations are developed to estimate the border curve separating the two most important operational regimens.

5.2 Definition of the operational phase border curve

Looking at the characterisation plots for progressive operational time depicted in Figure 4.24, a general pattern can be observed. Considering progressive characterisation plots, all batch operations initiate with RT1 and develop into either RT2 (case of primary acetate scarcity) or RT4 (case of primary ammonia scarcity) on the vicinity of the ammonia or acetate concentration axes respectively. RT2 grows into RT3 with total PHB concentration drop which indicates a “famine” phase operation. A batch process under “famine” phase undergoes total PHB reduction due to shortage of at least one element required for growth or replication of cells.

The fourth regime type (RT4) grows into either RT5 which also represents another “famine” phase regime type or it grows to RT6 when process is under continues PHB augmentation with a “feast” phase operation. In a “feast” phase batch, all elements for growth or maintenance of the total PHB content is available. As mentioned before, RT7 and RT8 appear following identification of RT6 in the vicinity of the acetate axis. Formation of RT9 occurs in the vicinity of RT5 and within the region already covered by RT8 when acetate scarcity leads to PHB consumption.

Figure 5.1 is drawn to show general pattern in progressive characterisation plots for the case of PHB production process. In this figure, Δt_x is defined as $(t_x - t_0)$ where t_0 is the time for batch process initiation and t_x represent the analytical time period of the process. Considering the process simulator as a representation of the PHB batch process, Δt_1 is around 2 to 5 hours, Δt_2 is around 4 to 10 hours, Δt_3 is around 8 to 25 hours and Δt_4 is about 100 hours or longer. It should be mentioned that t_4 is

considerably greater than t_3 to emphasise prolonged duration of the operation for formation of RT9.

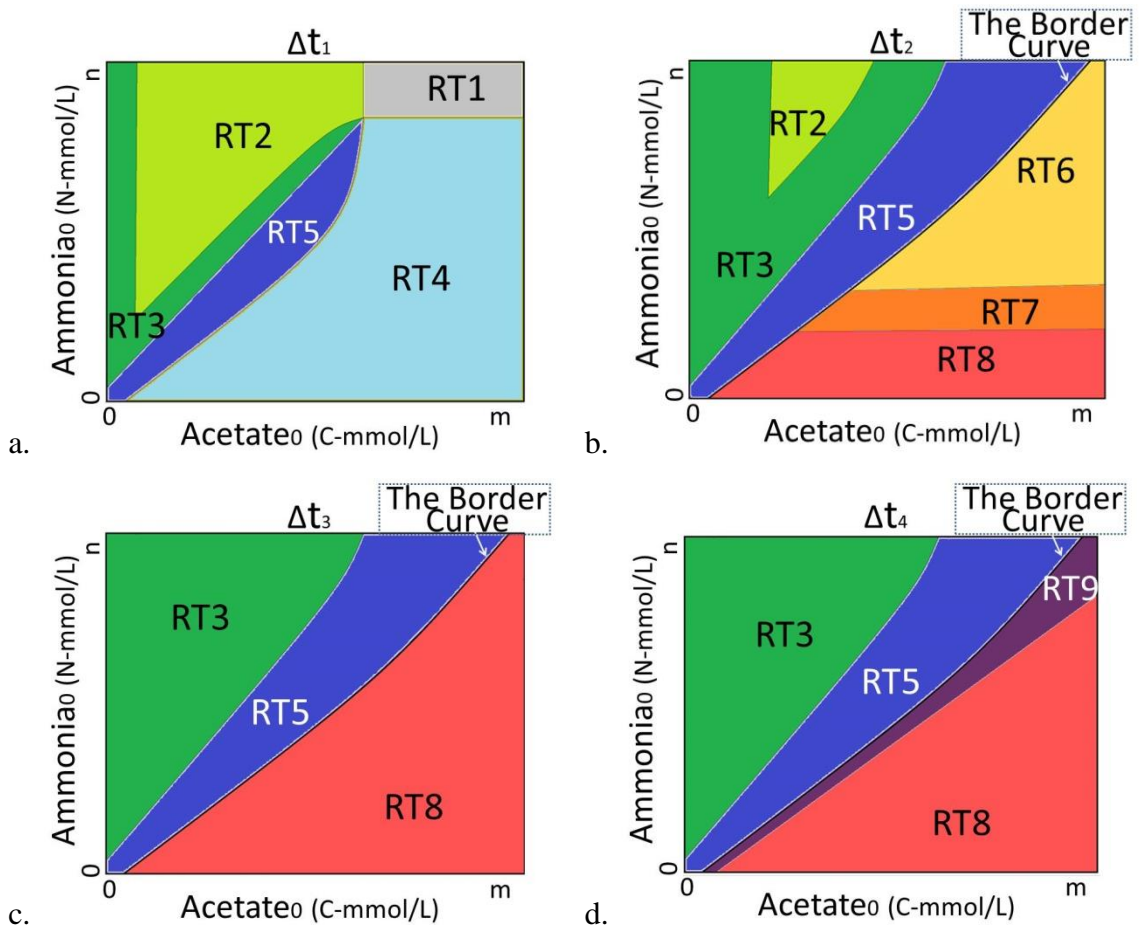


Figure 5.1 Progressive characterisation plot pattern in the case of PHB production process (operational time wise)

As depicted in Figure 5.1, operational regions can be separated by different border curves on a characterisation plot at a certain stage of the process progression. For a mature batch operation in which required time is allocated to a batch process, Figure 5.1.c shows an illustration associated to its characterisation plot. Figure 5.1.a and Figure 5.1.b depict characterisation plots of batch operations in their initial underdeveloped stages while Figure 5.1.d shows the plot for batches operated for prolonged duration which is unfavourable. Looking at Figure 5.1.c, three dominant regime types can be identified with one border curve separating RT3 region from RT5 region and the second border curve separating RT5 region from RT8. The later border curve appears identical in Figure 5.1.b and Figure 5.1.d as well to demonstrate that this curve remains unchanged as soon as regime phases are established. The initial, “feast” phase, and “famine” phase regimes are indicated separately in the three groups shown in

Figure 5.2. RT9 is an unfavourable regime type occurring in “feast” phase regimens since undesirable PHB concentration drop occurs at the late stage of the batch operation.

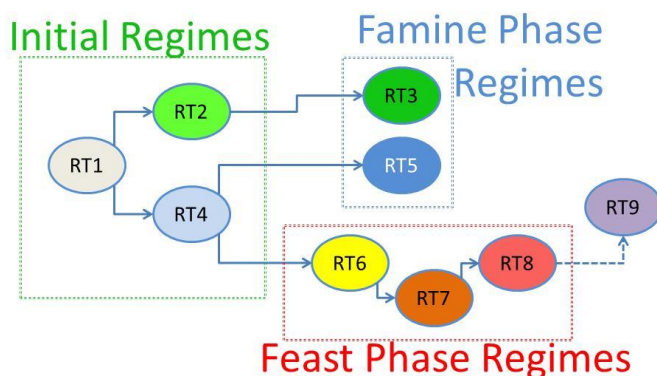


Figure 5.2 Classification of operational regimes based on their operational pathway

Looking at Figure 5.1 and Figure 5.2 it can be deduced that the border curve separating RT5 operational region from the operational regions of RT6, RT7, RT8 and RT9 plays a crucial role when distinction of the two major process behavioural patterns is required to be addressed. Therefore in this context, the border curve refers to the highly significant border separating RT5 from RT6, RT7, RT8 and RT9. As shown in the depiction of Figure 5.1 and the characterisation plots generated by simulation results given in Figure 4.24, the border curve appears as soon as RT5 or RT6 regime appear and it retains its coordination in all the other characterisation plots generated for that process with longer operational duration.

In the next section, simulation results are used to develop mathematical equations capable of estimating coordination of the border curve.

5.3 Identification of the “Border Line” on characterisation plots

With the aim of finding mathematical representations of the border curve, a simplifying assumption is made to facilitate implementation of mathematical equations into the simulated data. Based on this assumption, mathematical representation of the border curve is a linear equation (a straight line) with its coordination depending on the initial biomass concentration and the percentage of its PHB content. The validity of this assumption are confirmed by observing simulation results at the end of this chapter.

Figure 5.3 shows two characterisation plots for batch simulations initiating with extensive unrealistic biomass concentration of 1,000 C-mmo/L containing different initial PHB factor of 0% (Figure 5.3.a) and 100% (Figure 5.3.b). Since RT6 appears on

both plots, it is possible to draw the “Border Line” separating RT5 from the “feast” phase operational regime types (RT6, RT7, RT8 or RT9). For this purpose, two points are denoted by the “ \square ” mark with their co-ordination on each characterisation plot.

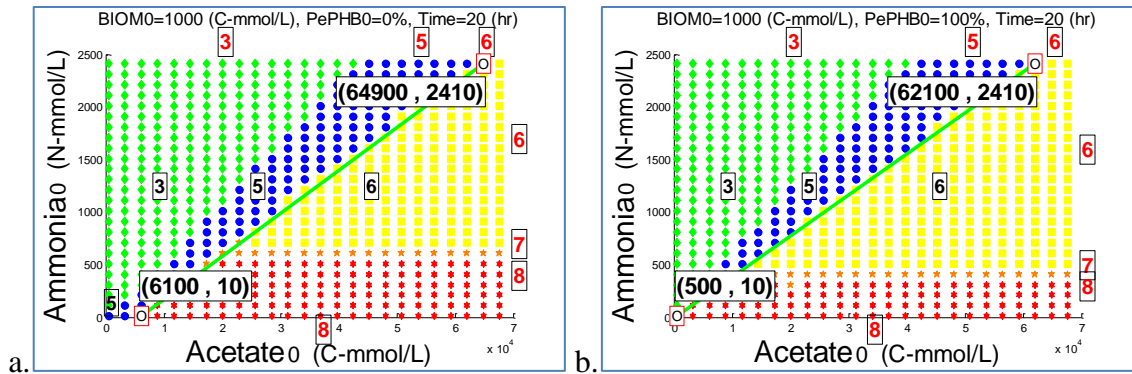


Figure 5.3 Characterisation plots with the border curves (BIOM0=1000 C-mmol/L)

Similar to the previous chapter, for the nine RT groups, iconic symbols “+”, “★”, “◆”, “▼”, “●”, “●”, “★”, “★” and “△” are used to demonstrate appearance of RT1 to RT9 respectively. In addition to the iconic symbols, RT numbers are also shown in black boxes for the bottom, middle, top iconic rows and the right edge of the characterisation plot.

The first point (referred to as Point1) specifies the batch simulation result for which initial acetate concentration is the lowest when a “feast” phase regime type appears for the minimum value of initial ammonia concentration on the characterisation plot. For example, In Figure 5.3.a, Point1 has co-ordination of (6100, 10). Likewise, the second point (referred to as Point2) shows the coordination of the simulation result for which initial acetate concentration is the lowest when a “feast” phase regime type appears for the maximum value of initial ammonia concentration on the characterisation plot. For instance in Figure 5.3.a, Point2 has co-ordination of (64900, 2410). The co-ordinations of these two points are depicted on the plots along with a straight line connecting the two points.

Looking at Figure 5.3 it can be deduced that a straight line is an appropriate approximation for the border curve. In addition to this outcome, mathematical equation of this line is a function of initial intracellular PHB content of cells (PePHB0 value). The initial comparison of the two plots in Figure 5.3 suggests that coordination of the “Border Line” moves towards the ammonia axis when PePHB0 is increased from 0% to 100%.

Similar plots are also generated for initial biomass concentration of 100 C-mmol/L in Figure 5.4. Approximation of a straight line in place of the border curve is not as accurate as the case shown in Figure 5.3; however, it provides satisfactory estimation especially when the “feast” phase operational region is addressed. Similar to the case of Figure 5.3, the “Border Line” move towards the ammonia axis when PePHB0 is increased. The coordination difference between the results depicted in Figure 5.3 and Figure 5.4 confirms dependency of the “Border Line” equation on the initial biomass concentration applied to the simulations. The iconic symbols “+”, “*”, “♦”, “◀”, “●”, “●”, “●”, “★”, “★” and “△” are used to demonstrate appearance of RT1 to RT9 respectively.

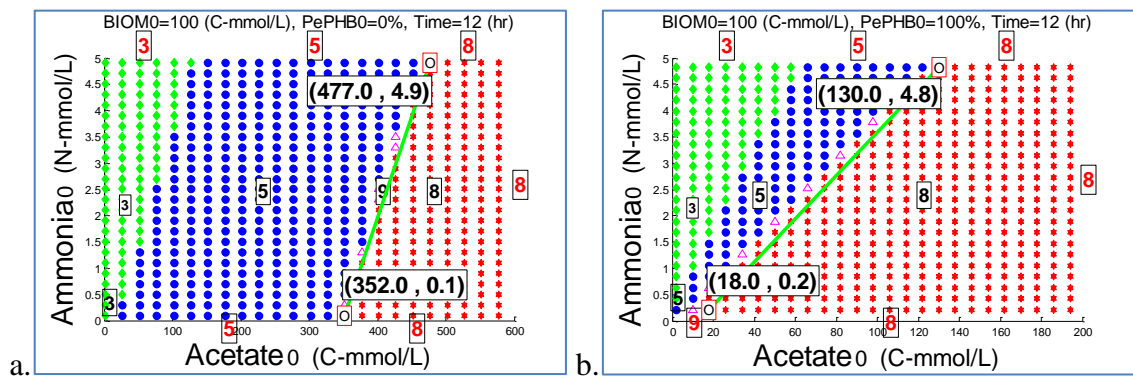


Figure 5.4 Characterisation plots with the border curves (BIOM0=100 C-mmol/L)

Observation of Figure 5.3 and Figure 5.4 suggests that the border curves differentiating the “feast” phase area from the “famine” phase area form a locus of curves for different initial PHB content values. For a given initial biomass concentration and batch operational period a locus for border curves can be considered to reflect dependency of the “Border Line” co-ordination on the initial PHB content of the biomass. Figure 5.5 shows a depiction of the border curve locus on a typical characterisation plot regarding PHB production process for a given initial biomass concentration and operational time.

In Figure 5.5, the straight line connecting “Point1” to “Point2” is called “line- α ” for the case of PePHB0 value of zero. In a similar manner, “line- β ” is a straight line connecting “Point1” to “Point2” when initial PHB content is 100%. The area confined by “line- α ”, “line- β ” and the axes of the characterisation plot is the border curve locus as depicted on Figure 5.5.

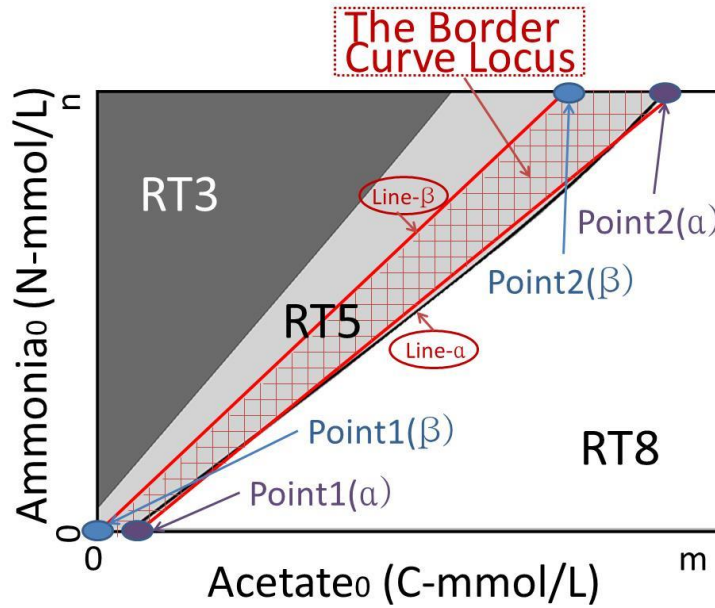


Figure 5.5 Qualitative pattern of the border curve area in a characterisation plot

In order to estimate equation of the border curve for a PePHB0 value in between 0% and 100%, the first step is to estimate the two border curves with PePHB0 value of 0% and 100%, and then genuine border curve is estimated as a linear ratio of the overall interval. Based on the illustrative description provided in this section, mathematical equations are developed in the next section for estimation of the border curve.

5.4 Mathematical representation of the border curve equation

Based on the illustrative description provided, the following steps are proposed to develop mathematical representations of the “Border Lines” as a function of both initial biomass concentration and their PHB content.

1. Characterisation plots are drawn for a range of different initial biomass concentrations with PePHB0 values of 0% and 100%.
2. For each characterisation plot, Point1 and Point2 are identified.
3. The gradient of the line connecting the two points is calculated as follows:

$$LG = \frac{\text{ammonia}_{0(\text{Point}2)} - \text{ammonia}_{0(\text{Point}1)}}{\text{acetate}_{0(\text{Point}2)} - \text{acetate}_{0(\text{Point}1)}} \quad (5.1)$$

where LG is the line gradient in (N-mmol/C-mmol). The gradients are specified for both PePHB0 value of zero (LG_{α}) and one hundred percent (LG_{β}).

4. Two first order polynomial equations are fitted to the data in order to build equations predicting LG values as functions of the initial biomass concentration,

one for PePHB0 values of zero and the other for PePHB0 value of one hundred percent.

$$f_1(Z) = LG_\alpha = (E_\alpha \cdot Z + F_\alpha) \quad (5.2)$$

$$f_2(Z) = LG_\beta = (E_\beta \cdot Z + F_\beta) \quad (5.3)$$

where Z is the initial biomass concentration in (C-mmol/L), used when generating the characterisation plot procedure. E_α , F_α , E_β and F_β are the parameters of the polynomial equation fitted to the data.

5. The line intercept crossing the acetate₀ axis is specified using the following equation.

$$\begin{aligned} & acetate_{Intercept} \\ &= acetate_{0(Point2)} \\ &- ammonia_{0(Point2)} \left(\frac{acetate_{0(Point2)} - acetate_{0(Point1)}}{ammonia_{0(Point2)} - ammonia_{0(Point1)}} \right) \end{aligned} \quad (5.4)$$

where $acetate_{Intercept}$ is the measure on acetate₀ axis where crossed by the “Border Line”.

6. Two first order polynomial equations are fitted to the data in order to build equations predicting $acetate_{Intercept}$ values as functions of the initial biomass concentration, one for PePHB0 values of 0% ($acetate_{Intercept_\alpha}$) and the other for PePHB0 value of 100% ($acetate_{Intercept_\beta}$).

$$f_3(Z) = acetate_{Intercept_\alpha} = (B_\alpha \cdot Z + C_\alpha) \quad (5.5)$$

$$f_4(Z) = acetate_{Intercept_\beta} = (B_\beta \cdot Z + C_\beta) \quad (5.6)$$

where B_α , C_α , B_β and C_β are the parameters of the polynomial equation fitted to the data.

7. The two line equations defining the straight lines connecting the Point1 to Point2 for the case of PePHB0 of 0% and 100% are given in the following equations.

$$Y_\alpha - (E_\alpha \cdot Z + F_\alpha) \cdot (X_\alpha - (B_\alpha \cdot Z + C_\alpha)) = 0 \quad (5.7)$$

$$Y_\beta - (E_\beta \cdot Z + F_\beta) \cdot (X_\beta - (B_\beta \cdot Z + C_\beta)) = 0 \quad (5.8)$$

where Y is the initial ammonia concentration in (N-mmol/L) and X is the initial acetate concentration in (C-mmol/L) on the straight line for PePHB0 equal to 0% (Y_α, X_α) and PePHB0 equal to 100% (Y_β, X_β).

8. The “Border Line” separating the two operational regimes in a characterisation plot generated for a certain initial biomass concentration and PHB content level of *PePHB0* can be obtained using the following equation.

$$Y - P.(X - Q) = 0 \quad (5.9)$$

where P and Q are defined as

$$P = (E_\alpha.Z + F_\alpha) + PePHB0.((E_\beta.Z + F_\beta) - (E_\alpha.Z + F_\alpha)) \quad (5.10)$$

$$Q = (B_\alpha.Z + C_\alpha) + PePHB0.((B_\beta.Z + C_\beta) - (B_\alpha.Z + C_\alpha)) \quad (5.11)$$

The steps aforementioned are to be taken to develop the mathematical equation of the “Border Line”. The first step is to generate characterisation plots for different initial biomass concentrations and PePHB0 of 0% and 100%. These characterisation plots are generated and depicted in three set of initial biomass concentrations given in Appendix-C.

In the first set of data given in Appendix C, 24 characterisation plots are depicted for initial biomass concentration in between 2 C-mmol/L and 200 C-mmol/L. On each plot, co-ordination of the points appearing in between the RT5 and the “feast” phase regime types for the maximum and minimum initial ammonia concentrations (Point2 and Point1) are noted. At the end, coordination of the Point1 and Point2 are tabulated along with the specifications obtained for the lines connecting the two points using Equation (5.1) and Equation (5.4). From Table 5.1 to Table 5.6, coordination of the Point1 and Point2 tabulated for PePHB0 value of 0% and 100% for various initial total biomass concentration. Characterisation plots were generated in three ranges of total biomass concentrations with the first group ranging in between 2 and 200 C-mmol/L, the second group ranging in between 200 and 1,000 C-mmol/L and the third group ranging between 1,000 and 15,000 C-mmol/L.

Table 5.1 Point1 and Point2 coordination and the specifications of the straight line crossing the two points (Biomass range 2-200 C-mmol/L, PePHB0=0%)

PePHB0=0%							
Simulation run number	Initial Biomass (C-mmol/L)	Point1 Acetate ₀ (C-mmol/L)	Point1 Ammonia ₀ (N-mmol/L)	Point2 Acetate ₀ (C-mmol/L)	Point2 Ammonia ₀ (N-mmol/L)	LG_{α} ($\frac{N-mmol}{C-mmol}$)	$acetate_{Intercept}$ (C-mmol/L)
1	2	11	0.1	133.4	5.1	0.04084	8.552
2	10	41.6	0.2	154	5.2	0.04448	37.104
3	20	77.8	0.3	200.2	5.3	0.04084	70.456
4	40	147	0.4	269.4	5.4	0.04084	137.20
5	60	218	0.5	340.4	5.5	0.04084	205.76
6	80	288.8	0.6	411.2	5.6	0.04084	274.11
7	100	358	0.7	480.4	5.7	0.04084	340.86
8	120	428.8	0.8	551.2	5.8	0.04084	409.21
9	140	499.8	0.9	620.4	5.9	0.04145	478.09
10	160	569	1	691.4	6	0.04084	544.52
11	180	648.8	1.1	773	6.1	0.04025	621.47
12	200	725.2	1.2	849.4	6.2	0.04025	695.39

Table 5.2 Point1 and Point2 coordination and the specifications of the straight line crossing the two points (Biomass range 2-200 C-mmol/L, PePHB0=100%)

PePHB0=100%							
Simulation run number	Initial Biomass (C-mmol/L)	Point1 Acetate₀ (C-mmol/L)	Point1 Ammonia₀ (N-mmol/L)	Point2 Acetate₀ (C-mmol/L)	Point2 Ammonia₀ (N-mmol/L)	$LG_{\alpha} \left(\frac{N\text{-mmol}}{C\text{-mmol}} \right)$	$acetate_{Intercept}$ (C-mmol/L)
13	2	3.8	0.1	128	5.1	0.04025	1.316
14	10	7.4	0.2	129.8	5.2	0.04084	2.504
15	20	9.2	0.3	133.4	5.3	0.04025	1.748
16	40	12.8	0.4	138.8	5.4	0.03968	2.72
17	60	14.6	0.5	138.8	5.5	0.04025	2.18
18	80	18.2	0.6	142.4	5.6	0.04025	3.296
19	100	20	0.7	144.2	5.7	0.04025	2.612
20	120	23.6	0.8	147.8	5.8	0.04025	3.728
21	140	25.4	0.9	151.4	5.9	0.03968	2.72
22	160	32.6	1	156.8	6	0.04025	7.76
23	180	30.8	1.1	156.8	6.1	0.03968	3.08
24	200	34.4	1.2	156.8	6.2	0.04084	5.024

Table 5.3 Point1 and Point2 coordination and the specifications of the straight line crossing the two points (Biomass range 200-1000 C-mmol/L, PePHB0=0%)

PePHB0=0%							
Simulation run number	Initial Biomass (C-mmol/L)	Point1 Acetate ₀ (C-mmol/L)	Point1 Ammonia ₀ (N-mmol/L)	Point2 Acetate ₀ (C-mmol/L)	Point2 Ammonia ₀ (N-mmol/L)	LG_{α} ($\frac{N-mmol}{C-mmol}$)	$acetate_{Intercept}$ (C-mmol/L)
25	200	725.2	1.2	849.4	6.2	0.04025	695.39
26	275	1012	2	1588	25	0.03993	961.9130
27	350	1308	3	1866	26	0.04121	1235.217
28	425	1584	4	2232	30	0.04012	1484.307
29	500	1864	5	2488	30	0.04006	1739.2
30	575	2164	6	3004	39.6	0.04	2014
31	650	2442	7	3530	49.7	0.03924	2263.639
32	725	2724	8	4020	60	0.04012	2524.615
33	800	3008	9	4548	70	0.03961	2780.786
34	875	3300	10	5050	80	0.04	3050
35	950	3616	11	5540	89.4	0.04074	3346.051
36	1000	3792	12	5976	98.4	0.03956	3488.666

Table 5.4 Point1 and Point2 coordination and the specifications of the straight line crossing the two points (Biomass range 200-1000 C-mmol/L, PePHB0=100%)

PePHB0=100%							
Simulation run number	Initial Biomass (C-mmol/L)	Point1 Acetate₀ (C-mmol/L)	Point1 Ammonia₀ (N-mmol/L)	Point2 Acetate₀ (C-mmol/L)	Point2 Ammonia₀ (N-mmol/L)	$LG_{\alpha} \left(\frac{N\text{-mmol}}{C\text{-mmol}} \right)$	$acetate_{Intercept}$ (C-mmol/L)
37	200	34.4	1.2	156.8	6.2	0.0408	5.024
38	275	72	2	632	25	0.04107	23.3043
39	350	100	3	660	26	0.04107	26.9565
40	425	121	4	767	30	0.04024	21.6153
41	500	146	5	776	30	0.03968	20
42	575	194	6	1010	39.6	0.04117	48.2857
43	650	212	7	1276	49.7	0.04013	37.5737
44	725	254	8	1514	60	0.04126	60.1538
45	800	296	9	1766	70	0.04149	79.1147
46	875	302	10	2052	80	0.04	52
47	950	326	11	2270	89.4	0.04032	53.2448
48	1000	362	12	2522	98.4	0.04	62

Table 5.5 Point1 and Point2 coordination and the specifications of the straight line crossing the two points (Biomass range 1000-1500 C-mmol/L, PePHB0=0%)

PePHB0=0%							
Simulation run number	Initial Biomass (C-mmol/L)	Point1 Acetate ₀ (C-mmol/L)	Point1 Ammonia ₀ (N-mmol/L)	Point2 Acetate ₀ (C-mmol/L)	Point2 Ammonia ₀ (N-mmol/L)	LG_{α} ($\frac{N\text{-mmol}}{C\text{-mmol}}$)	$acetate_{Intercept}$ (C-mmol/L)
49	1000	3792	12	5976	98.4	0.03956	3488.666
50	2000	7440	15	10800	150	0.04017	7066.666
51	3000	11120	25	16720	250	0.04017	10497.77
52	4000	14980	35	22680	350	0.04090	14124.44
53	5000	18800	55	28700	447	0.03959	17410.96
54	6000	23400	100	34600	550	0.04017	20911.11
55	7000	27720	130	40640	650	0.04024	24490
56	8000	31880	160	46640	748	0.03983	27863.67
57	9000	36100	180	52480	840	0.040	31632.72
58	10000	40400	220	58400	948	0.04044	34960.43
59	12500	50000	250	68400	990	0.04021	43783.78
60	15000	59500	280	79500	1080	0.04	52500

Table 5.6 Point1 and Point2 coordination and the specifications of the straight line crossing the two points (Biomass range 1000-1500 C-mmol/L, PePHB0=100%)

PePHB0=100%							
Simulation run number	Initial Biomass (C-mmol/L)	Point1 Acetate₀ (C-mmol/L)	Point1 Ammonia₀ (N-mmol/L)	Point2 Acetate₀ (C-mmol/L)	Point2 Ammonia₀ (N-mmol/L)	$LG_{\alpha} \left(\frac{N\text{-mmol}}{C\text{-mmol}} \right)$	$acetate_{Intercept}$ (C-mmol/L)
61	1000	362	12	2522	98.4	0.04	62
62	2000	522	15	3852	150	0.04054	152
63	3000	860	25	6380	250	0.04076	246.666
64	4000	1080	35	9000	350	0.03977	200
65	5000	1560	55	11360	447	0.04	385
66	6000	3040	100	14220	550	0.04025	555.5555
67	7000	3960	130	17080	650	0.03963	680
68	8000	4680	160	19640	748	0.03930	809.2517
69	9000	5520	180	21860	840	0.0439	1063.63
70	10000	6320	220	24800	948	0.03939	1035.38
71	12500	7440	250	25770	990	0.04037	1247.43
72	15000	8680	280	28280	1080	0.04081	1820

The LG_α , LG_β , $acetate_{Intercept_\alpha}$ and $acetate_{Intercept_\beta}$ values were obtained and tabulated. It can be noted from the tables that the obtained LG_α values are very close to a constant value. Therefore, constants can be applied in place of Equation (5.2) and Equation (5.3) when LG is independent of the initial biomass concentration. The average for LG_α and LG_β values along with their standard deviations are given in Table 5.7. The standard deviation values are two orders of magnitude smaller than their average values. This indicates that variation of data around their average value is insignificant and hence the whole set can be replaced by the average value.

Table 5.7 The average for the LG_α and LG_β values along with their standard deviations

	Initial biomass concentration (C-mmol/L)					
	Biom0 <200		200 < Biom0 <1000		1000 < Biom0 <15000	
	A_α	A_β	A_α	A_β	A_α	A_β
Average gradient (N-mmol/C-mmol)	0.04110	0.0402	0.0400	0.0406	0.04013	0.0401
Standard deviation	0.001	0.0003	0.0004	0.0005	0.0003	0.0004

These average values are called A_α and A_β respectively in case of PePHB0 of 0% and 100% which take the place of Equation (5.2) and Equation (5.3). As the result, Equation (5.7) and Equation (5.8) are modified to the following formations:

$$Y_\alpha - A_\alpha \cdot (X_\alpha - (B_\alpha \cdot Z + C_\alpha)) = 0 \quad (5.12)$$

$$Y_\beta - A_\beta \cdot (X_\beta - (B_\beta \cdot Z + C_\beta)) = 0 \quad (5.13)$$

First order polynomial equations for prediction of $acetate_{Intercept}$ values as functions of initial biomass concentrations in the form of Equation (5.5) and Equation (5.6) are built. In Figure 5.6, polynomial equations are given along with the coefficient of determination values for each case scenario.

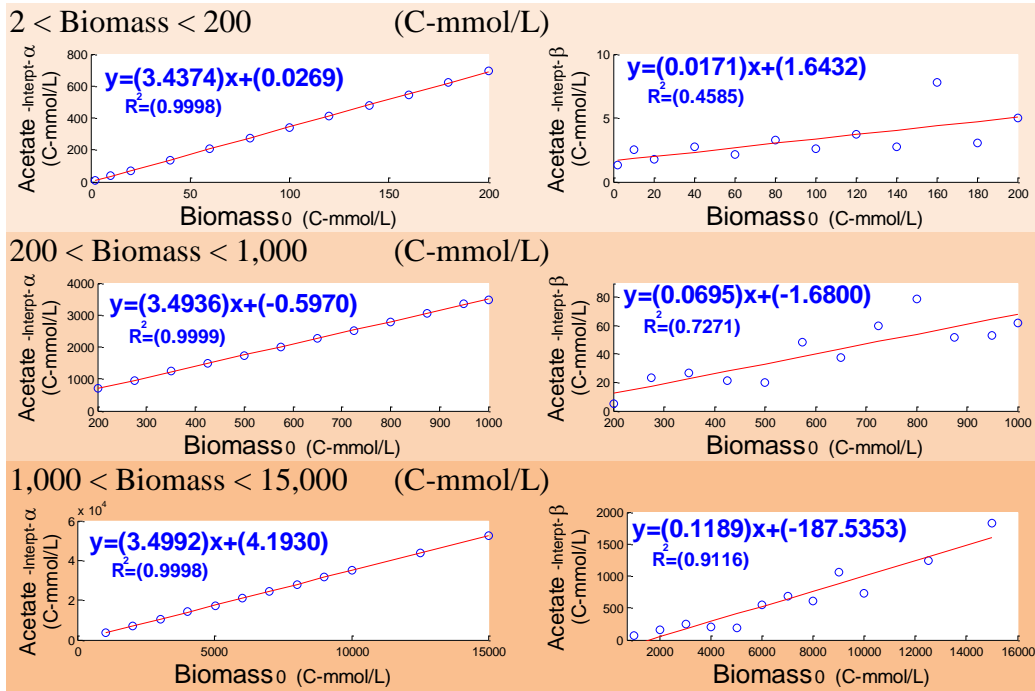


Figure 5.6 Presentation of the linear equations predicting $acetate_{Intercept}$

It can be seen in Figure 5.6 that the coefficient of determination values are close to 1 for the equations related to the simulations with PePHB0 value of 0%. This confirms high capability of these equations to provide accurate prediction with minimal prediction error values. On the other hand, the coefficient of determination values for the simulations with PePHB0 values of 100% are significantly less than 1. However, since the magnitude of the $acetate_{Intercept}$ values is considerably lower in the case of $acetate_{Intercept}_\beta$ when compared to $acetate_{Intercept}_\alpha$ values, the effect of model error would not be significant on the overall estimation of the border curve co-ordination.

In Table 5.8, equation parameters to be applied in Equation (5.12) and Equation (5.13) are given based on the results obtained from Table 5.8 and Figure 5.6.

Table 5.8 Equation parameters for the Line- α and the Line- β to be applied on Equation (5.12) and Equation (5.13)

	Initial biomass concentration (C-mmol/L)								
	2<BIOM0<200			200<BIOM0<1,000			1,000<BIOM0<15,000		
Line- α	A_α	B_α	C_α	A_α	B_α	C_α	A_α	B_α	C_α
	0.04110	3.4374	0.0269	0.0400	3.4936	-0.597	0.04013	3.4992	4.193
Line- β	A_β	B_β	C_β	A_β	B_β	C_β	A_β	B_β	C_β
	0.0402	0.0171	1.6432	0.0406	0.0695	-1.68	0.0401	0.1189	-187.5

At the end, the equation of the “Border Line” separating the “feast” from the “famine” phase operational regimes on a characterisation plot with PePHB0 value in between 0% and 100% is obtained from the following equation.

$$Y - (A_{\alpha} + PePHB0 \cdot (A_{\beta} - A_{\alpha})) \times (X - ((B_{\alpha} \cdot Z + C_{\alpha}) + PePHB0 \cdot ((B_{\beta} \cdot Z + C_{\beta}) - (B_{\alpha} \cdot Z + C_{\alpha})))) = 0 \quad (5.14)$$

This equation is a modified version of Equation (5.9) when line gradients are assumed to be constant. This equation will be referred to as the “Phase Differentiating Equation” since it enables segregation of the two “feast” and “famine” phase operations from each other.

5.5 Validation of the “Phase Differentiating Equation”

Six batch operations are considered for the validation purpose in this section. Table 5.9 tabulates the simulation parameters associated with PHB batch operations for validation of the “Phase Differentiating Equation” or the “Border Line” obtained in this Chapter.

Table 5.9 Simulation parameters for “Phase Differentiating Equation” validation

Simulation Setting No	Biom0 (C-mmol/L)	PePHB0 %	Time (hr)	Deterministic Simulator Run	Random Behaviour Simulator Runs
1	70	30	12	Figure 5.7	Figure 5.8
2	150	70	13	Figure 5.9	Figure 5.10
3	400	15	18	Figure 5.12	Figure 5.13
4	700	85	16	Figure 5.14	Figure 5.15
5	3000	45	17	Figure 5.16	Figure 5.17
6	9000	65	150	Figure 5.18	Figure 5.18

The initial biomass concentrations imposed to the system are assigned such that two validation examinations are provided for each of the three biomass intervals considered in the equation development stage. In the first two simulation settings, the PePHB0 value associated with initial PHB content of the cells are chosen to be 30% and 70% for initial biomass concentration of 70 C-mmol/L and 150 C-mmol/L respectively. The batch operational periods are considered such that majority of the simulated batch operations reach to their operational maturity stage by formation of either “feast” or “famine” phase regime types.

The validation process presented in this chapter is rather graphical than quantitative. In Section 6.4.3 and Section 6.5.5, qualitative assessment of the “Phase Differentiating Equation” for validation of the method accuracy will be carried out for the “feast” and “famine” phase regimen.

The mathematical equation obtained in the previous section (Equation (5.14)) is validated to examine its capability to differentiate “feast” phase region from the “famine” phase region in different characterisation plots generated for different case

scenarios. The “Phase Differentiating Equation” is first validated by deterministic process simulator. Additionally, reliability of the equation is investigated by drawing the “Border Line” using the “Phase Differentiating Equation” on a series of characterisation plots generated using random behaviour process simulator. In this section, 4 examination runs are carried out using random behaviour process simulator in addition to the reference plot obtained using the deterministic behaviour process simulator. In order to assess reliability of the equation, comparison of the “Border Line” estimation accuracy is made using the reference plot.

On each characterisation plot, three lines are depicted using the Equation (5.12), Equation (5.13) and Equation (5.14) for the case of PePHB0 of 0% (line- α), PePHB0 of 100% (line- β) and the operational PePHB0 per cent (the “Border Line”). The acetate intercept values are also calculated and noted for each line on the graph. Similar to the Chapter 4, iconic symbols “+”, “★”, “◆”, “▼”, “●”, “●”, “★”, “★”, “★” and “△” are used to demonstrate occurrence of RT1 to RT9 regime types respectively. It is worthwhile mentioning that the “feast” phase regime types are RT6, RT7 and RT8 while the “famine” phase regime types are RT3 and RT5.

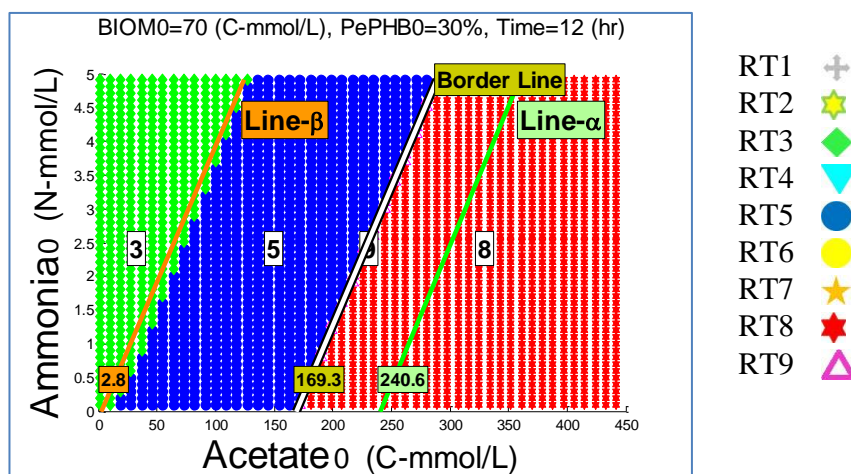


Figure 5.7 Simulation setting No.1, validation of “Phase Differentiating Equation”-Deterministic behaviour system

Figure 5.7 shows a characterisation plot generated for the first examination study. As shown in this figure, the “Border Line” drew on the plot presents an accurate estimation of the “feast” and “famine” phase region boundary when deterministic behaviour process simulator is used for generation of the characterisation plot.

In Figure 5.8, four examination runs are performed to generate four characterisation plots using random behaviour process simulator explained in Chapter 3 with identical operational parameters. Since biological behaviour of bacteria differs from one batch

simulation to another, process profiles of two batches with identical operational parameters may vary. As the result of the biological random behaviour, characterisation plots shown in Figure 5.8 differ from one experimental run to another.

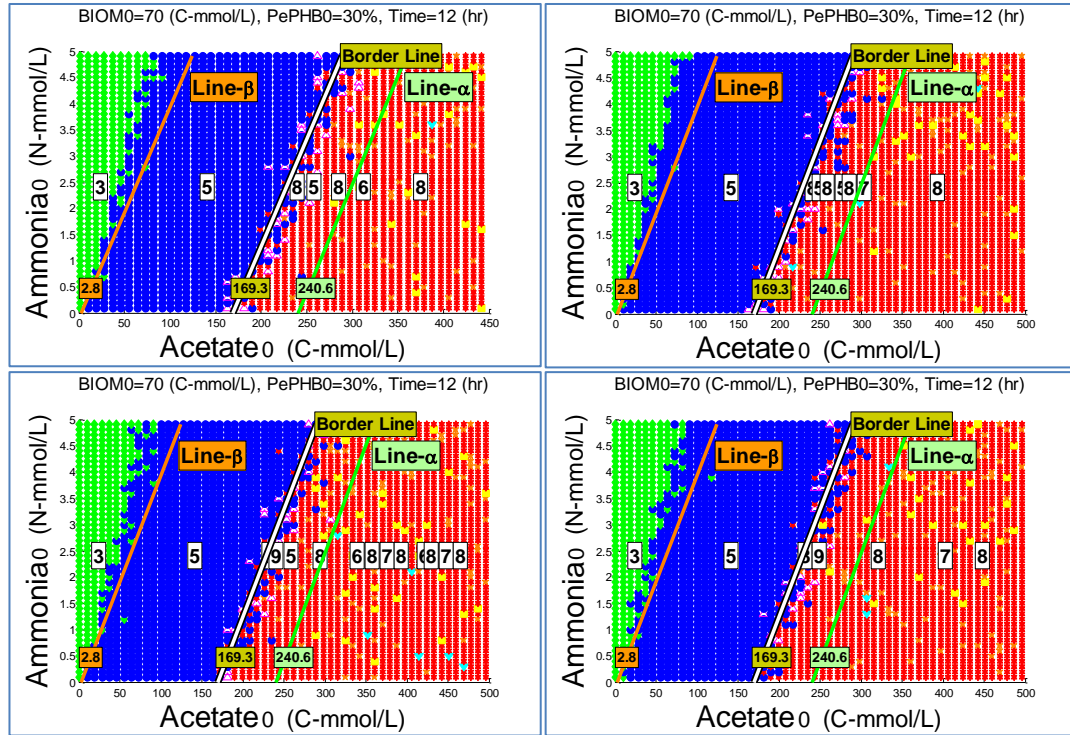


Figure 5.8 Simulation setting No.1, validation of “Phase Differentiating Equation”- Random behaviour system

In the five characterisation plots depicted in Figure 5.7 and Figure 5.8, the three equations for line- α , line- β and the “Border Line” are the same as Equation (5.12), Equation (5.13) and Equation (5.14) are considered to be independent of the operational behaviour randomness. Due to biological randomness of behaviour, “feast” and “famine” phase operational regions overlap and it is not possible to consider a border curve that differentiates the “feast” and “famine” phase with high accuracy. However, the “Border Line” generated using Equation (5.14) provides an acceptable estimation of the two phase boundaries as depicted in Figure 5.8 for the four experiments.

In the second examination case study, initial biomass concentration is 150 C-mmol/L with initial PHB content level of 70% as for PePHB0. The batch operation period is considered to be 13 hours for the process to reach maturity. In Figure 5.9, the characterisation plot generated using deterministic behaviour process simulator is shown along with the line- α , line- β and the “Border Line”. The accuracy of Equation (5.14) to draw the “Border Line” separating RT5 region area from RT8 region area is shown to be very high. In effect, the “Border Line” covers the batch operation

points represented by the “ Δ ” symbol to indicate occurrence of RT9 regime operation. As mentioned in Chapter 4, RT9 is the regime type that appears in the boundary of the two operational phases and cannot be considered as either one.

Comparison of the acetate intercept points in Figure 5.7 and Figure 5.9 for the first and second examination runs shows considerable increase for line- α and line- β while acetate intercept value associated with the “Border Line” demonstrates a significant decrease from the first examination run to the second examination run. As mentioned in the “Border Line” equation development section, since both line- α and line- β are defined for constant values of PePHB0, they are independent of the operational PePHB0 value. Therefore, an increase in PePHB0 value from 30% to 70% does not affect co-ordination estimation of these two lines. However, the acetate intercept is relative to the initial biomass concentration and higher acetate intercept value is estimated when initial biomass concentration increases.

The “Border Line” equation is a function of PePHB0 value. For the case of batch operations initialised by low level of intracellular PHB content, the “Border Line” appears in the vicinity of the line- α with relatively high acetate intercept value. On the other hand, the “Border Line” shifts towards the line- β when PePHB0 value is high. Since initial biomass concentration has increased from 70 C-mmol/L to 150 C-mmol/L in the two examination runs, the acetate intercept value was expected to increase if the PePHB0 value remained the same in the two cases. However, PePHB0 value has increased from 30% to 70% and consequently the “Border Line” has been shifted towards the line- β resulting in a lower acetate intercept value obtained for the second examination run.

In Figure 5.10, the four characterisation plots generated by the random behaviour process simulator are shown along with the “Border Line” obtained using “Phase Differentiating Equation”. Similar to the first examination run, “feast” and “famine” phase areas overlap and no clear boundary can be considered to differentiate these two areas on the characterisation plots. Despite the uncertainty, the “Border Line” drew on the plots can provide an acceptable approximation of the line that separates the two regions.

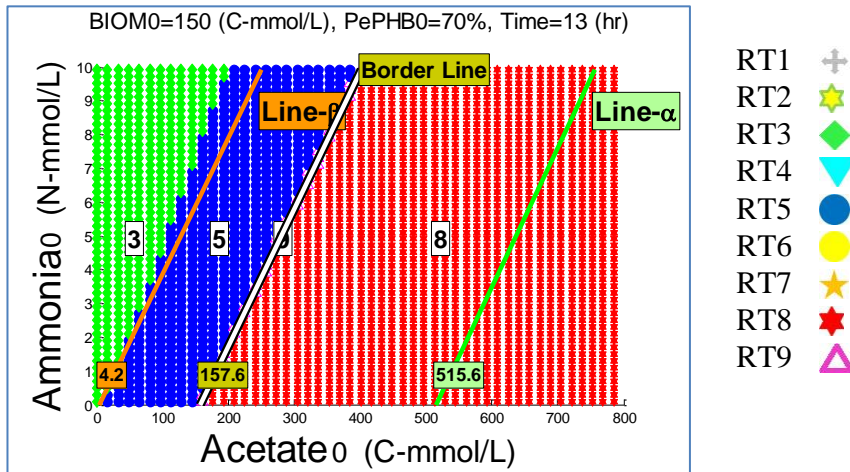


Figure 5.9 Simulation setting No.2, validation of “Phase Differentiating Equation”- Deterministic behaviour system

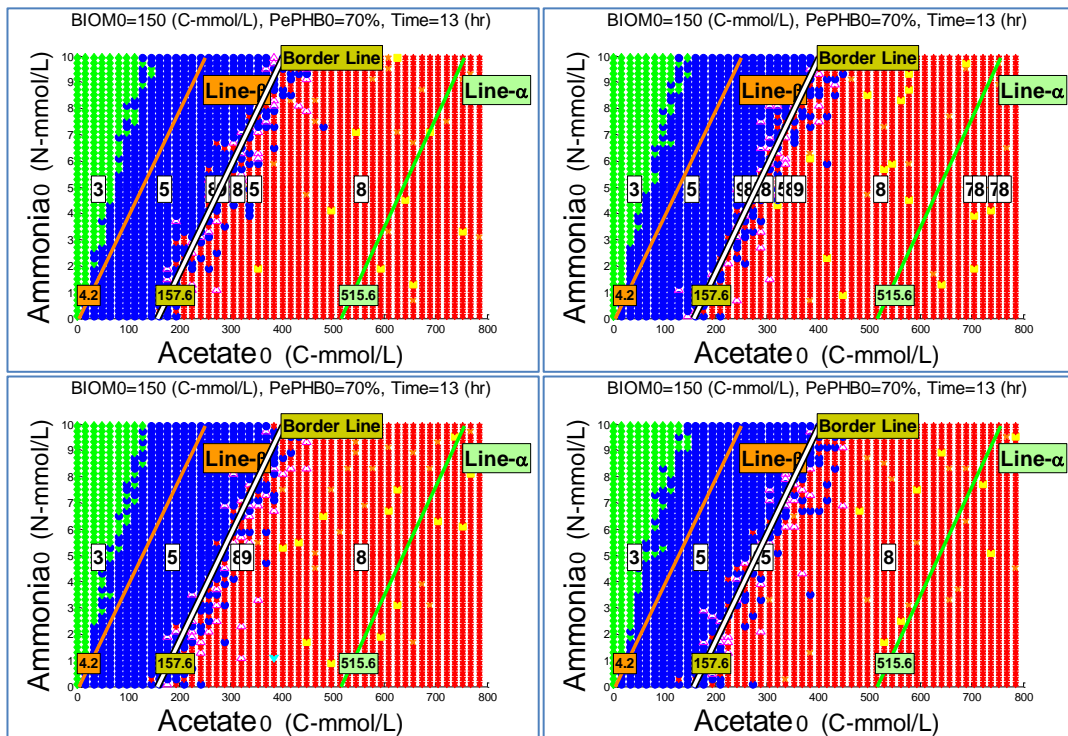


Figure 5.10 Simulation setting No.2, validation of “Phase Differentiating Equation”- Random behaviour system

In order to investigate the effect of PePHB0 value on dispersion rate of the “famine” phase batches into the “feast” phase area as specified by the “Border Line”, Figure 5.11 is depicted for characterisation plots obtained from batch simulations carried out with PePHB0 value of 30%. In generation of this figure, simulation parameters were assigned to be the same as used in generation of Figure 5.10 with exception of the PePHB0 value.

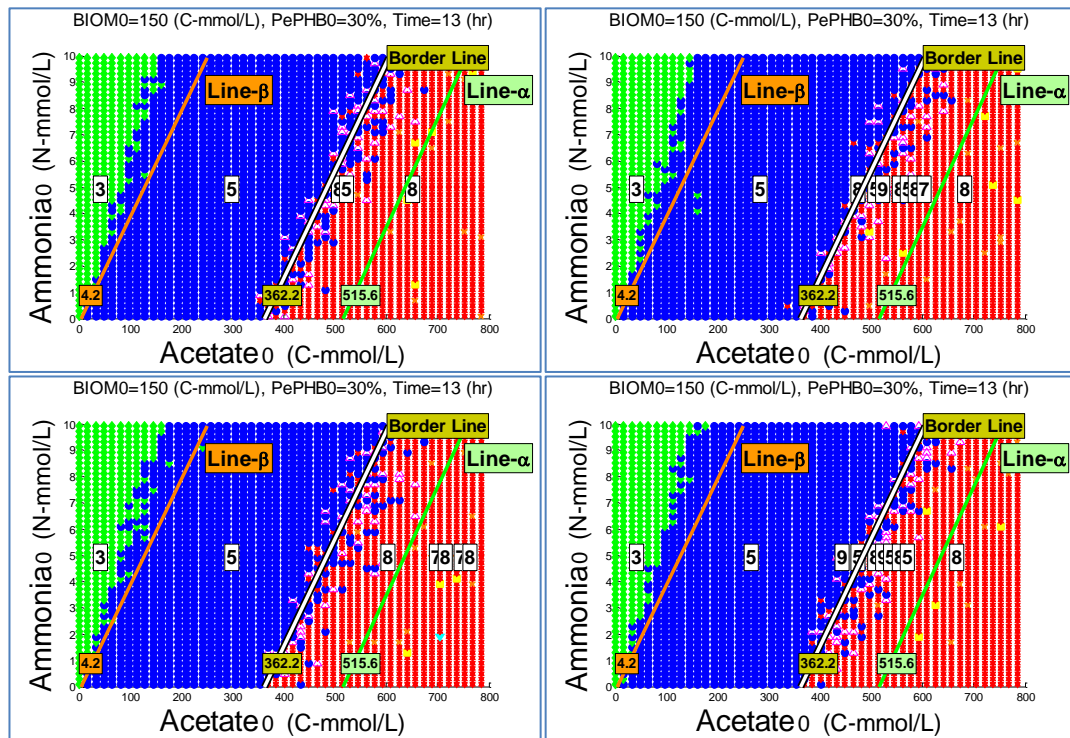


Figure 5.11 Validation of PePHB0 reduction on regimen dispersion

Comparison of characterisation plots shown in Figure 5.10 and Figure 5.11 suggests that dispersion of “feast” phase batches into the “famine” phase region (specified by the “Border Line”) does not significantly change when PePHB0 value is changed. Similar statement can also be made about dispersion of “famine” phase batches into the “feast” phase area as specified by the “Border Line”.

Since the PePHB0 value assigned for generation of Figure 5.11 is the same as this value for generation of Figure 5.8, a comparison of these two figures can be made to investigate the effect of initial biomass concentration on dispersion of “feast” phase batches into the “famine” phase region or “famine” phase batches into the “feast” phase region. Considering the change of scale in the two figures, the overall comparison indicates no significant change of dispersion when initial biomass concentration is changed for generation of characterisation plots.

For the second biomass interval in which Equation (5.14) is obtained, initial biomass concentration of 400 C-mmol/L and 700 C-mmol/L is considered. The PePHB0 values are assigned such that the “Border Line” appears in vicinity of their two extreme Border Lines (line- α and line- β) with PePHB0 value of 15% and 85%.

In Figure 5.12, the third simulation setting is defined to generation a characterisation plot using deterministic behaviour process simulator for initial biomass concentration of

400 C-mmol/L and PePHB0 value of 15%. Batch operation time is considered to be 18 hours for each simulated batch to perform analysis on mature process operations.

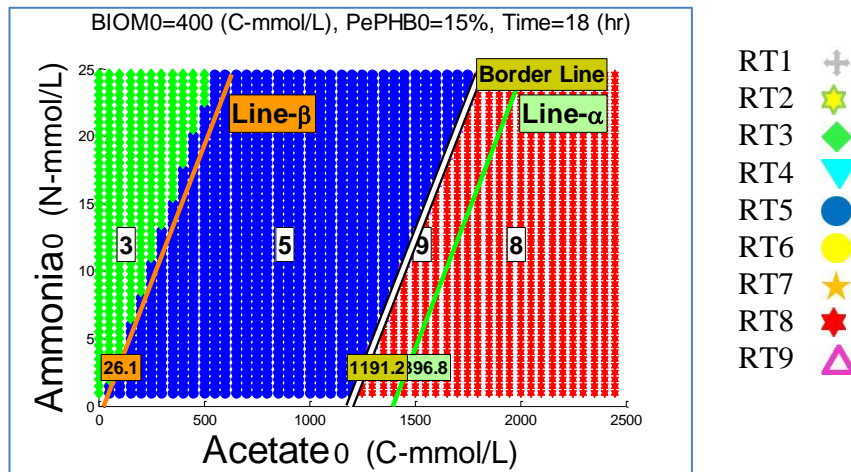


Figure 5.12 Simulation setting No.3, validation of “Phase Differentiating Equation”- Deterministic behaviour system

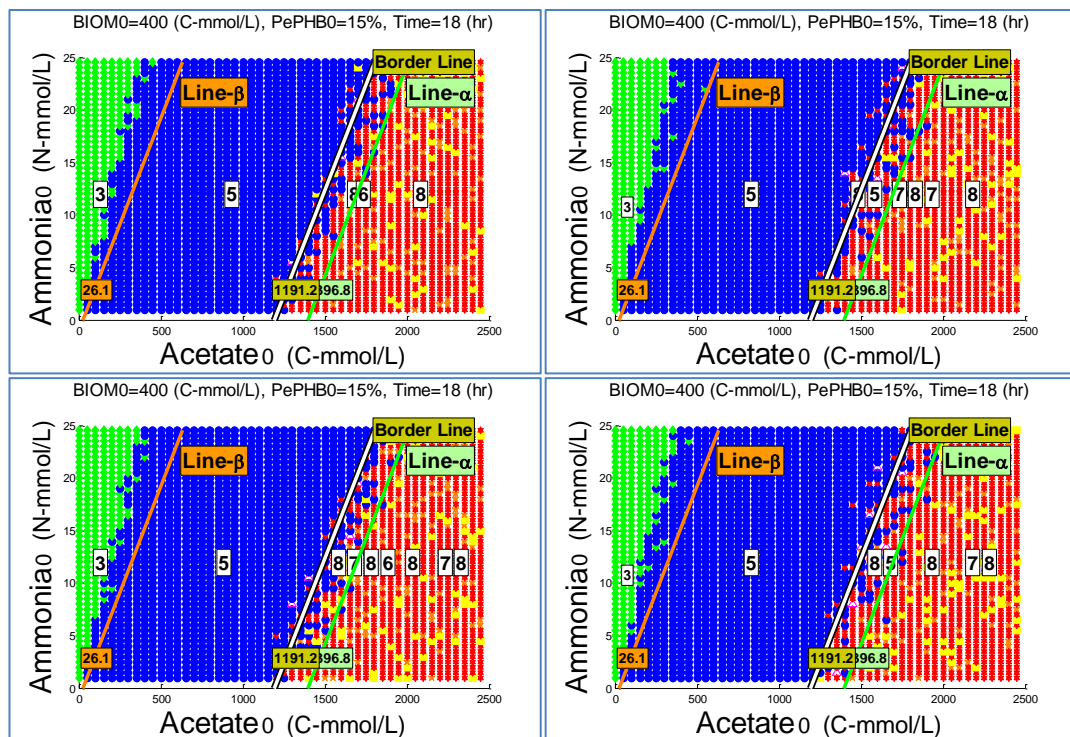


Figure 5.13 Simulation setting No.3, validation of “Phase Differentiating Equation”- Random behaviour system

Figure 5.12 demonstrates high accuracy of the equation obtained to segregate “feast” and “famine” operational regions on a characterisation plot generated by deterministic behaviour process simulator. Reliability of the “Border Line” is investigated when random behaviour process simulator is used to generate four characterisation plots with the same simulation parameters considered to produce Figure 5.12. As shown in

Figure 5.13, the “Border Line” provides a reliable estimation of the boundary between the two phase regime areas.

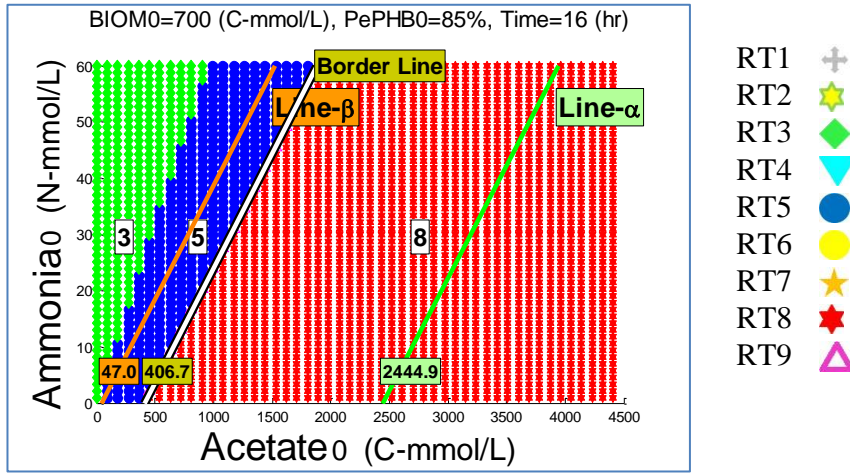


Figure 5.14 Simulation setting No.4, validation of “Phase Differentiating Equation”- Deterministic behaviour system

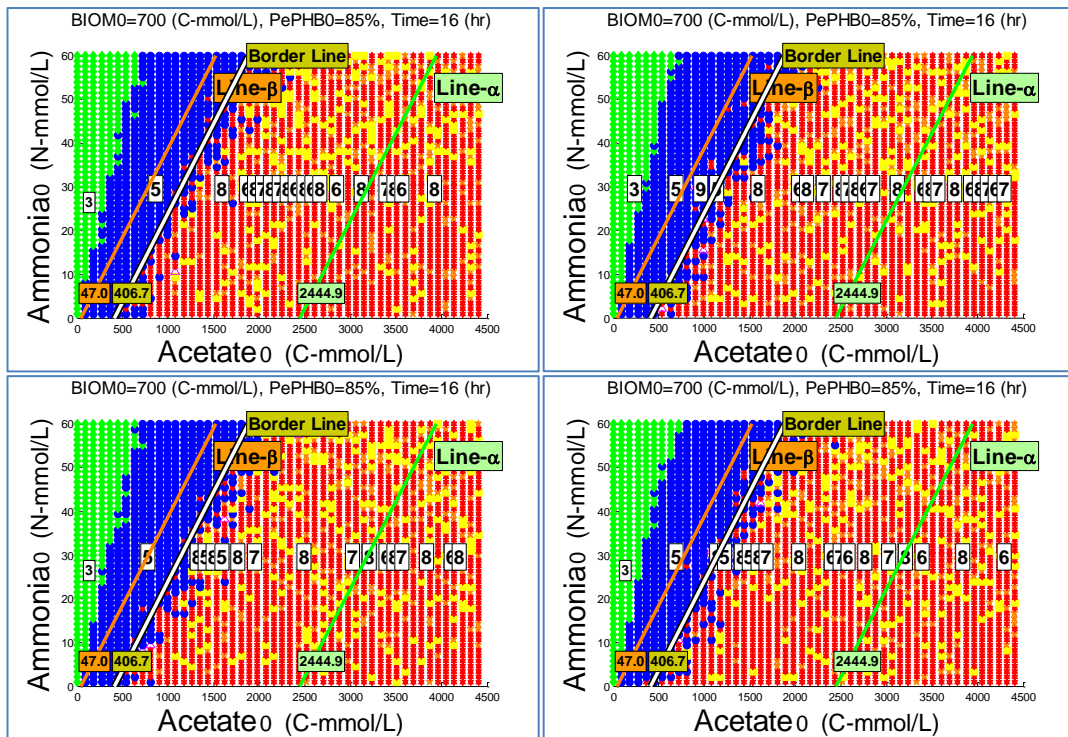


Figure 5.15 Simulation setting No.4, validation of “Phase Differentiating Equation”- Random behaviour system

In generation of the characterisation plots depicted in Figure 5.14 and Figure 5.15, deterministic and random behaviour process simulators are used respectively to simulate batch operations with initial biomass concentration of 700 C-mmol/L and PePHB0 value of 85%. Both accuracy and reliability of the “Border Line” separating the “feast” and “famine” phase regime areas can be confirmed by observing these two figures.

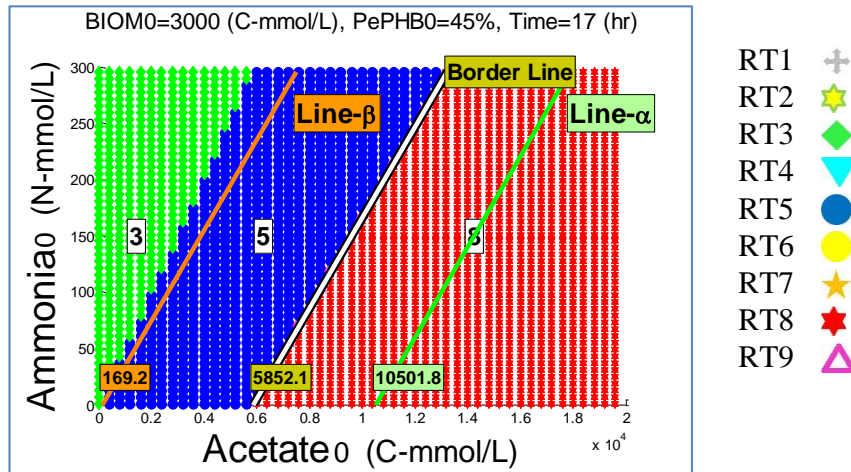


Figure 5.16 Simulation setting No.5, validation of “Phase Differentiating Equation”- Deterministic behaviour system

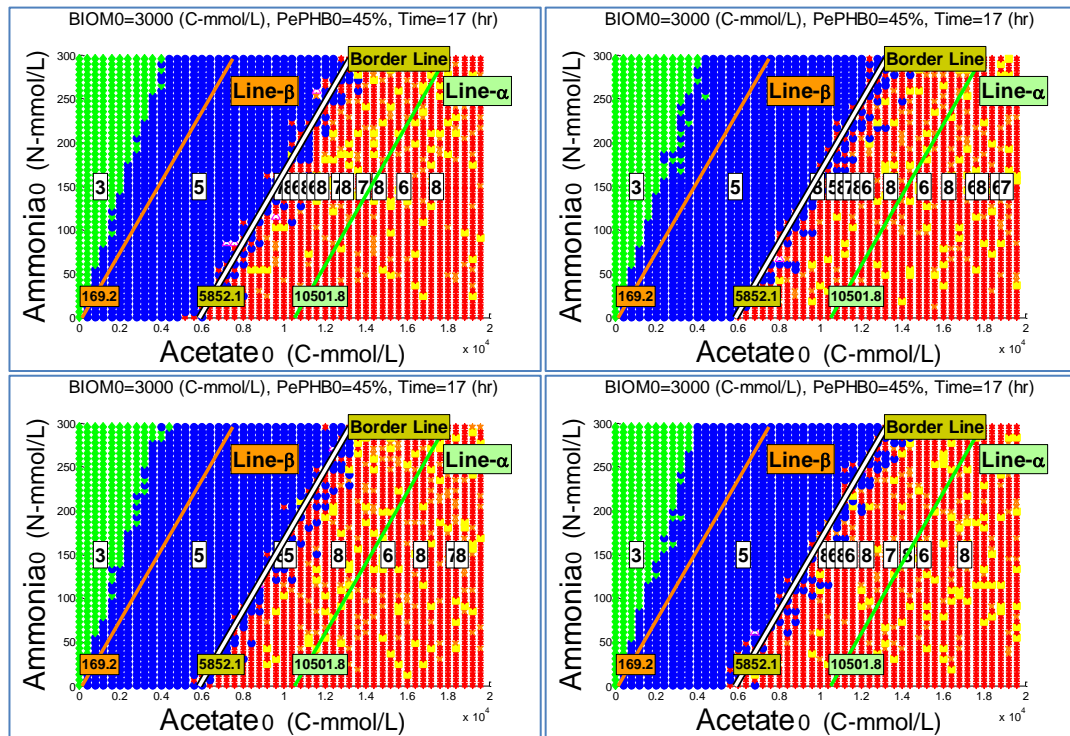


Figure 5.17 Simulation setting No.5, validation of “Phase Differentiating Equation”- Random behaviour system

The last two simulation settings in this chapter are defined such that equation parameters associated with the third biomass interval in “Phase Differentiating Equation” can be validated. Figure 5.16 and Figure 5.17 show characterisation plots generated using deterministic and random behaviour process simulators respectively for initial biomass concentration of 3,000 C-mmol/L, PePHB0 value of 45% for duration of 17 hours. The accuracy and reliability of the “Phase Differentiating Equation” can be confirmed by observing proper approximation of the two regime boundaries.

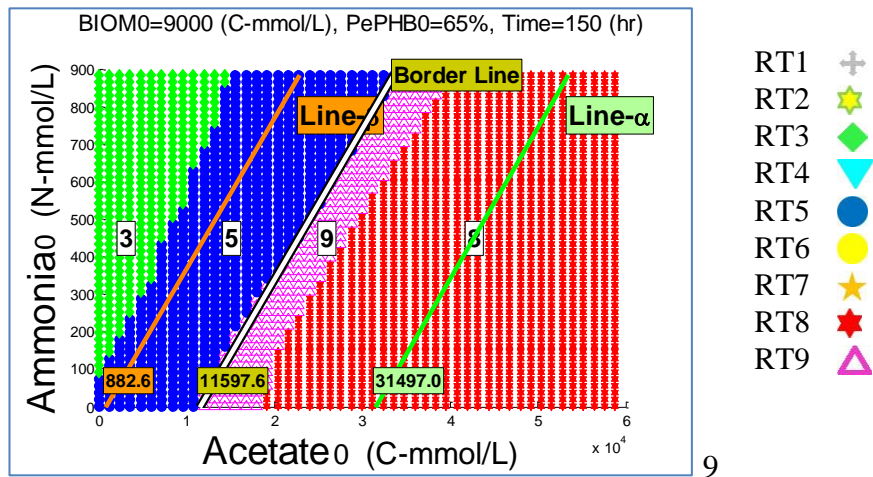


Figure 5.18 Simulation setting No.6, validation of “Phase Differentiating Equation”- Deterministic behaviour system

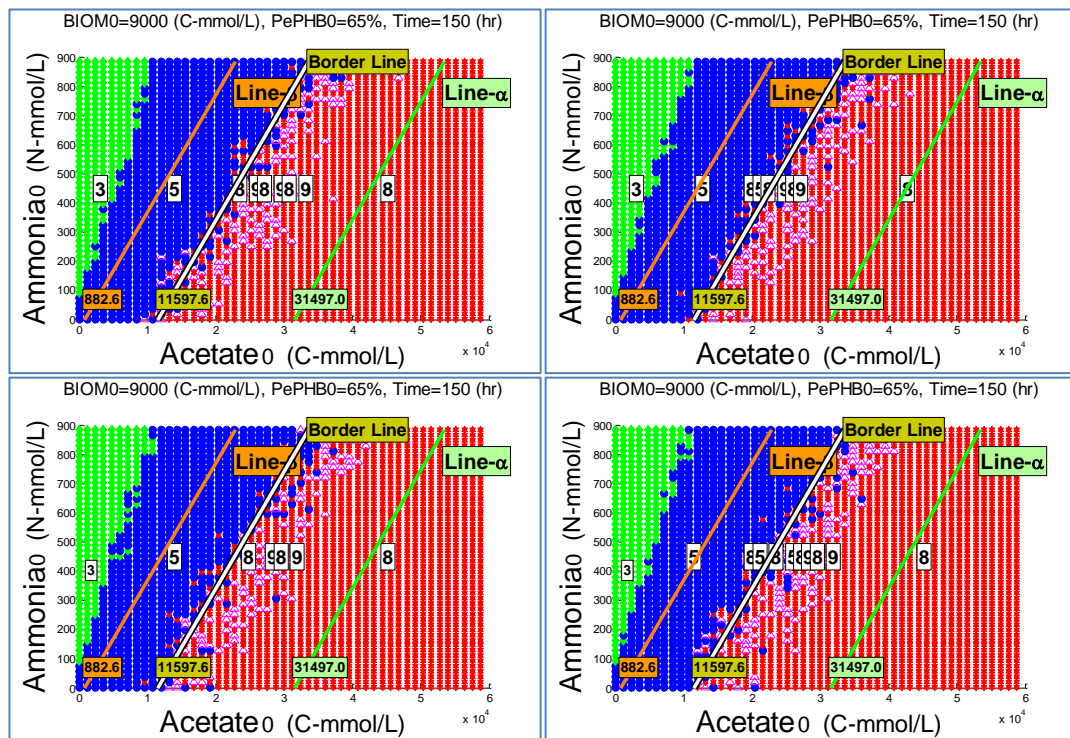


Figure 5.19 Simulation setting No.6, validation of “Phase Differentiating Equation”- Random behaviour system

In the last simulation setting, initial biomass concentration of 9,000 C-mmol/L is considered with PePHB0 value of 65% for the deterministic and random behaviour process simulators used in generation of Figure 5.18 and Figure 5.19 respectively. In this examination run, batch operational duration is assigned to be 150 hours to investigate accuracy and reliability of the “Phase Differentiating Equation” for segregation of the “feast” and “famine” phase operational regions for the case of batch operations with prolonged duration. Appearance of RT9 regimen (presented by “△” in the characterisation plots) is the indication of PHB drop due to carbon source shortage

during a “feast” phase batch operation. As expected, RT9 region forms in the “feast” phase areas and in the vicinity of the RT5 “famine” phase region. The “Phase Differentiating Equation” provides proper estimation of the boundary between the two phase regions as depicted in Figure 5.18 and Figure 5.19.

The “Phase Differentiating Equation” obtained in this chapter was successfully validated for the three biomass intervals considered in the development stage of the equation. This equation will play a crucial role in estimation of process pathway using the initial state of the batch. In Chapter 6, the “Phase Differentiating Equation” will be used to segregate “feast” phase batch data from “famine” phase batch data with the aim of developing empirical models targeting each phase separately. It is evident that models developed separately for each case of “feast” and “famine” phase batch data sets will be more accurate than the models developed without prior classification of the data sets.

In Chapter 7, the “Phase Differentiating Equation” will be applied to design a recipe structure for production of PHB using Sequential Batch Reactors. This equation will be implemented within the recipe to assure occurrence of the “feast” and “famine” phase operations in the particular stages assigned in the recipe. Application of the recipe on the production reactors will reduce the costs associated with process monitoring and control. Additionally, it provides a window in direction of process automation with less labour work.

5.6 Conclusions

Prior to this study, there is no record of any reliable tool for segregation or prediction of biological operational phases based on information obtained from process initial state regarding PHB production using Mixed Microbial Cultures. The mathematical tool obtained in this chapter using the innovative method developed in Chapter 4 is a significant contribution of the author to improve PHB process understanding.

Operational regions associated with the “feast” and “famine” phase were recognised on the characterisation plots generated by the procedure developed in Chapter 4. With the aim of formulating a mathematical equation that can differentiate the two phase operational regions, a series of characterisation plots were drawn and analysed in this chapter. The “Phase Differentiating Equation” was obtained using characterisation plots generated by deterministic behaviour process simulator.

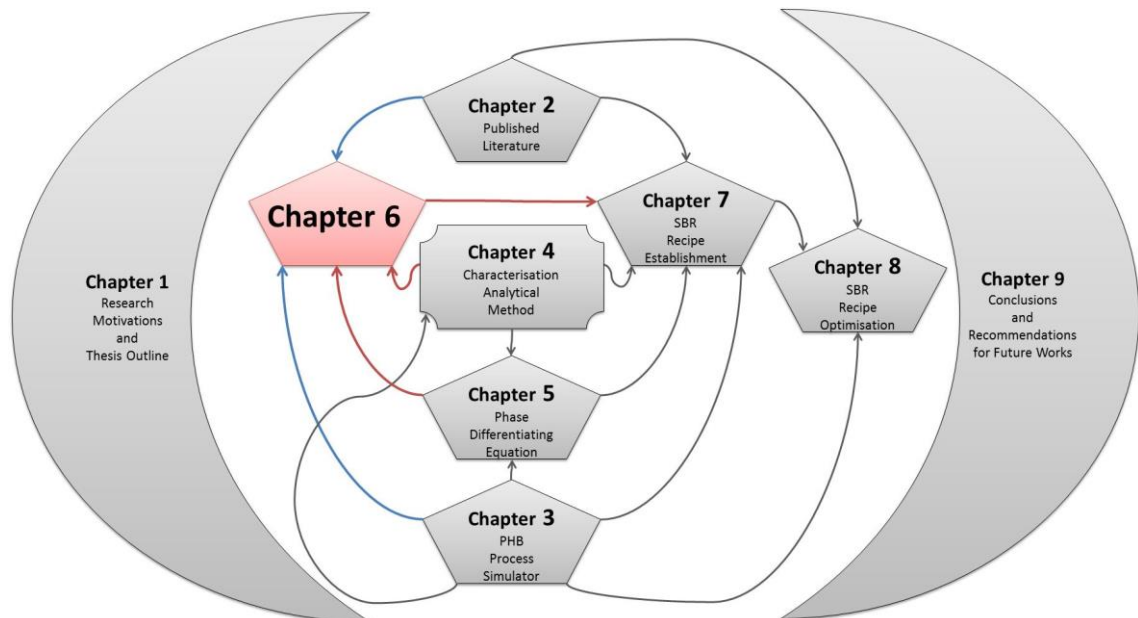
The outcome of observing a cluster of characterisation plots was that the curve separating the two regions can be estimated with a straight line connecting two batch points on the boundary of the “feast” and “famine” phase regions. The author claims that the “Phase Differentiating Equation” developed in this research study is the only tool available for prediction of PHB batch operational phase based on initial state of the process when using mixed microbial cultures.

The “Phase Differentiating Equation” is an indispensable and valuable tool which can play essential role in different analytical studies considering the PHB production process. Two applications of the equation will be discussed in Chapter 6 and Chapter 7 where a novel PHB production recipe is developed and established.

It was demonstrated that the “Phase Differentiating Equation” developed in this chapter was accurate and reliable when four variables including initial acetate, ammonia, biomass concentrations along with the intracellular PHB content of the cells were considered. The “Phase Differentiating Equation” was successfully validated using characterisation plots generated by both deterministic and random behaviour process simulators. The validation process was carried out for six different case scenarios to investigate reliability of the equation to cover a wide range of initial biomass concentration and intracellular PHB content values.

In the next chapter, the “Phase Differentiating Equation” will be applied for development of more accurate empirical models targeting classified operational data.

Chapter 6
Empirical Modelling of the Most Significant Elements of PHB Batch
Process using Mixed Microbial Culture Cultivation



6.1 Introduction

In this chapter, a novel mathematical tool is developed to construct quantitative representations of the PHB production process using mixed microbial cultures in batch operations. In this context, the term “mathematical model” is abbreviated to “model” to represent any consistent set of mathematical equations which correspond to some entity of the PHB process. In this study, the empirical models are trained using PHB process simulator introduced in Chapter 3. Empirical models are inexpensive and are known to be less effort demanding in comparison to mechanistic models for estimation of some specific attributes of the process. Different structure of empirical models will be tested to find the best model structures for estimation of the most important process attributes. These structures build the foundations for empirical model development using real experimental process data. There are a number of useful applications encountered for models developed using experimental process data. In addition to making quantitative predictions for the most important elements of the process, a robust relationship between process elements can be made in model development procedure (if available) to provide a comprehensive picture of the overall process.

In the first step, empirical models are developed using a bulk of process data exclusive of any data classification. Unable to provide acceptable model predictions for the final total PHB concentration, the “Characterisation Method” analytical method developed in Chapter 4 will be used to classify process data prior to model development stage. An appropriate data management and organisation procedure offers the opportunity of target modelling with the prospect of obtaining more accurate models. The “Characterisation Method” and the classifications carried out by introduction of nine “Regime Types” for PHB process profiles will be used in this chapter for systemic identification of the “feast” and “famine” phase operational regimes.

The “feast” and “famine” phase profiles are scrutinised in Section 6.4.2, Section 6.5.2, and Section 6.5.3 in order to identify the most significant elements of the process. The “famine” phase batch data are divided into the two groups based on their “Regime Types”. Additionally, empirical modelling of the most significant process occurrences during a batch operation, such as optimal batch termination time or exhaustion point of carbon or nitrogen sources will also be investigated in this chapter. These models can potentially be used for advanced process optimisation and control.

At first, simple linear MLR models are developed to use initial batch conditions for prediction of the most significant elements of the process. Furthermore, more

sophisticated non-linear BANN models are built to demonstrate their proficiency over their linear counterparts. Additionally, high proficiency of BANN models over single structured neural networks will be demonstrated in the quest of an accurate and reliable modelling technique. Various structures for input-output modelling will be investigated in order to provide the most appropriate model structure for prediction of critical process attributes of the PHB production process.

In the next section, an overview of empirical model development procedure is given.

6.2 Empirical model development procedure

The procedure of model development is discussed in this section. These stages are considered from data generation to the model validation procedure. Various structures are examined to find the most appropriate model input/output arrangements for specific applications using real experimental process data.

6.2.1 Data generation

In this stage, the simulation program provides batch operational data to be applied for development of mathematical models. With the aim of data generation, initial biomass, acetate and ammonia concentrations are assigned using MATLAB's random value generator in pre-specified intervals respective to each element. Initial PHB content (PePHB0) is the fourth element assigned arbitrarily in a range between 0% and 100%. The "Phase Differentiating Equation" (Equation (5.14)) is applied to enable prediction of "feast" from the "famine" phase operational occurrence based on initial batch condition. Data generated within the predicted "feast" and "famine" phase operations are stored separately.

6.2.2 Outlier detection

In a typical model development procedure, a subset of the data collected from practical or simulated processes is not applied in analytical methods due to experimental errors, data corruption or undesired variability in the measurement. Outliers are discarded or replaced using statistical methods prior to model development.

6.2.3 Data grouping

Filtered data stored from the previous stage is divided randomly into two main groups as for model development and model validation. In this study, 70% of the batch data stored for a phase operation is used for training-testing and the remained 30% is used for validation purposes.

6.2.4 Data pre-processing

One of the important stages after organised data collection and before model development is data pre-processing for the type of modelling designated for implementation. The type of pre-processing method is based on the type of data available for modelling and the modelling technique used to train the model. In this study, process data is scaled to the range between -1 and 1 for the minimum and maximum value of each variable respectively. After specifying the minimum and maximum values from the set of data stored for each variable for the model development data, data is transformed by a direct linear equation. These minimum and maximum values are stored for scaling the validation data and also unscaling of the model predictions to their original scale.

6.2.5 Empirical model development

Quantitative representation of a batch process can provide useful information about the process that is modelled. The golden rule is to build required models using the simplest modelling technique with the acceptable level of accuracy. Prior to model development, comprehensive process understanding is essential to identify the most significant and influential variables of the process being modelled. Based on the type of relationship observed in between the dependant and independent variables, an appropriate modelling technique is proposed and implemented. Evaluation of the modelling technique can be carried out when a suitable criterion is applied to compare models developed using different modelling structures or techniques.

In this study, the most common mathematical algorithms to develop models for linear and non-linear process data are investigated and compared. In this section, data flowchart applied for neural network model development will be explained.

The theory behind the neural network modelling was mentioned in Section 2.6.3. In this section, programing structure implemented using MATLAB to generate, manage and model empirical data in this study is described. Figure 6.1 shows data flowchart in three segments, (1) data generation, (2) data management and (3) data modelling.

Simulated data is generated by “BIOSIM”, the coded program that simulates PHB production by mixed microbial cultures by Dias *et al.* (2005) and described in Chapter 3. Outlier detection, data grouping, and pre-processing of the data stored from the process simulation are depicted under data management block.

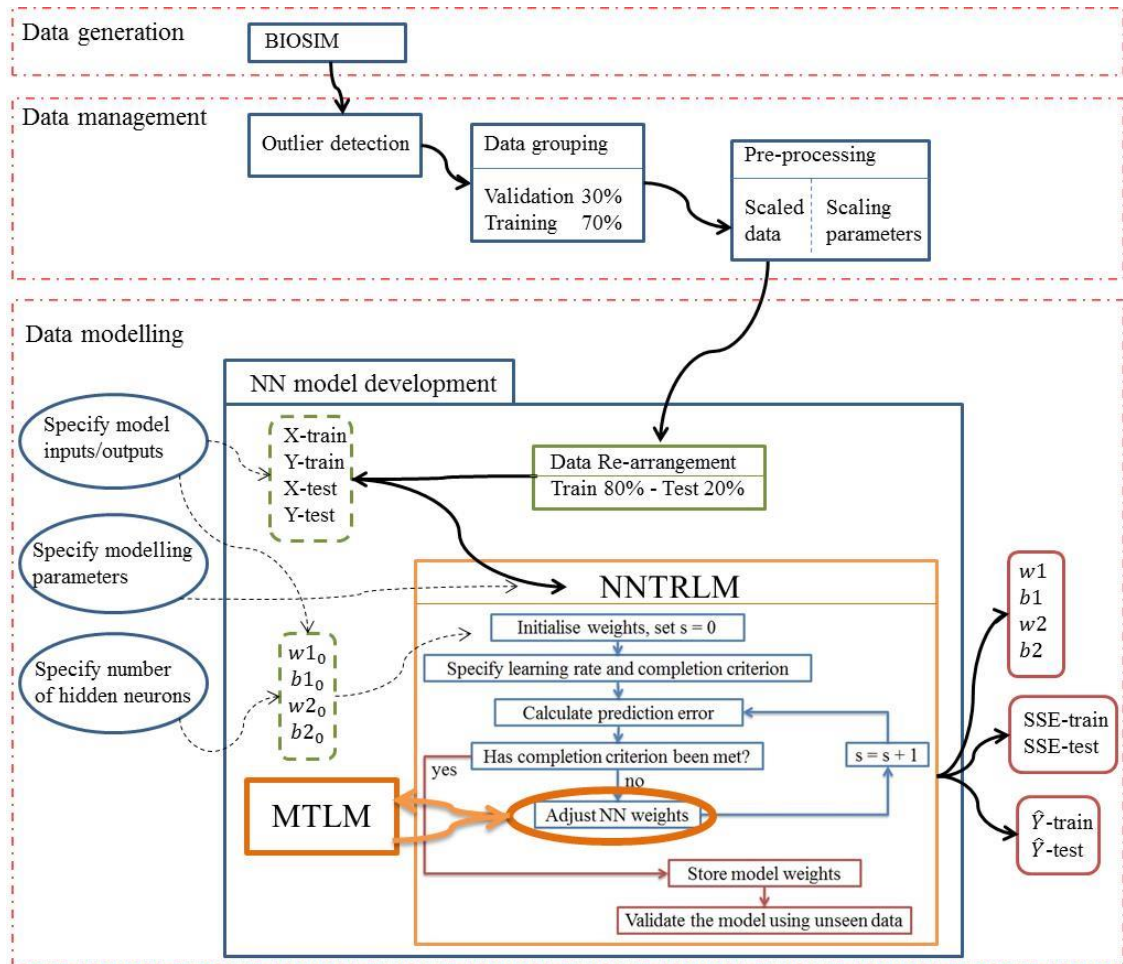


Figure 6.1 Data flowchart for developing neural network models

For the purpose of neural network modelling, the scaled training data is divided randomly into two groups of the train and the test sets with a ratio of 4 to 1 respectively. As shown in data modelling block of Figure 6.1, prior to the model development, three important sets of modelling elements should be specified. This includes specification of the number of the model inputs and outputs, the number of neurons in the hidden layer of the NN model and modelling parameters including the damping factor and target SSE value.

The feedforward neural network model with single hidden layer is applied with modelling structure consists of a number of dependant and independent variables (model inputs/outputs) and a number of neurons in the hidden layer. In Figure 6.1, w_{1_0} is associated with the weight synapses for initial random values assigned to w_{1ik} ($i = 1 \rightarrow p$), p being the number of model inputs and ($k = 1 \rightarrow h$), h being the number of hidden neurons.

The weight synapses for the input bias is assigned by b_{1_0} that can be associated with w_{10k} , ($k = 1 \rightarrow h$), in Figure 2.6. For the synapses connecting the hidden layer to the

single output neuron, $w2_0$ is considered to contain initial values for the weights associated with w_{0k1} , ($k = 1 \rightarrow h$), and $b2_0$ for the bias weight associated with w_{001} in Figure 2.6.

Therefore, for a NN model with single hidden layer, p number of model inputs, h number of hidden neurons predicting one dependant variable, a random matrix of ($h \times p$), a random vector of ($1 \times h$), a random vector of ($h \times 1$) and a single random value are considered in range between -0.1 and 0.1 for $w1_0$, $b1_0$, $w2_0$ and $b2_0$ respectively.

As depicted in Figure 6.1, ($X - \text{train}$), ($Y - \text{train}$), ($X - \text{test}$) and ($Y - \text{test}$) are the four matrixes containing scaled process data stored in two subsets of train data and test data. ($X - \text{train}$) is a ($n_1 \times p$) matrix with n_1 being the number of observations classified in the train data for model inputs and ($Y - \text{train}$) is a ($n_1 \times 1$) vector containing n_1 number of train data for the model output. In similar manner, ($X - \text{test}$) is a matrix of ($n_2 \times p$) and ($Y - \text{test}$) is a vector of ($n_2 \times 1$) whose elements are the input and output data with n_2 being the number of observation classified in the test subset.

In Figure 6.1, “NNTRLM”, a coded MATLAB function that establishes neural network weights using the modelling parameters specified. This function operates based on the algorithm depicted in Figure 2.7 and it employs another coded function called “MTLM” to update NN weights using Levenberg-Marquardt method explained in Section 2.6.3.

At the end of the operation, model weights ($w1$, $b1$, $w2$ and $b2$) are established and the final/best prediction results for the train and the test subsets are store in ($\hat{Y} - \text{train}$) and ($\hat{Y} - \text{test}$) vectors respectively. ($SSE - \text{train}$) and ($SSE - \text{test}$) are also reported for evaluation purpose demonstrating prediction accuracy capabilities.

With a NN model development coding programs in hand, Bootstrapping Aggregated Neural Network (BANN) models can be made by aggregating the individual NN models. Un-scaling of the prediction results will be carried out using the “scaling parameters” and validation of the BANN models will be investigated afterwards to assess prediction capability of the model on a set of unseen data.

6.2.6 Model validation

Validation of the models built in previous stages is carried out using data stored for validation purpose which has not been used in model development procedure. Model prediction errors are quantified using root mean squared errors (RMSE).

$$RMSE = \sqrt{\frac{\sum_{i=1}^V (Residual_i)^2}{V}} \quad (6.1)$$

Where (V) is the number of validation data and *Residual* values are the differences between prediction values obtained from the model and the true value of the data stored in the validation data set.

In this study, data sets are scaled to -1 and 1. Therefore, the overall data range is a 2-unit magnitude. RMSE value of 0.2 calculated for data with 2-unit magnitude, demonstrates prediction error of 10% (0.2 divided by the 2-unit magnitude) or 90% of prediction accuracy. Therefore, for model prediction accuracy of 90%, RMSE values of equal or less than 0.2 is acceptable for a scaled validation data set.

6.2.7 Unscaling

Scaling parameters used in the scaling stage is used to unscale prediction results of the models to return the data to their original scale.

In the next sections, PHB batch process data are modelled for unclassified data (Section 6.3), classified “feast” phase data (Section 6.4) and classified “famine” phase data (Section 6.5). The aim is to investigate model prediction accuracy improvement using the classification tools developed in Chapter 4 and Chapter 5.

6.3 Empirical modelling for unclassified operational data

In this section, PHB batch process data comprising of both “feast” phase and “famine” phase batch operations are used to build empirical models predicting critical process attributes at the end of a well-developed batch operation. It is expected to observe considerable prediction accuracy improvement when model developing data are segregated into separate sub-sets of “feast” phase and “famine” phase data in the subsequent sections. Table 6.1 tabulates simulation parameters assigned to generate process data for the modelling purpose. Five random numbers are considered for each simulator parameters associated with initial biomass (BIOM0), acetate (ADDHA) and ammonia (ADDN) concentrations by iterative operators of “RandNo1”, “RandNo2” and “RandNo3” respectively. The range of random values are between a1 and b1 for initial biomass concentrations, a2 and b2 for acetate concentrations and a3 and b3 for ammonia concentrations as observed in practical recipes reported in Chapter 3. The

initial intracellular PHB content is randomly assigned in between 0% to 100% as the minimum and maximum capacity of the cells to restore PHB.

Table 6.1 Process data generation contemplating “feast” and “famine” operational phases

Programming parameters		
Iteration operator	Minimum value	Maximum value
RandNo1 (BIOM0)=5	a1=2 (C-mmol/L)	b1=140 (C-mmol/L)
RandNo2 (ADDHA)=5	a2=100 (C-mmol/L)	b2=700 (C-mmol/L)
RandNo3 (ADDN)=5	a3=0.1 (N-mmol/L)	b3=10 (N-mmol/L)
PePHB0	0%	100%

For each one of the five initial biomass concentration, five different values are randomly assigned for acetate concentrations for which 25 different values are randomly selected for ammonia concentration. The five BIOM0 values randomly selected are shown along with the 25 ADDHA and 125 ADDN values in Figure 6.2.a, Figure 6.2.b and Figure 6.2.c respectively.

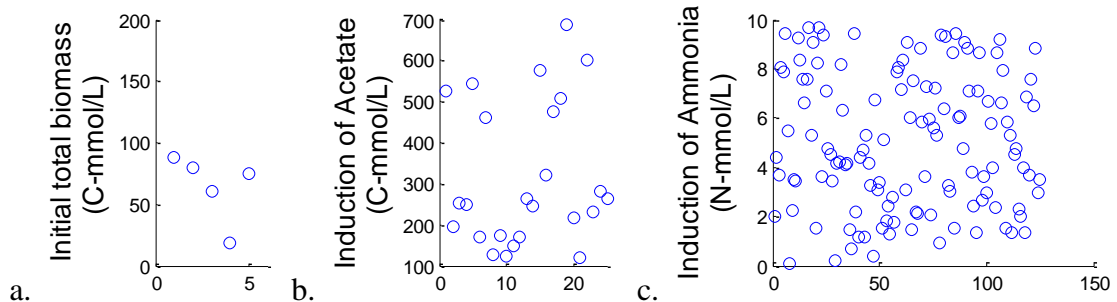


Figure 6.2 Random values assigned to process parameters for data generation

The PHB process simulator explained in Chapter 3 is used to generate 125 process data sets using the parameters assigned randomly as aforementioned. The batch operational duration is set to 25 hours which is sufficient for batch operations to reach to the process maturity conditions. In Figure 6.3 and Figure 6.4 the critical process attributes are depicted at the initial (T_0) and final (Point-Z) operational batch points respectively for the model training and validation data sets. Around 70% of the 125 data is used for model training purpose (88 batch operations) and the remained (37 batch operations) is used for model validation.

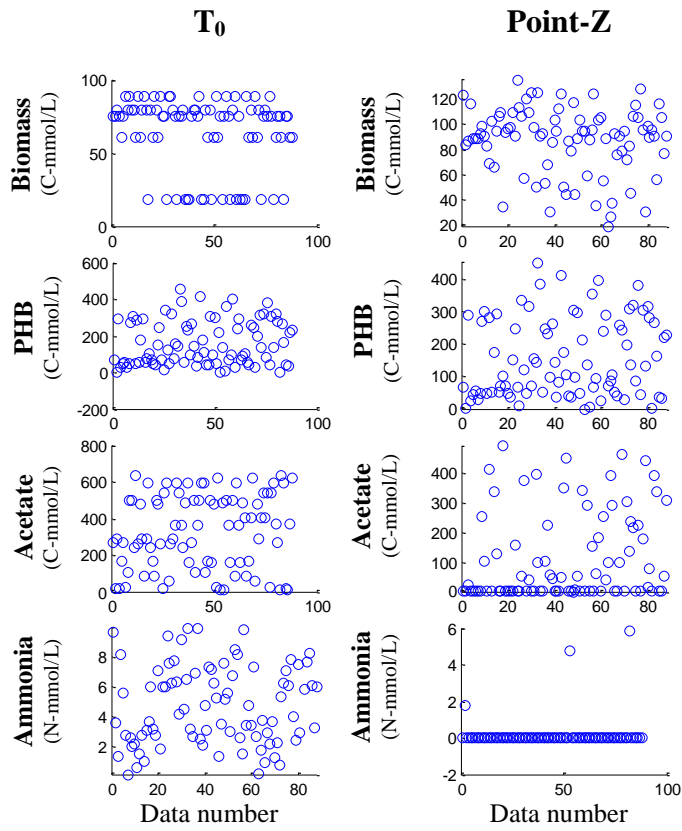


Figure 6.3 Training data for model development

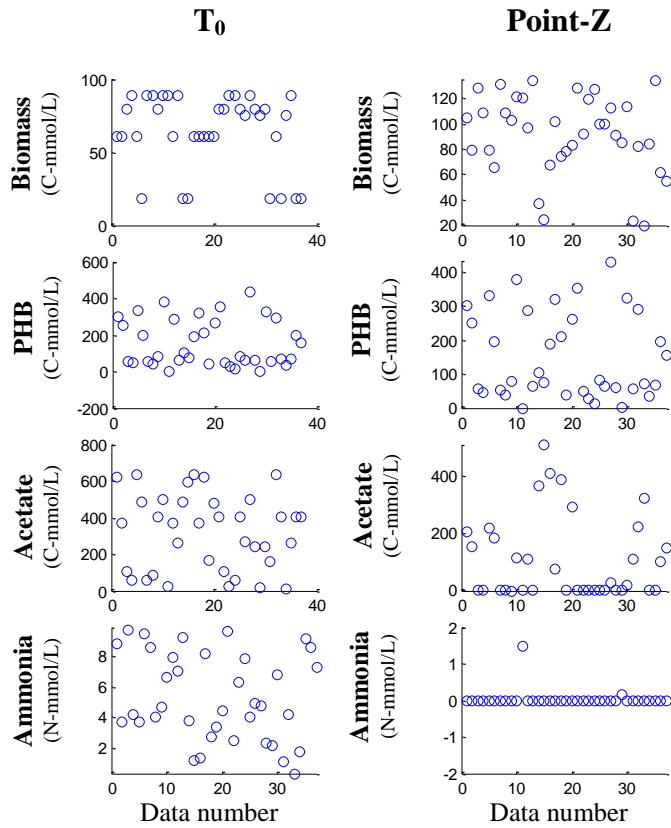


Figure 6.4 Validation data for model development

BANN is a sophisticated empirical modelling technique explained in Section 2.6.4 to build empirical models predicting biomass, PHB, acetate and ammonia concentrations after 25 hours of batch progression using four-input models. Initial biomass and intracellular PHB concentrations are input variables along with total acetate and ammonia concentrations injected to the batch processes.

In Figure 6.5, model predictions are marked by “ \bullet ” and the true/ target values are shown by “ \circ ”. The RMSE values for the set of validation data are also calculated and noted on each plot. The RMSE values obtained for the scaled data sets can be used to compare model prediction capability regardless of the size of validation data set and data magnitude range.

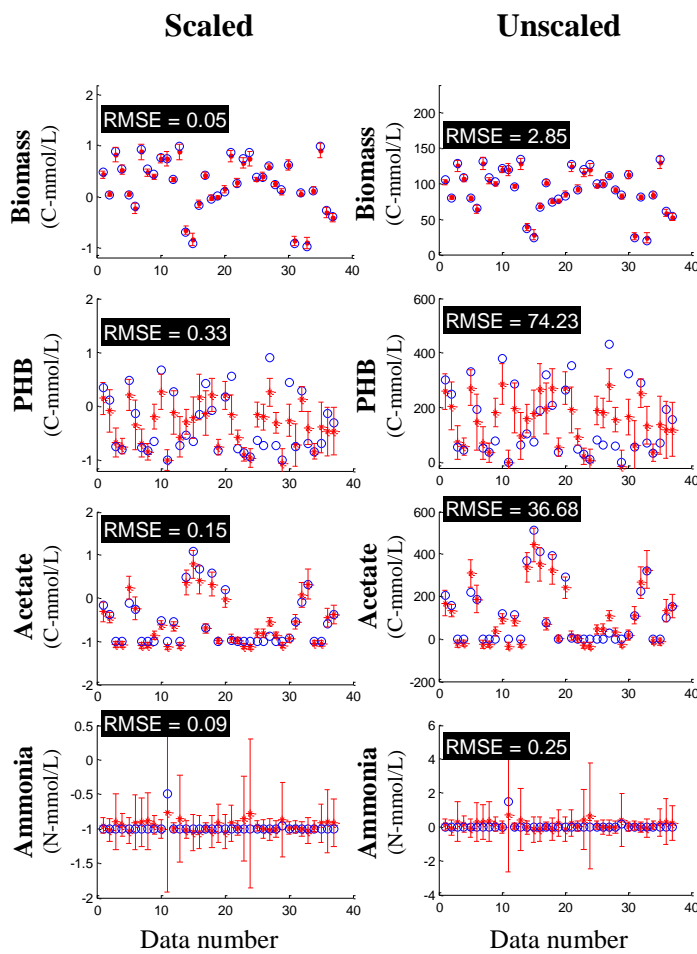


Figure 6.5 BANN model validation for critical process attributes at batch final operation point (Point-Z)

As mentioned, data sets are scaled to -1 and 1. Therefore, the overall data range for each data set is a 2-unit magnitude range. An RMSE value of 0.2 calculated for data with a 2-unit of overall magnitude, demonstrates prediction error of 10% (0.2 divided by a 2-unit range) or 90% of prediction accuracy. Therefore, for model prediction accuracy of 90%, RMSE values of equal or less than 0.2 are considered as acceptable values for scaled data sets in this study.

Since ammonia concentration at the end of a PHB batch process is insignificant, empirical models predicting this value is inconsequential. While final biomass concentration was predicted with high precision (with scaled RMSE of 0.05) and final acetate concentration prediction is in the acceptable range (with scaled RMSE of less than 0.2), the final PHB concentration prediction is poor (with scaled RMSE of 0.33). Since PHB is the process product and its model accuracy is highly demanded, investigations will be carried out in the subsequent sections to improve model predictions using segregated process data.

6.4 The “feast” phase operational modelling

6.4.1 Introduction

Prior to model development, an understanding of the process profiles is required to identify the most significant elements of the process being modelled. With the aim of developing empirical models, process profiles are investigated in the two major operational phase groups classified as the “feast” phase and the “famine” phase.

In order to generate process data for the modelling purpose, the PHB program simulator introduced in Chapter 3 is used. The original simulation program is embedded in a new program code structure that separates the “feast” phase data from the “famine” phase data using the “Phase Differentiation Equations” obtained in Chapter 5. The new structure is shown in Figure 6.6 where three iteration loops are considered to allocate random values to the initial biomass, acetate and ammonia concentrations. The “BIOSIM” program in this section is a modified version of the original program along with the supplement of the “Characterisation Method” module (CharMeth). Within the simulation program, Equation (5.14) is embedded in the “Phase Differentiation Equations” box where operational phase is predicted based on the initial state of the simulated batch. When a “feast” phase operation is predicted by the equation, the simulation result is stored in the “feast” phase memory box. On the other side, if prediction is towards “famine” phase occurrence, the simulation results are stored in the “famine” phase memory box based on the analysis carried out by the “CharMeth” module.

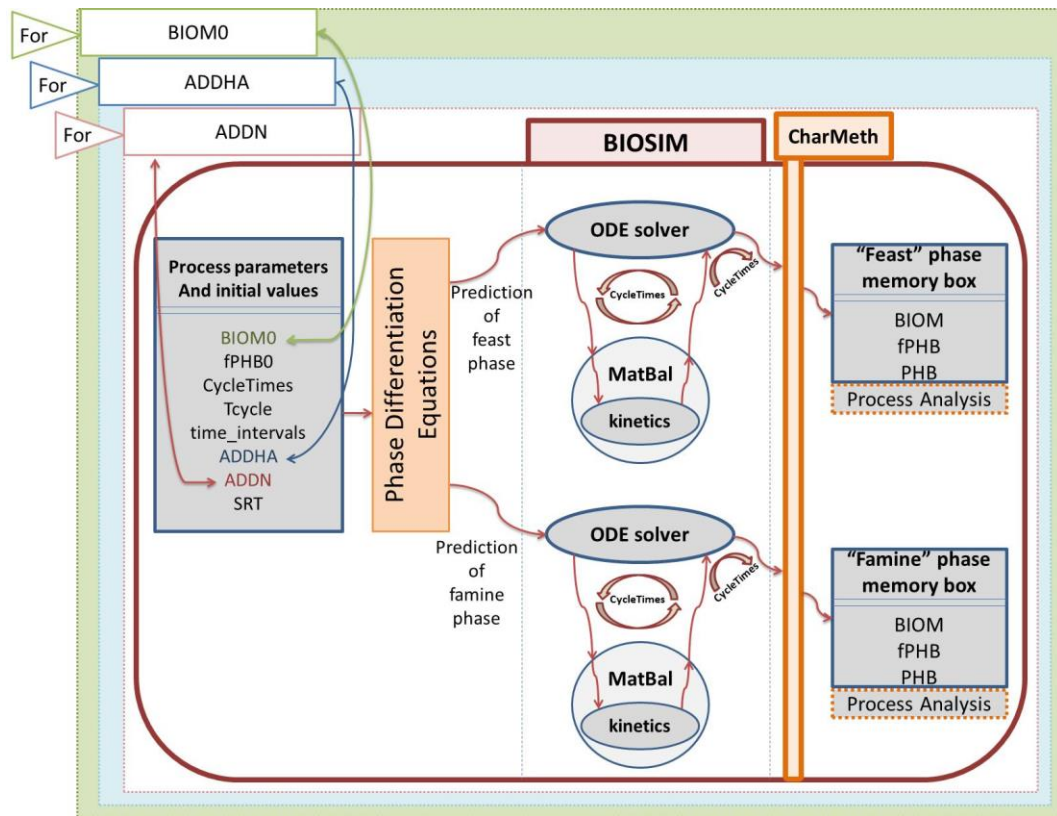


Figure 6.6 Data generation program structure separating operation phases

The capability of empirical models in prediction of some significant elements of the process is investigated in this study by developing linear (MLR) and non-linear (BANN) models using data obtained from batch simulations.

6.4.2 Description of the “feast” phase profile

For the case of the “feast” phase operational profile in a mixed microbial culture of 32 populations, “fPHB summation” is a factor defined as the summation of all the 32 fPHB values at any operational time. As mentioned in Chapter 3, fPHB indicates the ratio of PHB concentration over the PHB-free biomass concentration. PHB formation inside cells can be reflected by “fPHB summation” incline, and PHB consumption by “fPHB summation” declines during operational period.

In Figure 6.7, two “feast” phase simulation results are depicted. On the left, two plots are shown for a low ratio of the PePHB0 factor; and on the right, two plots are given for a case of high PePHB0 ratio. These two simulation results are shown to demonstrate two different “fPHB summation” while their PHB profiles are similar. In Figure 6.7.a, PHB formation and biomass growth occur simultaneously; whereas in Figure 6.7.b, PHB stored in the cells is consumed initially to provide additional carbon in direction of biomass growth and then PHB formation takes place afterwards in presence of external feed source. As mentioned in Chapter 4, ammonia, acetate, PHB stability points are

specified along with the first additional analytical point with (\blacktriangle), (\blacktriangledown), (\bullet), and (\star) signs respectively in Figure 6.7 (Dias *et al.*, 2005).

On the PHB profiles depicted in Figure 6.7, the illustrative indicators developed in Chapter 4 for acetate, ammonia and PHB stability point detection are shown as well. “Point-A”, “Point-B”, “Point-C” and “Point-D” are defined as the ammonia stability point, acetate stability point, PHB stability point and maintenance of the PHB stability detection point in a “feast” phase batch operation. This naming system will be used to assign model input/output structure.

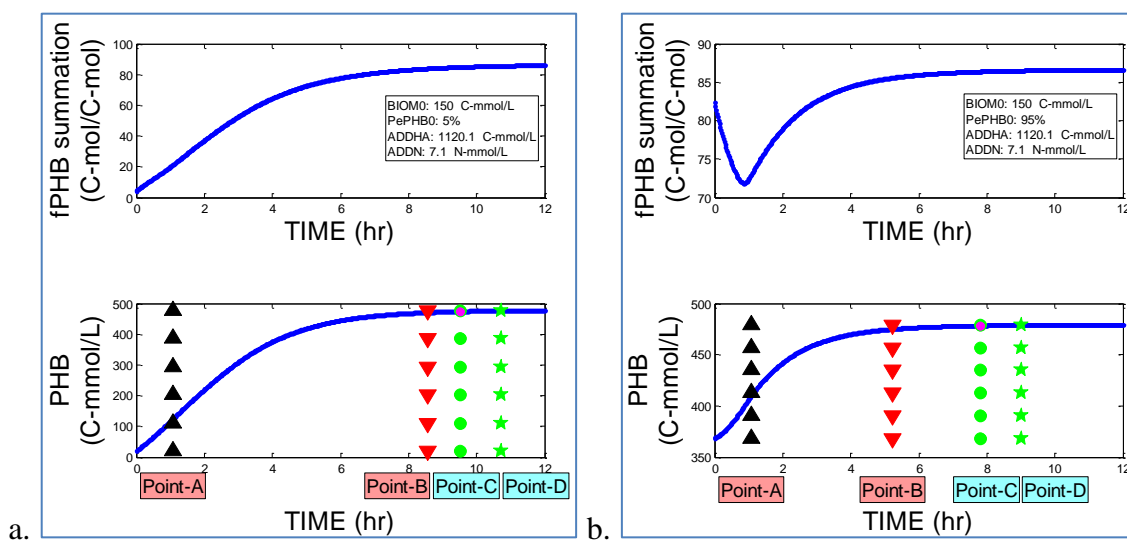


Figure 6.7 “Feast” phase PHB profiles (RT8) for low PePHB0 (left) and high PePHB0 (right) values

Comparison of the two simulation results suggest that continues inclination of PHB profile cannot be associated with continues formation of PHB within the cells. Additionally, it is not sufficient to observe and analyse the triple plots of acetate, ammonia and PHB to provide a detailed assessment of the batch process. Application of other process profile such as the “fPHB summation” factor can provide useful and interesting information about the process which is applied in the “famine” phase profile investigations with more tangible outcomes.

In the next sections, modelling development procedure is performed for the “feast” phase operation data using linear and non-linear model development techniques.

6.4.3 Data generation targeting “feast” phase batch operations

In this section, data generation is carried out with the aim of developing empirical models predicting critical process elements in the “feast” phase operations. Therefore, simulation parameters are specified so that these parameters are appropriate for generation of data representing “feast” phase operations.

Simulation program is used to consider batch operations initiating with cells containing low level of PHB. In practice, “feast” phase operations are conducted to increase PHB content of cells. Initiating a “feast” phase operation with high PHB content cells results into PHB consumption towards cell replication with consequent PHB accumulation in presence of carbon source and nitrogen source limitation. Moreover, in an ideal SBR operation, a batch process is directed towards a “feast” phase operation after a “famine” phase operation is completed. As the result, PHB content of the cells should be low at the initial point of a “feast” phase operation after a successful “famine” phase occurrence (Dias *et al.*, 2005).

The “PePHB0” value that determines the “fPHB0” parameter to specify the PHB content of the initial biomass is randomly assigned in a range between 0% and 20% for each batch simulation since low PHB content cells are expected to initiate a “feast” phase batch process. In Table 6.2, the program parameters used to design a series of batch simulations is tabulated. The programing parameters are to assign random values to the initial biomass (BIOM0), acetate (ADDHA) and ammonia (ADDN) concentrations. The number of random numbers is specified by “RandNo1”, “RandNo2” and “RandNo3” for BIOM0, ADDHA and ADDN respectively. These numbers are generated in a range of numbers starting from “a1”, “a2” and “a3” and to the “b1”, “b2” and “b3” for BIOM0, ADDHA and ADDN respectively.

Table 6.2 Process data generation targeting “feast” phase operation

Programing parameters		
Iteration operator	Minimum value	Maximum value
RandNo1 (BIOM0)=10	a1=2 (C-mmol/L)	b1=140 (C-mmol/L)
RandNo2 (ADDHA)=5	a2=100 (C-mmol/L)	b2=700 (C-mmol/L)
RandNo3 (ADDN)=5	a3=0.1 (N-mmol/L)	b3=10 (N-mmol/L)
PePHB0	0%	20%

In Table 6.2, simulation results of 250 batch processes are given for 10 different values of initial biomass concentrations. For each initial biomass concentration, five different values are randomly assigned for acetate concentrations for which 25 different values are randomly selected for ammonia concentration introduced to the batch. The numbers of random values are selected so that the “feast” phase batch data is close to 125 as in Section 6.4 to make reliable comparisons. The 10 initial biomass concentrations, along with the 50 acetate concentration values and 250 ammonia concentrations assigned by

random generator function are depicted in Figure 6.8.a, Figure 6.8.b, and Figure 6.8.c respectively.

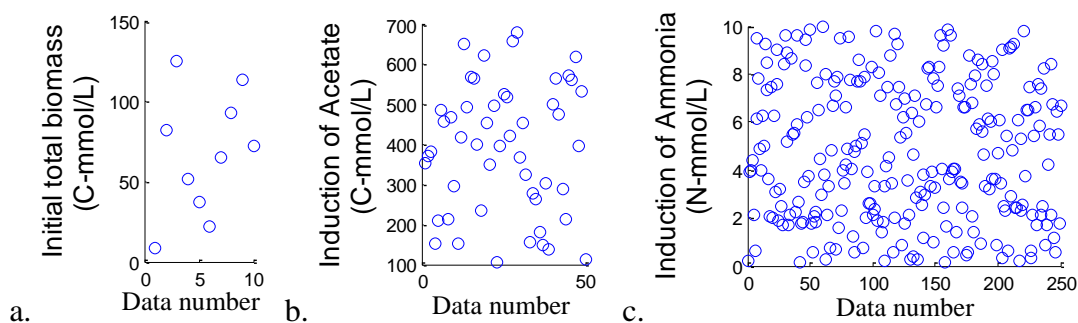


Figure 6.8 Random values assigned to process parameters for data generation targeting the “feast” phase

The random values are used to simulate 250 batch operations. Based on the initial condition of the batches, occurrence of “feast” or “famine” phase operations were predicted using “Phase Differentiating Equation” (Equation (5.14)) derived on the basis of the “Characterisation Method” analysis. As the result, 128 batches were predicted to operate under the “feast” phase operation and the other 122 batches were expected to run under the “famine” phase.

Simulation of the 250 batch operations provide concentration profiles to be analysed by the “CharMeth” module to identify the “Regime Type” number of each batch as defined in Chapter 4. Identification of RT6, RT7 and RT8 are associated with the “feast” phase operation and RT3 and RT5 represent “famine” phase operation. An operation under RT9 experiences PHB drop due to carbon source scarcity after PHB saturation. Therefore RT9 is neither a complete “feast” nor a “famine” phase operation in this context.

Figure 6.9 shows four plots validating the prediction capability of the “Phase Differentiating Equation” (Equation (5.14)) by means of profile analysis represented by “Regime Type” numbers. Figure 6.9.a declares that 113 batch operations out of the total 128 batches predicted to operate under the “feast” phase were executed under RT6, RT7 or RT8 which confirms occurrence of the “feast” phase operation. The remained 15 batches presented by RT4, RT5 or RT9 cannot be considered as a “feast” phase operation and therefore are depicted in Figure 6.9.c as incorrect prediction of the phase operation at the initial point of the batch.

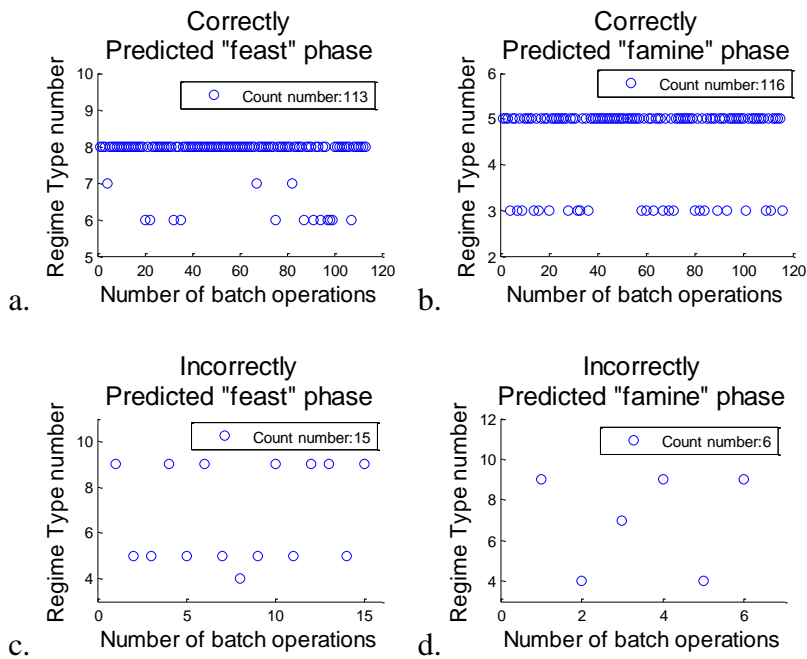


Figure 6.9 Identification of valid “feast” phase data set

The batch operations estimated to operate under the “famine” phase based on their initial conditions were also validated by the “Characterisation Method” to confirm that 116 out of the 122 batches predicted for “famine” phase operation operated under either RT3 or RT5 which represent “famine” phase “Regime Types” as shown in Figure 6.9.b. The remaining 6 batches operated under RT4, RT7 or RT9 cannot be considered as a “famine” phase operations and depicted in Figure 6.9.d. These results show that phase prediction using the “Phase Differentiating Equation” (Equation (5.14)) is valid for more than 90% of the simulated batch processes.

In this section, the focus of empirical model development is on process data obtained from the “feast” phase batch operations. With the aim of developing models targeting significant elements of the “feast” phase batch operation of the PHB production process, data set with the “feast” phase “Regime Type” numbers is considered. Around 70% of the data is used for model training purposes and the remaining is stored for the model validation. Therefore, 80 observations out of the total 113 “feast” phase batch data will be used as the training data set and the remaining 33 observations will be stored for model validation.

The training and validation data are represented in Figure 6.10 and Figure 6.11. In these plots, biomass, PHB, acetate and ammonia concentrations at the initial point of batch operation (T_0), ammonia stability point (Point-A), acetate stability point (Point-B) and PHB saturation point (Point-C) are depicted along with the time of Point-A, Point-B and Point-C occurrences for the “feast” phase operations.

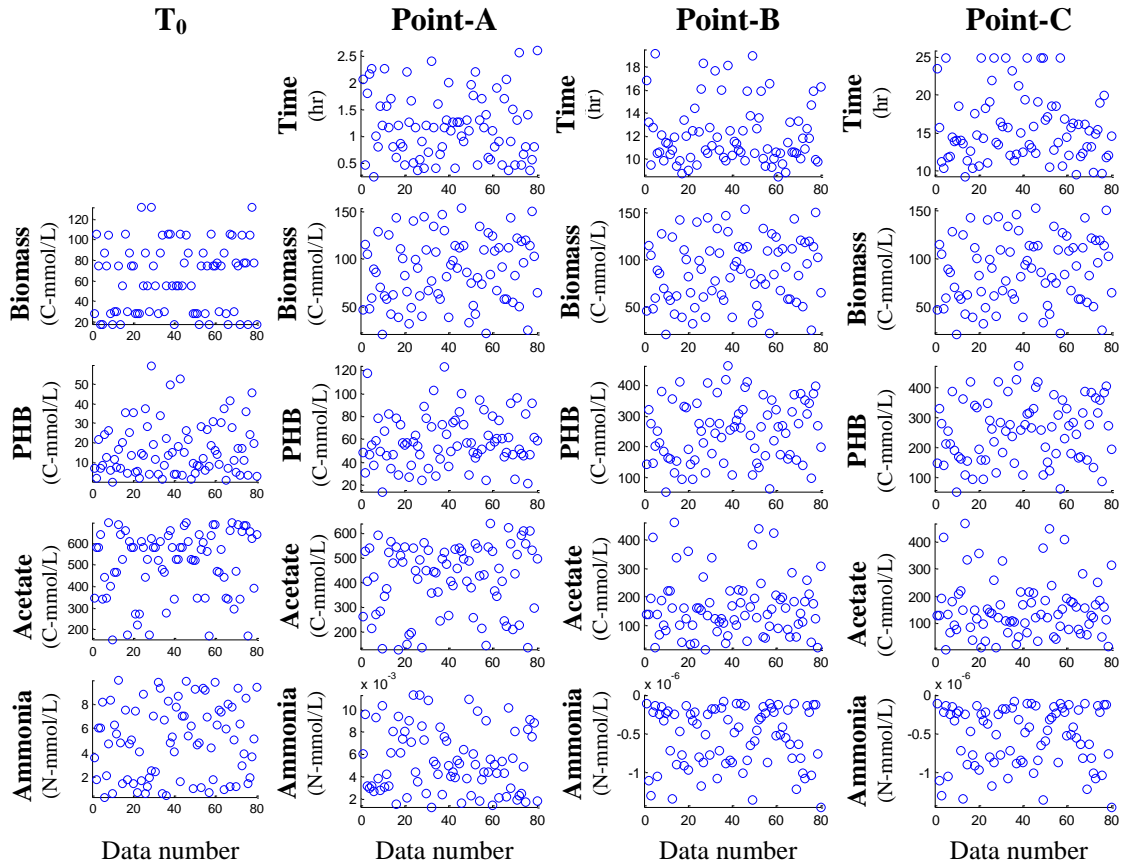


Figure 6.10 Training data for the “feast” phase model development

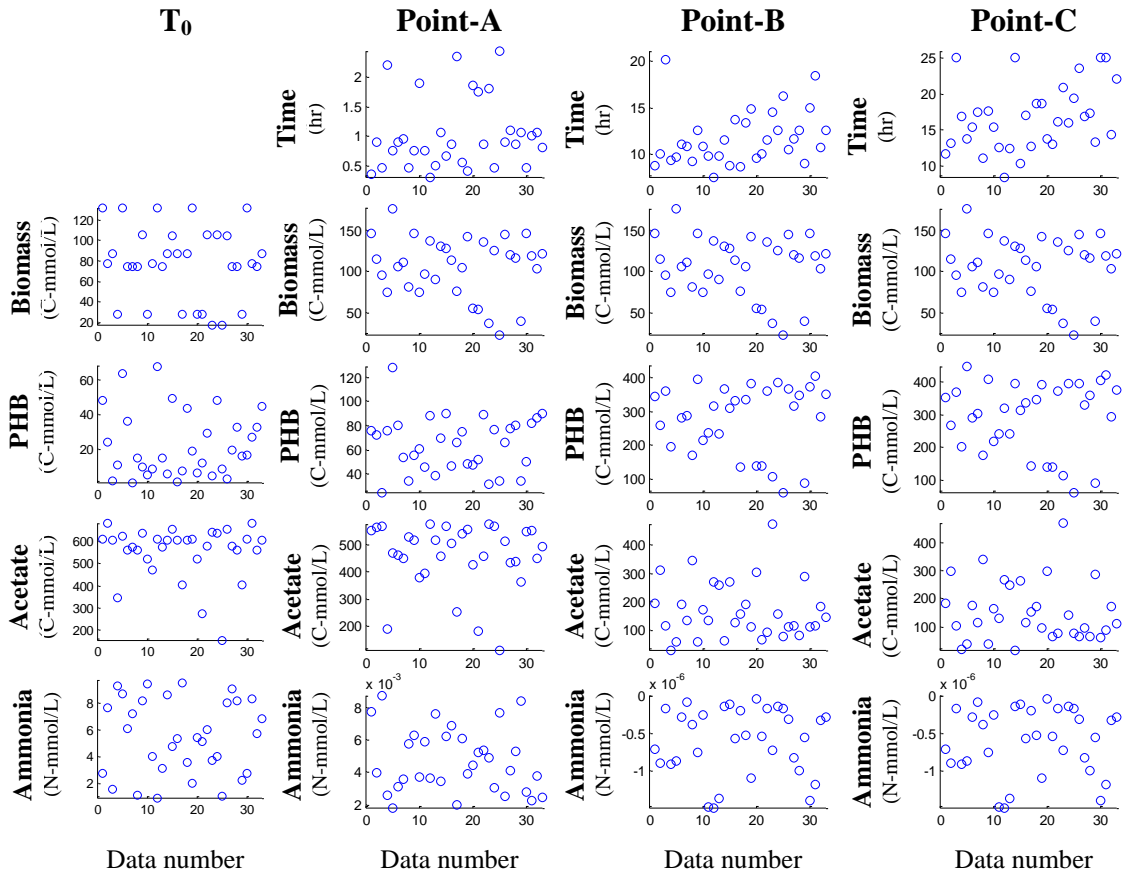


Figure 6.11 Validation data for the “feast” phase model development

For empirical model development, training and validation data sets are pre-processed (scaled to -1 to 1) and stored. The scaling parameters are the minimum and maximum values for each subset of training data as tabulated in Table 6.3.

Table 6.3 Scaling parameters for the “feast” phase data sets

	T ₀		Point-A		Point-B		Point-C	
	Min	Max	Min	Max	Min	Max	Min	Max
Time (hr)	0	0	0.2	2.6	8.5	19.1	9.2	24.9
Biomass (C-mmol/L)	17.6	131.7	21	153.3	21.0	153.3	21.0	153.3
PHB (C-mmol/L)	0.1	53.8	13.7	123.5	13.7	123.5	53.2	473.3
Acetate (C-mmol/L)	153.8	696.94	128.0	641.3	128.0	641.3	4.2	467.3
Ammonia (N-mmol/L)	0.3	9.9	0	0.01	0	0.01	0	0

The scaled training and validation data will be used to develop both MLR and BANN models. In the following section, MLR models are developed and validated.

6.4.4 MLR modelling targeting “feast” phase process data

The first modelling structure proposed to build MLR models has four inputs with the following formation:

$$y = \theta_0 + \theta_1 x_1 + \theta_2 x_2 + \theta_3 x_3 + \theta_4 x_4 \quad (6.2)$$

where x_1 , x_2 , x_3 and x_4 are total biomass, PHB, acetate and ammonia concentrations at the initial point of the batch simulations and θ_0 , θ_1 , θ_2 , θ_3 and θ_4 are MLR model parameters. The MLR modelling technique explained in Section 2.6.2 is applied to determine model parameters. The BLS solution of Equation (2.16) is used to obtain the MLR model parameters tabulated in Table 6.4.


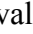
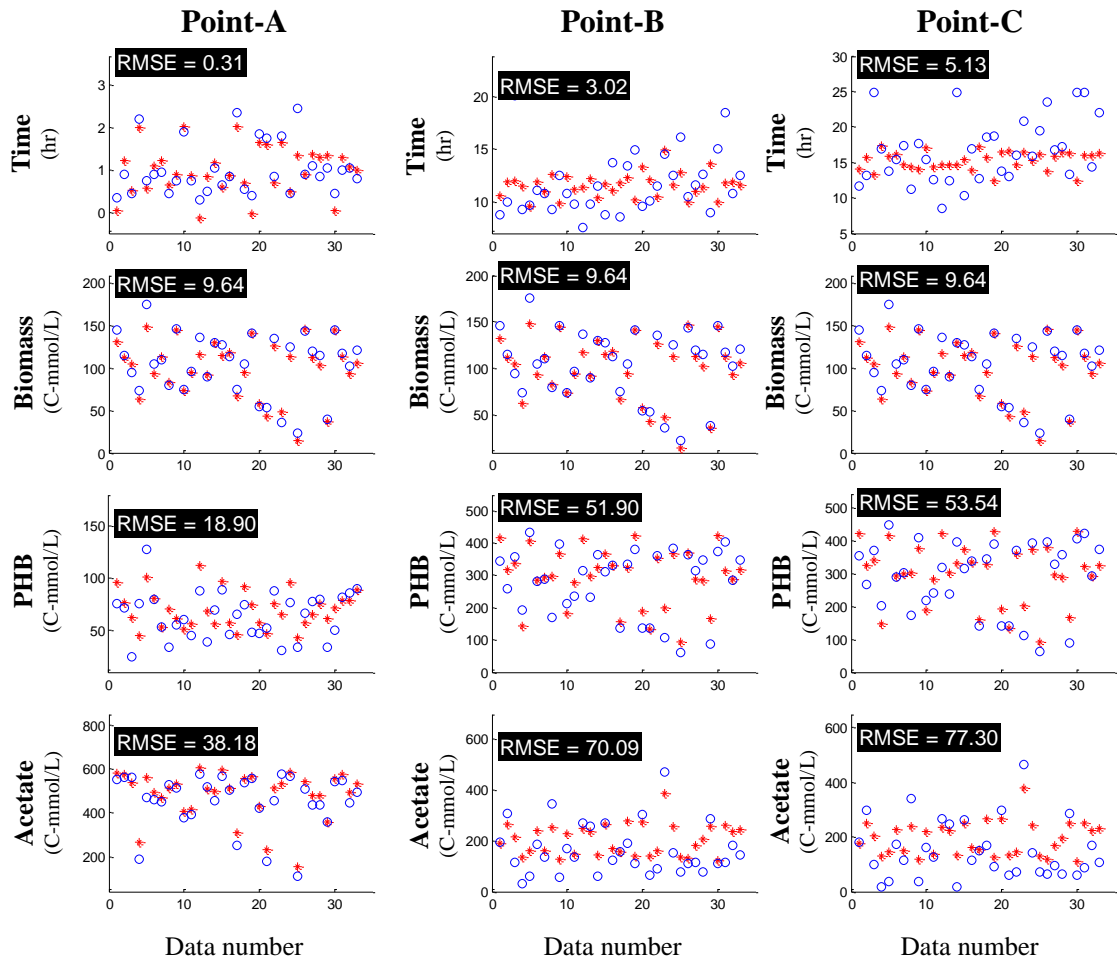
The prediction results are depicted for the unscaled validation data in Figure 6.12. In the plots depicted in this figure, the model predictions are marked by “” and the true/target values are shown by “”. The RMSE values for the set of validation data are calculated and noted on each plot. Since ammonia concentrations are insignificant in the process, empirical models are not trained for their predictions.

Table 6.4 MLR model parameters to predict significant occurrences in the “feast” phase operations

$y = f(x_1, x_2, x_3, x_4)$		θ_0	θ_1	θ_2	θ_3	θ_4
Model outputs						
Point-A	Time	-0.3584	-0.6448	-0.0080	0.0195	0.3818
	Biomass	0.8068	-0.1862	0.1422	0.1855	0.2786
	PHB	-0.0209	0.4114	-0.4969	0.2959	-0.1106
	Acetate	-0.0016	0.0655	0.0797	0.8681	-0.1173
Point-B	Time	-0.4955	-0.4038	0.1088	0.2988	-0.2132
	Biomass	0.8070	-0.1863	0.2173	0.1855	0.2784
	PHB	0.5597	-0.0311	0.2516	0.2921	-0.0381
	Acetate	-0.3746	-0.6295	0.2732	0.7351	-0.2516
Point-C	Time	-0.1680	-0.2790	0.1854	-0.0038	0.1054
	Biomass	0.8070	-0.1863	0.2684	0.1855	0.2784
	PHB	0.5620	-0.0291	-0.0928	0.2958	-0.0271
	Acetate	-0.3962	-0.6172	0.2589	0.6955	-0.2370

**Figure 6.12 MLR model prediction results for the validation data**

Looking at Figure 6.12, it can be deduced that MLR models are not capable of providing accurate predictions for the “feast” phase process elements. Therefore investigations to develop more reliable models will be conducted. Evaluation of model prediction capability will also be carried out after BANN model development stage in Section 6.4.6. In the next section, the same set of data used for MLR modelling will be applied to develop and validate non-linear neural network models to be compared with the results obtained from MLR model predictions.

6.4.5 BANN modelling targeting “feast” phase process data

With the aim of improving prediction capabilities of the empirical models, BANN modelling method is investigated in this section. In Section 6.2.5, general description of the data flowchart is given for development of an individual neural network model. In this section, scaled training data is used to develop a series of neural network models comprising of a single hidden layer. For a certain set of training data set, “train” and “test” data subsets are partitioned randomly to develop a series of neural networks with initial parameters arbitrarily generated to tune model parameters. This procedure is repeated for a range of different number of hidden neurons in the hidden layer denoted by (hn_{min}) for the minimum number of hidden neurons and (hn_{max}) for the maximum number of hidden neurons. The best model is the one presenting the lowest SSE value on the “test” data set and the neural network structure and the weights associated with the minimum SSE value is stored to be applied in the BANN structure. In Figure 6.13, development of N number of neural networks using a certain set of pre-processed training data is depicted.

As depicted in Figure 6.13, random functions generate random values to initialise NN weights and also to set an arrangement for selection of the “train” and the “test” subsets from the original “training” data set. The first neural network model is built with hn_{min} number of hidden neurons using the Levenberg-Marquardt method mentioned in Section 2.6.3. The NN model is stored with its SSE value obtained on the “test” data set. Afterwards, one hidden neuron is added to the hidden layer and the NN weights are tuned to obtain the SSE value of the second NN model. This procedure is repeated until a NN model is developed for (hn_{max}) number of hidden neurons. The best model structure is selected via cross validation for the minimum SSE value for test data set.

The second individual neural network model is built and selected by repeating the procedure mentioned with a random alteration in the selection of the “train” and the “test” subsets and initial model tuning parameters as depicted in Figure 6.13. This

procedure is repeated to build N number of individual neural networks to be implemented in the BANN model structure.

In order to compare performance of the neural network models and the MLR models developed previously, the same set of training and validation data is used to predict process elements of significant importance. With the aim of building a BANN structure from N number of individual neural networks, MATLAB program is applied to implement the algorithm described in Figure 6.13. In this program, thirty neural networks are selected to model each element of high interest from the process ($N = 30$) and the number of neurons in the hidden layer varies in between 1 to 40 ($hn_{min} = 1$, $hn_{max} = 40$). The models selected for aggregation have the minimum SSE value on the “test” data among the models built with different number of hidden neurons. Figure 6.14 shows SSE_{test} values obtained for neural networks predicting total PHB concentration at its stability point in a “feast” phase profile (Point-C). As shown in Figure 6.14 and mentioned in description of Figure 6.13, 40 neural networks are developed with different number of hidden neurons for each of the 30 data sets obtained from re-arrangement of the training data. The points associated with the minimum SSE_{test} value in the set of models developed for a certain set of data are marked by “○” in Figure 6.14. This figure is generated in modelling procedure carried out to predict total PHB concentration at its stability point using initial concentrations of biomass, PHB, acetate and ammonia as the independent variables.

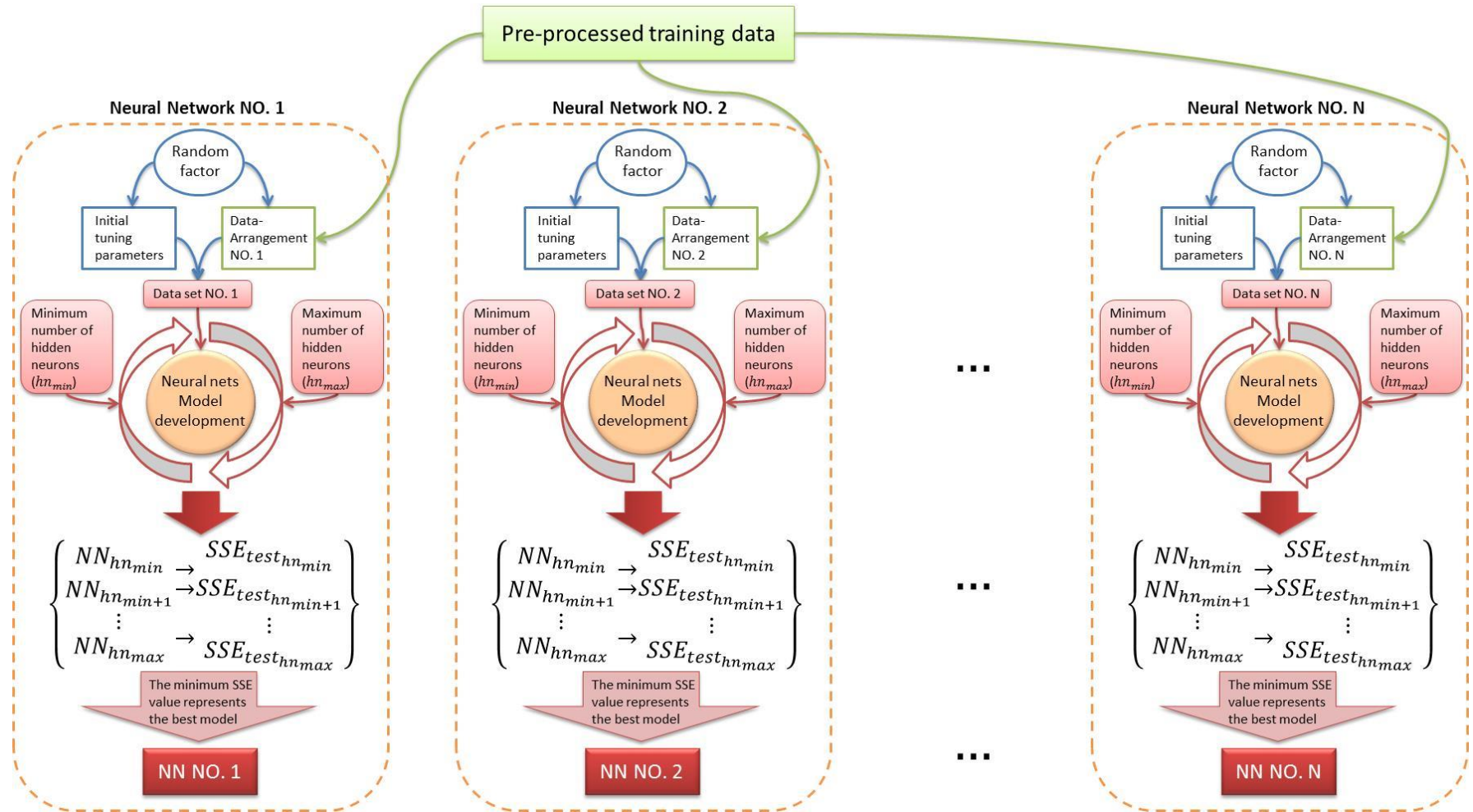


Figure 6.13 Development of N number of individual neural networks for a certain set of training data

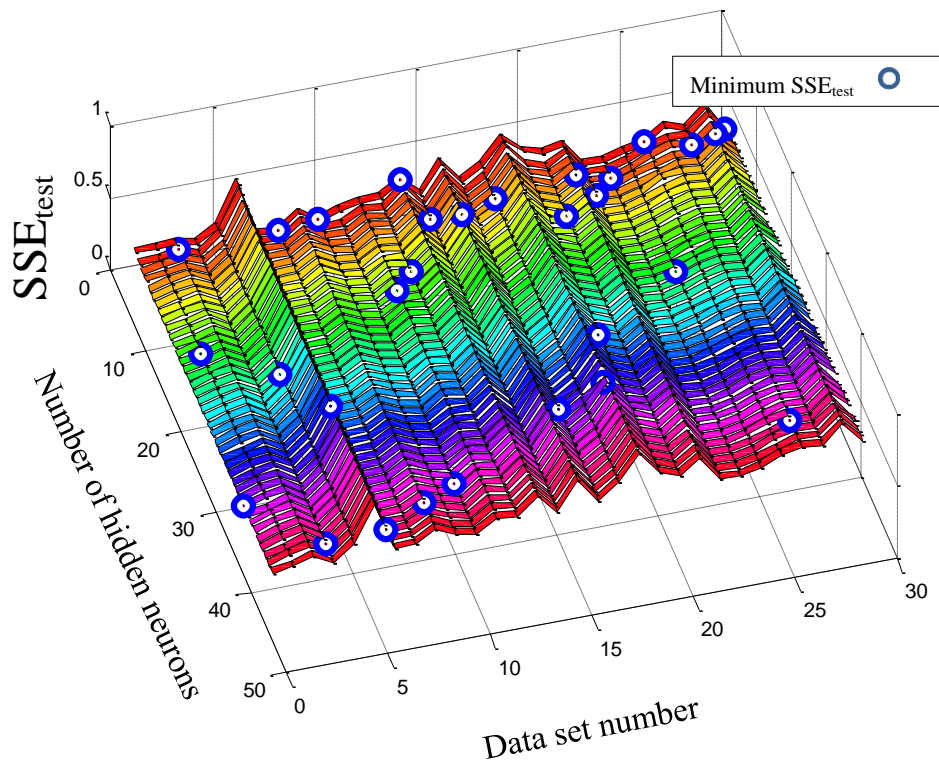


Figure 6.14 SSE_{test} values obtained for NN models predicting PHB concentration at its stability point in “feast” phase profile

Figure 6.14 shows that optimal number of hidden neurons varies from one model to another. In Figure 6.15 optimal numbers of hidden neurons are depicted for the models developed to predict PHB concentration at PHB saturation point. Considering Figure 6.14 and Figure 6.15 it can be deduced that a high number of hidden neurons cannot be associated with the best model performance.

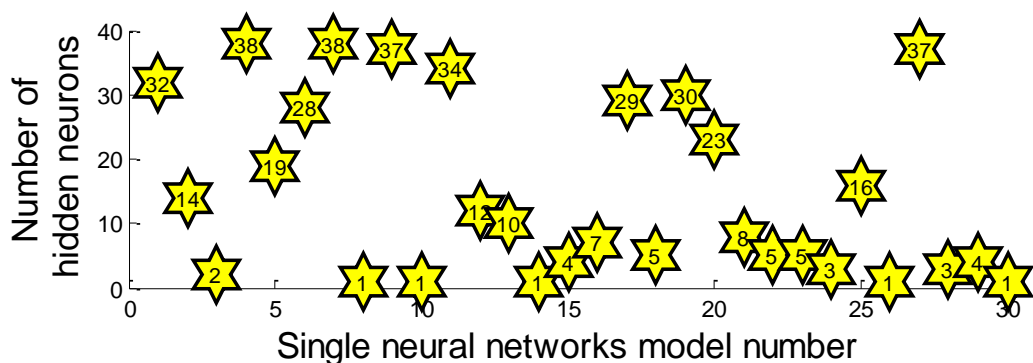


Figure 6.15 Optimal number of hidden neurons obtained for each selected single NN model

The thirty selected models are aggregated to form a single structure BANN model as explained in Section 2.6.4. Figure 6.16 shows SSE values obtained for the individual

neural network models along with the aggregated BANN model validated using the 33 data sets stored for validation purpose of the model built for PHB at Point-C.

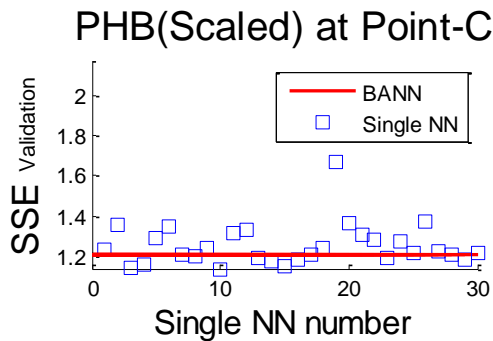


Figure 6.16 Comparison of the single NN models with the BANN model SSE values

It can be seen that the SSE value calculated for BANN is lower than the average value of single models SSE values. Although BANN model does not provide the most accurate predictions when compared to some single models with low SSE values, it presents predictions that are more reliable and acceptable in comparison to the least accurate single model predictions. Therefore, aggregation of the single models provided a robust prediction capability for the BANN model as demonstrated in Figure 6.16.

The prediction capability of the BANN model developed to estimate total PHB concentration at the PHB saturation point of the “feast” phase operations is shown in Figure 6.17 for the unscaled validation data. The RMSE value of about 40 demonstrates prediction capability of around 90% for the range of validation data given between 100 and 500 C-mmol/L. In addition to the predicted values by the BANN model and their true values as the target, prediction confidence bounds are calculated and shown in the figure.

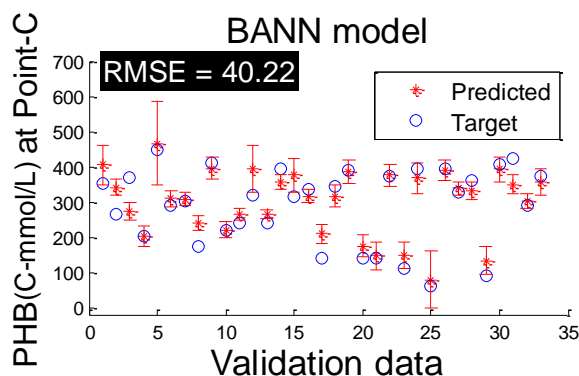


Figure 6.17 Validation of the model predicting PHB concentration at Point-C

The case of BANN model development procedure for PHB concentration at Point-C was discussed as a standard procedure to present model structure and prediction results.

The other modelling results obtained for the significant elements of the “feast” phase profile using the same four input variables of initial biomass, PHB, acetate and ammonia concentrations are depicted in Figure 6.18, Figure 6.19 and Figure 6.20 for hidden neuron numbers (HNN), SSE values of prediction accuracy for scaled data, and aggregated model validation respectively.

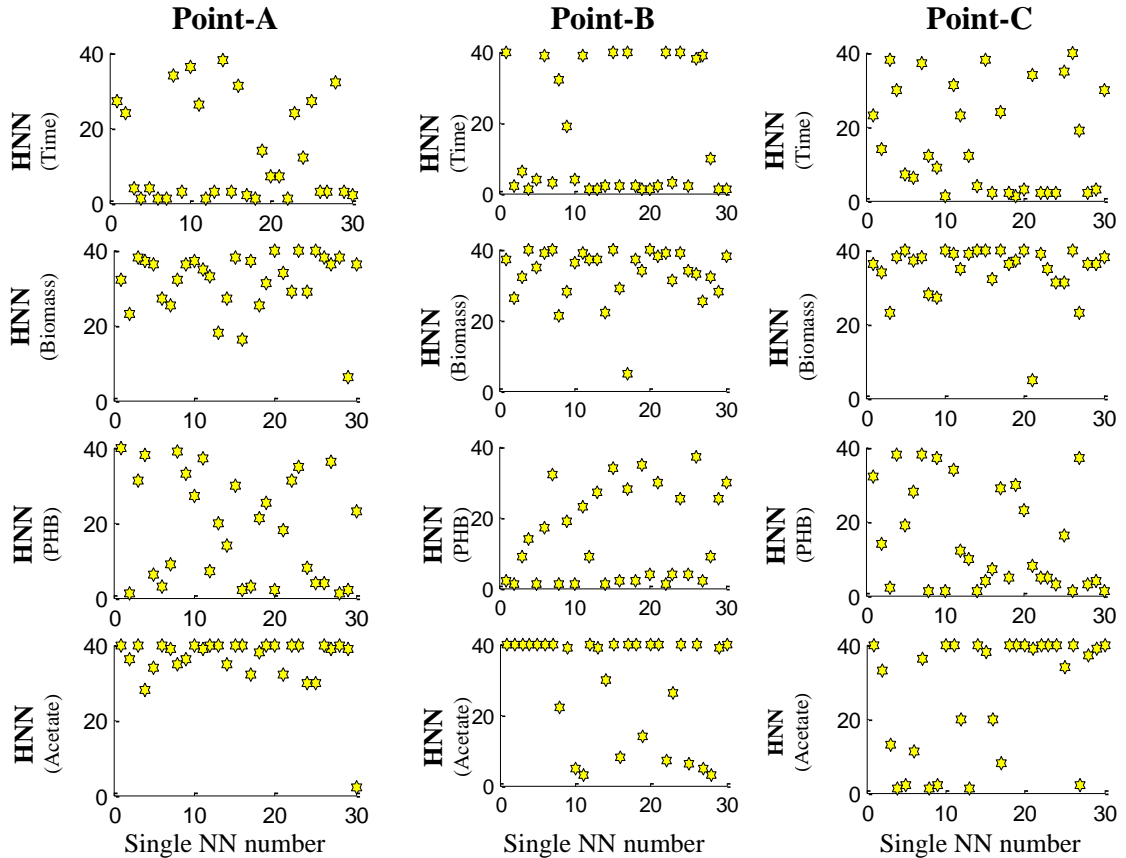


Figure 6.18 Number of hidden neurons for each single NN structure

In Figure 6.18, the number of hidden neurons selected to produce the lowest prediction errors for a specific arrangement of train-test data and the initial tuning parameters are shown for all modelling output targets. As mentioned in description of Figure 6.14 and Figure 6.15, optimal number of neurons in the hidden layer varies when initial model training parameters alter and that a NN model with high number of hidden neurons does not guarantee the most accurate predictions.

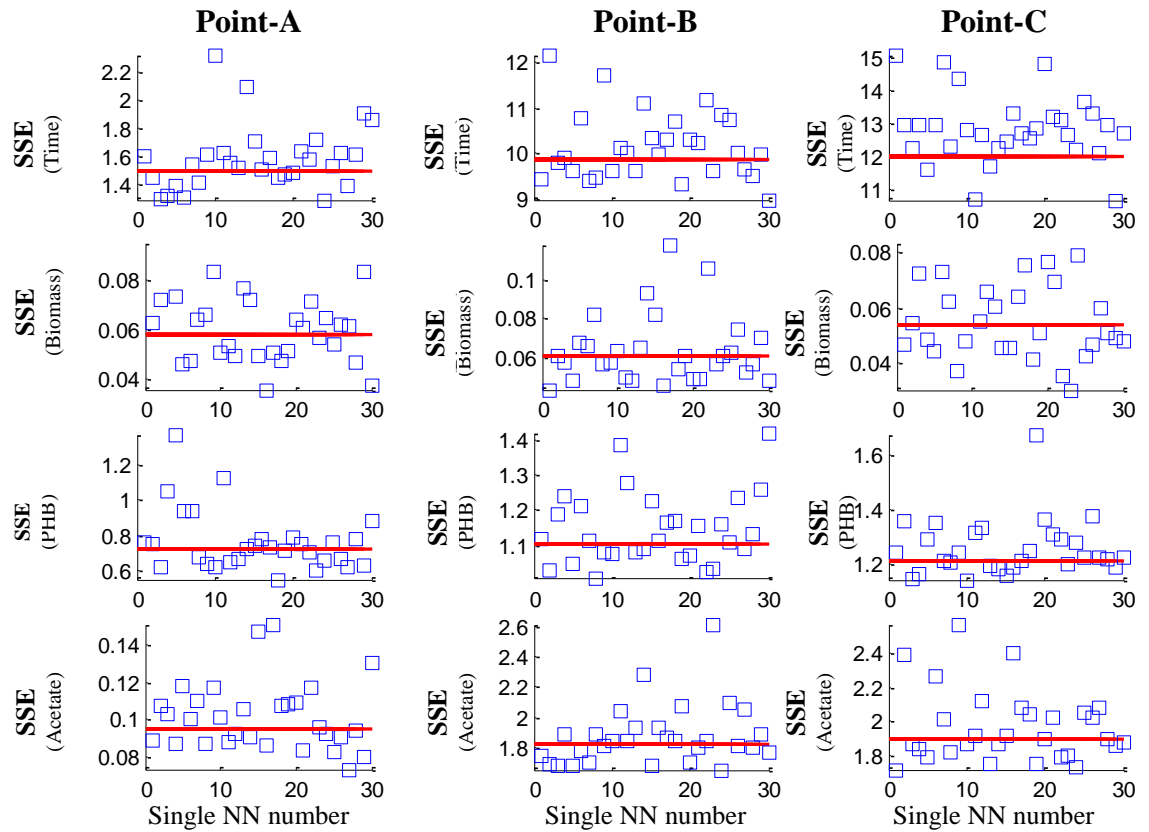


Figure 6.19 Sum square errors of single and aggregated model predictions for “fast” phase scaled data

Figure 6.19 shows the SSE values for the validation data set using the single NN models along with their counterpart produced by the aggregated BANN model. This figure confirms the validity of the statement made in description of Figure 6.16, arguing that the residual value of BANN modelling technique is approximately equal or less than the average value of the single models embedded within the BANN model.

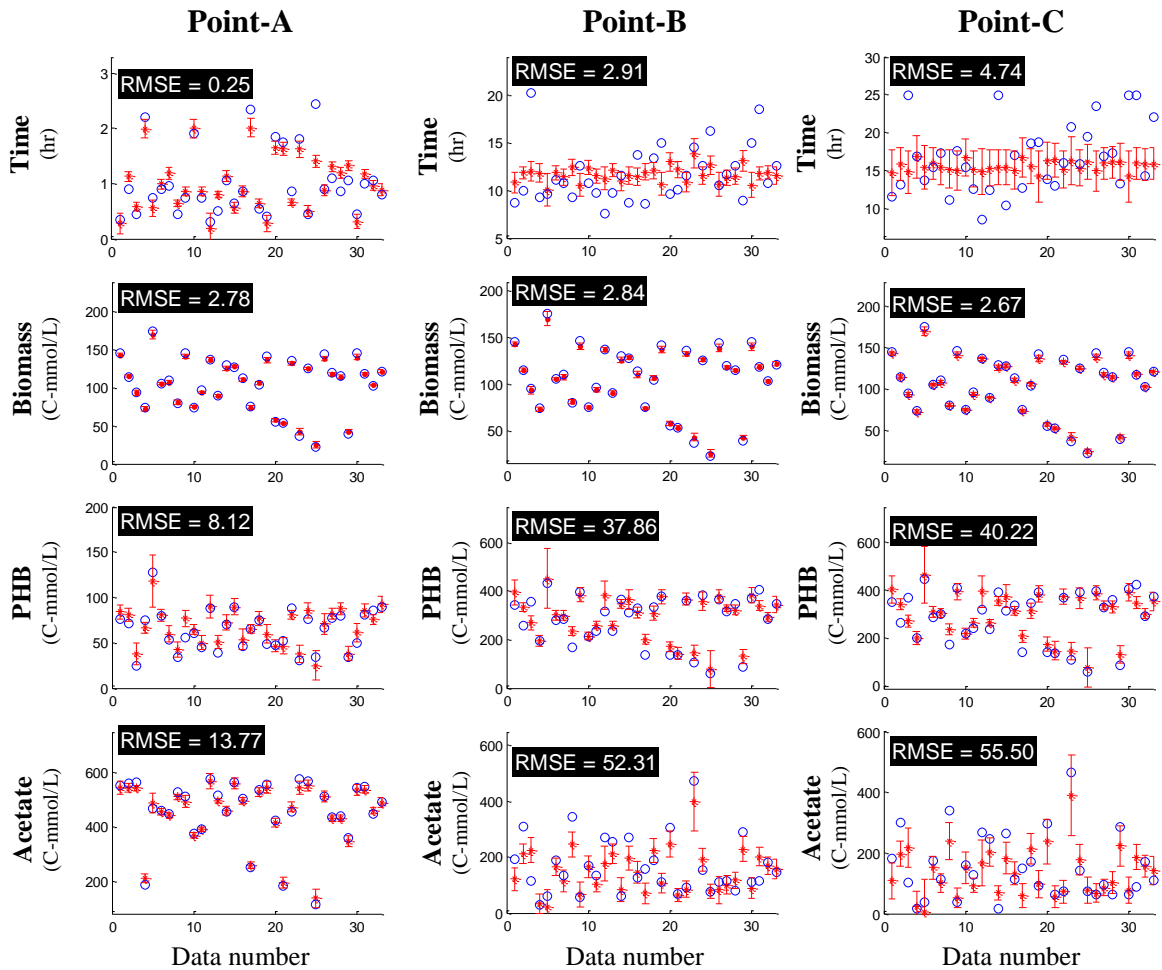


Figure 6.20 BANN model validation for significant elements of the “feast” phase profiles

Looking at Figure 6.20, it is evident that prediction capability of the models estimating the acetate, ammonia and PHB stability time points are not very satisfactory, especially when compared with MLR model prediction shown in Figure 6.12. On the other side, the most accurate estimations are presented for total biomass concentration at the three operational time points of Point-A, Point-B and Point-C. The accuracy of the models developed to estimate total PHB concentrations at the three operational time points is also very satisfying. However, for the case of models predicting acetate concentration at the three operational time points, the model estimating acetate concentration at ammonia exhaustion point (Point-A) is much more accurate than the other two models.

In the next sub-section, capability of the linear MLR models will be compared with their equivalent non-linear BANN models based on the RMSE values obtained in the model validation procedure.

6.4.6 Comparison of the MLR and BANN model results

The RMSE criterion used to specify prediction accuracy of the models built on the set of scaled data can also be used to compare prediction capability of different modelling techniques. Table 6.5 tabulates RMSE values obtained in Section 6.4.4 and Section 6.4.5 respectively in validation process of the linear MLR and non-linear BANN models. As it can be seen in the table, the non-linear BANN models produced better estimation of the target variables compared to the linear MLR models. Therefore, the appropriate modelling method for the practical experimental data is suggested to be a non-linear BANN technique based on this study.

Table 6.5 Comparison of the MLR and BANN model prediction capabilities

$y = f(x_1, x_2, x_3, x_4)$		RMSE (validation data)			
		Scaled data		Unscaled data	
		MLR	BANN	MLR	BANN
Point-A	Time	0.26	0.21	0.31	0.25
	Biomass	0.15	0.04	9.64	2.78
	PHB	0.34	0.15	18.9	8.12
	Acetate	0.15	0.05	38.18	13.77
Point-B	Time	0.57	0.55	3.02	2.91
	Biomass	0.15	0.04	9.64	2.84
	PHB	0.25	0.18	51.9	37.86
	Acetate	0.32	0.24	70.09	52.31
Point-C	Time	0.65	0.60	5.13	4.74
	Biomass	0.15	0.04	9.64	2.67
	PHB	0.25	0.19	53.54	40.22
	Acetate	0.33	0.24	77.30	55.5

The overall assessment of the models predicting time elements of the “feast” phase process (including the ammonia depletion time at Point-A, acetate stability time at Point-B and PHB saturation at the Point-C process time) leads to the conclusion that models associated with process time provide inaccurate estimations. However, prediction of the biomass concentrations at the three operational points is much more accurate when modelled by BANN rather than the MLR modelling technique. The BANN modelling technique also produces better results for estimation of the PHB and acetate concentrations at the three operational points.

It was mentioned that a RMSE value of less than 0.2 for a scaled data set demonstrates prediction accuracy of more than 90%. Table 6.5 shows that RMSE values for prediction of total biomass and PHB concentrations using BANN models are in the acceptable range. BANN modelling of acetate concentrations is slightly out of the acceptable range and models predicting Point-A, Point-B and Point-C occurrence times are not accurate. These results also confirm high accuracy level for prediction of final PHB concentration when process data is classified for “feast” phase operations prior to model development. It was shown in Section 6.3 that acceptable prediction of final PHB concentration was not achievable without data classification.

In the subsequent section, reduction of model input number is investigated to improve model generalisation capability by eliminating unnecessary model inputs using the BANN modelling technique.

6.4.7 Development of BANN models with reduced number of inputs

In this section, BANN models are developed using different combination of inputs with less than four variables applied in the previous sections. Reduction of model input variable number while maintaining prediction accuracy has a number of benefits that can be summarised into reduction model development effort and improvement of model generalisation capability. The first effort is to develop three-input models using the same data presented in the previous sections. The following formations are considered for BANN model development.

$$y = f(x_1, x_2, x_3)$$

$$y = f(x_1, x_2, x_4)$$

$$y = f(x_1, x_3, x_4)$$

$$y = f(x_2, x_3, x_4)$$

where x_1 , x_2 , x_3 and x_4 are total biomass, PHB, acetate and ammonia concentrations at the initial point of the batch simulations. Table 6.6 tabulates RMSE values on the scaled validation data for the four model structures.

Table 6.6 RMSE values for BANN models developed on three-input structures

		$y = f(x_1, x_2, x_3)$	$y = f(x_1, x_2, x_4)$	$y = f(x_1, x_3, x_4)$	$y = f(x_2, x_3, x_4)$
		RMSE	RMSE	RMSE	RMSE
		(Scaled data)	(Scaled data)	(Scaled data)	(Scaled data)
Point-A	Time	0.27	0.22	0.21	0.35
	Biomass	0.21	0.03	0.04	0.37
	PHB	0.29	0.14	0.29	0.14
	Acetate	0.16	0.37	0.05	0.05
Point-B	Time	0.56	0.54	0.54	0.53
	Biomass	0.21	0.03	0.04	0.37
	PHB	0.23	0.19	0.18	0.33
	Acetate	0.35	0.41	0.26	0.40
Point-C	Time	0.62	0.61	0.60	0.58
	Biomass	0.21	0.03	0.04	0.37
	PHB	0.24	0.20	0.18	0.36
	Acetate	0.37	0.41	0.26	0.42

Looking at Table 6.6, it can be observed that model prediction capability is increased for a number of cases by considering three-input model structure. In the four-input models, introduction of some process variables as the model input have destructive effect on the model accuracy when model output is independent of the input variable.

The BANN models that predict biomass concentrations at the Point-A, Point-B and Point-C are highly accurate when model formations $f(x_1, x_2, x_4)$ and $f(x_1, x_3, x_4)$ are applied. This outcome suggests application of two-input model formation of $f(x_1, x_4)$ to confirm dependency of biomass concentration on only two initial process elements biomass and ammonia concentrations. Table 6.7 shows RMSE values calculated for the scaled validation data set stored using the random behaviour system.

As given in Table 6.7, RMSE values obtained from the scaled validation data set is the lowest achieved for the prediction of biomass concentrations at different stages of the “feast” phase process. This indicates that biomass prediction is best performed using only the initial biomass and ammonia concentrations provided that the data is acquired from “feast” phase operations.

Table 6.7 RMSE values for models developed on initial biomass and ammonia concentrations by BANN

$y = f(x_1, x_4)$		RMSE (Scaled data)
Point-A	Time	0.22
	Biomass	0.01
	PHB	0.28
	Acetate	0.34
Point-B	Time	0.54
	Biomass	0.01
	PHB	0.19
	Acetate	0.42
Point-C	Time	0.58
	Biomass	0.01
	PHB	0.19
	Acetate	0.42

Looking at Table 6.6, model formations $f(x_1, x_2, x_4)$ and $f(x_2, x_3, x_4)$ have the lowest RMSE values for the models predicting PHB concentration at the Point-A. In order to test model prediction improvement by applying only two put variables to the model, initial PHB and ammonia concentrations are implemented in BANN model development. Table 6.8 shows RMSE values for the models predicting the significant elements of the “feast” phase process.

Table 6.8 RMSE values for models developed on initial PHB and ammonia concentrations by BANN

$y = f(x_2, x_4)$		RMSE (Scaled data)
Point-A	Time	0.43
	Biomass	0.47
	PHB	0.12
	Acetate	0.46
Point-B	Time	0.53
	Biomass	0.47
	PHB	0.45
	Acetate	0.43
Point-C	Time	0.57
	Biomass	0.48
	PHB	0.47
	Acetate	0.43

Looking at Table 6.8, it is evident that model predictions have degraded except for the case of PHB concentration at the Point-A. This outcome suggests that prediction of the PHB concentration at the ammonia depletion point is best performed when only two input variables of initial PHB and ammonia is considered for modelling.

Table 6.9 RMSE values for models developed on initial PHB and ammonia concentrations by BANN

$y = f(x_3, x_4)$		RMSE (Scaled data)
Point-A	Time	0.37
	Biomass	0.42
	PHB	0.34
	Acetate	0.04
Point-B	Time	0.54
	Biomass	0.42
	PHB	0.35
	Acetate	0.40
Point-C	Time	0.58
	Biomass	0.41
	PHB	0.36
	Acetate	0.42

The third type of models developed with two model inputs is based on initial acetate and ammonia concentrations. Since models predicting acetate concentration at the Point-A have the lowest RMSE values with model formations $f(x_1, x_3, x_4)$ and $f(x_2, x_3, x_4)$, the two-input model formation of $f(x_3, x_4)$ is also considered in the investigations. Table 6.9 confirms prediction improvement for the model estimating acetate concentration at the ammonia depletion point.

The later model formation demonstrate poor prediction capability for estimation of significant process elements other than the acetate concentration at the Point-A. In the next section, the most appropriate model structure is proposed to predict each significant element of the “feast” phase process by the means of the RMSE criterion based on the studies carried out in the previous sections.

6.4.8 Recommendations for development of appropriate model structure targeting “feast” phase batch operations

In this section, RMSE values obtained for the BANN and MLR models developed in the previous sections are compared to find the best model structure for each element of the “feast” phase operation. The training and validation data is the same obtained from the

random behaviour simulator system and stored to develop the models. Based on the RMSE criterion, the most appropriate model structures are proposed in Table 6.10.

When modelling precision is the same for two model structures, the structure with lower number of input variables is selected. In practice, data acquisition and model development is less challenging when the number of process variables involved in the modelling technique is less.

In Table 6.10, the lowest scaled RMSE values obtained for the models predicting the significant elements of the “feast” phase process are tabulated along with their modelling formulations. Based on RMSE values, the most accurate models are those predicting the biomass concentrations at the three process stages. The RMSE values for PHB concentration predictions at the three process stages are slightly less than 0.2 and can be considered as reliable models. In case of the acetate concentration models, high precision prediction is observed at the ammonia depletion point of the process; however, RMSE values are slightly higher than 0.2 when estimating acetate concentrations at Point-B and Point-C. The high RMSE values for the models predicting the time of significant occurrences for Point-B and Point-C in a “feast” phase batch indicate unreliable model predictions. Model prediction of ammonia depletion time point has scaled RMSE value of 0.21 which is not much more than the acceptable RMSE value of 0.2.

Table 6.10 Proposition of the model structure for the significant elements of the “feast” phase operations

		Modelling formulation	RMSE (scaled validation)
Point-A	Time	$f(x_1, x_3, x_4)$	0.21
	Biomass	$f(x_1, x_4)$	0.01
	PHB	$f(x_2, x_4)$	0.12
	Acetate	$f(x_3, x_4)$	0.04
Point-B	Time	$f(x_2, x_4)$	0.53
	Biomass	$f(x_1, x_4)$	0.01
	PHB	$f(x_1, x_4)$	0.19
	Acetate	$f(x_1, x_2, x_3, x_4)$	0.24
Point-C	Time	$f(x_2, x_4)$	0.57
	Biomass	$f(x_1, x_4)$	0.01
	PHB	$f(x_1, x_4)$	0.19
	Acetate	$f(x_1, x_2, x_3, x_4)$	0.24

It is important to mention that the conclusions made in this study are mainly based on the data obtained using the simulation program explained in Chapter 3. In order to confirm the best modelling technique and structure, experimental data from real production process is required for each specific production unit. The aim of this study was to demonstrate reliability and prediction accuracy obtained using the BANN modelling in comparison to the single NN and linear MLR models when building empirical models targeting the “feast” phase PHB production batches.

In the next section, empirical models are developed to estimate some significant elements of the “famine” phase operations.

6.5 The “famine” phase operational modelling

6.5.1 Introduction

In this section, “famine” phase operational profiles are targeted in order to develop empirical models estimating critical process attributes. In production of the PHB using mixed microbial cultures, the main characteristic of the “famine” phase process is consumption of the intracellular PHB content in the absence of external feed source.

In Chapter 4, “famine” phase operations were classified into two main “Regime Types” referred to as RT3 and RT5. In this section, process profiles associated with RT3 and RT5 are studied and their significant elements of the “Regime Types” are identified. The empirical models are developed for the case of batch simulation results obtained from a random behaviour process simulator reflecting PHB production using mixed microbial cultures.

6.5.2 Description of the “famine” phase operational profile – RT3

A production “feast” phase process should be followed by a “famine” phase in order to maintain biological wellbeing of the production cells (Dias *et al.*, 2005). The success and effectiveness of the “famine” phase operation highly depends on the final status of the active biomass. The lower the intracellular PHB content of the cells at the end of the operation, the more efficacious the “famine” phase operation. The “famine” phase profiles appear in the form of either RT3 or RT5. The focus of this section is on RT3 with the description given in Chapter 4. At first, a description of the batch profile is given prior to the model development stage.

The process profile of this “Regime Type” can be divided into three operational intervals by two significant occurrences within the operational time. The first

occurrence is acetate depletion which is referred to as “Point-P” in this study. Followed by the appearance of the “Point-P”, ammonia depletion takes place as the second significant occurrence in a process under RT3. The operational time in which ammonia depletion occurs is referred to as the “Point-Q” in this section.

Figure 6.21 shows two batch operation plots under RT3 with “fPHB summation” subplot shown on the top and PHB concentration subplot shown in the bottom of the each plot. The “fPHB summation” was defined in Section 6.4.2 in description of the “feast” phase profiles. The same formulation is used as an indicator of the PHB content level within the cells.

In the presence of both acetate and ammonia, a RT3 batch operation initiating with low intracellular PHB content undergoes a period of PHB storage until carbon source is depleted in the medium. Afterwards, intracellular PHB is consumed to maintain cell growth and replication (shown in Figure 6.21.a). On the other side, when initial intracellular PHB content is high, the cells consume their PHB as an energy source in parallel with the carbon sources available in the medium. The PHB consumption continues after acetate depletion in the medium (shown in Figure 6.21.b).

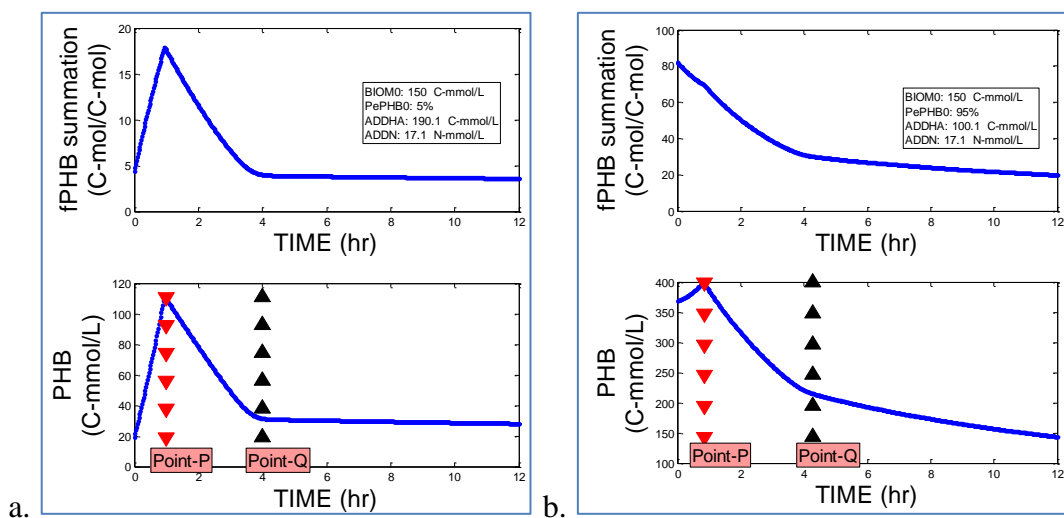


Figure 6.21 “Famine” phase profile with RT3

As it can be seen in Figure 6.21, in the first division of the profile prior to “Point-P”, “fPHB summation” factor can be either increasing or decreasing by a very high ratio. In the second division of the profile between “Point-P” and “Point-Q”, “fPHB summation” factor decreases with a steep decline. It is in the third division of the RT3 occurring after “Point-Q” that the “fPHB summation” value reaches to a favourably low magnitude. Assessment of the plots shown in Figure 6.21 suggests that a successful “famine” phase operation under RT3 initiates when acetate depletion takes place.

Additionally, optimal batch termination point can be associated with ammonia exhaustion point when “famine” phase operation runs under RT3.

In the next section, “famine” phase profiles under RT5 will be scrutinised.

6.5.3 Description of the “famine” phase operational profile – RT5

In addition to RT3, the “famine” phase operation also takes place under RT5 where unlike the former “Regime Type”, ammonia depletion occurs prior to acetate exhaustion. Figure 6.22 shows two batch operations under RT5 with different initial intracellular PHB contents. It can be observed that “fPHB summation” decline occurs after acetate complete depletion in the medium.

Looking at Figure 6.21 and Figure 6.22, it is evident that continuous reduction of the “fPHB summation” factor (which is the subject of a “famine” phase operation) can be maintained in both “Regime Types” when acetate is completely exhausted in the medium. An additional outcome is that the “fPHB summation” factor reaches to a high magnitude by acetate consumption prior to its depletion point. Therefore, when optimal termination time for a “famine” phase operation is under investigation, acetate depletion point is the only process element that needs to be considered. However, since “fPHB summation” is at its high for “Point-P”, a different factor should be identified to specify operation duration after occurrence of the “Point-P”.

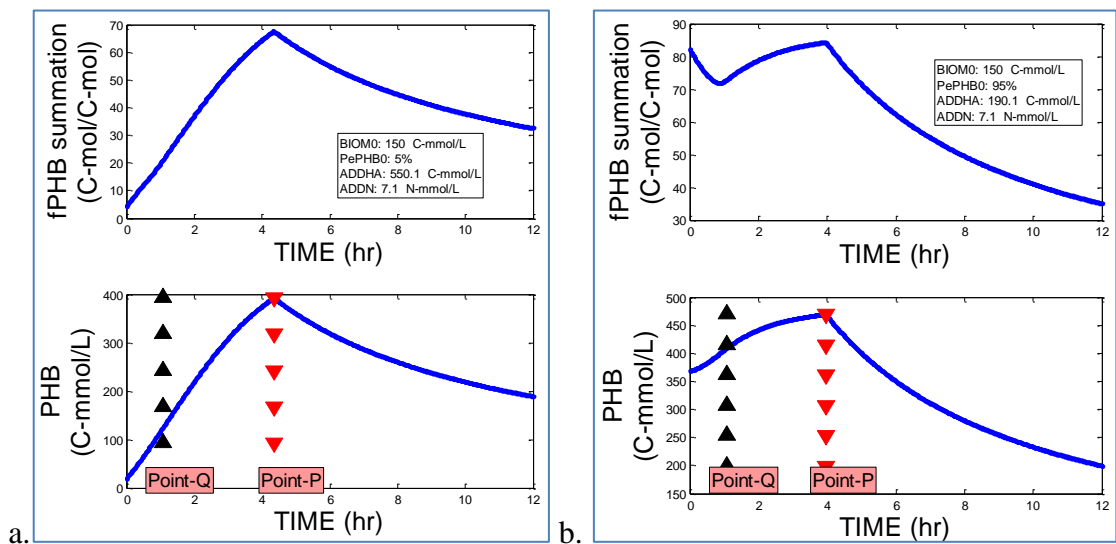


Figure 6.22 “Famine” phase profile with RT5

The “famine” phase proficiency highly depends on the process operational duration. The longer a “famine” phase batch operates after acetate exhaustion, the higher the yield of the famine phase operation. On the other side, a prolonged famine phase operation is associated with higher operational running cost. Therefore, a balance should be made to

specify the optimal batch duration considering the acetate exhaustion point. In the next section, a new process factor is defined to be applied as a criterion for optimal batch termination time of the “famine” phase operations.

6.5.4 Batch termination criterion for historic data of “famine” phase process

In this section, “famine” phase batch termination point is identified using a series of historical batch data. Assessment of the “famine” phase profiles using the analytical tool introduced in this section provides a platform to estimate optimal “famine” phase batch termination time using empirical models developed on appropriate set of process data. First, the analytical tool to assess the historical batch data will be introduced and later BANN models will be developed to estimate the optimal duration of the “famine” phase batch operations.

Looking at Figure 6.21 and Figure 6.22, it can be deduced that termination of the “famine” phase batch prior to the acetate exhaustion point is not favourable. In the case of RT3, “fPHB summation” level is close to its maximum at the acetate depletion point and “fPHB summation” level reaches to a local maximum which is the least desirable point to terminate a “famine” phase operation in RT5. Therefore, the proposed batch termination time should be an operation time occurring after detection of the acetate exhaustion point. In order to determine the “famine” phase operational duration, “fPHBsumEND” factor is defined as a criterion that regulates process termination in the simulation program. The following equation is used to calculate the “fPHBsumEND” value using “fPHB-summation” profile obtained from a complete “famine” phase batch profile.

$$fPHBsumEND = fPHBsumMIN + fPHBsumENDratio \times (fPHBsumMAX - fPHBsumMIN) \quad (6.3)$$

where “ $fPHBsumMIN$ ” and “ $fPHBsumMAX$ ” are the minimum and maximum values for “fPHB-summation” during a “famine” phase batch operation respectively. The “ $fPHBsumENDratio$ ” factor is specified by the operator to determine the extent of PHB consumption by the cells through the “famine” phase operation. In order to address a successful “famine” phase batch operation, “ $fPHBsumENDratio$ ” should have a small value in the range of zero to the unit value.

In the simulation studies, the operational time in which “fPHB summation” is equal to the “ $fPHBsumEND$ ” value is recorded as the optimal point for “famine” phase batch termination. As an example, Figure 6.23 demonstrates a “fPHB summation” profile for

a “famine” phase batch operating under RT3 with “ $fPHBsumENDratio$ ” value of 15%.

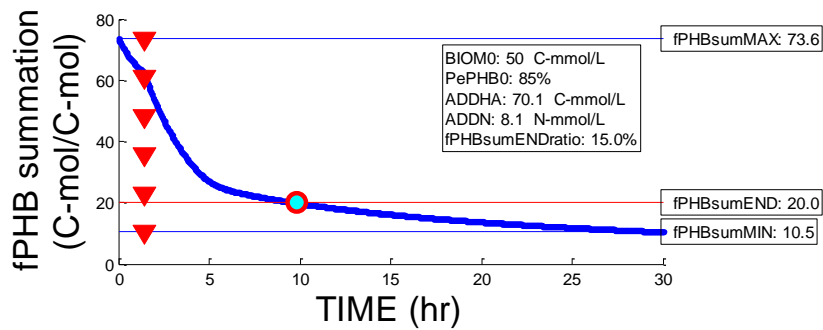


Figure 6.23 Identification of “famine” phase batch termination criterion

As shown in the figure, “ $fPHBsumMAX$ ”, “ $fPHBsumMIN$ ” and “ $fPHBsumEND$ ” values are specified to be equal to 73.6 C-mol/C-mol, 10.5 C-mol/C-mol and 20 C-mol/C-mol respectively. The optimal batch termination time is specified by the symbol “ \bullet ” on the “fPHB summation” curve at about 10 hours after batch initiation. The acetate depletion point is also marked by the symbol “ \blacktriangledown ” on the graph.

Identification of the “ $fPHBsumEND$ ” point is not always as straightforward as shown in the case of Figure 6.23. The analytical tool to assess the historical batch profiles should be capable of finding the desirable “ $fPHBsumEND$ ” point in various profile case scenarios. Therefore, a sophisticated algorithm is required to be developed in order to identify the most appropriate time point to terminate the operation. In Figure 6.24, an “fPHB summation” profile is shown for a “famine” phase batch operating under RT5.

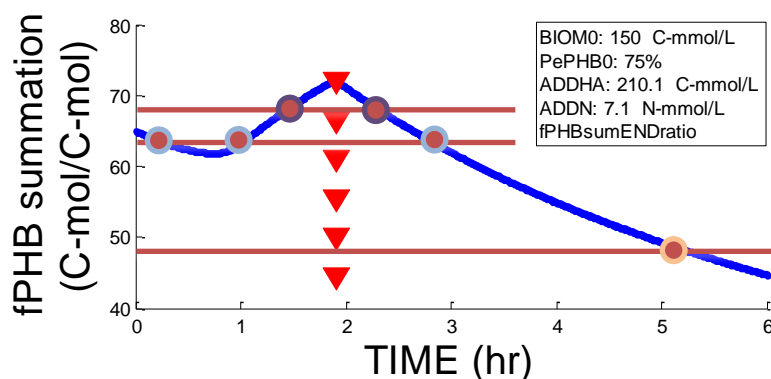


Figure 6.24 Detection of various “fPHBsumEND” points on a “famine” phase profile

As shown in the figure, the “fPHB summation” curve crosses the “ $fPHBsumEND$ ” level in more than one operational time points when “ $fPHBsumEND$ ” value is high. In such cases, the algorithm identifying the batch termination time should specify the time

point which appears after the acetate exhaustion point in the process profile in order to address the appropriate time point. Figure 6.25 shows that the analytical tool correctly records the longest operational time point when “fPHBsumEND” criterion crosses the “fPHB-summation” curve in three points.

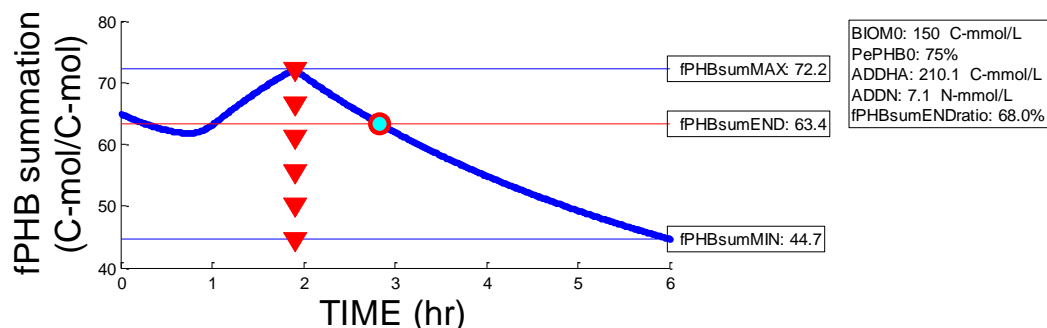


Figure 6.25 Identification of “famine” phase batch termination point by the analytical tool

The algorithm developed in this section will also be used in the next section to identify the optimal “famine” phase batch operation using a series of historic profiles for model development. Additionally, this tool will be applied in the next chapter to assess the yield of “famine” phase operation in the production recipe. The algorithm is embedded within the “CharMeth” module. In this study, the “*fPHBsumENDRatio*” is considered to be at the 20% of the overall range of “fPHB summation” range.

6.5.5 Data generation targeting “famine” phase batch operations

In this section, “famine” phase data is used to develop empirical models using the linear MLR and non-linear BANN structures. In order to differentiate the “famine” phase from the “feast” phase data, the same program structure introduced in Section 6.4.3 to separate the two phase data is applied. The process simulation program applied in this section is the same used for the “feast” phase operational simulations.

The simulation parameters applied in the simulation program are the same used in Section 6.4.3 for “feast” phase data generation except for the minimum and maximum initial acetate and PePHB0 values. For the case of the “famine” phase data generation, the minimum and maximum range of initial acetate is decreased from 100 C-mmol/L to 2 C-mmol/L and from 700 C-mmol/L to 300 C-mmol/L respectively. This modification is to assure targeting “famine” phase operations when generating simulation data. Based on the results obtained from the characterisation plots, for the same range of initial ammonia concentration, high initial acetate concentration is potent to direct the batch

into a “feast” phase operation while low initial acetate concentration directs the process into a “famine” phase operation.

Since “famine” phase operations should be occurring after a “feast” phase operation, the PHB content of the cells should be high at the initial point of the operation. Therefore, the range of PePHB0 values is increased to 70% and 100% for the minimum and the maximum values of the PePHB0 range respectively.

The rest of the simulation parameters applied in this section are identical to those used in Section 6.4.3 for the “feast” phase data generation stage. In Table 6.11, the program parameters used to design 250 batch simulations are tabulated for 10 different values of initial biomass concentrations.

Table 6.11 Process data generation targeting “famine” phase operation

Programing parameters		
Iteration operator	Minimum value	Maximum value
RandNo1 (BIOM0)=10	a1=2 (C-mmol/L)	b1=200 (C-mmol/L)
RandNo2 (ADDHA)=5	a2=2 (C-mmol/L)	b2=300 (C-mmol/L)
RandNo3 (ADDN)=5	a3=0.1 (N-mmol/L)	b3=10 (N-mmol/L)
PePHB0	70%	100%

For each initial biomass concentration, five different values are randomly assigned for acetate concentrations for which 25 different values are randomly selected for ammonia concentration introduced to the batch. The 10 initial biomass concentrations, along with the 50 acetate concentration values and 250 ammonia concentrations assigned by random generator function are depicted in Figure 6.26.a, Figure 6.26.b, and Figure 6.26.c respectively.

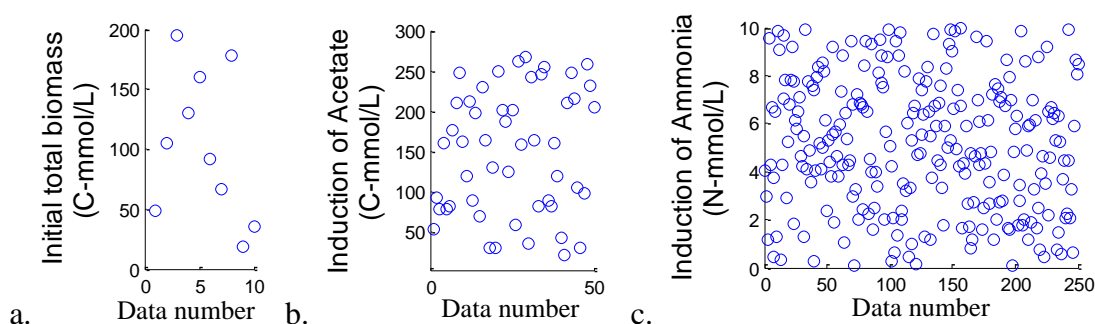


Figure 6.26 Random values assigned to process parameters for data generation targeting the “famine” phase

In Figure 6.27, simulation results of 250 batch processes are given for 10 different values of initial biomass concentrations. For each value of initial biomass concentration, five different values are randomly assigned for initial acetate concentrations and for each acetate value 25 different values are randomly selected for initial ammonia concentrations in their specified range. As shown in Figure 6.27.a and Figure 6.27.c, 115 batches were predicted to operate under the “feast” phase as oppose to the 135 batches predicted for operation under the “famine” phase. These predictions were made applying the “Phase Differentiating Equation” obtained in Chapter 5.

Analysis of the simulation profiles provides “Regime Type” numbers of the 250 batch operations. Based on the “Regime Type” numbers, 221 out of the 250 batches were correctly differentiated according to their “Regime Types”. The remaining batches consist of RT9 operations which represent neither “feast” nor “famine” phase operations. The other batches that operated under RT5 but predicted to operate under the “feast” phase can be considered as the error results of the “Phase Differentiating Equation” depicted in Figure 6.27.c. The two batches with RT4 depicted in Figure 6.27.d are immature operations that could not be considered as complete “famine” phase operations.

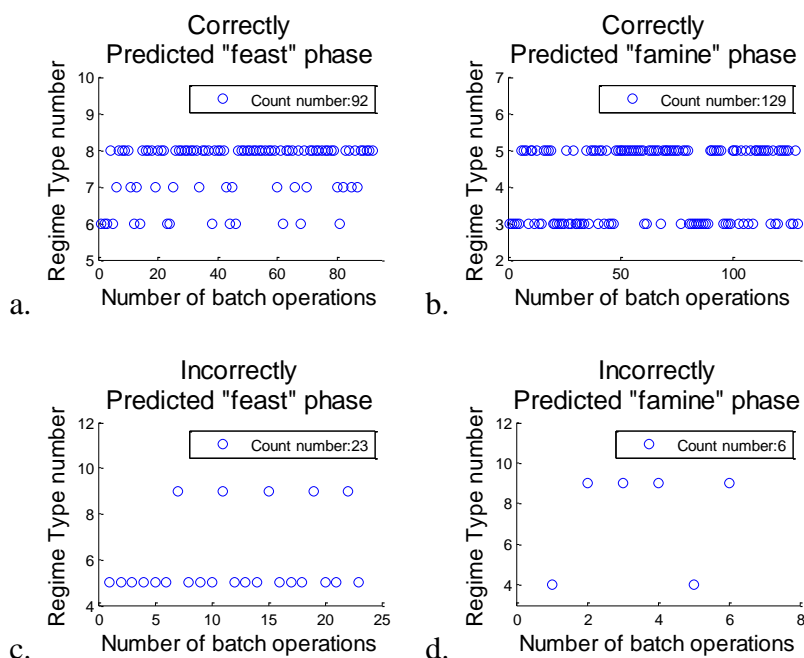


Figure 6.27 Identification of valid “famine” phase batch data set

The 129 batch data predicted and operated as “famine” phase batches are applied for model development and validation in this section. This data set includes batch operations with “famine” phase operations under both RT3 and RT5. Assessment of the

results specifies that 74 out of the 129 batches operated under RT5 and 55 batches operated under RT3. Additionally, analysis of the batch profiles provide suggestions for optimal batch termination time (Point-T) with “fPHBsumENDratio” criterion of 20% as depicted in Figure 6.28. According to this figure, batch operations under RT5 required longer batch duration in order to achieve the same level of PHB content when compared to the batches running under RT3.

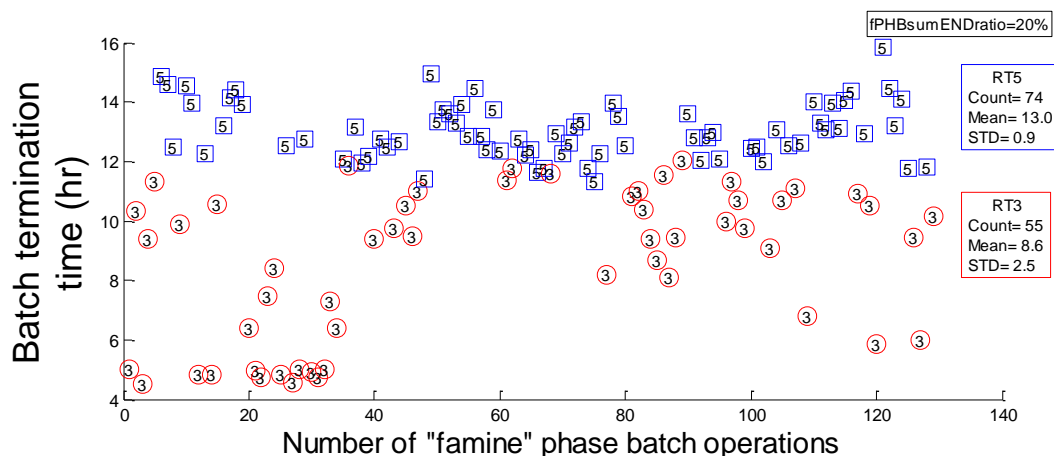


Figure 6.28 “Famine” phase batch durations with “fPHBsumENDratio” criterion of 20%

It can be deduced from Figure 6.28 that batch operation under RT3 is more favourable than the RT5 when “famine” phase operational duration is considered. This is due to the fact that acetate depletion is the first significant occurrence in a RT3 operation which accelerates early consumption of the PHB contents of the cells.

The first significant point in a “famine” phase batch operation is the initial point of the operation (T_0), the second significant point is considered to be the acetate depletion point (Point-P) and the third significant point is the batch termination point (Point-T) specified by the batch termination criterion in this study. Similar to the “feast” phase modelling section, around 70% of the “famine” phase data is used for the model training and the remained is used for model validation purpose. Figure 6.29 shows training data sets for the time, biomass, PHB, acetate and ammonia concentrations at the three points. Out of total 129 “famine” phase batches, 91 data sets were randomly selected for model training purposes and the remained 38 data sets were stored for model validation stage depicted in Figure 6.30.

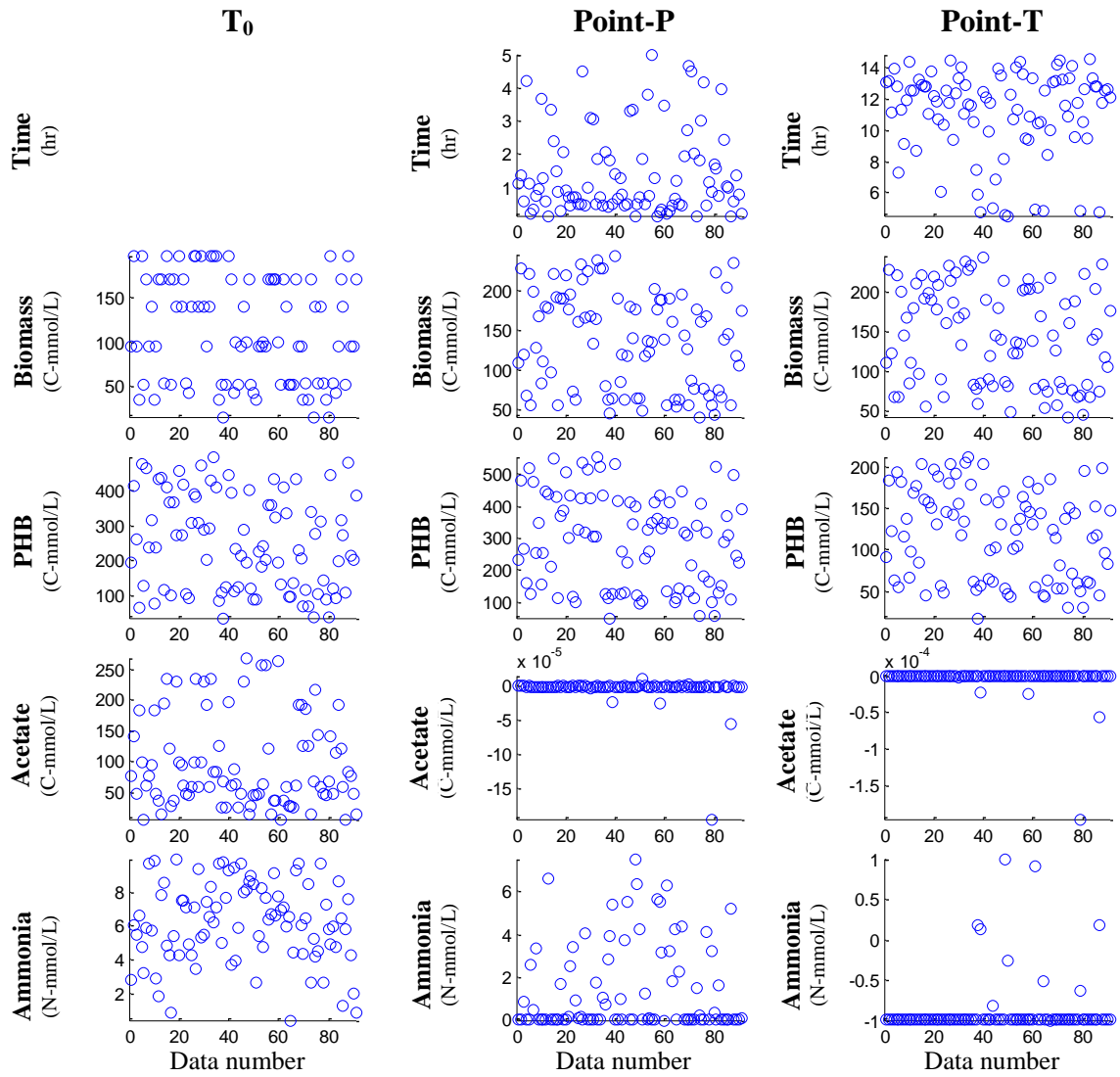


Figure 6.29 Training data for the "famine" phase model development

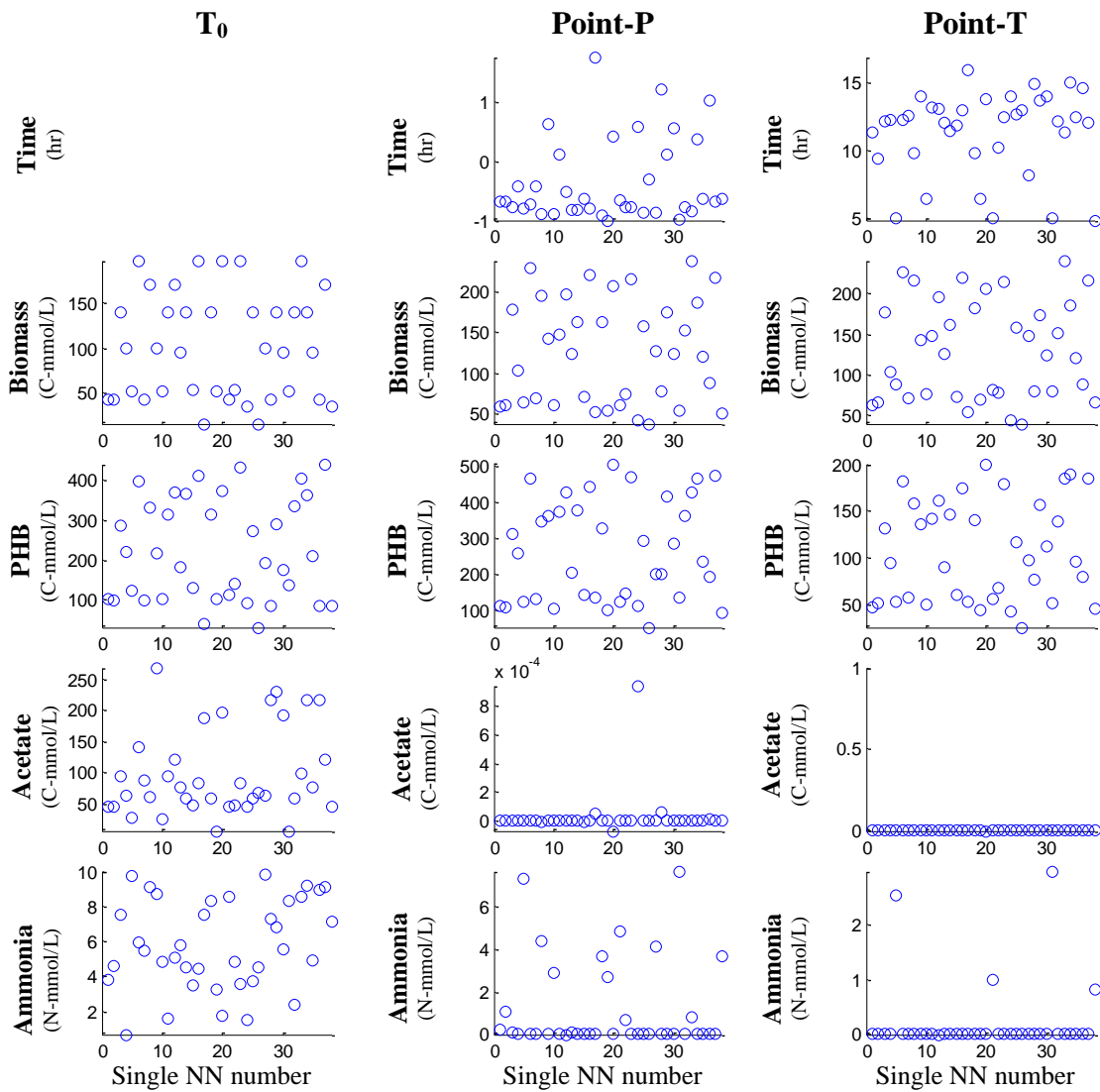


Figure 6.30 Validation data for the “famine” phase model development

Using the minimum and maximum values of each training data set (Appendix-D, Table D.1), training and validation data sets are scaled and used in the modelling development procedure. In the following sections, “famine” phase operations are modelled with both RT3 and RT5 “Regime Types” considered together to model “famine” phase significant occurrences and later each “famine” phase operation is considered separately.

6.5.6 MLR modelling targeting “famine” phase process data

The modelling structure proposed to build the MLR models consists of the same four inputs considered in the “feast” phase model development sections as given in Equation ((6.2)). The MLR model parameters are obtained and tabulated in Appendix-D (Table D.2). The models are validated and the predictions are unscaled and depicted in Figure 6.31. In the plots depicted in Figure 6.31, the model prediction values are marked by “★” and the true/ target values are shown by “○”. The RMSE values for validation data are also depicted on these plots.

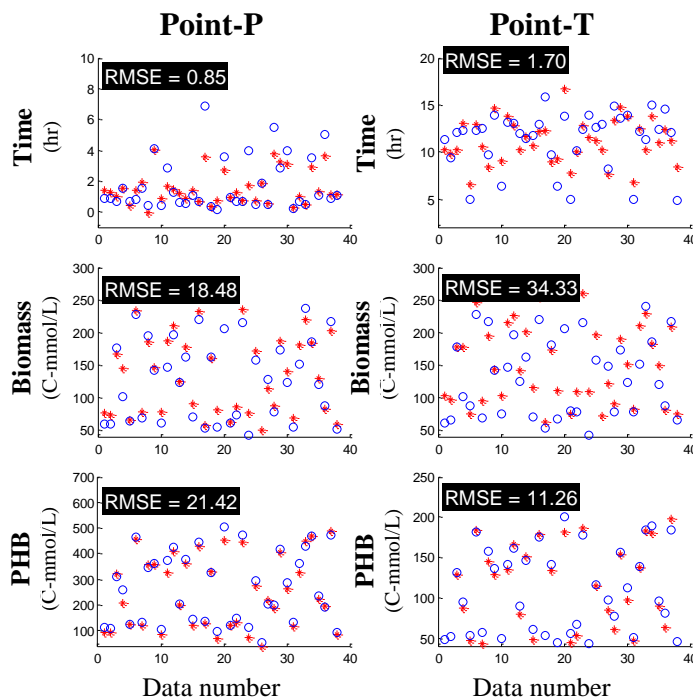


Figure 6.31 MLR model validation developed for the “famine” phase data sets

In the next section, the same set of data used for MLR modelling will be applied to develop and validate BANN models.

6.5.7 BANN modelling targeting “famine” phase process data

The BANN models developed in this section are built under the same input-output structure used in the models built in the previous section. Optimal number of hidden neurons and the SSE values in the validation process of the individual NN models are given in Appendix-D (Figure D.1 and Figure D.2 respectively).

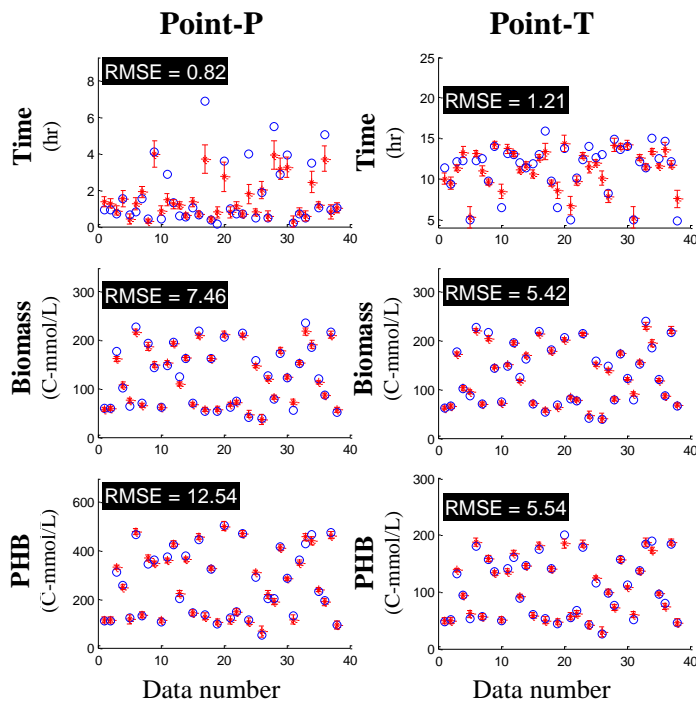


Figure 6.32 BANN model validation for significant elements of the “famine” phase profiles

In Figure 6.32, BANN model prediction results are depicted for validation data sets. In this figure, model estimations are depicted for unscaled predictions along with the confidence bounds obtained using the results of single neural network models.

Comparing the RMSE values of the linear MLR models and the non-linear BANN models demonstrate proficiency of BANN models over the linear models. In Appendix-D (Table D.3), RMSE values obtained in model validation procedure are given for five-input and three-input models. The additional model input in the five-input model is the time of acetate depletion in “famine” phase operations. The three-input models are designed to encounter the four possible combination of models with four different variables.

In Table 6.12, the most appropriate model formulations are proposed based on the RMSE values and the number of model input variables obtained from simulation studies.

Table 6.12 Proposition of the model structure for the significant elements of the “famine” phase operations

<i>Recommendations</i>		Modelling formulation	RMSE (scaled)
Point-P	Time	$f(x_1, x_3, x_4)$	0.34
	Biomass	$f(x_1, x_3, x_4)$	0.06
	PHB	$f(x_2, x_3)$	0.04
Point-T	Time	$f(x_1, x_2, x_3, x_4, x_5)$	0.22
	Biomass	$f(x_1, x_4)$	0.03
	PHB	$f(x_2, x_3)$	0.06

As mentioned, RMSE values of scaled validation data with magnitude less than 0.2 indicate models performing with acceptable accuracy level. In the next sections, BANN models are developed on the two “famine” phase “Regime Type” numbers, RT3 and RT5 separately. This is to investigate model accuracy improvement when two “Regime Types” are modelled independently.

6.5.8 BANN modelling targeting “famine” phase process operating under RT3

In this section, a subset of the “famine” phase data set used in the previous section is considered containing data sets associated with batch operations operating under RT3. As noted on Figure 6.28, 55 batch data were identified to present the phase operation under RT3. Following the same procedure explained in the previous sections, 70% of the data which is 39 batch data is used for BANN model development and the remained 16 batch data is applied for model validation. The optimal number of hidden neurons for each individual NN model and the SSE values obtained in the validation process of the individual NN models are given in Appendix-D (Figure D.3 and Figure D.4 respectively).

In Figure 6.33, BANN model prediction results are depicted for validation data sets. In this figure, model estimations are depicted for unscaled predictions along with the confidence bounds obtained using the results of single neural network models.

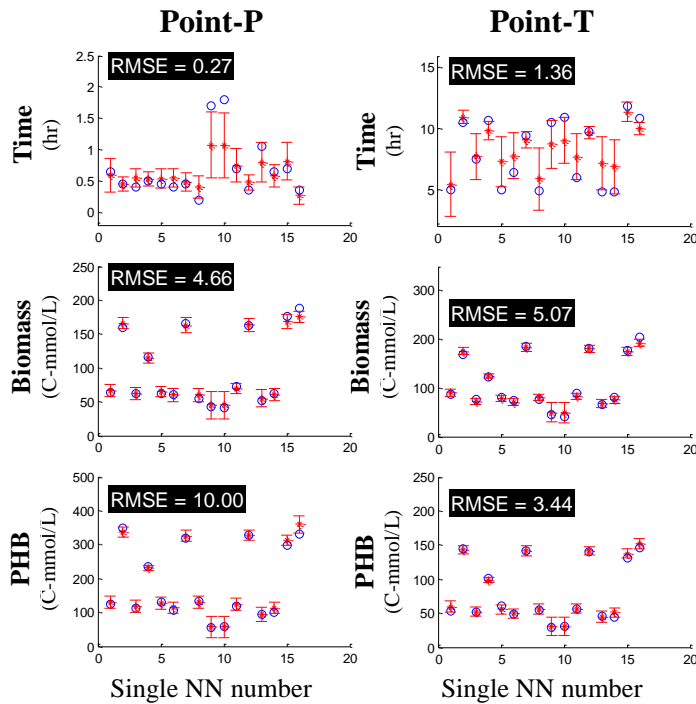


Figure 6.33 BANN model validation for significant elements of the RT3 data sets

Similar to the previous section, RMSE values are obtained for models developed under various combinations of independent input variables. In Appendix-D (Table D.4), the five-input model has an additional acetate depletion time along with the other four input variables applied in modelling. The three-input models are designed to encounter the four possible combination of models with four different variables. In addition, one case of two-input models is also investigated with model formation of $y=f(x_3, x_4)$ to examine prediction improvement for estimation of batch termination time. As given in Appendix-D (Table D.4), the lowest RMSE values are obtained for the three-input models to establish the most appropriate model structure to estimate other significant elements of a “famine” phase process under RT3.

In Table 6.13, the most appropriate model formulations are proposed for the “famine” phase processes under RT3, based on their RMSE values and their number of model input variables obtained from simulation studies.

In the next section, RT5 “famine” phase batch data will be applied for modelling.

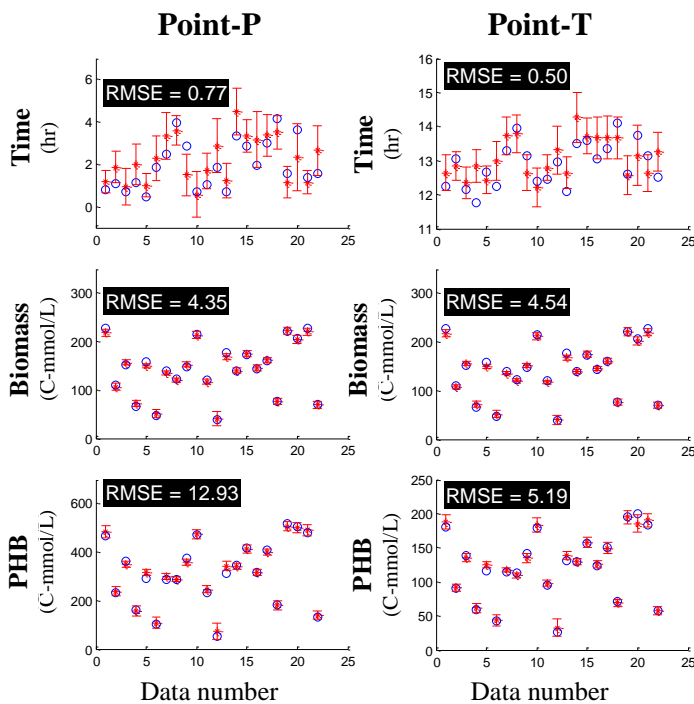
Table 6.13 Proposition of the model structure for the significant elements of the RT3 data sets

<i>Recommendations</i>		Modelling formulation	RMSE (scaled)
Point-P	Time	$f(x_1, x_2, x_3)$	0.26
	Biomass	$f(x_1, x_3, x_4)$	0.02
	PHB	$f(x_2, x_3, x_4)$	0.01
Point-T	Time	$f(x_3, x_4)$	0.31
	Biomass	$f(x_1, x_3, x_4)$	0.03
	PHB	$f(x_2, x_3, x_4)$	0.03

6.5.9 BANN modelling targeting “famine” phase process operating under RT5

Similar to the previous section, “famine” phase data associated with the RT5 is used for BANN model development and validation. 74 batch data was stored for RT5 with 52 batch data for model development and 22 batch data for validation purposes. The number of hidden neurons used in development of the individual neural networks and the SSE values in the validation process of the individual NN models are given in Appendix-D (Figure D.5 and Figure D.6 respectively).

In Figure 6.34, BANN model prediction results are depicted for validation data sets. In this figure, model estimations are depicted for unscaled predictions along with the confidence bounds obtained using the results of single neural network models.

**Figure 6.34** BANN model validation for significant elements of the RT5 data sets

Similar to the previous section, RMSE values are obtained for models developed under various combinations of independent input variables. In Appendix-D (Table D.5), the five-input model has an additional acetate depletion time along with the general four input variables applied in modelling. The three-input models are designed to encounter the four possible combination of models with four different variables. One case of two-input models is also investigated with model formation of $y=f(x_2, x_3)$ to examine prediction improvement for estimation of PHB concentration at acetate depletion point. As given in Appendix-D (Table D.5), the lowest RMSE values are obtained for the three-input models to establish the most appropriate model structure to estimate the significant factors of the “famine” phase process under RT5.

In Table 6.14, the most appropriate model formulations are proposed for the “famine” phase processes under RT5, based on their RMSE values and their number of model input variables obtained from simulation studies.

Table 6.14 Proposition of the model structure for the significant elements of RT5 batch profiles

<i>Recommendations</i>		Modelling formulation	RMSE (Scaled)
Point-P	Time	$f(x_2, x_3, x_4)$	0.22
	Biomass	$f(x_1, x_3, x_4)$	0.01
	PHB	$f(x_2, x_3)$	0.04
Point-T	Time	$f(x_1, x_2, x_3, x_4, x_5)$	0.14
	Biomass	$f(x_1, x_3, x_4)$	0.01
	PHB	$f(x_1, x_2, x_3)$	0.05

In the next section, recommendations are made for modelling structures under “famine” phase operations.

6.5.10 Recommendations for development of appropriate model structure targeting “famine” phase batch operations

In Table 6.15, the lowest RMSE values obtained in prediction of significant process elements in the case of RT3 and RT5 ensemble (Table 6.12), only RT3 (Table 6.13) and only RT5 (Table 6.14) are shown.

Table 6.15 Lowest RMSE values obtained for prediction of significant elements in “famine” phase regimes

<i>RMSE (Scaled)</i>		RT3 and RT5	RT3	RT5
Point-P	Time	0.34	0.26	0.22
	Biomass	0.06	0.02	0.01
	PHB	0.04	0.01	0.04
Point-T	Time	0.22	0.31	0.14
	Biomass	0.03	0.03	0.01
	PHB	0.06	0.03	0.05
Summation		0.75	0.63	0.47

Overall assessment of the prediction capabilities between the “famine” phase data considered together and separately shows that separating the two “Regime Types” can increase model prediction accuracy. This is deduced from the summation of 6 significant elements of the process for the three cases given in Table 6.15. However, for estimation of biomass and PHB concentrations, accuracy of the empirical models is found to be very high and segregation of the “famine” phase data into two subsets of RT3 and RT5 process data prior to model development is unnecessary.

6.6 Conclusions

Application of the “Characterisation Method” developed in Chapter 4 and the “Phase Differentiating Equation” developed in Chapter 5 proved to be beneficial for data classification prior to modelling. While empirical modelling of the process data bulk for product concentration (PHB) was demonstrated to be unreliable and inaccurate, identification of the different operational behaviour and model development using classified data sets proved to be effective for prediction improvement. It was shown that model development using classified data sets increased model prediction accuracy for estimation of almost every critical process attributes under investigation.

Various modelling input-output structures were examined to obtain the appropriate formulations for prediction of the most significant elements of the “feast” and “famine” phase operations using their initial process state. It was shown that models with less number of input variables can provide more accurate predictions in some cases and additional input variables prevent sophisticated model training process. Reduction of model input variables can decrease model development effort and improvement of model generalisation capacity.

Linear MLR modelling technique provided less accurate predictions when compared to the non-linear BANN models due to the non-linearity of the process data. Bootstrapping aggregation of a number of individual neural network models proved to increase model reliability. Comparison of the SSE values obtained from single structured neural network models and the models aggregated by bootstrapping method conformed that the residual value of BANN modelling technique is less than the average value of the single models embedded within the BANN model. It was also demonstrated that optimal number of neurons in the hidden layer of neural network structures varies when initial training parameters alter and that a model with high number of hidden neurons does not guarantee the most accurate predictions.

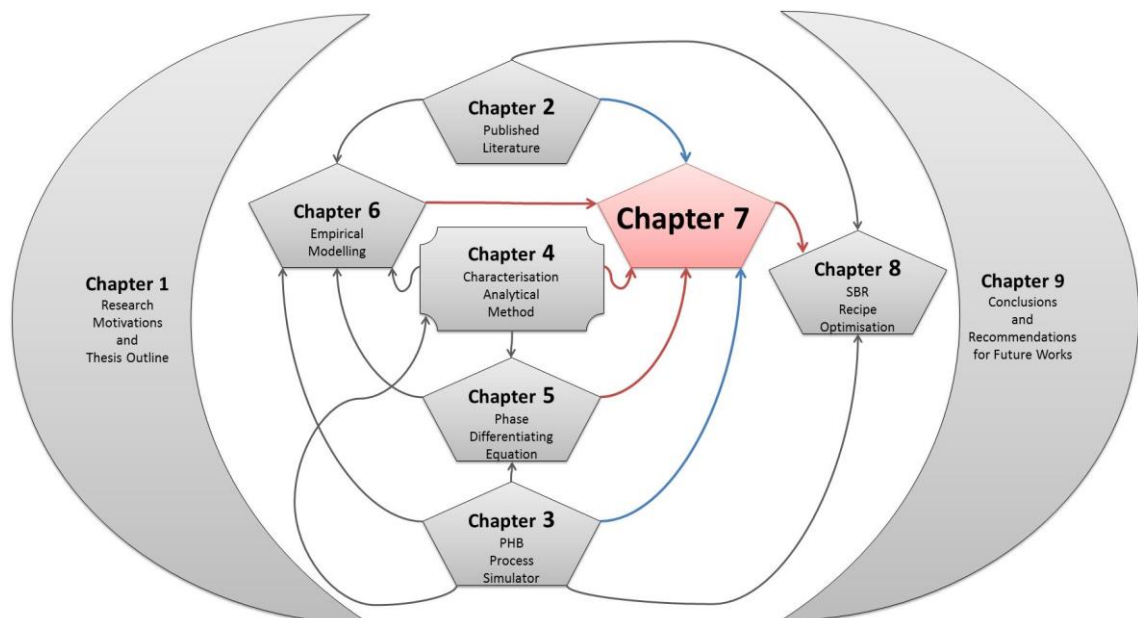
The overall assessment of the models predicting time elements of the “feast” phase process leads to the conclusion that models associated with process time provide inaccurate estimations especially at the point of PHB saturation. Models predicting total biomass concentration provide accurate prediction using two-input models with initial biomass concentration and total ammonia concentration. For prediction of total PHB concentrations at different stages of a “feast” phase process, initial PHB concentration and total ammonia concentration builds acceptable empirical models. Prediction of acetate concentration at the final stage of a “feast” phase operation requires models with

input variables consisting of initial total biomass and PHB concentrations and total acetate and ammonia used in the process to make estimations close to the acceptable range.

Unlike the “feast” phase operation with unique operational pathway, “famine” phase operation can be observed in two different pathways ending to RT3 or RT5. Analysis of the “famine” phase data led to the conclusion that batch operation under RT3 is more favourable than the RT5 when more efficient operation is required. Prediction of “famine” phase optimal termination point by empirical models is less accurate for the case of RT3 operations when compared to the RT5 counterparts. For estimation of biomass and PHB concentrations, accuracy of the empirical models was found to be very high and segregation of the “famine” phase data into two subsets of RT3 and RT5 process data prior to model development found to be unnecessary. For estimation of final biomass concentration, a 2-input model of initial biomass concentration and total ammonia concentration is required. Moreover, a 2-input model of initial PHB concentration and total acetate concentration is capable of provide accurate prediction for final PHB concentration at the end of a “famine” phase operation.

The empirical model structures providing accurate and reliable predictions will play an important role for assignment of production recipe parameters which will be discussed in Chapter 7.

Chapter 7
Generation of PHB Production Recipe Using the
“Phase Differentiating Equation”
for Sequential Batch Reactors



7.1 Introduction

Intracellular accumulation of PHB has been reported for a number of bacteria in either their wild form or by recombinant strains. Up to recent years, industrial scale production of PHB has been carried out using single strain microbial cultures. However, high cost of production associated with sterilization and process significant sensitivity against minor changes in operational condition lead to investigations towards PHB production under Mixed Microbial Cultures (MMC). Successful production is reported in both bench scale and full scale under a process type known as “feast” and “famine”. Sequential batch production method is a technique used to continuously maintain production condition by repetitively undertaking a series of operational practices.

As mentioned in Chapter 2, an operation in nutrition shortage state is said to run in the “famine” phase; and on the other side, when nutrition abundance results into cell replication and augmented growth, operation is said to be under “feast” phase.

In this chapter, based on “Characterisation Method” developed in Chapter 4, sequential batch production procedure known as SBR recipe is designed to impose occurrence of the two major biological phases in each sequence of the SBR for sustainable production. Feasibility studies are carried out to ensure validity of the approach using mechanistic models and the “Characterisation Method” developed in Chapter 4. The key element of innovation in the SBR recipe is application of the “Phase Differentiating Equation” (Equation (5.14)) to assure occurrence of the “feast” and the “famine” phase operations at the predefined SBR operational steps. Implementation of the “Phase Differentiating Equation” within the proposed SBR structure imposes another advantage in process execution which enables automated alleviation of the load effect. The proposed production procedure will be studied using the batch simulation program. Once the SBR recipe structure is established, recipe parameters will be assigned using empirical models developed in Chapter 6.

At the end, a thorough study on the capability of the proposed SBR structure will be carried out to investigate reliability of the SBR process in occurrence of operational disturbances.

7.2 Generation of the SBR recipe

7.2.1 Introduction

Occurrence of both “feast” and “famine” phase operations in the majority of SBR cycles is crucial (Dias *et al.*, 2005). Based on “Characterisation Method” studies carried out in Chapter 4, PHB production under MMC was identified under a number of process “Regime Types” classified into nine RT groups. Further studies demonstrated that process progression regimes consists of three pathways while two pathways end in the “famine” phase operation and the other ends in a “feast” phase operation at process maturity stage.

In summary, RT1 is the initial regime with both acetate and ammonia available in the process. In the first “famine” phase pathway, RT1 is followed by RT2 (when acetate stability occurs) which later leads to RT3 by exhaustion of both feeding sources. The second “famine” phase pathway appears with initial ammonia depletion which is characterised by RT4 and terminates with acetate complete exhaustion in RT5. The last pathway is a “feast” phase operation with initial ammonia depletion in RT4 followed by acetate concentration stability in RT6. Further progression of a batch operation under RT6 leads to RT7 and RT8 where process primary exploitation and process maturity points are formed over operational time respectively. The ninth “Regime Type” (RT9) appears at the end of the third pathway when acetate is completely exhausted in the medium and cells start to consume their PHB content to provide metabolic activities of cells; hence, its occurrence is undesirable.

With the aim of maximising PHB production, “feast” phase operation is the operational pathway to be addressed. On the other side, despite consumption of PHB in a “famine” phase operation, its occurrence is required to provide process conditions for sustainable SBR productions. Cells with low PHB content have more tendencies to replicate in presence of nutrient rich medium. Whereas PHB saturated cells are reluctant for reproduction and have no capacity to form further PHB within. Therefore, a “feast” phase operation should be followed by a “famine” phase operation prior to initiate subsequent production cycle to ensure presence of active culture in a production “feast” phase operation. This is the fundamental principle in design of production recipes which will be discussed in this chapter.

7.2.2 General structure of the recipe

The SBR configuration proposed in this study consist of six operational steps within each sequence of the overall process. Each of these steps is schematically shown in Figure 7.1 in a separate division. At the initial point of a SBR run, for a given initial biomass concentration, a pair of feeding concentrations is imposed to the medium so that occurrence of the “feast” phase batch is assured. Process characterisation studies and the analysis providing mathematical equations to direct a PHB batch process into a particular phase operation is reported in Chapter 4 and Chapter 5.

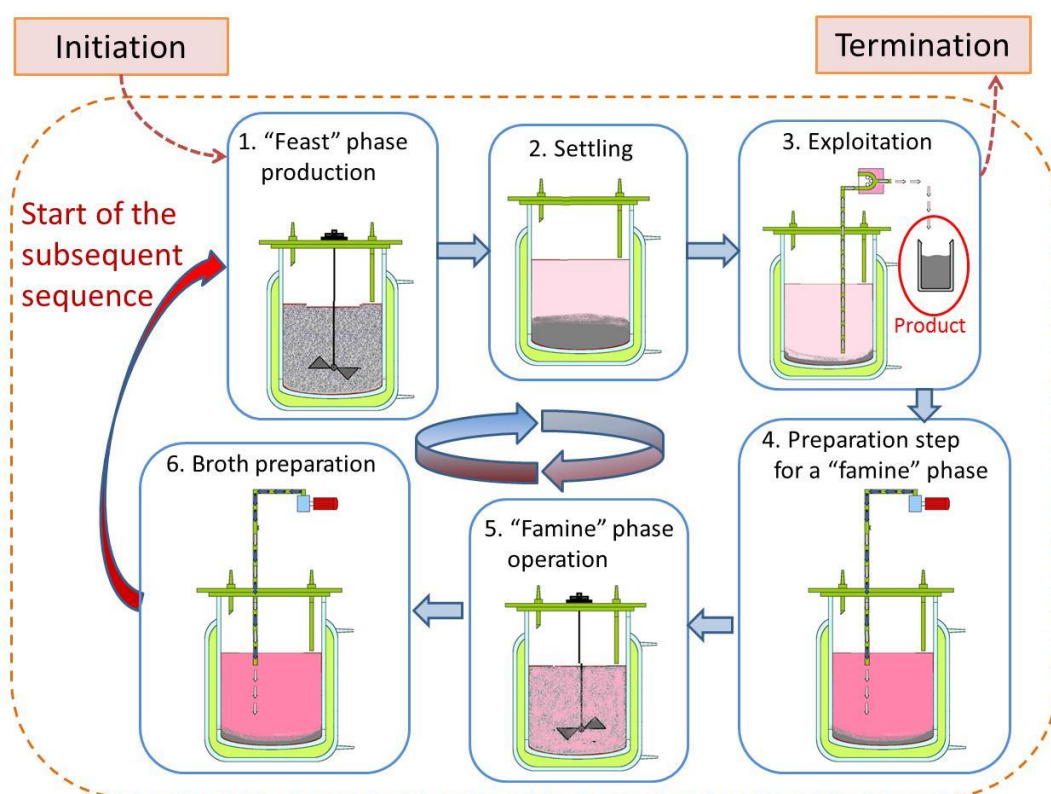


Figure 7.1 General structure of the SBR configuration

Following completion of the “feast” phase batch process in the first step of the first cycle, batch reactor undergoes a period of quiescence so that majority of the biomass concentration precipitates. This settling step is noted as the second step of the SBR run. In the third step, a ratio of the biomass saturated with PHB after a “feast” phase operation is exploited for downstream processing. The proposed method has a number of advantages over other possible options such as partial reservation or constant exploitation of biomass. The most important advantage is process stability enforcement by extraction of process biomass variability. It is proposed to measure and set the remaining biomass sediment level to a certain point associated with the biomass concentration specified as per the SBR recipe. It will also be shown in Section 7.3.5 that

operational fluctuation in practical execution of the recipe would not paralysed the SBR operation under the proposed recipe.

The biomass remaining inside the vessel also contains high level of PHB content which should be consumed by the cells to regain their reproduction capabilities. The second portion of biomass can also be transferred to a smaller volume reactor for a “famine” phase operation. In the fourth step, feeding concentrations are monitored and additional substances are added to the reactor such that operational conditions for “famine” phase operation is satisfied. Consequently, the batch reactor is actuated to complete a “famine” phase batch in the fifth step of the SBR cycle. During the “famine” phase, cells consume ammonia as the external nitrogen source along with their PHB content as the intracellular carbon source for replication and maintenance. By the end of this step, biomass concentration is increased in reflection of PHB consumption in the operational system. In the sixth step, condition of the medium containing activated biomass is monitored and manipulated in accordance with the “feast” phase requirements by application of the “Phase Differentiating Equation” developed in Chapter 5. The subsequent sequence follows a “feast” phase operation in its first step and follows similar procedure aforementioned for the subsequent SBR sequence/cycle.

7.2.3 Implementation of the SBR recipe

Practical execution of the proposed SBR recipe requires identification of the essential process elements in the SBR architecture. These elements are specified in this section to draw a general picture of SBR execution with a number of process sequences or cycle number. Figure 7.2 illustrates the general architecture for execution of the SBR recipe for infinite number of cycles. This figure is a practical depiction of the SBR structure shown in Figure 7.1.

STEP 1. In order to initiate a SBR process, the operational tank is prepared to initiate a “feast” phase operation with initial biomass ($Biomass_0$), acetate ($Acetate_0$) and ammonia ($Ammonia_0$) concentrations along with the other essential materials required for successful execution of the batch process. In the SBR recipe, duration of the “feast” phase batch process is also specified. Specification of the initial biomass, acetate and ammonia concentrations are the requirement of the first step operation in the first cycle of the SBR run. For the second cycle and onwards, batch operation duration is the only batch element required to be specified in the SBR recipe since materials are taken from the sixth step of the former cycle to the first step of the executing first step.

STEP 2. After a successful “feast” phase operation in the first step of SBR cycle, cells should reach to their PHB maturity point while ammonia is completely exhausted and acetate concentration is reduced to a positive entity. At this stage, the SBR process undergoes an operational quiescence for precipitation of biomass in the tank. The quiescence operational period should be specified in the SBR recipe to be applied for every second step operation of each cycle.

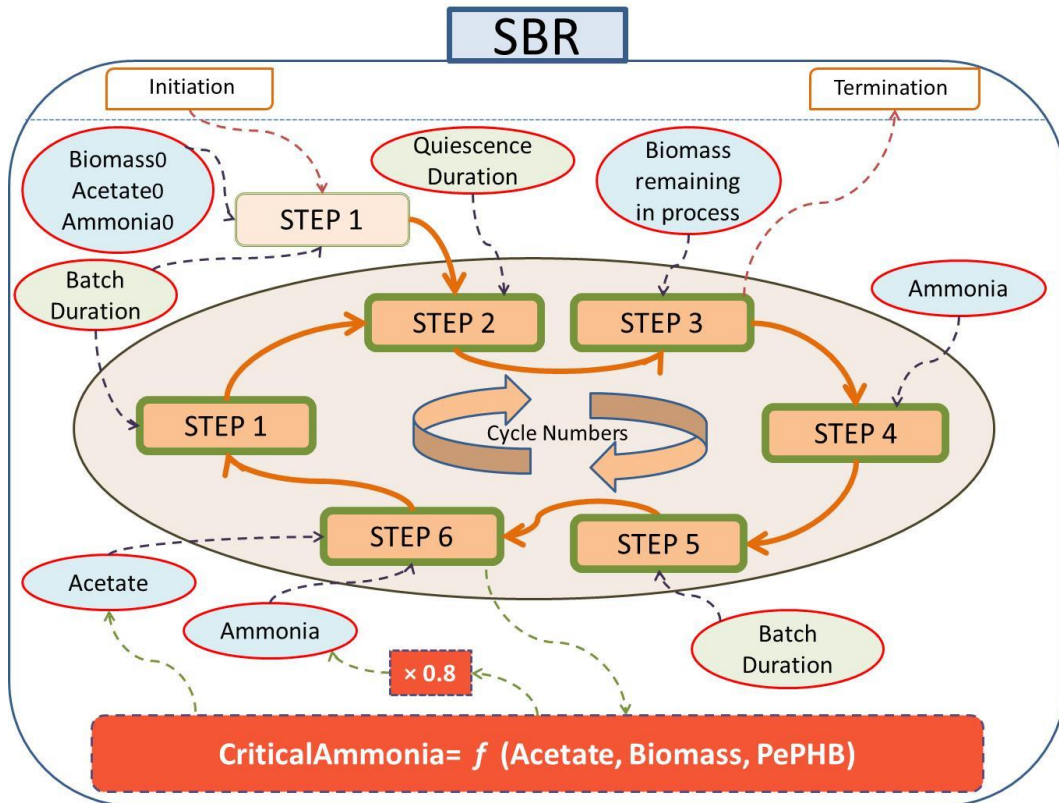


Figure 7.2 Structure of the SBR recipe for execution

STEP 3. The third SBR step is the exploitation stage in which a portion of the total biomass containing PHB saturated bacteria is exploited from the operational tank. In the execution recipe, it is proposed to maintain a certain level of biomass at the end of the third step of the SBR as defined in the recipe. Therefore, a straight forward method is suggested to maintain SBR process operability by exploitation of different biomass concentrations in the event of operational deviation from its steady state conditions. These advantages favour selection of the proposed method over other possible options such as partial reservation or constant exploitation of biomass. This stage is the last stage of the SBR operation if the total number of operational cycles is met according to the recipe.

STEP 4. In the fourth step of the SBR recipe, a feed stream containing ammonia is injected to the operational system with the aim of directing the batch process into a “famine” phase operation. Ammonia injection increases bacteria replication in parallel to acetate consumption. As the result, the rate of acetate consumption increases significantly until acetate is exhausted in the operational system. Bacteria start to consume their intracellular PHB content to provide for their metabolic actives.

STEP 5. The fifth step of the SBR process is the “famine” phase batch operation led by the injection of ammonia in the previous step. Importance of the “famine” phase operation is in reduction of PHB concentration inside bacteria in order to maintain their biological tendency for reproduction and PHB storage. The SBR process element that is required to be defined for this stage of the recipe is the operational duration.

STEP 6. In the sixth step of the SBR process, a mixture of acetate and ammonia is injected to the operational system with the aim of directing the subsequent batch process into a “feast” phase operation. The major point of innovation in this recipe is the application of the “Phase Differentiating Equation” (Equation (5.14)) in specification of the appropriate acetate and ammonia added to the operational system. This equation was formulated as

$$Y - (A_{\alpha} + PePHB0 \cdot (A_{\beta} - A_{\alpha})) \times \quad (5.1)$$

$$(X - ((B_{\alpha} \cdot Z + C_{\alpha}) + PePHB0 \cdot ((B_{\beta} \cdot Z + C_{\beta}) - (B_{\alpha} \cdot Z + C_{\alpha})))) = 0$$

where X is the initial acetate concentration in (C-mmol/L), Y is the initial ammonia concentration in (N-mmol/L), Z is the initial biomass concentration in (C-mmol/L), $PePHB0$ value specifies PHB content percentage and A_{α} , B_{α} , C_{α} , A_{β} , B_{β} , and C_{β} are equation parameters tabulated in Table 5.8 (Section 5.4).

With application of the “Phase Differentiating Equation” (Equation (5.14)), critical ammonia concentration is specified for a given biomass concentration with PHB content level of $PePHB0$ value and acetate concentration specified in the recipe. If subsequent batch operation follows the general trend of its biological behaviour, providing less than the critical ammonia (specified using Equation (5.14)) to the system would result a “feast” phase operation. On the other side, maintaining more than the identified critical ammonia would lead to a “famine” phase operation. In order to direct the batch process into a “feast” phase operation, 80% of the critical ammonia value is considered to be provided to the batch operation in this study. The 80% ratio is proposed on the following two bases:

1. This ratio is high enough to maximise biomass replication with high ammonia concentration exposed to the system.
2. It is not too high to impose risk of “famine” phase occurrence when “feast” phase is favourable.

Acetate concentration should be increased to a level specified in the SBR recipe. For the specified acetate concentration and available biomass with their level of PHB content, the critical ammonia concentration is calculated using the “Phase Differentiating Equation” (Equation (5.14)) and 80% of this value is set as the target to increase ammonia concentration by the end of the sixth step of the SBR recipe execution.

As depicted in Figure 7.2, termination of the sixth step is followed by initiation of the first step which is a “feast” phase batch operation with pre-defined duration specified in the SBR recipe. In the same manner, the subsequent sequence of the SBR process is carried out to complete all the cycles as specified in the recipe. Total exploitation of the biomass occurs in the third step of the final SBR cycle for process termination.

In the next section, procedure of recipe parameter assignment will be discussed in detail.

7.2.4 Procedure of assigning values to the SBR recipe parameters

In this section, a procedure to allocate appropriate values to the parameters of the SBR recipe is discussed. This method is based on the amount of biomass concentration required to be produced/exploited from the operational system in different cycle stages. In other words, production scale is specified by assigning appropriate values to the recipe parameters associated with the biomass concentrations. This includes an approximation for the initial biomass injected to the operational system and the amount of biomass concentration kept in the SBR operation in the exploitation stage. The other parameters related to the inlet/outlet flow of materials to the system are specified in accordance with the biomass concentrations.

In the initial step of parameter assignment, the amount of biomass kept in the operational system in the exploitation stage of the SBR process (STEP 3) is specified. The next step is to specify ammonia concentration at the end of the fourth step of the SBR cycle. Since ammonia is added to the system with the aim of directing the subsequent “famine” phase operation in the fifth step of the SBR, empirical models developed in Section 6.5 can be used to identify the ammonia augmentation level in the STEP 4.

Based on the amount of biomass and ammonia available in the initial state of the “famine” phase operation, biomass production would occur. A Bootstrapping Aggregated Neural Network (BANN) model predicting biomass concentration at the end of the “famine” phase operation (defined as Point-T in Chapter 6) can be used for reverse calculation. Table 6.12 shows that prediction of biomass concentration at the end of the “famine” phase operation is a function of initial biomass and ammonia concentration values. This model can be used for the given value of biomass concentration kept in the SBR process from STEP 3 to estimate the required value associated with biomass concentration at the end of the “famine” phase operation. The initial ammonia concentration is the variable to be identified by the BANN model. Prior to adding ammonia in STEP 4, insignificant amount of ammonia is available in the operational system since ammonia was completely exhausted in the former “feast” phase operation. Additionally, with the application of “Phase Differentiating Equation”, it is possible to calculate the maximum permissible acetate concentration available at the beginning of STEP 4 stage.

Assuming that STEP 5 “famine” phase operation takes place successfully, the final biomass concentration should be close to the value predicted by the BANN model. The acetate and ammonia concentrations is manipulated in STEP 6 for the given biomass concentration to ensure occurrence of a “feast” phase operation in STEP 1 of the subsequent cycle.

As biomass concentration is the basis of the recipe design, final concentration of biomass at the end of STEP 1 “feast” phase operation should be specified. Since initial and final concentration of biomass for the “feast” phase process are known, the empirical model proposed in Table 6.10 can be used to associate initial biomass and ammonia concentrations to the final biomass concentration in a “feast” phase operation. The appropriate ammonia concentration required to be injected to the operational system in STEP 6 can be identified using the model.

In order to specify the appropriate acetate concentration for injection in this stage, “Phase Differentiating Equation” is applied. To assure “feast” phase operation, the specified ammonia concentration should meet the specified acetate concentration when ammonia concentration is 80% of its critical value. Therefore, appropriate acetate concentration can be obtained using the “Phase Differentiating Equation” for an ammonia value equal to 125% of the specified ammonia (125% is the ratio of 100 over

80, the reverse ratio of 80%). With the specified acetate and ammonia concentrations for STEP 6, SBR process is prepared to operate a “feast” phase batch operation.

Empirical model structure proposed in Table 6.10 for prediction of final acetate concentration using initial biomass, PHB, acetate and ammonia concentrations can be used to check that the final acetate concentration does not exceed from the maximum permissible acetate concentration previously specified in STEP 4.

In the SBR recipe, initial biomass, acetate and ammonia concentrations for SBR initiation in STEP 1 can be assigned by the concentration values expected at the end of the STEP 6 for these materials. Later, these values can be modified by the dominant steady state values of these materials at the initial point of STEP 1.

Other than the recipe parameters assigned up to this point, parameters related to batch durations need to be specified as well. The best practice is to assign these values based on experiment results. Moreover, simulation studies can also be useful in this regard. The analytical tool to generate characterisation plots mentioned in Chapter 4 can provide useful information regarding the optimal duration of a “feast” phase batch process. In case of the “famine” phase optimal batch termination point, analysis of the historical data can provide a platform to assign the batch duration. For instance, in accordance with the Figure 6.28, optimal batch duration is longer when dominant “famine” phase operation runs under RT5 in comparison to RT3. As a proposition, average value of optimal batch termination times plus a ratio of their standard deviation can be used as the termination point of “famine” phase batch operations.

The BANN model structure given in Table 6.10 for estimation of PHB saturation point in a “feast” phase operation can also be used to assign “feast” phase batch duration in the SBR recipe. It should be noted that the models predicting the most significant operational points do not perform accurately. For “famine” phase batch termination estimation, the model structure proposed in Table 6.12 can be used. When occurrence of one of the two “famine” phase “Regime Types” is more probable, one of two model structures given in Table 6.13 and Table 6.14 for RT3 and RT5 respectively is more favourable for more accurate estimation of batch termination points.

At the end, a list of SBR Recipe Factors (RF) defined in this section for the SBR process aiming to produce PHB under MMC is tabulated in Table 7.1 along with brief description of the factor.

Table 7.1 SBR recipe factors

SBR Recipe Factors	Description
RF1	SBR cycle numbers
RF2	Total biomass concentration introduced to the SBR at the initial point (STEP1). (C-mmol/L)
RF3	PHB ratio available in the initial biomass relative to its maximum capacity (STEP1).
RF4	Acetate concentration introduced to the SBR at the initial point (STEP1). (C-mmol/L)
RF5	Ammonia concentration introduced to the SBR at the initial point (STEP1). (N-mmol/L)
RF6	STEP 1 operational duration (hour)
RF7	STEP 2 operational duration (hour)
RF8	Total biomass concentration remained in the operation in STEP 3 (C-mmol/L)
RF9	Ammonia concentration maintained by the end of STEP 4 (N-mmol/L)
RF10	STEP 5 operational duration (hour)
RF11	Acetate concentration maintained by the end of STEP 6 (C-mmol/L)

In the next section, a typical SBR recipe is designed and later implemented by the simulation program.

7.2.5 Design of a typical SBR recipe

Following the procedure mentioned in the previous section, a typical SBR recipe is generated in this section based on the magnitude of the process variables reported in the literature. The biomass concentration considered in the SBR recipe alters in a range between 10 C-mmol/L and 40 C-mmol/L which is within the range of practical experiments reported in the literature (Serafim *et al.*, 2004; Dias *et al.*, 2006; Dias, 2008).

The biomass concentration kept in the SBR process in STEP 3 is considered to be 10 C-mmol/L (RF8=10). The biomass replication in the “famine” phase operation increases the biomass concentration from 10 C-mmol/L to 20 C-mmol/L. In the “feast” phase operations, biomass growth is designed to be from 20 C-mmol/L to 30 C-mmol/L.

Based on these biomass concentrations, acetate and ammonia feeding concentrations are specified as discussed in the previous section. The BANN model developed to predict biomass concentration at the final point of a “famine” phase operation (Point-T) is used to assign an appropriate value for addition of ammonia in STEP 4 of the SBR process.

Table 7.2 shows prediction results for a two-input model with x_1 being initial biomass concentration and x_4 being initial ammonia concentration. For a constant initial biomass of 10 C-mmol/L and variable initial ammonia concentration between 1 N-mmol/L and 3 N-mmol/L, final biomass concentrations are estimated.

Table 7.2 BANN model predictions for final biomass concentration in a “famine” phase batch operation

x_1 (Initial biomass)	x_4 (Initial ammonia)	$y=f(x_1, x_4)$ (Final biomass)
10 (C-mmol/L)	1 (N-mmol/L)	15.5 (C-mmol/L)
10 (C-mmol/L)	1.5 (N-mmol/L)	17.9 (C-mmol/L)
10 (C-mmol/L)	2 (N-mmol/L)	19.8 (C-mmol/L)
10 (C-mmol/L)	2.5 (N-mmol/L)	22.1 (C-mmol/L)
10 (C-mmol/L)	3 (N-mmol/L)	24.5 (C-mmol/L)

Since biomass concentration of 20 C-mmol/L is favourable, ammonia concentration of around 2 N-mmol/L is assigned to the SBR recipe (RF9=2). Therefore, ammonia augmentation level should be about 2 N-mmol/L in STEP 4 of the SBR process. Using “Phase Differentiating Equation” maximum permissible acetate concentration can be identified to assure occurrence of “famine” phase operations in the consecutive batch operation. The “Phase Differentiating Equation” is used for biomass concentrations less than 200 C-mmol/L:

$$Y - (0.0411 + PePHB0 \cdot (0.0402 - 0.0411)) \times (X - ((3.4374 \cdot Z + 0.0269) + PePHB0 \cdot ((0.0171 \cdot Z + 1.6432) - (3.4374 \cdot Z + 0.0269)))) = 0$$

where Y is the initial ammonia concentration in N-mmol/L, X is the initial acetate concentration in C-mmol/L and Z is the initial biomass concentration in C-mmol/L. For initial biomass concentration of 10 C-mmol/L ($Z=10$ C-mmol/L), and ammonia concentration of 2 N-mmol/L ($Y=2$ N-mmol/L) the above equation takes the following format:

$$2 - (0.0411 + PePHB0 \cdot (-0.001)) \times (X - (34.4 - PePHB0 \times 32.56)) = 0$$

At the initial state of a “famine” phase operation, $PePHB0$ value should be close to 100%. For $PePHB0$ equal to 1, critical acetate concentration is calculated to be about 50 C-mmol/L ($X=50$ C-mmol/L). This is the maximum acetate concentration that should be available at the beginning of STEP 4.

For STEP 6, acetate and ammonia feeding concentrations should be defined so that “feast” phase operations are assured in the subsequent STEP 1 batch operation. As mentioned, biomass concentration is expected to increase from 20 C-mmol/L to 30 C-mmol/L in the “feast” phase operation. The proposed BANN model structure given in Table 6.10 is used to associate initial biomass and ammonia concentrations to final biomass concentration in a “feast” phase process. For a constant initial biomass concentration of 20 C-mmol/L, the BANN model is used to predict final biomass concentrations to target 30 C-mmol/L with various initial ammonia concentration values. In Table 7.3 prediction values are tabulated for 5 different initial ammonia values. As shown in this table, in order to reach to 30 C-mmol/L of biomass, augmentation of 2 N-mmol/L ammonia is required.

Table 7.3 BANN model predictions for final biomass concentration in a “feast” phase batch operation

x_1 (Initial biomass)	x_4 (Initial ammonia)	$y=f(x_1, x_4)$ (Final biomass)
20 (C-mmol/L)	1 (N-mmol/L)	25.8 (C-mmol/L)
20 (C-mmol/L)	1.5 (N-mmol/L)	27.9 (C-mmol/L)
20 (C-mmol/L)	2 (N-mmol/L)	30.1 (C-mmol/L)
20 (C-mmol/L)	2.5 (N-mmol/L)	32.2 (C-mmol/L)
20 (C-mmol/L)	3 (N-mmol/L)	34.3 (C-mmol/L)

In order to assure “feast” phase operation, “Phase Differentiating Equation” is used to find the critical acetate concentration equivalent to 125% of the ammonia concentration injected in STEP 6 of the process. Based on the “Phase Differentiating Equation” (Equation (5.14)):

$$Y - (0.0411 + PePHB0 \cdot (0.0402 - 0.0411)) \times (X - ((3.4374 \cdot Z + 0.0269) + PePHB0 \cdot ((0.0171 \cdot Z + 1.6432) - (3.4374 \cdot Z + 0.0269)))) = 0$$

For initial biomass concentration of 20 C-mmol/L ($Z=20$ C-mmol/L), and ammonia concentration of 2×1.25 N-mmol/L ($Y=2.5$ N-mmol/L) the above equation takes the following format:

$$2.5 - (0.0411 + PePHB0 \cdot (-0.001)) \times (X - (68.775 - PePHB0 \times 66.79)) = 0$$

At the initial state of a “feast” phase operation, $PePHB0$ value should be close to 0%. For $PePHB0$ equal to 0, critical acetate concentration is calculated to be about 130 C-mmol/L ($X=130$ C-mmol/L). This is the acetate concentration that should be

available at the end of STEP 6 and beginning of the consecutive STEP 1 batch operation (RF11=130).

In order to initiate the SBR operation, process conditions at STEP 1 steady state is considered. Therefore, initial biomass concentration is assigned to be equal to 20 C-mmol/L, with low level of PHB content after a “famine” phase operation, initial ammonia concentration of 2 N-mmol/L and initial acetate concentration of 130 C-mmo/L (RF2=20, RF3=10%, RF4=130, RF5=2). Up to this point, recipe parameters associated with feeding concentrations are all specified.

It is also favourable to estimate final concentration of acetate at the end of STEP 1 “feast” phase operation to ensure that the remained concentration is less than 50 C-mmol/L. The BANN model structure given in Table 6.10 for prediction of final acetate concentration using initial biomass, PHB, acetate and ammonia concentrations are applied in this regard. For initial biomass concentration of 20 C-mmol/L ($x_1=20$) with insignificant amount of intracellular PHB content ($x_2=0$), initial acetate concentration of 130 C-mmol/L ($x_3=130$) and initial ammonia concentration of 2 N-mmol/L ($x_4=2$) the final acetate concentration is predicted to be about 30 C-mmol/L by the BANN model. This value is considerably less than the maximum permissible amount for acetate concentration of 50 C-mmol/L that should be available at the beginning of STEP 4. Therefore, it does not produce any conflict for “famine” phase operation in the subsequent STEP 5 (For high initial intracellular PHB content ($x_2=1$), the predicted final acetate concentration is far less than 30 C-mmol/L which confirms validity of the recipe in case of occurrence of disturbance effecting the initial intracellular PHB content).

The batch duration parameters are assigned to 15 hours for the “feast” phase operations and 20 hours for the “famine” phase operations using BANN models with the structures proposed in Table 6.10 and Table 6.12 respectively (RF6=15, RF10=20). The quiescence period is considered to be 10 hours in simulations as proposed in the literature (RF7=10) (Dias, 2008). Assignment of a more accurate batch period time is a subject of experimental studies.

In the next section, the SBR recipe generated in this section will be executed using the simulation program.

7.2.6 Execution of the SBR recipe

In this section, computer simulation program discussed in Chapter 3 is used to implement the SBR recipe for production of PHB under mixed microbial cultures. The SBR production presented in this section is based on the SBR recipe developed in the previous section. The SBR recipe parameters presented in this section are assigned to generate a 50-cycle SBR run. This SBR recipe is tabulated in Table 7.4.

Table 7.4 A SBR recipe for production of PHB

SBR recipe				
RF1	Cycle Numbers		50	
	SBR stage	Entity	Value	Unit
RF2	Initiation	Biomass	20	C-mmol/L
RF3	Initiation	PePHB0	0.1	
RF4	Initiation	Acetate	130	C-mmol/L
RF5	Initiation	Ammonia	2	N-mmol/L
RF6	Step 1:	Time	15	hr
RF7	Step 2:	Time	10	hr
RF8	Step 3:	Biomass	10	C-mmol/L
RF9	Step 4:	Ammonia	2	N-mmol/L
RF10	Step 5:	Time	20	hr
RF11	Step 6:	Acetate	130	C-mmol/L

Detailed simulation results for ammonia, acetate, PHB and biomass concentrations are depicted in different subplots shown for the first and the second sequence of the SBR in Figure 7.3 and Figure 7.4 respectively. Each column in the figures represents one step of the SBR recipe as designed in Section 7.2.2.

- *Demonstration of the first two SBR recipe cycles*

Cycle 1-STEP 1: As shown in the first column of Figure 7.3, SBR initiates with ammonia concentration of 2 N-mmol/L, acetate concentration of 130 C-mmol/L and total biomass concentration of 20 C-mmol/L. The total biomass concentration is composed of the biomass concentrations for each 32 populations of bacterial used as the mixed microbial cultures producing PHB. For simulation purpose, initial biomass concentration of cultures is randomly assigned to sum up to the total biomass concentration specified by the SBR recipe. The intracellular PHB content of the biomass at the initial point is 10% of the maximum capacity of each 32 populations.

Looking at the first column of subplots shown in Figure 7.3, it can be deduced that the 15 hour batch operation in the first step of the SBR recipe is operating under the “feast”

phase operation specifications. The concentration of total PHB increases to a maximum saturation point by the end of the batch without any PHB drop. This is in conformity with the SBR recipe in which the first step was designed to perform a “feast” phase operation. This operation represents an RT8 “Regime Type” in accordance to the “Characterisation Method” analysis with initial ammonia depletion followed by acetate concentration stability. The plots depicting total biomass and total PHB concentrations were obtained by summation of the 32 biomass and PHB values for each 32 active bacterial populations respectively. The ammonia depletion point is marked by (Δ), acetate stability point is marked by (∇) and PHB saturation is marked by (\circ). The PHB saturation is maintained for 10% of the overall batch duration confirmed by (\star) on the PHB plot.

Cycle 1-STEP 2: The final state of the batch operation in the first step is used to define the initial state of the batch in the second step which is the settling step. In this stage, batch operation undergoes a period of quiescence in order to allow precipitation of the biomass. The quiescence stage requires 10 hours of quiescence with no input/output stream of materials into/from the operational system. The plots presenting critical process attributes are shown in the second column of the Figure 7.3. In this step, apart from a small portion of acetate consumed to maintain cells metabolic activities, no significant concentration alteration occurs in the biomass and PHB profiles.

Cycle 1-STEP 3: The final state of the batch in quiescence step is used to define the initial process state in the third step of the recipe (exploitation step). The graphs showing the initial and final state of the process at this stage are given in the third column of plots in Figure 7.3. Since this stage of the SBR is not an operational process, a short instant is considered for biomass exploitation in this simulation study. However, this stage may require considerably more time in real operation practice. At this stage, the high intracellular PHB content cells are divided into two portions. One portion remains inside the operational system to be used in the consecutive steps of the SBR process assigned as RF8 in the recipe. The other portion is exploited from the system for PHB purification and downstream processing. As shown in Figure 7.3, total biomass concentration in the operational system drops from 30 C-mmol/L to 10 C-mmol/L in accordance with the recipe specifications. The biomass concentration of 20 C-mmol/L exploited from the reactor contains about 52 C-mmol/L intracellular PHB as the product of the first cycle of SBR operation. Since simulation period is considered to be short, process alteration in acetate or ammonia concentration is insignificant.

Cycle 1-STEP 4: In the fourth step, operational system is prepared to undergo a “famine” phase operation in the subsequent step. For that purpose, ammonia is introduced to the operational system in accordance with the specification given by RF9 in the SBR recipe. Similar to the previous step, the time period considered for this simulated stage is short since injection of ammonia occurs instantly in practice. As shown in the fourth column of Figure 7.3, ammonia concentration is increased to 2 N-mmol/L by the end of this step.

Cycle 1-STEP 5: In the fifth step of the cycle, a batch process operation occurs. Execution of a well-designed SBR recipe leads to a “famine” phase operation in this step. The graphs shown in the fifth column of Figure 7.3 confirms “famine” phase operation for the first cycle of the SBR operation under RT3. In this process, both acetate and ammonia are consumed in direction of biomass replication. When acetate is completely exhausted in the operational system, cells start to consume their intracellular PHB content to maintain their metabolic activities. Consumption of the intracellular PHB is reflected in fPHB, PHB and total PHB plots. The operational duration is set to 20 hours as specified in the SBR recipe (RF10=20).

Cycle 1-STEP 6: by the end of the “famine” phase operation, cells should be in proper state to initiate a “feast” phase production stage. In the sixth step of the recipe, process preparations are carried out to direct the operational system into a “feast” phase process. Similar to the third and the fourth steps, the sixth step occurs instantly and a short time is considered for simulation of the step. The acetate augmentation concentration is specified by the SBR recipe using the “Phase Differentiating Equation” and accordingly ammonia is added to the operational system to insure “feast” phase operation in the consecutive step. The acetate augmentation factor is 130 C-mmol/L in the SBR recipe (RF11=130).

Equation (5.14) is applied to assign appropriate ammonia augmentation concentration:

$$Y - (0.0411 + PePHB0 \cdot (0.0402 - 0.0411)) \times (X - ((3.4374 \cdot Z + 0.0269) + PePHB0 \cdot ((0.0171 \cdot Z + 1.6432) - (3.4374 \cdot Z + 0.0269)))) = 0$$

where Y is the initial ammonia concentration in N-mmol/L, X is the initial acetate concentration in C-mmol/L and Z is the initial biomass concentration in C-mmol/L. The average $PePHB0$ value for the 32 populations at the initial stage of the sixth step in the first cycle is about 15% ($PePHB0 = 0.15$). The initial biomass concentration is 20 C-mmol/L ($Z=20$) and the initial acetate concentration should be about 130 C-mmol/L

($X=130$) as given in the recipe. Using equation mentioned above, the critical ammonia concentration is calculated to be about 2.8 N-mmol/L ($Y=2.8$).

As mentioned in the recipe description section, in the sixth step of the SBR cycle ammonia is added to the operational system so that its concentration reaches to 80% of the critical ammonia concentration calculated. As shown in the sixth column graphs of Figure 7.3, acetate and ammonia concentrations are augmented to 130 C-mmol/L and 2.2 N-mmol/L at the final operational state of the sixth step.

Cycle 2-STEP 1: the second cycle of the SBR process initiates from the first step operational batch process. The initial state of the batch process is the final state of the batch from the previous sixth step. As shown in the first column of graphs in Figure 7.4, the operational batch undergoes a “feast” phase operational process as expected.

Cycle 2-STEP 2: precipitation is carried out during the 10 hours of operational quiescence.

Cycle 2-STEP 3: in this step, 22 C-mmol/L of biomass is exploited from the process and 10 C-mmol/L remains in the vessel for the consecutive step of the cycle.

Cycle 2-STEP 4: ammonia concentration is increased to 2 N-mmol/L as specified in the SBR recipe.

Cycle 2-STEP 5: a batch operation occurs to reduce PHB content of the cells by operating under a “famine” phase operation. As shown in the fifth column graphs of Figure 7.4, “famine” phase operation is occurred under RT3 “Regime Type”.

Cycle 2-STEP 6: in this step, acetate and ammonia is added to the operational system in order to prepare the batch for the subsequent “feast” phase operation.

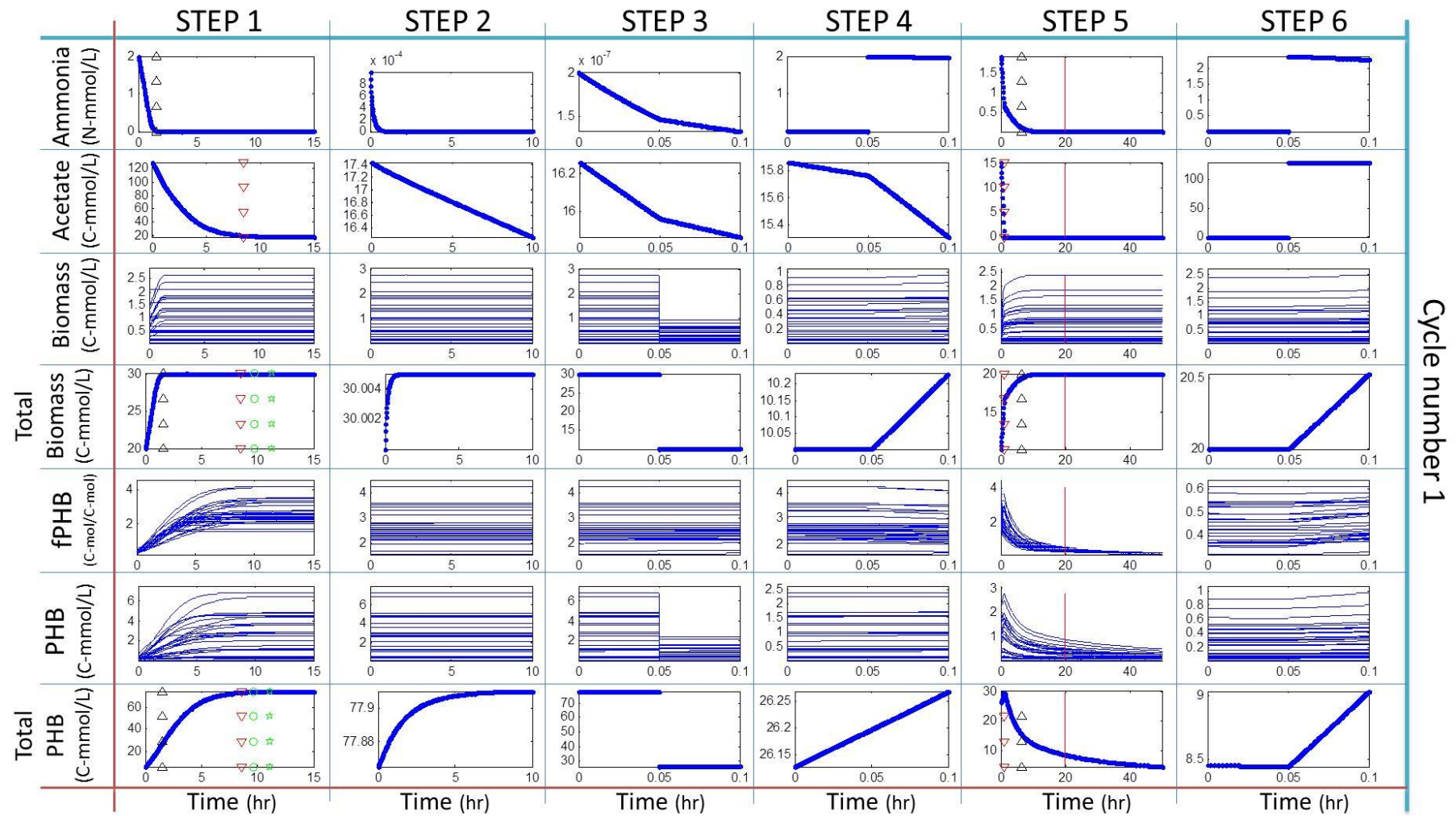


Figure 7.3 Detailed presentation of simulation results for the first cycle of PHB production under proposed SBR recipe

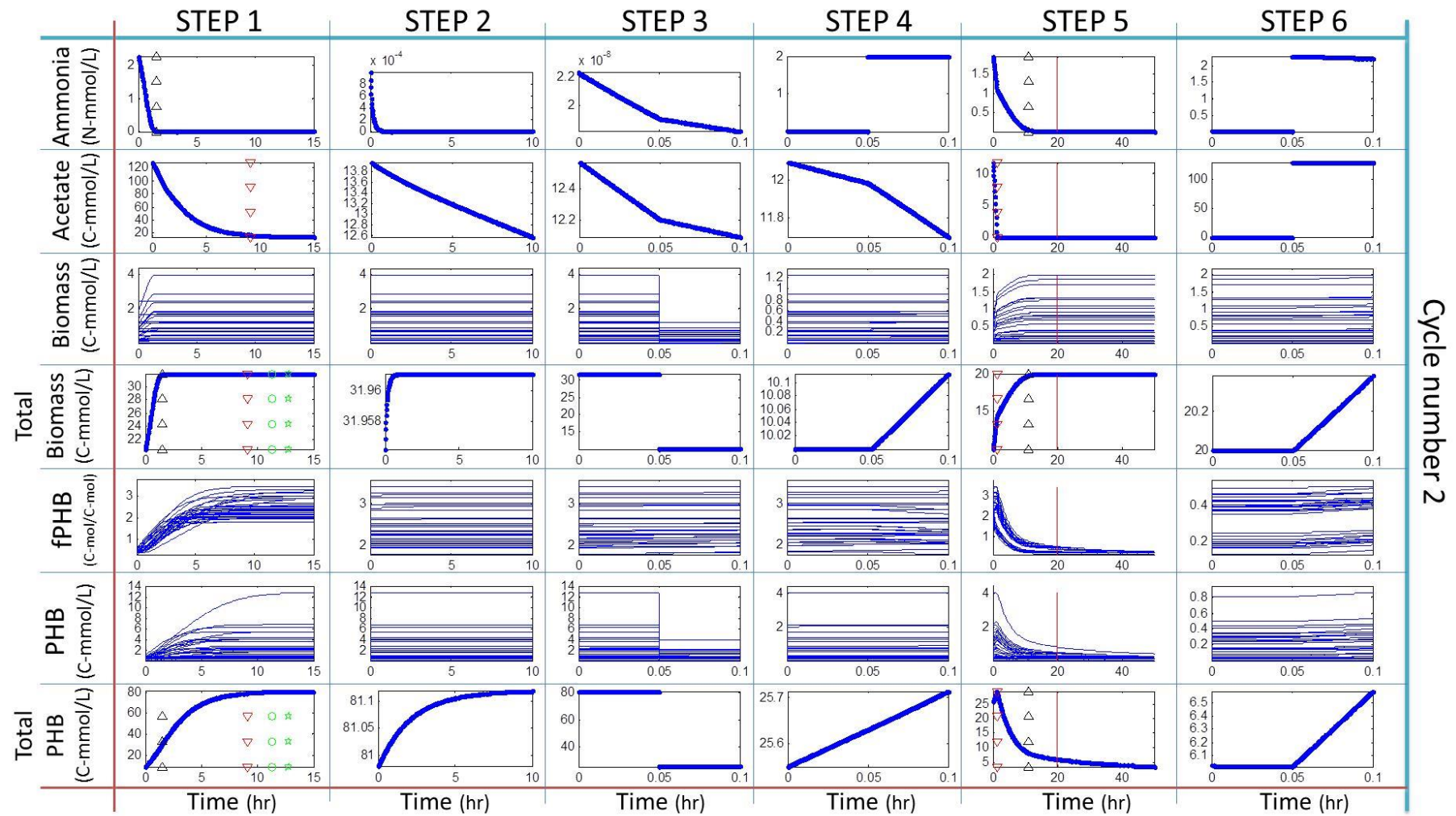


Figure 7.4 Detailed presentation of simulation results for the second cycle of PHB production under proposed SBR recipe

- *Demonstration of the first five SBR recipe cycles*

Detailed description of the process elements for the first two SBR cycles was depicted in Figure 7.3 and Figure 7.4. In Figure 7.5, simulation results are shown for the first five cycles of this recipe. In this figure, significant elements of the process are depicted showing the initial and final state of each batch in each SBR step. Additionally, “Regime Type” numbers are given in the plots of the first row in order to provide qualitative description of the operational batch process carried out in each cycle. For each SBR step, one column of plots is allocated in Figure 7.5.

In order to validate the SBR recipe, occurrence of the “feast” and “famine” phase operations in the first and the fifth SBR steps are investigated at first. The appearance of RT8 in STEP 1 and RT3 in STEP 5 confirms occurrence of the “feast” phase and the “famine” phase operations in conformity of the SBR structure respectively. Successful quiescence stage is characterised by RT4 in STEP 2. Otherwise, acetate shortage results in occurrence of RT5 which is a failure in STEP 2.

The total biomass concentration profile follows the description designed in creation of the SBR recipe. In the five cycles, total biomass concentration increases from 20 C-mmol/L to about 30 C-mmol/L in the first step SBR operations. In the third step SBR operations, 10 C-mmol/L of the total biomass concentration remain in the SBR operation while the second portion is exploited. In the “famine” phase operation stages, total biomass concentration increases from 10 C-mmol/L to 20 C-mmol/L as considered in the SBR recipe generation procedure.

Looking at the first column graphs depicted in Figure 7.5, it can be seen that “feast” phase process characteristics are observable in the initial and final states of the process elements. PePHB values increased from less than 10% to more than 90% in each cycle and their effect on the total PHB concentrations is reflected on the PHB profile.

In the second column of graphs shown Figure 7.5, concentration profiles are depicted for the quiescence stage of the SBR. These graphs demonstrate that acetate consumption is the only significant occurrence that takes place to maintain biological activities of the cells. As shown in the graphs, total biomass concentration, total PHB concentration and ammonia concentration remain the same during the quiescence stage.

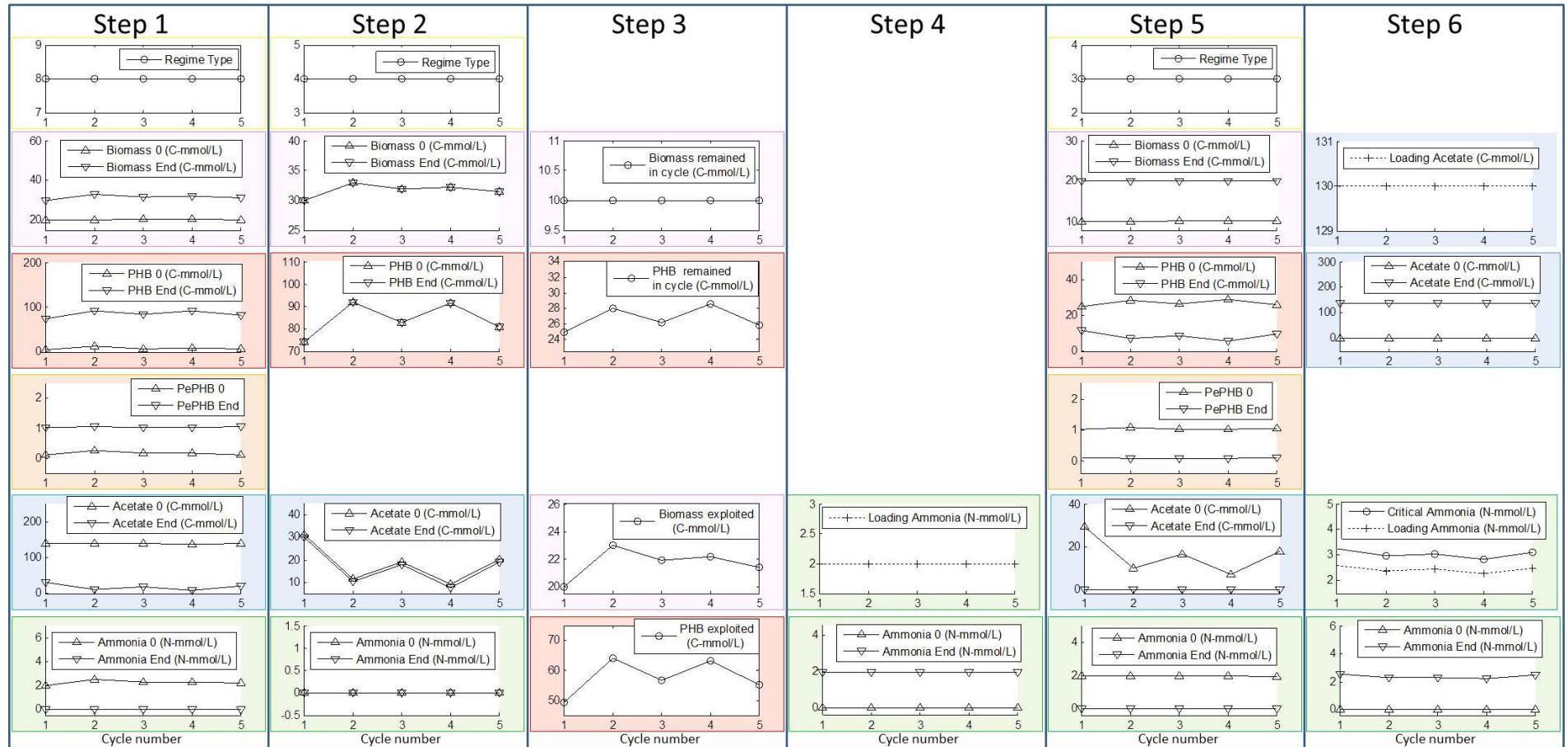


Figure 7.5 Execution of the SBR recipe in five cycles

In the third column of Figure 7.5, the process graphs associated with the exploitation stage are depicted. In the five cycles, the total biomass concentration exploited from the process varies in between 20 C-mmol/L to 23 C-mmol/L. This variation is mainly due to the variation of the loading ammonia concentration in the sixth step of the earlier cycle. For instance, maximum total biomass concentration exploited in the third step occurred in the second cycle when maximum ammonia concentration is assigned for the sixth step of the earlier cycle. The variation observed for the total PHB profiles are due to the variations in the total biomass concentration and the “feast” phase operations occurred prior to the exploitation stage.

For the fourth step of the SBR, the loading concentration of ammonia is depicted on the top graph in the fourth column of Figure 7.5. On the bottom graph, the initial and final concentrations of ammonia are depicted to demonstrating ammonia increase from zero to the amount introduced to the process in this stage of the SBR.

In the fifth column of Figure 7.5, PePHB profile is depicted to demonstrate effectiveness of the “famine” phase operation in reduction of PHB content of the operational cells. The initial PePHB values decreased from more than 95% to less than 5% during the five “famine” phase operations in the SBR cycles. The complete exhaustion of the acetate and ammonia is depicted in their concentration profiles in this column of graphs.

In the sixth column of Figure 7.5, initial, loading and final concentrations of acetate and ammonia are depicted in the graphs. As mentioned in the previous section, the acetate loading concentration is specified in the SBR recipe whereas the ammonia loading concentration is calculated using the “Phase Differentiating Equation”.

Figure 7.5 demonstrates a successful release of the SBR recipe for a SBR process in the first five cycles. In Figure 7.6, a complete set of operational elements are shown for the 50 cycles of the SBR recipe.

- *Demonstration of a complete SBR recipe with 50 cycles*

The first step in process analysis is carried out by observing the “Regime Type” numbers on the top graphs depicted for the first, second and fifth steps of the SBR operation. As shown on the “Regime Type” plot of the first step operations in Figure 7.6, the majority of the operations perform under RT8 which indications occurrence of a “feast” phase operation. In three cycles RT5 and in one cycle RT9 are the “Regime Types” observed in STEP 1 operations which are not favourable. In

STEP 2, six out of fifty operations encountered acetate exhaustion during the quiescence period by observing unfavourable RT5 in place of RT4. In STEP 5, RT3 and RT5 are the only “Regime Types” observed in the “Regime Type” plot to confirm “famine” phase occurrence in all cycles of the process.

The overall assessment of the “Regime Type” plot leads to the conclusion that the SBR recipe is able to provide a successful SBR operation with low failure rate of less than 10% in the “feast” phase operational stage (in 4 out of 50 cycles “feast” phase did not occur). This failure is mainly due to the unpredictable/randomness associated with the biological behaviour of the PHB process that is reflected in the simulation program.

The loading concentration of ammonia in the sixth step of the SBR operation is specified using the “Phase Differentiating Equation”. As mentioned in Chapter 5, the “Phase Differentiating Equation” fails in a small ratio of the total predictions when random behaviour process simulator is applied. Unfortunately, failure of the equation to provide accurate estimation has negative effect on overall performance of the SBR process. However, this failure does not paralyse the overall process and the operation manages to retain its pre-defined pathway in the subsequent stages.

Close observation of the concentration profiles in different stages of the SBR operation depicted in Figure 7.6 leads to the conclusion that the operational system follows the specifications defined in the SBR recipe except for a minority of the cycles. These deviations of the expected concentration profiles can be noted in the cycles with appearance of unexpected “Regime Types”.

Execution of the SBR recipe with large number of cycles demonstrates the reliability of the method to perform successful PHB production under MMC using the SBR process with the proposed recipe structure. The success of the proposed recipe structure and its parameters can also be confirmed when no accumulation of substances is recorded over SBR process. The intracellular PHB content of the cells reduce to its minimal level in the “famine” phase operations while cells accumulate PHB to their maximum capacity in the majority of the “feast” phase operations as depicted in Figure 7.6.

In the next section, capability of the SBR process operating under the generated recipe in rejection of different types of load disturbances will be investigated.

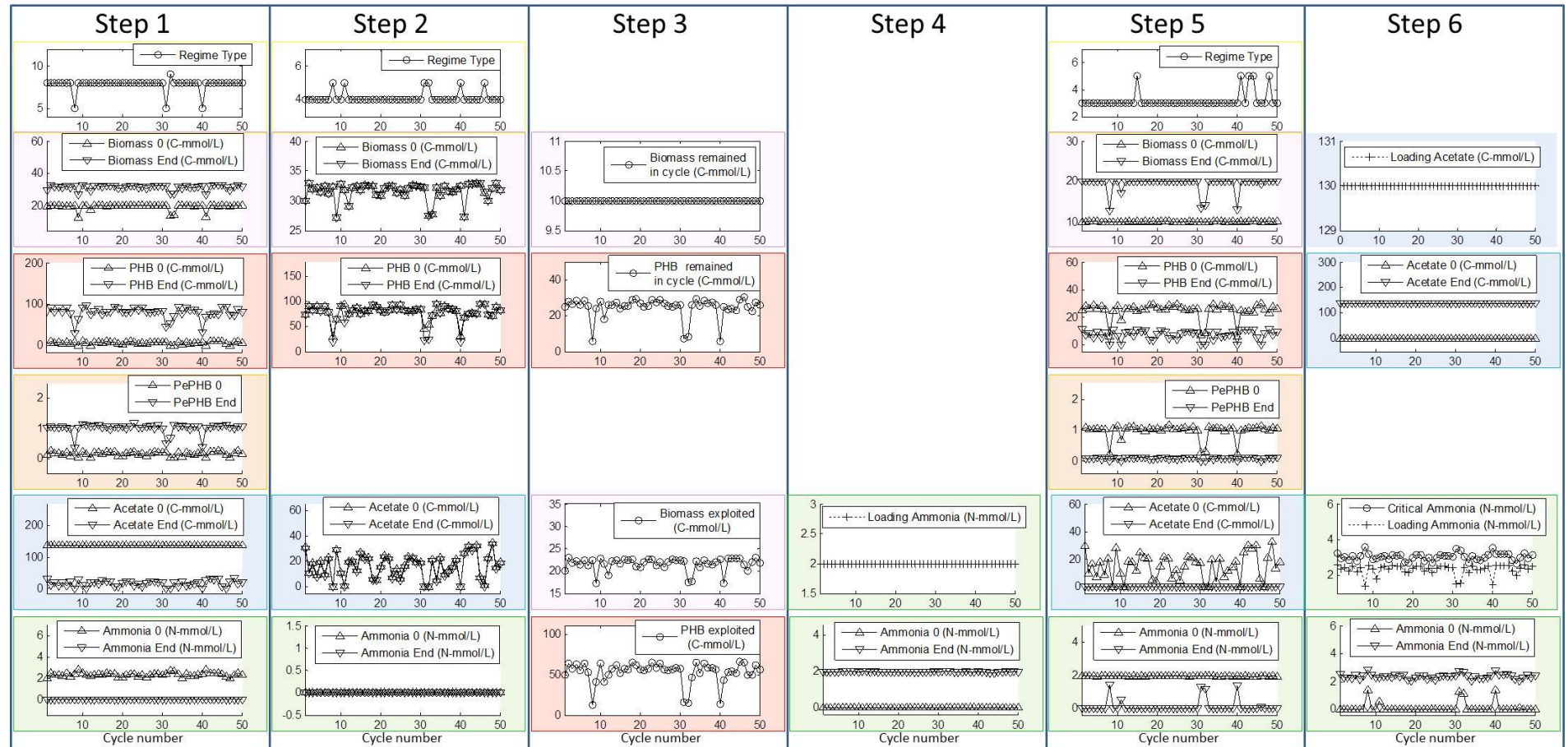


Figure 7.6 Execution of the SBR recipe (demonstration of the 50 cycles)

7.3 Capability of the SBR recipe in disturbance rejection

7.3.1 Introduction

Application of the SBR recipe created for production of PHB under MMC is straightforward. However, execution of the recipe on the operational units might be coupled with disturbances that can potentially paralyse the process. For instance, if ammonia concentration is not maintained at exact 2 N-mmol/L, deviation of the operational recipe occurs with no predictable outcome and it can be considered as a disturbance to the operational recipe.

In this section, both positive (external effect to the system is more than the specified value in the recipe) and negative (external effect to the system is less than the specified value in the recipe) disturbances are imposed to the recipe parameters that are associated with the substances injected or exploited from the operational system.

With the aim of analysing the effect of executional disturbances to the operational process, deterministic behaviour process simulator is applied in the first step for a more clear observation of the disturbance effect on the SBR process. The SBR recipe generated in Section 7.2.5 is executed for 50 cycles and the results of a simulation run are depicted in Figure 7.7. Since deterministic behaviour process simulator is used to generate data depicted in Figure 7.7, the produced plots are more informative when compared with the plots depicted in Figure 7.6 where random behaviour process simulator is used for data generation.

The deterministic behaviour process simulator produces identical results when two batch operations undergo the same operational conditions. Additionally, the “Phase Differentiating Equation” applied in the sixth step of the SBR cycles is very accurate for the case of deterministic behaviour system as mentioned in Chapter 5.

The three recipe factors that can be imposed to load disturbances are RF8, RF9 and RF11 during the course of the SBR operation. The three graphs demonstrating the remaining biomass concentration in the third step (RF8), the ammonia augmentation concentration in the fourth step (RF9) and the acetate augmentation concentration in the sixth step (RF11) are the identical graphs when comparing Figure 7.6 with Figure 7.7. These three profiles are identical since no operational disturbance is considered in simulation studies of the two systems.

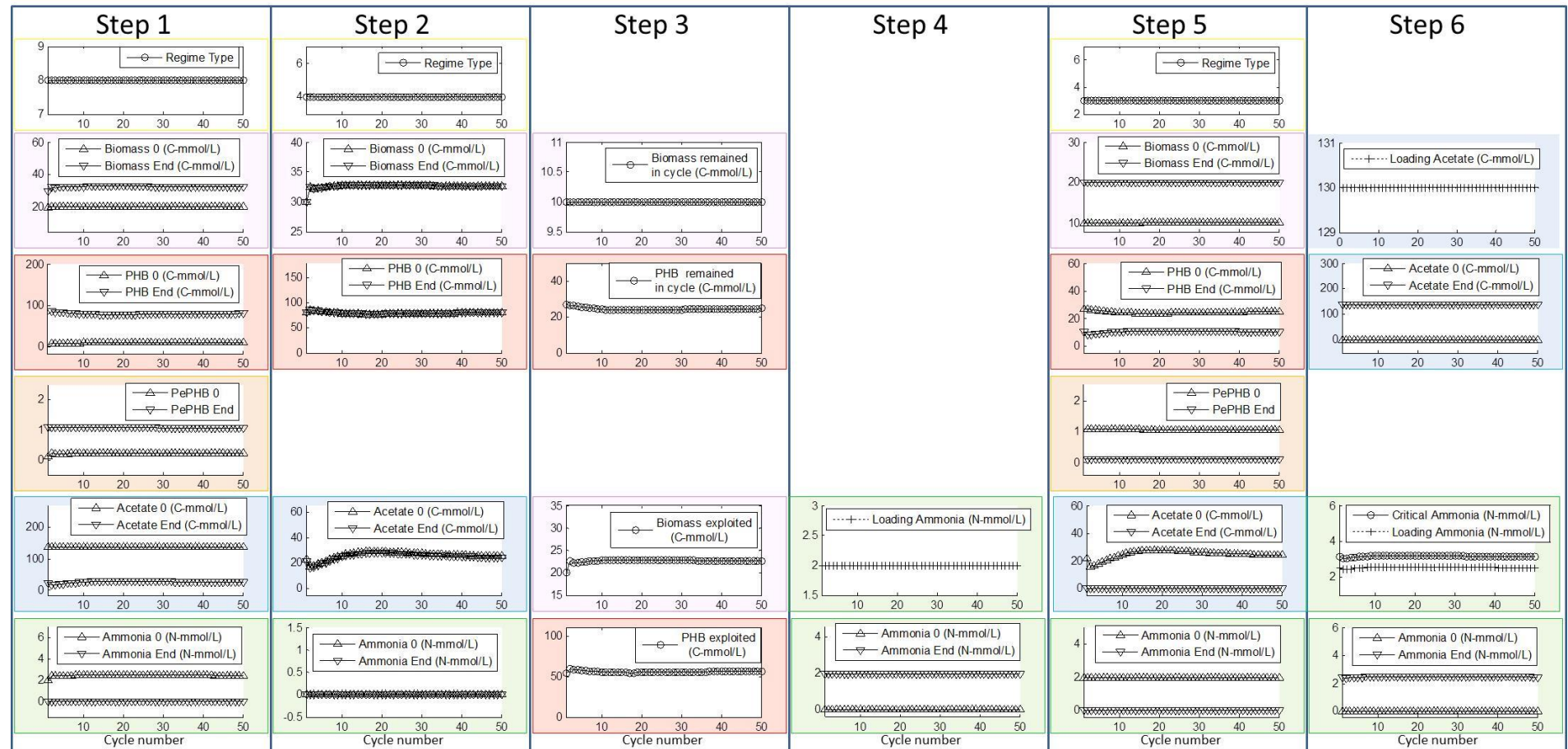


Figure 7.7 Execution of the SBR recipe using deterministic behaviour process simulator

The analysis of the SBR recipe reaction to the load disturbances on RF8, RF9 and RF11 are discussed in Section 7.3.2, Section 7.3.3 and Section 7.3.4 respectively. A brief summary of the figures depicted to illustrate the effect of disturbances on the SBR recipe is tabulated in Table 7.5.

Table 7.5 Illustrative investigations on the recipe reactions to the load disturbances

Source of load disturbance	Deterministic behaviour simulator	Random behaviour simulator
RF8-The remained biomass concentration in STEP3	Section 7.3.2 Figure 7.8	Section 7.3.2 Figure 7.9
RF9-The ammonia augmentation concentration in STEP4	Section 7.3.3 Figure 7.10	Section 7.3.3 Figure 7.11
RF11-The acetate augmentation concentration in STEP11 (disturbance recognition without delay)	Section 7.3.4.A Figure 7.12	Section 7.3.4.A Figure 7.13
RF11-The acetate augmentation concentration in STEP11 (disturbance recognition with delay)	Section 7.3.4.B Figure 7.14	Section 7.3.4.B Figure 7.15

Investigations on the effect of RF11 disturbance on the recipe is carried out on two cases considering immediate (Section 7.3.4.A) or gradual recognition of the disturbance (Section 7.3.4.B). At the end, realisation of the SBR process operation is carried out by imposing operational execution variation of maximum 50% in RF8, RF9 and RF11. Moreover, histograms are shown to demonstrate PHB production variation in reflection of operational variations in Section 7.3.5.

The effect of positive and negative load disturbances on these three SBR variables will be investigated in the next three sections.

7.3.2 *The effect of load disturbance on the total biomass concentration remained inside the reactor in the 3rd step of the SBR process - RF8*

In order to investigate the effect of load disturbance on the amount of biomass remained in the operational system in the exploitation stage; both deterministic and random behaviour process simulators are used. The load disturbances are imposed on the 10th and 25th cycle numbers with a positive value and a negative value respectively.

In Figure 7.8, simulation results for a SBR process operated under the recipe tabulated in Table 7.4 is depicted for the deterministic behaviour system. In this process, the biomass concentration remained in the operational system is considered to be 20 C-mmol/L in the 10th cycle and 1 C-mmol/L in the 25th cycle in place of the 10 C-mmol/L specified in the recipe.

Looking at the “Regime Type” profiles in the first and the fifth steps of the operation, it can be observed that both “feast” phase and “famine” phase operations occur in each operational cycle. This figure demonstrates that disturbances on RF3 does not deviate the overall process from the original pathway considered in the SBR recipe. The operational recipe is capable of mitigating the effect of disturbances by two means. The first is alteration of ammonia concentration injected to the system in the sixth step of the same cycle and the second is biomass compensation in the third step of operation in the subsequent sequence.

As it can be seen in Figure 7.8, the critical and loading ammonia graphs in the sixth column of plots drop to almost half of their steady state values in the 10th cycle. This reaction from the operational process is caused by application of the “Phase Differentiating Equation” in assignment of appropriate concentration of ammonia in the sixth step of the process. Since additional biomass is available in the system, injection of less ammonia lead to less production of biomass in the subsequent “feast” phase. This reaction to the disturbance directs the process to its steady state pathway.

The reverse effect is observable when only 1 C-mmol/L of biomass is maintained in the 25th cycle of the operational process. In the sixth step of the same sequence, the amount of ammonia injected into the system is more than its steady state to produce more biomass in the subsequent “feast” phase operation.

The second mitigating reaction to the biomass shock can be observed in the subsequent cycle when biomass concentration remained in the operational system is the same as defined in the SBR recipe. In the third step of the 11th cycle, more biomass is exploited

from the operational system to retain the 10 C-mmol/L of total biomass concentration in the process. On the other side, in the third step of the 26th cycle the opposite occurrence is observed to bring the process back to its steady state pathway.

The simulation graphs depicted in Figure 7.9 are generated using the random behaviour process simulator to investigate the effect of disturbance on RF3. The random function applied in the simulation program generates the same set of random values each time the simulation program is run. Therefore, without the disturbances, simulation graphs in Figure 7.9 should be identical to those of Figure 7.6.

Comparing the “Regime Type” graphs in Figure 7.6 and Figure 7.9 suggests that disturbances on RF3 have minimal effect on the “Regime Types” of the operational systems. The “Regime Type” graphs for the second and the fifth steps are identical in the two figures. The first step operation in the 11th cycle undergoes a RT9 “Regime Type” which is an unfavourable “feast” phase operation. The appearance of RT9 can also be associated with random behaviour of the biological system more than the effect of the biomass concentration disturbance.

The same two mitigating effects of the recipe in the consecutive steps of the operation can be observed on the random behaviour systems after imposing the disturbances. The change in loading ammonia concentrations in the 10th and 25th cycles and the amount of biomass exploited from the system in the 11th and 26th cycles minimise the effect of two disturbances on the overall process.

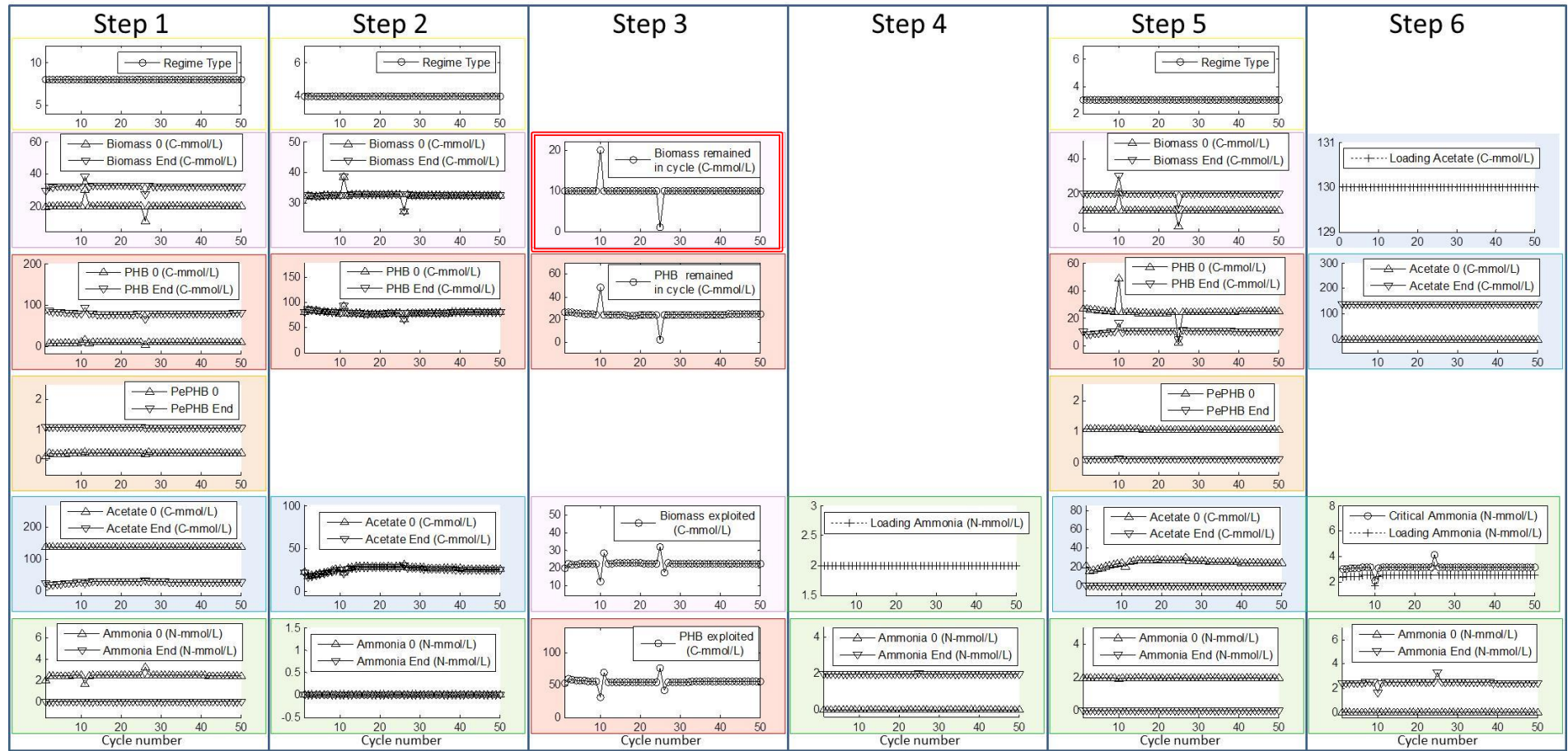


Figure 7.8 Execution of the SBR recipe with load disturbances on RF8 (deterministic behaviour process simulator)

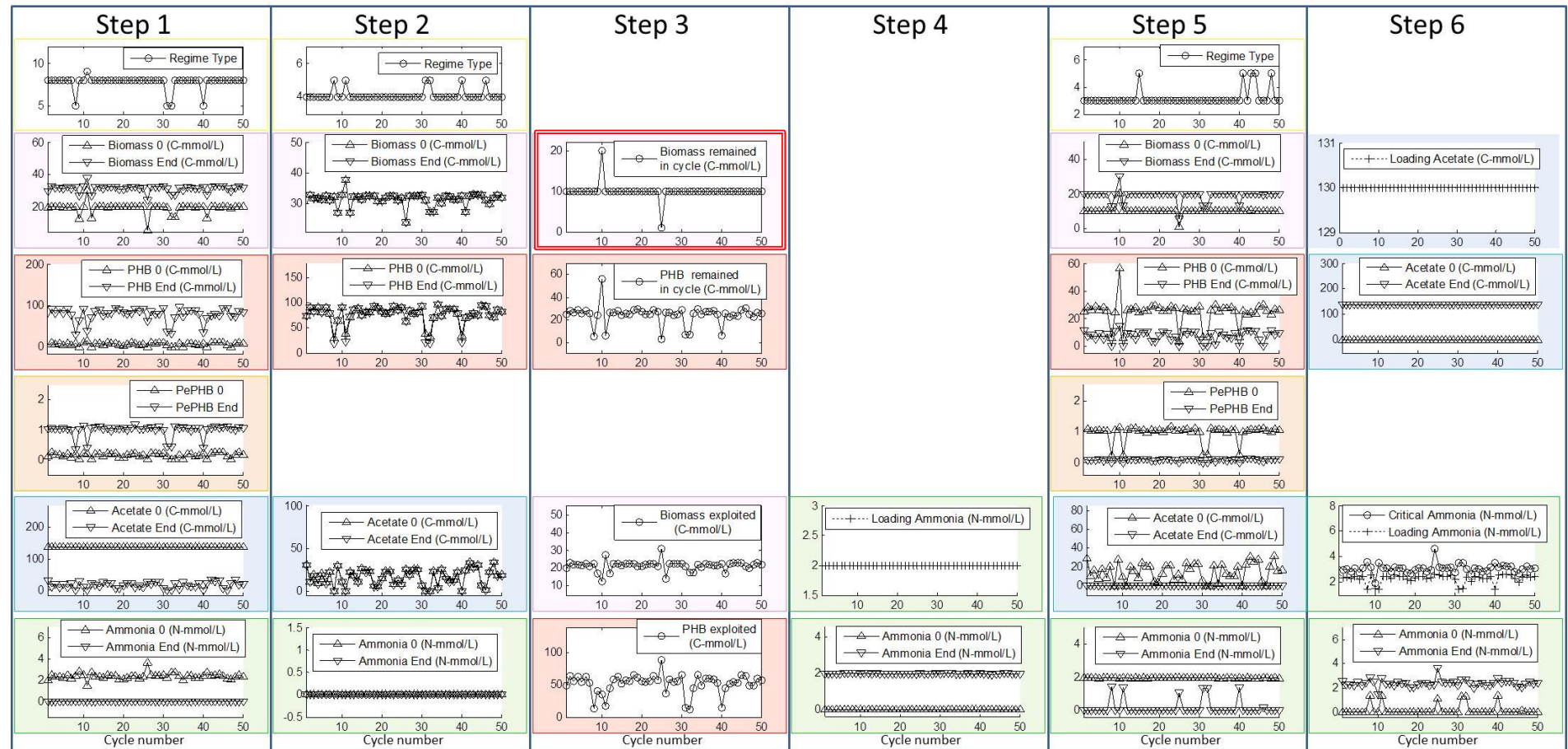


Figure 7.9 Execution of the SBR recipe with load disturbances on RF8

7.3.3 *The effect of load disturbance on the amount of ammonia introduced in the 4th step of the SBR process – RF9*

The second type of load disturbance investigated in this study is the effect of loading change on the amount of ammonia introduced to the operation in the fourth step of the process. In the simulation results shown in Figure 7.10, two load disturbances are imposed to the fourth step of the SBR process. In the 10th sequence, ammonia concentration is considered to be 4 N-mmol/L as opposed to the steady state 2 N-mmol/L. Subsequently, in comparison to the steady state conditions, more biomass is produced in the fifth step of the same sequence and less ammonia is injected to the process in the sixth step. The additional biomass is exploited in the third step of the 11th cycle in order to redirect the process into the operational pathway defined in the SBR recipe.

The second disturbance is imposed on the 25th sequence of the simulation run. In the fourth step of this cycle, no ammonia is injected to the process. Subsequently, the fifth step operation turns into a quiescence stage instead of a “famine” phase operation. The fifth step operational regime is RT4 in the 25th sequence which is not favourable. Insignificant amount of acetate is consumed during the fifth step and all is available in the sixth step. The “Phase Differentiating Equation” specifies more ammonia to be introduced into the sixth step when compared to the steady state value. This is to assure occurrence of the “feast” phase operation in the subsequent first step operation. The result of the “feast” phase operation is additional biomass production to compensate for the biomass lost in the previous fifth step operation. The additional biomass is exploited in STEP 3; however, acetate concentration remained higher than the steady state value. The additional acetate directs STEP 5 operation of the 26th cycle into a “feast” phase operation with RT8 which is not favourable. The amount of ammonia injected in the sixth step of 26th cycle remained high to reduce the effect of additional acetate in the operational system. The 27th cycle is a successful cycle with “feast” phase operation in the first step and “famine” phase operation with RT5 in the fifth step. The process retains its steady state conditions after the 27th cycle.

The simulation results in Figure 7.10 demonstrate that “famine” phase operations are missed in two cycles after negative disturbance on RF9 recipe factor. In Figure 7.11, the simulation results are shown when the same disturbances are imposed to the random behaviour process system. Since random values are the same applied in generation of

Figure 7.6, the effect of ammonia load disturbances can be observed on random behaviour process systems when Figure 7.6 is compared with Figure 7.11.

Comparison of the “Regime Type” graphs in Figure 7.6 and Figure 7.11 demonstrates that positive disturbance on the ammonia injection in STEP 4, changed the “Regime Type” of the first step in the 11th cycle from expected RT8 to unfavourable RT9. Appearance of RT9 is due to the lack of external carbon source in STEP 1 that can be associated with the lower injection of acetate in STEP 6 operation of the 10th cycle. Moreover, the randomness in the operational behaviour of the system that require more acetate for that particular operation as seen in the same operation depicted in Figure 7.9.

When negative disturbance is imposed to the 25th cycle of the operation, unlike the results obtained from the deterministic behaviour process system, the “feast” phase operation occurs in fifth step of the same sequence. The additional ammonia introduced in the sixth step of the 25th cycle returns the process into its acceptable operational pathway with “feast” phase RT8 in the first step and “famine” phase RT5 in the fifth step of the 26th cycle.

As shown in Figure 7.11, the simulation results obtained from the random behaviour process simulator demonstrate that the effect of disturbances were mitigated after one cycle of operation and therefore the SBR recipe is capable of alleviating the effect of disturbances on ammonia concentration injected in the fourth step of the SBR process.

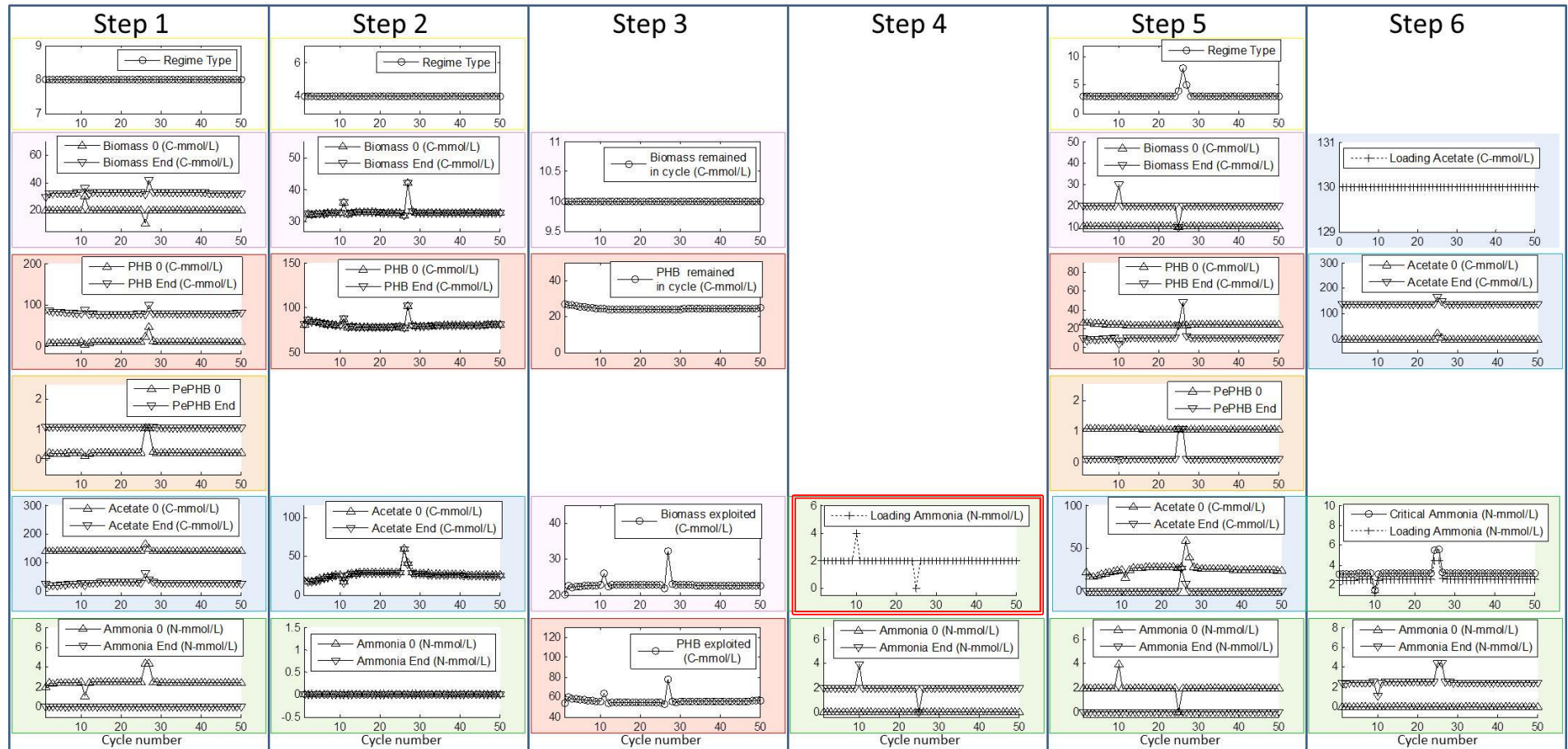


Figure 7.10 Execution of the SBR recipe with load disturbances on RF9 (deterministic behaviour process simulator)

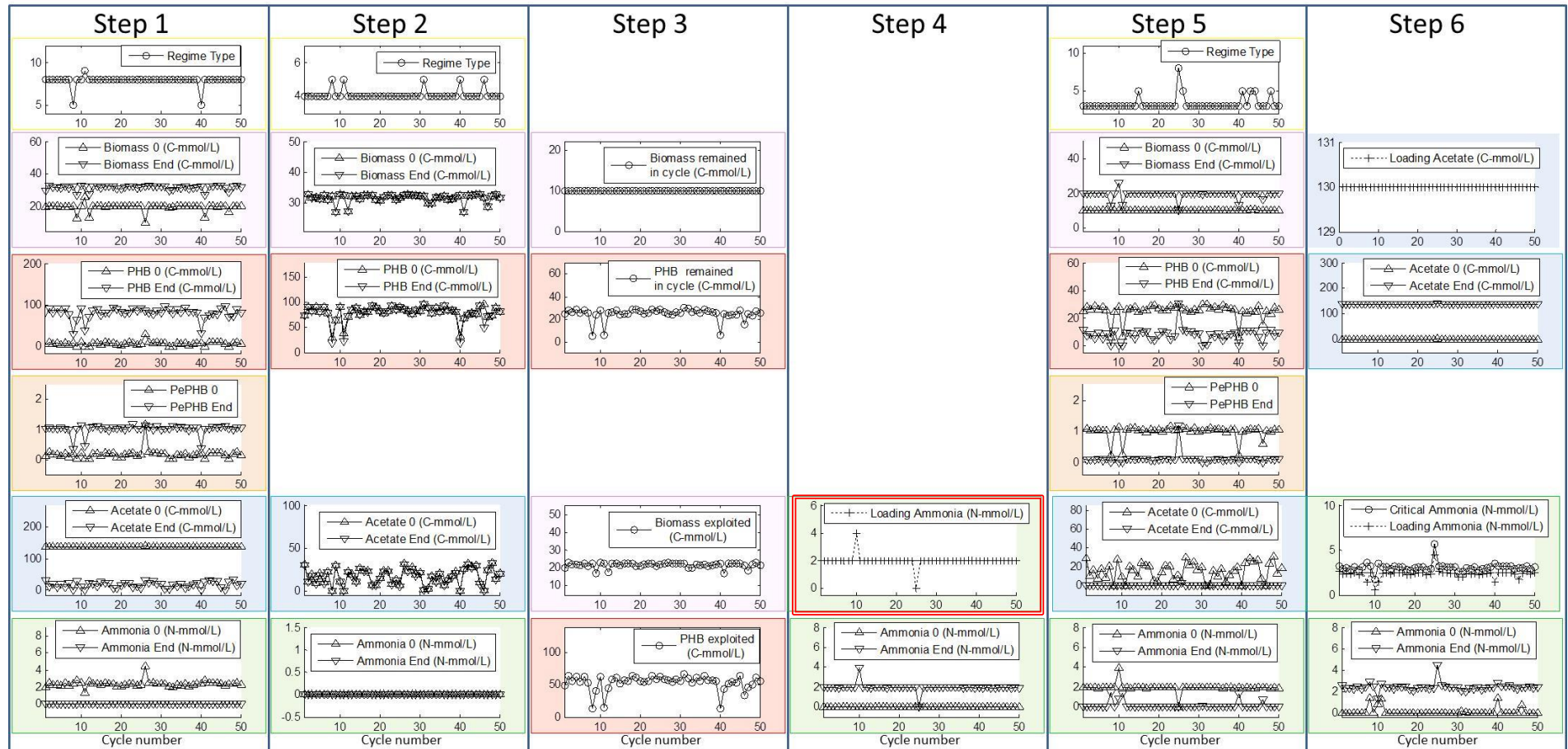


Figure 7.11 Execution of the SBR recipe with load disturbances on RF9

7.3.4 *The effect of load disturbance to the amount of acetate introduced in the 6th step of the SBR process – RF11*

In this section, load disturbance to the acetate introduced in the 6th step is considered in two cases. In the first case, critical ammonia concentration is specified based on the acetate concentration of the same sequence in which acetate disturbance occurs. In the second case, critical ammonia concentration is calculated based on the acetate value specified in the recipe. The effect of disturbance is observed in the subsequent step of operation. These two cases are considered in the next two sub-sections.

7.3.4.A Disturbance recognition as it occurs

The simulation results shown in Figure 7.12 are shown to investigate the effect of load disturbances on loading acetate concentrations in the sixth step of the deterministic behaviour SBR process. In the 10th cycle of the simulated process, loading acetate concentration is twice its steady state value and additional ammonia is injected in the same stage to mitigate the effect of the disturbance.

In the subsequent cycle, more biomass is produced in the “feast” phase operation and then exploited in the third step in order to increase the rate of acetate consumption in the process. In the fifth step of the same sequence, acetate concentration is still higher than its steady state value and RT8 “feast” phase operation occurs in place of “famine” phase operation in this stage. The ammonia loaded in the 11th cycle is higher than its steady state value in order to alleviate the effect of the additional acetate inside the operation. The subsequent “feast” phase operation initiates with high intracellular PHB content cells. The additional biomass is taken out of the operational system in the 12th cycle and the SBR returns to its steady state condition.

In order to simulate the effect of negative disturbance on the loading acetate concentration, no acetate is loaded to the sixth step of the process in the 25th cycle. The loading ammonia concentration drops significantly in comparison to the steady state conditions. Since no ammonia is available in the first step operation of the subsequent cycle and acetate concentration is insignificant, unfavourable RT3 operation occurs in place of the “feast” phase operation. The amount of biomass exploited in the third step drops significantly while cells lack intracellular PHB content. Since PHB level in the operational cells is low, “famine” phase occurrence in the fifth step has minimal operational benefits. The steady state process condition is retained with injection of acetate to the process in the sixth step of operation.

In Figure 7.13, simulation results are depicted for the random behaviour process simulator exposed to the same positive and negative disturbances on the loading acetate concentration. The effect of the disturbances on this system is similar to their effect on the deterministic behaviour process system aforementioned.

The effect of the additional acetate introduced to the system in the 10th cycle is mitigated by adding more ammonia and producing more biomass in the subsequent cycle. The majority of the additional acetate is consumed in the “feast” and therefore a successful “famine” phase operation occurs in the fifth step operation of the 11th cycle.

When no acetate is injected in the 25th cycle (in order to investigate the effect of negative disturbance on the system) ammonia loading in STEP 4 is low as directed by the “Phase Differentiating Equation” to direct the subsequent operation into a “feast” phase operation. Occurrence of the unfavourable RT5 which is a “famine” phase operation in the first step of the 26th cycle cannot be prevented. The amount of PHB product exploited from the system drops to zero in this cycle and an unnecessary “famine” phase occurs in the fifth step of this cycle. The process returns to its normal operational pathway when steady state loading acetate concentration is injected into the process in the sixth step.

Simulation results shown in Figure 7.12 and Figure 7.13 demonstrate the capability of the SBR process under the defined recipe in alleviation of the disturbances imposed on the loading acetate concentration. The “Regime Type” graphs deviate from the ideal operational regimes when disturbances occur; however, they retain the ideal regimes after one or two cycles after disturbance occurrence. Additionally, no accumulation of substances is observed during the SBR process.

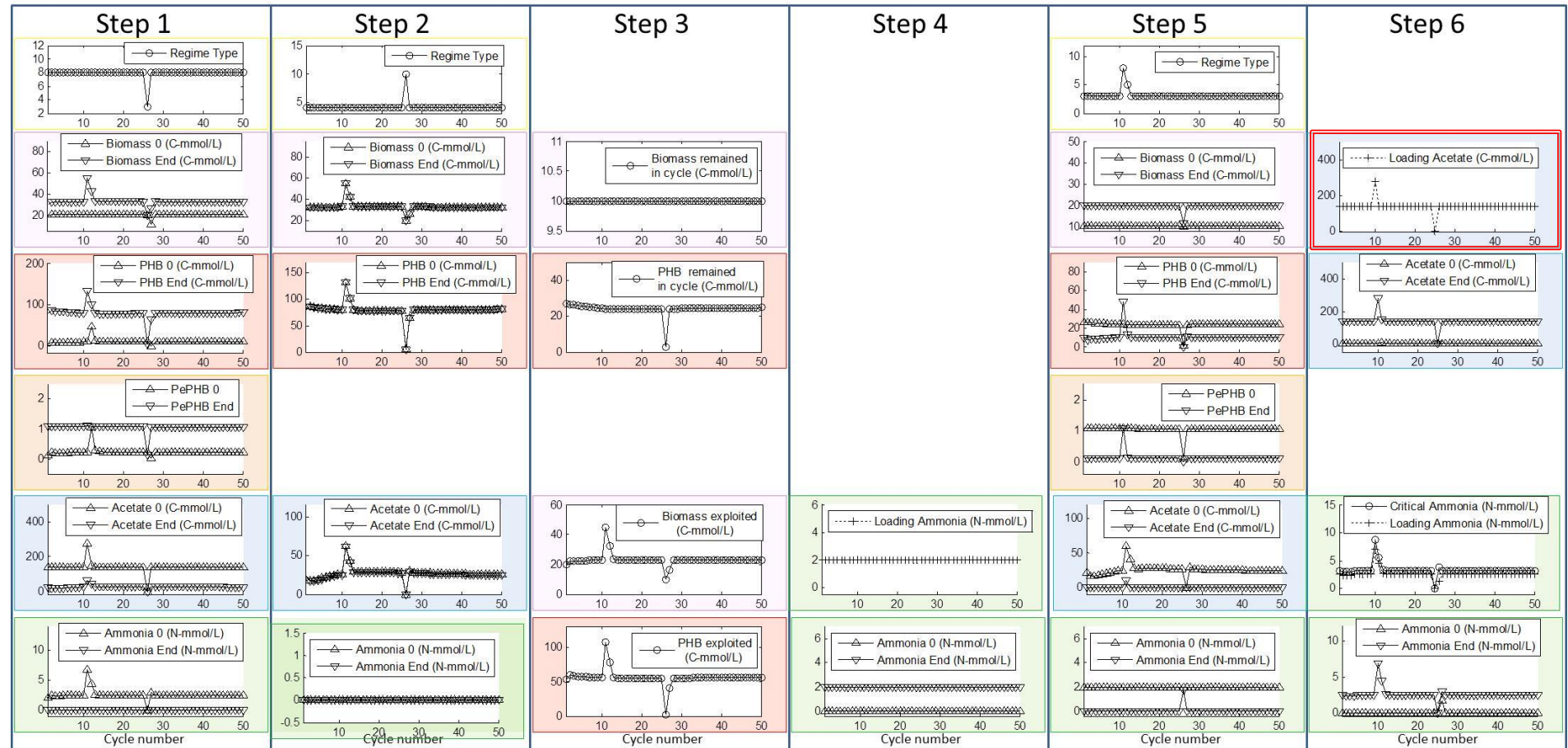


Figure 7.12 Execution of the SBR recipe with load disturbances on RF11 (deterministic behaviour process simulator)

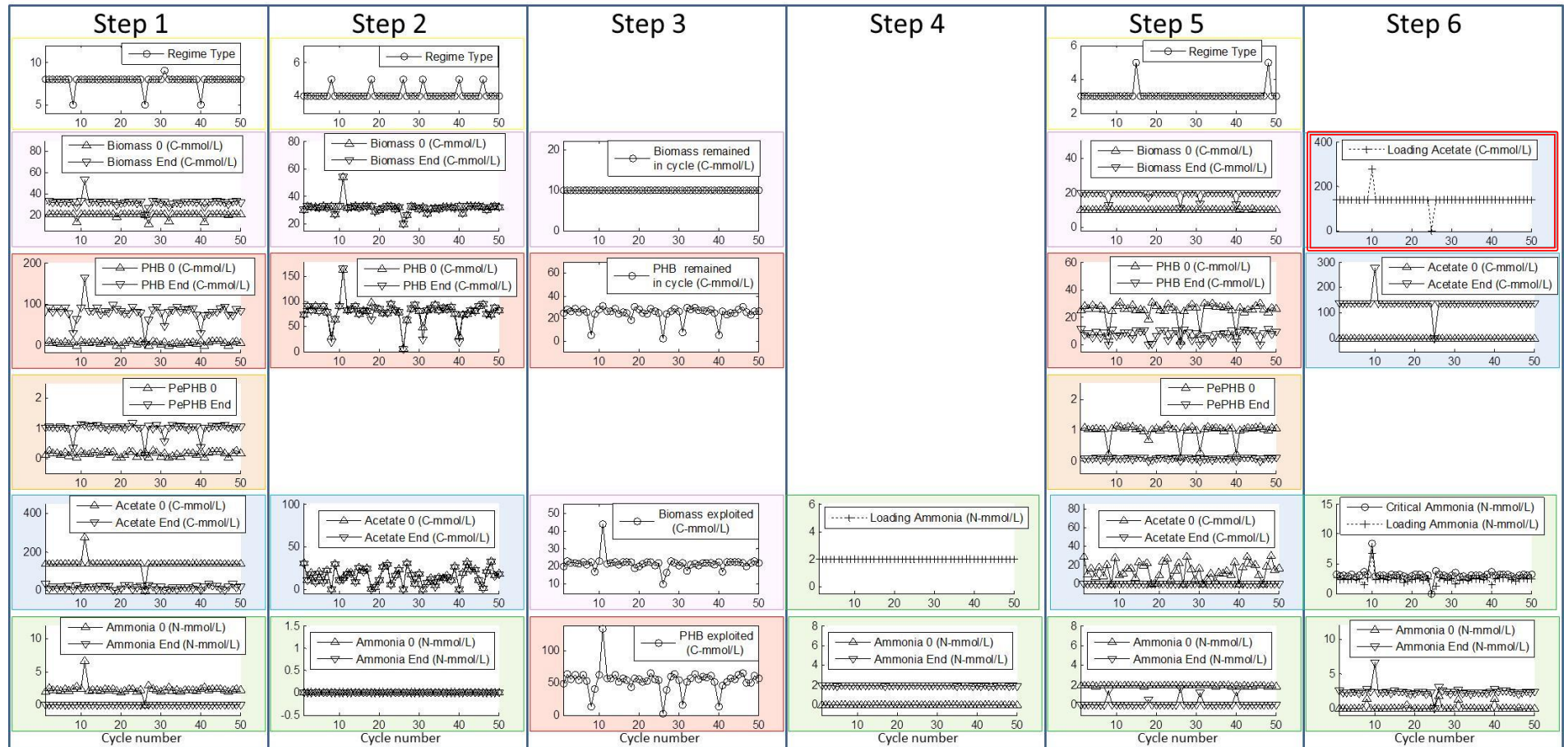


Figure 7.13 Execution of the SBR recipe with load disturbances on RF11

7.3.4.B Disturbance recognition with delay

In absence of online monitoring for acetate concentration in the operational solution, ammonia loading concentration is calculated based on the acetate concentration specified in the SBR recipe. Therefore, the acetate and ammonia concentrations injected into the operational process do not follow the specifications directed by the “Phase Differentiating Equation” in occurrence of the acetate disturbance.

In Figure 7.14, a positive disturbance is imposed on the loading acetate concentration in the 10th cycle of the deterministic behaviour simulated process. In this simulation, the loading ammonia concentration remains the same as for the steady state condition in the 10th cycle. Since ammonia concentration is the same as its steady state value, biomass and PHB production stays the same as for the steady state conditions in the first step operation of the subsequent cycle. At the end of the “feast” phase operation, high concentration of acetate is remained in the operation. The high concentration of acetate in the operation prevents “famine” phase occurrence in the fifth step of the 11th cycle. In the sixth step of the 11th cycle, additional acetate concentration is detected and more ammonia is injected to the process as specified by the “Phase Differentiating Equation”. Subsequently, more biomass is produced in the first step “feast” operations and more biomass is exploited from the process in this cycle. The remained additional acetate in the system prevents “famine” phase occurrence in the fifth step and more ammonia is injected to reduce the effect of additional acetate in the system.

For seven consecutive cycles, the “feast” phase operation is observed in both the first and the fifth steps of the process. Continuous production of PHB without PHB consumption in consecutive cycles is not desirable in a practical SBR operation. The process retains its steady state conditions when acetate concentration available in the fifth step operation returns to its steady state value.

In the case of examining the effect of negative disturbances, the loading acetate concentration is reduced to zero in the 25th cycle of the process. The ammonia augmentation concentration in the sixth step remains at its steady state value since no online measurement is presumed to be available to detect acetate shortage in the operational system. Subsequently, “famine” phase appears with RT3 “Regime Type” in the first step operation of the 26th cycle. The biomass production in this cycle is lower than the steady state condition and the exploited biomass lacks PHB content. Since less ammonia is consumed in the first step operation in this cycle, its concentration increases significantly with injection of ammonia in the fourth step of the process. The “famine”

phase occurrence in the fifth step of the 26th cycle is not significant since intracellular PHB content is low at the initial point of the operation. Assuming off-line measurement of the substrate concentration at the initial point of the sixth step operations, acetate concentration is augmented to the recipe specified value. The injected ammonia concentration in this stage is less than its steady state value since there is additional ammonia remained in the system from the unsuccessful first step operation in the 26th cycle. As shown in Figure 7.14, the SBR process retains its steady state conditions from the 27th cycle to the end of the process.

Analysis of the results shows that positive disturbance on the acetate loading concentration have more severe effect on the overall process than the negative disturbance. The effects of disturbances on loading acetate concentration using random behaviour process simulator are depicted in Figure 7.15. Comparison of the simulation results depicted in Figure 7.14 and Figure 7.15 shows that load disturbances on the acetate concentration lead to similar process behaviours in the both simulation results.

In the random behaviour simulator results, the effect of the positive disturbance alleviated in fewer cycle runs (4 against 8) when compared to its deterministic counterpart. This suggests that average acetate consumption rate for the activated cells after the positive disturbance occurrence in the random behaviour process system is higher than the consumption rate in the deterministic system. Process deviations in operational cycles that cannot be associated with the disturbances are due to randomness associated with process behaviour discussed in assessment of Figure 7.6.

As mentioned for the case of deterministic behaviour process simulator, positive loading acetate disturbance results into “famine” phase failures in the fifth step operations of consecutive cycles. On the other side, negative disturbance on acetate loading reduces biomass production of a few cycles and its effect mitigates without much disruption of the overall SBR operation.

In summary, Figure 7.15 shows that the SBR recipe is cable of managing the process in occurrence of the acetate loading disturbance. As shown, a few process cycles deviated from their pre-defined pathway in occurrence of a disturbance and then retained their productive pathway. Additionally, it is demonstrated that acetate loading disturbance does not lead to accumulation of substances in the SBR process which is favourable.

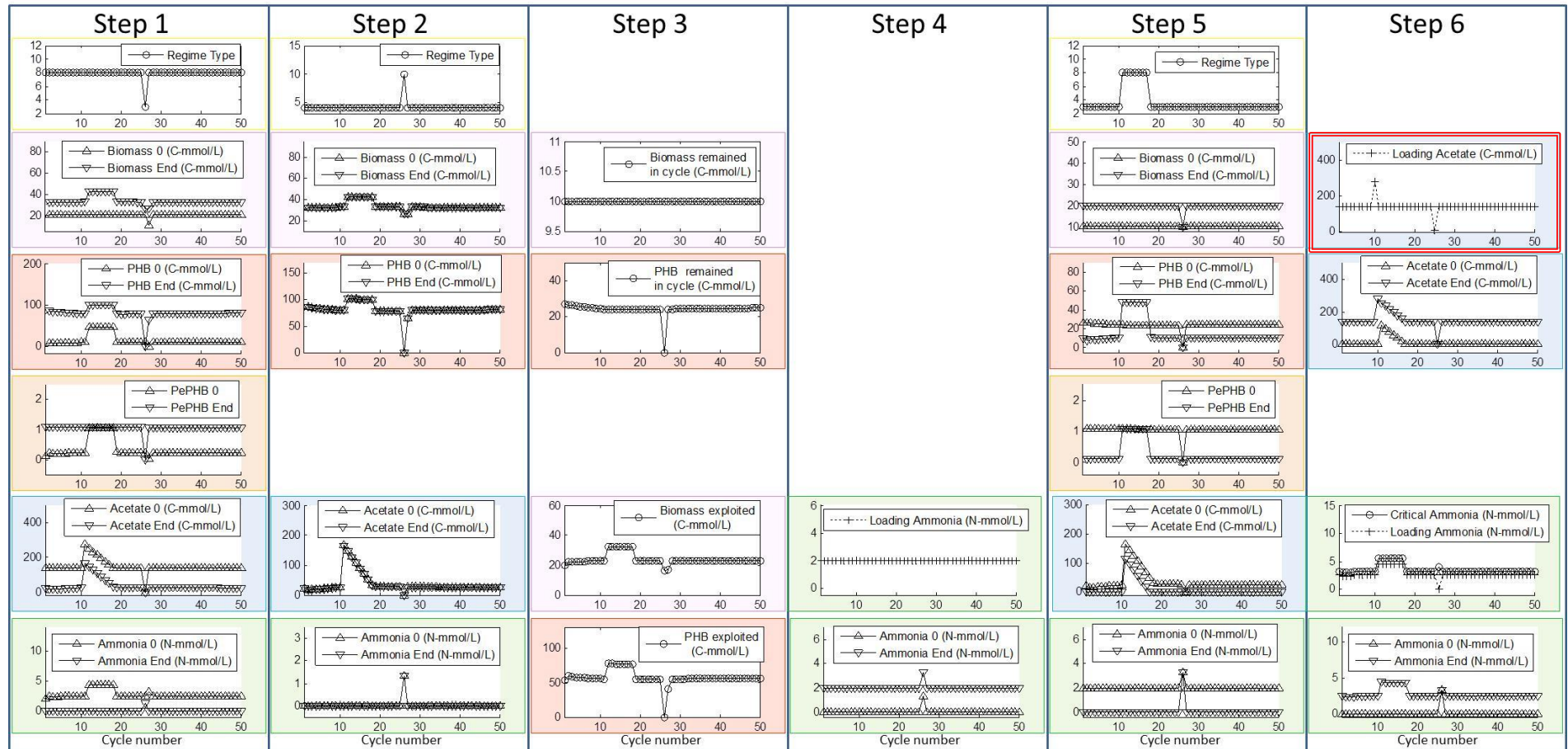


Figure 7.14 Execution of the SBR recipe with load disturbances on RF11 (deterministic behaviour process simulator)

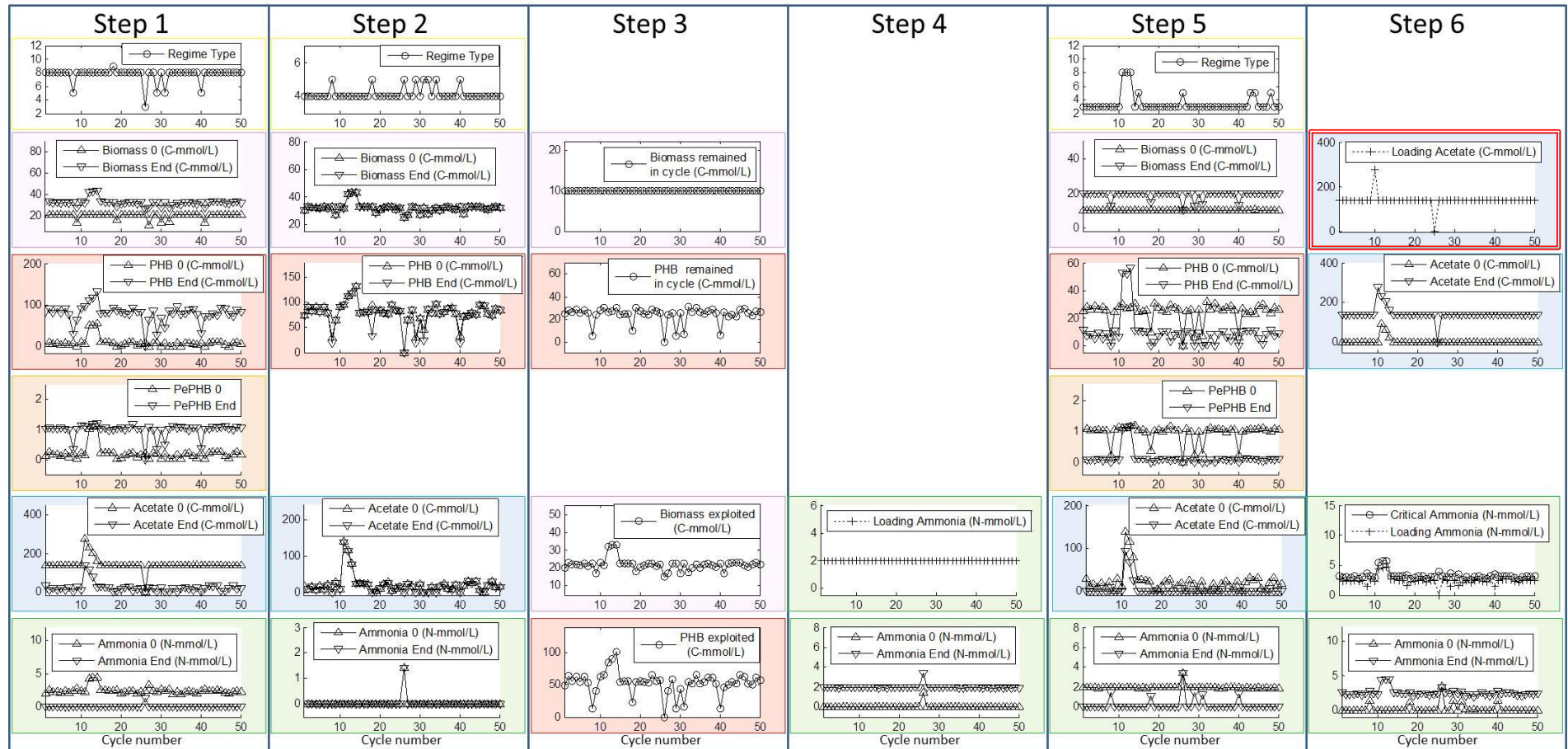


Figure 7.15 Execution of the SBR recipe with load disturbances on RF11

7.3.5 Realisation of practical SBR process execution

In simulation studies presented to this point, the concentration values assigned to the simulation program were exactly the same as they were specified in the recipe (except for the case of load disturbance cycles). In practical experiments, operational misconducts are inevitable in a course of operational SBR process. In other words, it is very difficult, if not impossible, to provide the exact amount of substances to the operational system as specified in the SBR recipe for each cycle. In this section, deviation from accurate execution of the recipe is taken to extremes in order to investigate recipe robustness despite operational abnormalities.

There are three recipe factors associated with concentration values for substances injected or exploited from the operational system. In this section, the three concentration values assigned to the simulation program are selected from three sets of random numbers normally distributed around the three values specified in the SBR recipe. These three recipe parameters are (1) the biomass concentration kept in the SBR process in the exploitation stage of STEP 3 (RF8), (2) loading ammonia concentration in the STEP 4 (RF9) and (3) loading acetate concentration in the STEP 6 (RF11). In Figure 7.16 simulation results are shown using the random behaviour process simulator to investigate process robustness in face of executional variability.

In Figure 7.16, maximum 50% deviation of the process variables is considered for the three process variables around their recipe specified values. This deviation percentage is so high that the tests can be considered as performance examination of the SBR recipe under significant level of operational misconduct. The “Regime Type” plots shown in Figure 7.16 confirm successful “feast” phase operations in 80% of the SBR process cycles. Since in the total fifty cycles of the SBR run, seven cycles failed in the first step “feast” phase operation and an additional three cycles failed in the second step quiescence operation. These failures occurred in the first or the second operational stages while “famine” phase operations successfully accomplished with RT3 and RT5 “Regime Types” in the all fifth step operations. The main source of “feast” phase failure is acetate shortage in the first step or the second step operations. Because there is no acetate injection in between the first and second step operations, if acetate depletion occurs in the first step its effect can also be detected in the immediate second step of the cycle. Therefore, occurrence of the unfavourable first step “Regime Type” is reflected in the second step “Regime Type” plot.

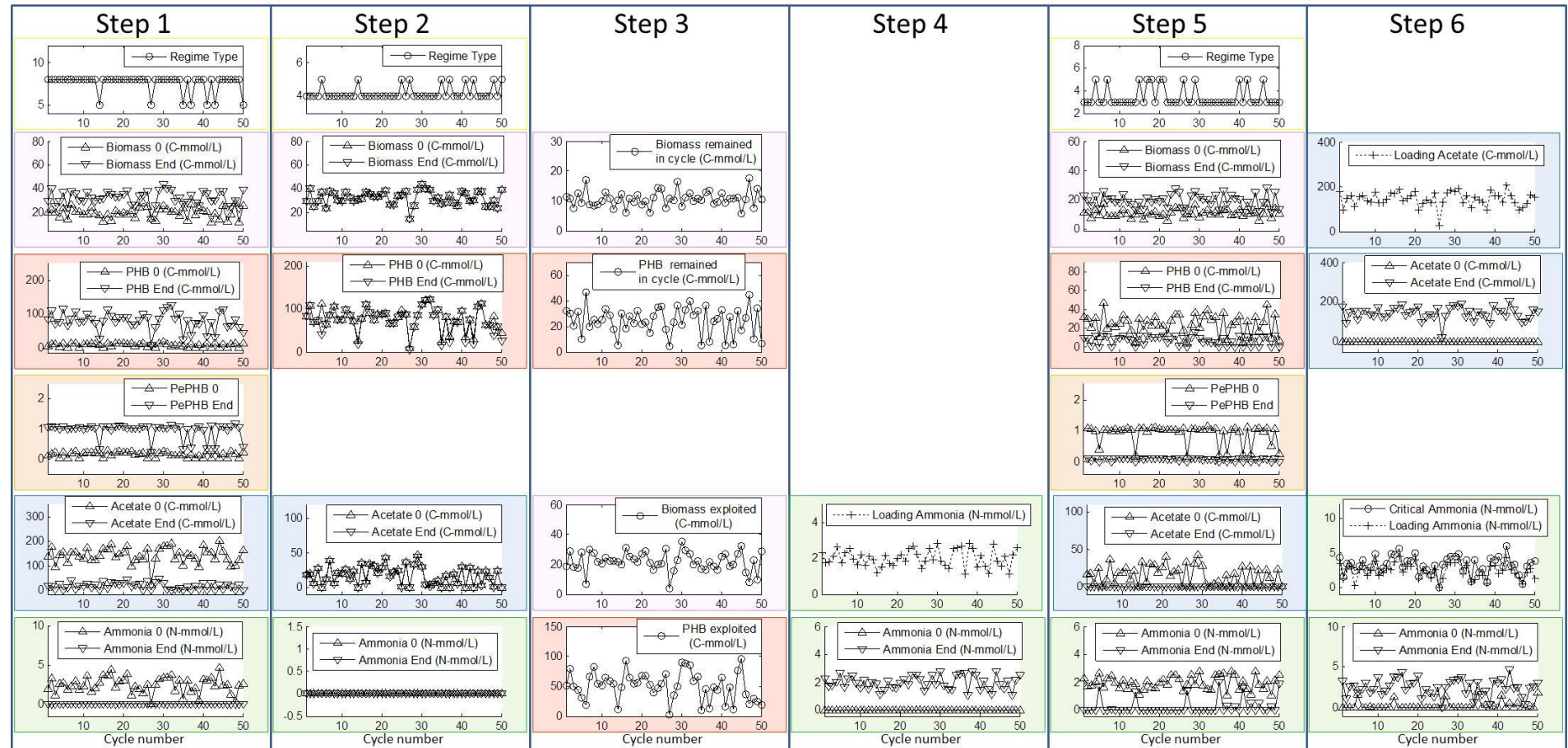


Figure 7.16 The third execution of the SBR recipe with maximum 50% deviation of RF8, RF9 and RF11 around their recipe specified values

In Figure 7.17, a histogram of total PHB concentration produced in 100 SBR runs with 50 cycles is depicted. The SBR processes were carried out under the recipe tabulated in Table 7.4 while values assigned to the RF8, RF9 and RF11 are normally distributed around the recipe specified values with maximum deviation of 50%. For each production range in Figure 7.17, the number of cycles failed to perform successfully in the second or the fifth steps of SBR sequences is recorded. On the histogram, the average number of cycles failed in the first two steps is given along with their standard deviation range. As mentioned before, process failure in the first two steps of a SBR cycle can be associated with acetate shortage in these two stage operations. In this histogram, total number of “famine” phase failures in the SBR processes ranged in a specified PHB production range is depicted as well.

Figure 7.17 shows that the less the number of failures in the first two steps of the SBR cycles, the higher the total amount of PHB production. Occurrence of acetate shortage in the first two step operations results into intracellular PHB consumption by the cells and reduction of the final PHB product.

When a “famine” phase operation fails, total PHB production augments by occurrence of a “feast” phase operation in the fifth step of the cycle. This can also be shown in Figure 7.17 where higher number of cycles with “famine” phase failure leads to higher amount of total PHB exploited from the process.

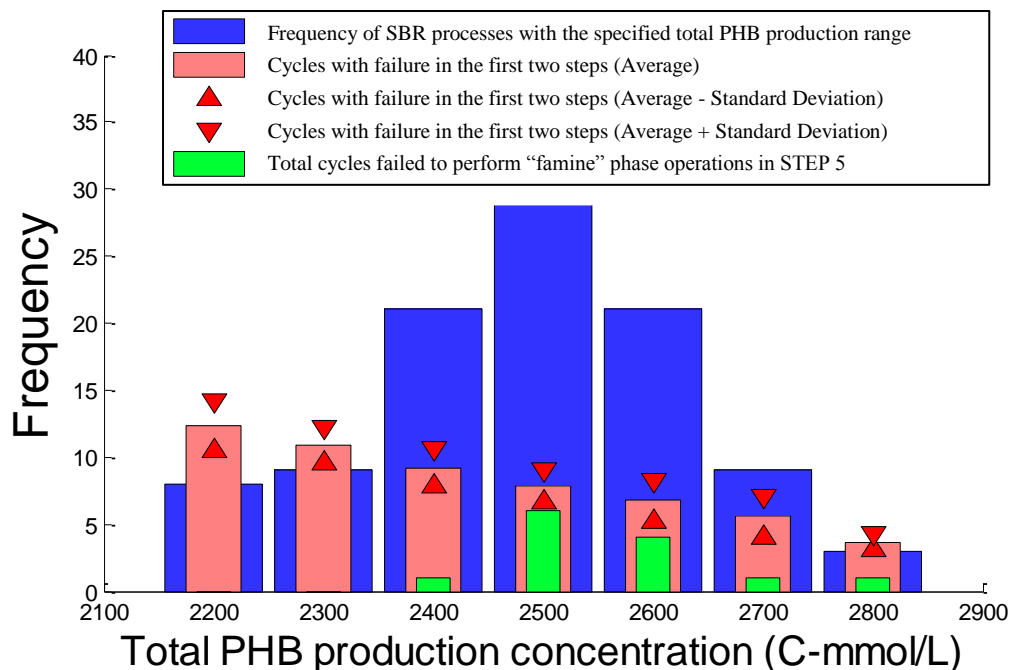


Figure 7.17 Histogram of total PHB production for 100 SBR runs under recipe given in Table 7.4 with maximum 50% deviation of RF8, RF9 and RF11

Figure 7.17 demonstrates that if the SBR recipe tabulated in Table 7.4 is executed with low level of accuracy (maximum 50% deviation from the recipe specified values for RF8, RF9 and RF11), there is about 30% chance of total PHB production in between 2450 and 2550 C-mmol/L with around 10% failures in the first two stages of the operational cycles. Additionally, it is probable to observe “famine” phase failure in operational cycles for this group of SBR processes.

Figure 7.17 also shows that the total chance of producing PHB in a range between 2350 and 2450 C-mmol/L or in between 2550 and 2650 C-mmol/L is about 40%. The high production processes with more than 2650 C-mmol/L of PHB have about 10% probability of occurrence while the chance of PHB production lower than 2350 C-mmol/L is about 20%.

This outcome will be compared with 100 SBR runs with more accurate execution of the recipe. Figure 7.18 shows similar histogram as depicted in Figure 7.17 with a difference in the simulation study to reflect level of accuracy in recipe execution. In this figure, the level of execution accuracy of the same SBR recipe is considered to be higher than the previous simulation runs (maximum 10% deviation from the recipe specified values for RF8, RF9 and RF11). As the result of high operational accuracy, the number of cycles with “famine” phase failure is less than the previous case.

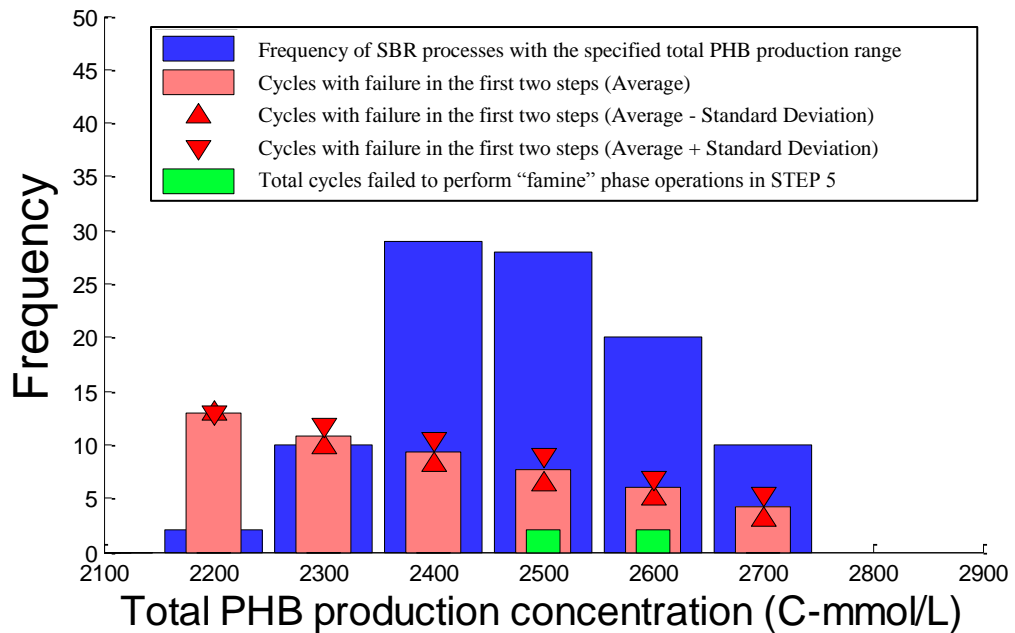


Figure 7.18 Histogram of total PHB production for 100 SBR runs under recipe given in Table 7.4 with maximum 10% deviation of RF8, RF9 and RF11

Comparison of the two figures also suggests that the possibility of PHB production with median concentration is higher when deviation from the recipe is minimised in operational execution. Total PHB production in between 2450 and 2550 C-mmol/L remained about the same in the two cases; however, total number of “famine” phase failures has decreased significantly from 7 to only 2 cycles.

The total chance of producing PHB in the range between 2350 and 2450 C-mmol/L or in between 2550 and 2650 C-mmol/L have increased from 40% to 50% while fewer cycles failed to perform “famine” phase operations. The additional 10% has been obtained from reduction of SBR run numbers with total PHB production of less than 2350 C-mmol/L due to more accurate execution of the recipe.

Simulation results confirm that proper and accurate execution of the proposed SBR recipe favours higher PHB production with fewer numbers of batches failing to perform a “famine” phase operation.

7.4 Conclusions

In this chapter, a novel method of SBR operational management was introduced for production of PHB with mixed microbial cultures. Since occurrence of both “feast” and “famine” phase operations is crucial in the majority SBR cycles for a successful and sustainable production process, the SBR architecture is designed to encompass both phases within each SBR sequence. The key element of this recipe is the implementation of the “Phase Differentiating Equation” developed in Chapter 5 which enabled process phase management to enforce occurrence of a particular phase in its specified SBR stage.

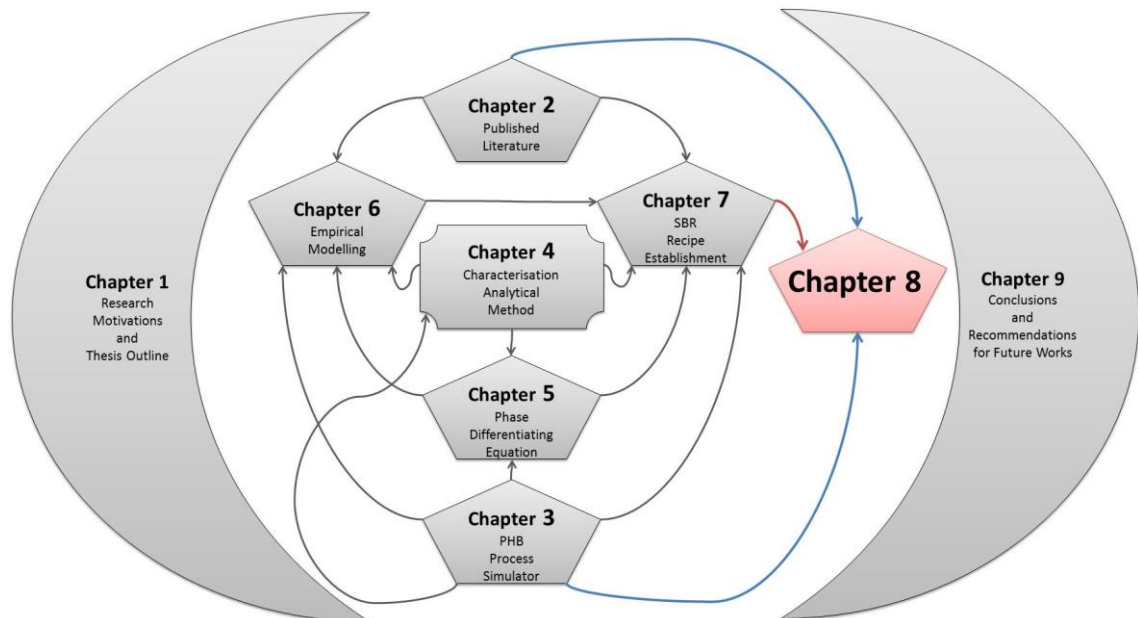
Prior to this study, the lack of a well-documented and reliable strategy for production of microbial products that required sequential operational switch between essential biological phases led to inefficient production approach for PHB production using mixed microbial cultures in the “feast” and “famine” phase alteration strategy. The analytical tool established in Chapter 4 and the mathematical equation capable of segregating the “feast” and “famine” phase operational regions (“Phase Differentiating Equation” found in Chapter 5) enabled generation of a systematic approach towards a more reliable SBR process. The proposed SBR recipe established in this chapter can potentially revolutionise mass production of PHB using the cost effective mixed microbial culture method.

The “Characterisation Method” developed in Chapter 4 proved to be a powerful tool for encapsulation of the process information into the form of meaningful “Regime Type” code numbers to evaluate operational proficiency in different stages of the SBR process. Based on the general SBR structure suggested in this chapter, operational parameters were specified using the empirical models developed in Chapter 6. The reliability of the SBR structure along with the recipe factors defined in the recipe generation procedure was examined successfully with promising outcomes. The capability of the SBR recipe structure to mitigate operational and load disturbances was investigated by imposing rigorous disturbances to the SBR process using random behaviour process simulator. Therefore, anarchic behaviour of biological systems is also reflected by the process simulator to provide a more realistic representation of the experimental process. The simulation studies demonstrate high capability of the SBR recipe structure to alleviate the effect of undesired disturbances to different process variables in the production system. As it was shown, implementation of the “Phase Differentiating Equation” developed in Chapter 5 was the most important element for process stability especially in the case of load disturbance rejection. Application of the “Phase Differentiating Equation” in the production recipe acts as a supplement that impose operational process control within the nature of the recipe in absence of advanced control algorithms.

In Chapter 8, PHB production will be optimised using Sequential Quadratic Programming algorithm for the production system that operate under the SBR recipe structure established in this chapter.

Chapter 8

Optimisation of the SBR Recipe using Sequential Quadratic Programming Algorithm for Sustainable PHB Production



8.1 Introduction

In simple words, mathematical optimisation is the selection of the best set of elements to meet a certain qualitative objective with regard to some criteria. More generally, in an optimisation problem a set of best available input values are selected from a defined domain with the aim of maximising or minimising an objective function while mathematical limitations are imposed by a set of constraints.

The complexity of the optimisation problem is escalated when more than one objective is enforced into the objective function. In the majority of the multi-objective optimisation problems, these objectives conflict and a trade-off should be made to reach an optimum conclusion. The choice of best design among the possible solutions is delegated to the decision maker by assigning the optimisation constraints and parameters.

In the last thirty years, emergence of cost effective and reliable computer machines capable of performing high speed computations increased. In the core of any capable optimisation problem solver, mathematical algorithms are implemented to find reliable solution using appropriate iterative methods. Classification of the iterative methods used to solve an optimisation problem is carried out according to the employment of Hessians, gradients or the simple function values. Sequential Quadratic Programming (SQP) is a Newton-based iterative method that evaluates Hessian of the objective function to converge to the solution of a constrained optimisation problem.

In Section 2.5.3, SQP is introduced in brief. In this chapter, this algorithm is used for optimisation of the SBR process operating on the production recipe established in Chapter 7 for sustainable PHB production using mixed microbial culture cultivation. The aim is to develop a reliable procedure for optimisation of real production plants operating under the developed SBR recipe and using empirical models built using the real process data.

8.2 Data generation for SBR optimisation purpose

The SBR recipe factors obtained in Section 7.2.5 will be used as the basis for the optimisation studies performed in this section. Since the effect of initial SBR condition on the overall PHB production is negligible, recipe parameters associated with the initial state of the SBR process are not considered in definition of the optimisation problem and remain identical to the values given in the SBR recipe.

The optimisation function will be defined to determine the optimum concentration values associated with the most effective operational elements in different steps of the SBR process. The operation variables that have significant effect on the SBR process are the biomass concentration kept in the operational system in the 3rd step of SBR cycles (RF8), ammonia augmentation concentration in every 4th step of SBR cycles (RF9), and acetate augmentation concentration in every 6th step of SBR cycles (RF11).

Variation of these three SBR variables opens a window of process operability for optimisation. With reference to Table 7.4, the random behaviour process simulator is used to generate process data for 100 SBR simulation runs with 50 cycles in each run. The SBR recipe factors RF8, RF9 and RF11 are randomly assigned between 1 C-mmol/L and 30 C-mmo/L (Figure 8.1.a), 0.2 N-mmol/L and 3 N-mmol/L (Figure 8.1.b), 10 C-mmol/L and 300 C-mmol/L (Figure 8.1.c) respectively. The simulated SBR operational data is used to develop empirical models for optimisation.

The set of 100 random values assigned to each one of the three SBR variables is shown in the three sub-plots of Figure 8.1 and is used to operate 100 SBR simulation runs. The simulation results are recorded for the process elements associated with the variables considered in definition of the objective function for optimisation. Two of the most important elements considered in optimisation of the SBR process are (1) the amount of total PHB produced in a complete SBR run and (2) the total number of SBR cycles with “famine” phase failure in the 5th step of the process.

The amount of total PHB concentration in the SBR operation can be associated with production efficiency of the process. The importance of the second optimisation element is for evaluation of process biological sustainability. Although PHB is formed only under “feast” phase, occurrence of “famine” phase is very important for the process feasibility. The cell physiological adaptation to nutrient limitation results in higher PHB formation rates once nutrition is in excess (Dias *et al.*, 2005). Therefore, occurrence of

“famine” phase operation in the majority of cycles is an essential element of a successful SBR process.

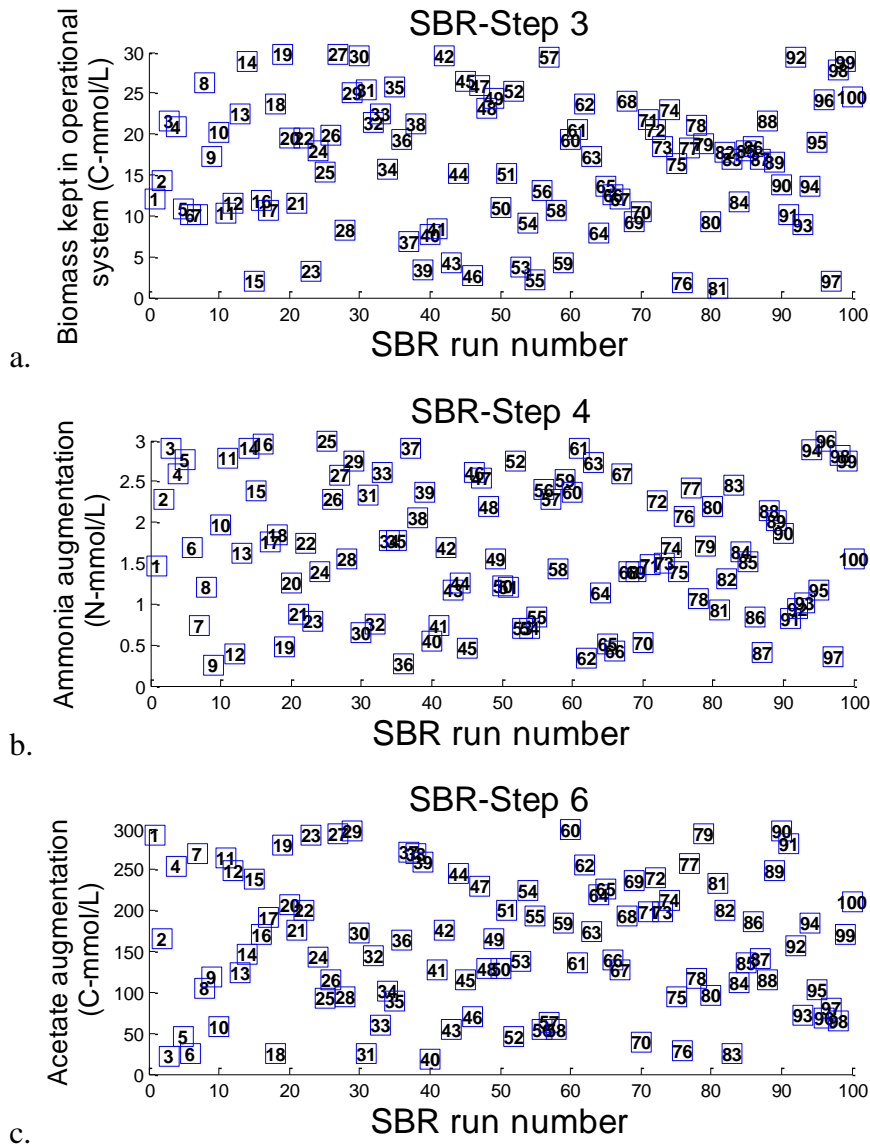


Figure 8.1 SBR variables randomly assigned for process modelling

As discussed in Chapter 7, PHB production increases when “feast” phase failure rate is minimised in the first two steps of the SBR process while “famine” phase while “famine” phase occurrence is dismissed in STEP 5. On the other side, process sustainability should be provided with occurrence of “famine” phase operation in each sequence of the SBR process to assure viable well-being of the bacteria in the operation. For this purpose, “famine” phase failure rate should be kept as minimal as possible in the 5th step of each SBR sequence. Therefore, PHB production should be obtained regarding sustainable production (viable biological well-being) with “famine” phase occurrence in each sequence of SBR process.

The total amount of PHB production and “famine” phase failed cycles are recorded for the case of 100 simulation runs conducted with the SBR recipe tabulated in Table 7.4 and the process variables given in Figure 8.1. These recorded values are shown for the total PHB product (Figure 8.2.a) and total number of cycles with “famine” phase failure in STEP 5 (Figure 8.2.b).

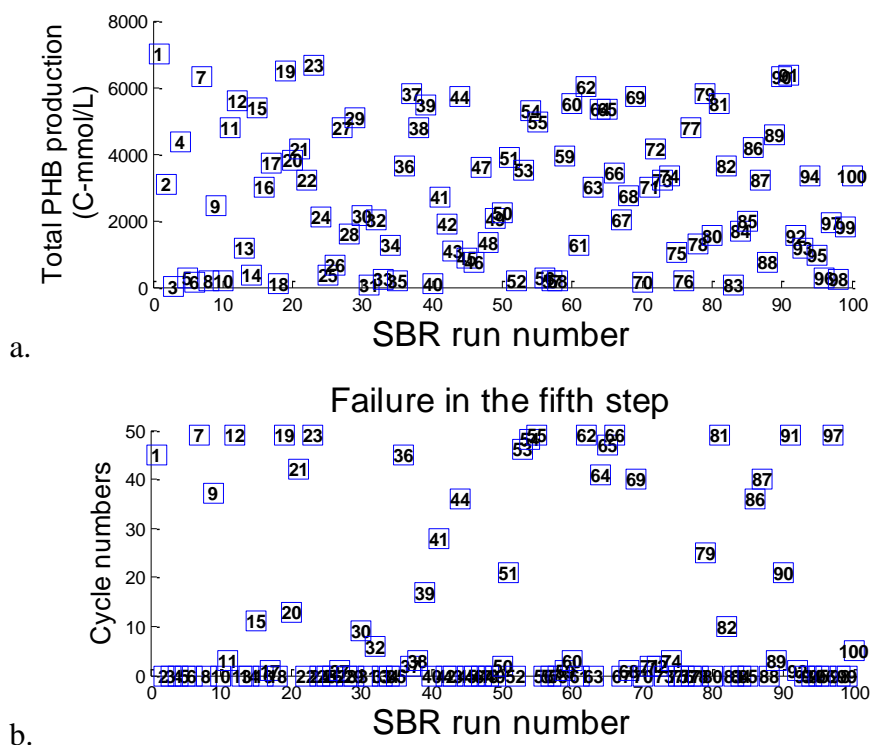


Figure 8.2 SBR process outcome for optimisation purpose

The recorded values associated with RF8, RF9 and RF11 variables used as the SBR process parameters are applied along with the simulation results obtained for the total PHB production and the number of cycles with “famine” phase failure for development of empirical models. As demonstrated in Figure 8.2.a, the total PHB production reaches to about 7,000 C-mmol/L in the SBR simulations with 50 cycles. However, with regards to Figure 8.2.b, the number of cycles in which “famine” phase failed to occur in STEP 5 is high for the SBR runs with maximum total PHB production. As mentioned, the high PHB production is not favourable when “famine” phase failure is dominant in STEP 5 since biological well-being is not maintained. Therefore, an optimisation study should be carried out to find optimal operational conditions.

The model input variables have normal distribution around their average values. Looking at Figure 8.2.a, it can be said that the total PHB production values are also scattered with an approximation of a normal distribution. However, Figure 8.2.b shows that “famine” phase failure rate is below 5 cycles in most of the simulation runs and the

distribution of data is not close to the pattern observed in the SBR process variables. Therefore, it is expected to develop more accurate models for prediction of the total PHB production concentration compared to the model predicting the total number of cycles in which “famine” phase failure occurred in STEP 5.

In the next section, empirical models will be developed. The prediction accuracy of the MLR models will be compared with non-linear ANN counterparts in the bootstrapping aggregated structure. The most accurate models will be used in optimisation algorithms to find optimal operational conditions in the subsequent sections.

8.3 Empirical model development by MLR

The MLR modelling technique explained in Section 2.6.2 is applied in this section to find the best parameters for the following 3-variable linear equation with the aim of generating the most accurate predictions for the model output. In the first case, the model output is the total PHB production amount in a SBE process. The total number of cycles with “famine” phase failure in STEP 5 is the output in the second model. The 3-variable input models have the following general formation:

$$y = \theta_0 + \theta_1 x_1 + \theta_2 x_2 + \theta_3 x_3 \quad (8.1)$$

where x_1 , x_2 and x_3 are biomass concentration kept in operational system in STEP 3, ammonia augmentation concentration in STEP 4, and acetate augmentation concentration in STEP 6 respectively. In the first and the second model, y is the total PHB production concentration and number of cycles with “famine” phase failure respectively. Eighty percent of the simulation data obtained in the previous section is scaled in between -1 and 1 to be applied in MLR model development algorithm. Applying the BLS solution using Equation (2.16) given in Section 2.6.2 the two empirical models are built and tabulated as presented in Table 8.1.

Table 8.1 MLR model parameters

$y = f(x_1, x_2, x_3)$	θ_0	θ_1	θ_2	θ_3
Model outputs				
Total PHB production	-0.187	-0.2714	-0.1027	0.9194
Cycles with “famine” phase failure in the 5th step	-0.4331	-0.4327	-0.7487	0.3965

These models are validated using the remaining 20% of the data set dismissed in the model development stage. The model prediction values are depicted along with the

scaled target simulation values for the total PHB production in Figure 8.3.a and the number of cycles failed to operate “famine” phase in STEP 5 in Figure 8.3.b.

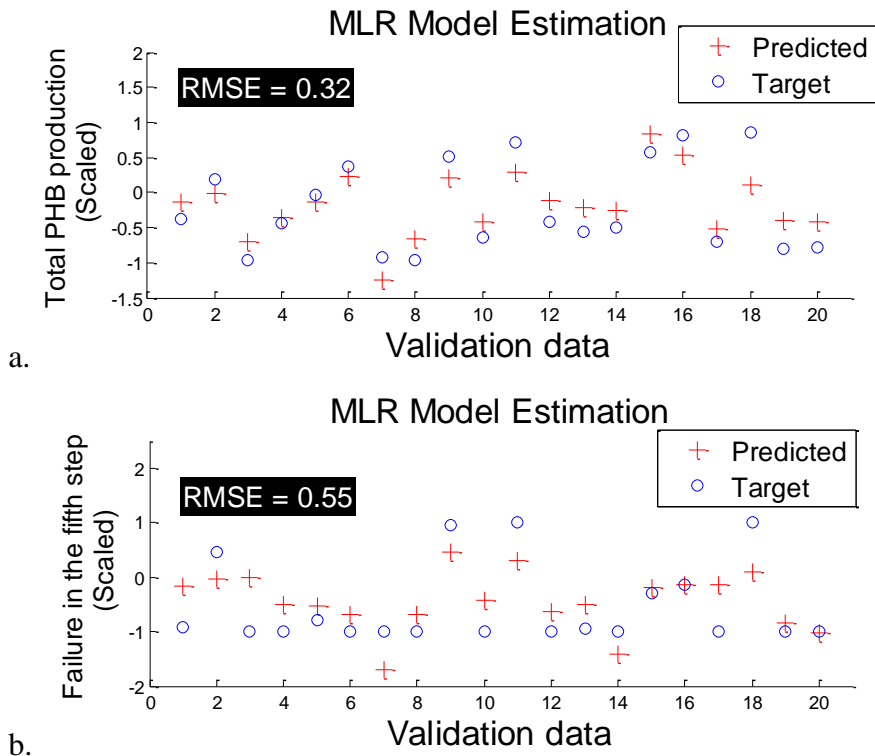


Figure 8.3 Validation of the MLR models

The RMSE values reported on the scaled validation plots determine model prediction accuracy. Validation plot depicted for total PHB production mode in Figure 8.3 shows that prediction results are not sufficiently accurate with RMSE of 0.32 for the scaled data. The performance of the MLR model predicting the total number of “famine” phase failure in STEP 5 is inferior to the first model with high RMSE value of 0.55 for scaled validation data.

As mentioned in Chapter 6, since overall data range is scaled to 2-unit magnitude, a RMSE value of 0.2 demonstrates prediction error of 10% (0.2 divided by the 2-unit magnitude) or 90% of prediction accuracy. Therefore, for model prediction accuracy of 90%, RMSE values of equal or less than 0.2 is acceptable for a scaled validation data set. Since RMSE values obtained for the two MLR models are larger than 0.2 for their scaled validation data sets, investigations are carried out to build more accurate empirical models.

In order to investigate model prediction improvement using non-linear methods, the BANN modelling technique discussed in Section 2.6.4 is applied in the next section on the same set of data obtained in this section.

8.4 Empirical model development by BANN

In this section, BANN modelling technique explained in Sections 2.6.3 and Section 2.6.4 is applied to develop non-linear models. Similar to the previous section, the first model predicts the total PHB production concentration and the second model estimates the total number of “famine” phase failure cycles in STEP 5. The same set of data used for model development in the previous section is used for training and testing the BANN models. These models are validated using the same set of validation data used in the MLR model validation stage.

For each BANN model, twenty individual neural network models are selected based on their optimal number of hidden neuron numbers. As mentioned in Section 2.6.3, the optimal number of hidden neurons is selected based on the minimum SSE value found on the “test” data set for each arrangement of the model developing data set from the original training data.

As demonstrated in Chapter 6, aggregation of twenty selected models provides a non-linear model with more reliable prediction capability. In Figure 8.4.a and Figure 8.4.c, the optimal numbers of hidden neurons are shown for the selected neural networks based on their minimal SSE values on “test” data set for the first and second models respectively.

The SSE values for validation data set are depicted in Figure 8.4.b and Figure 8.4.d for the first and second models respectively. As shown, the BANN models produce more reliable predictions compared to outcome variation of the individual neural networks.

In Figure 8.5.a and Figure 8.5.b, validation results are depicted for the scaled BANN model estimations and their confidence bounds versus their true target values for the two models. As shown, the non-linear BANN models for estimation of total PHB production concentration and “famine” phase failure cycles are more accurate than their MLR counterparts. The RMSE value obtained for the scaled validation data set of the first model is 0.15 which is within the acceptable range for accurate modelling since it is less than 0.2. The RMSE value calculated for the scaled validation data set of the second model is 0.28 which is unfavourable since it is higher than the 0.2 limit. However, application of the BANN modelling strategy reduced prediction error from RMSE of 0.55 for MLR model to RMSE of 0.28 for the same scaled validation data set.

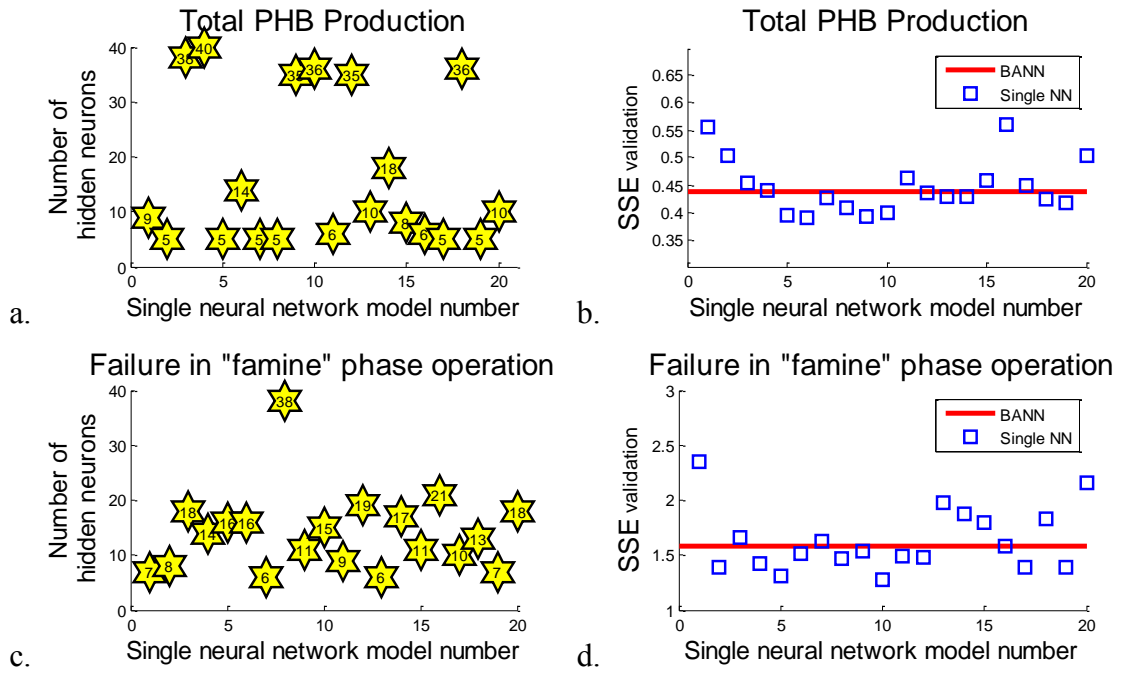


Figure 8.4 Number of hidden neurons and prediction performance of the neural network models

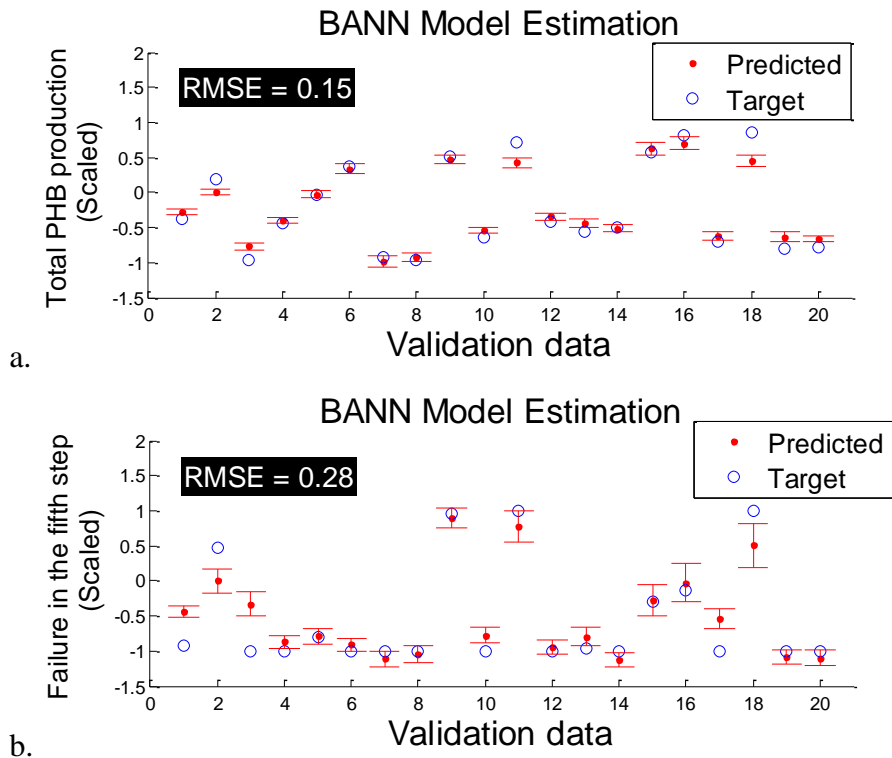


Figure 8.5 Validation of BANN models (scaled date)

Since non-linear BANN models are more accurate than their MLR counterparts, the SQP algorithm is an appropriate algorithm for optimisation of a non-linear cost

function. Application of the SQP algorithm for optimisation of the SBR recipe will be carried out in the next section.

8.5 Application of SQP for optimisation of the SBR recipe

In Section 2.5.3, Sequential Quadratic Programming (SQP) was introduced as an optimisation technique commonly used for non-linear objective functions. In this section, the optimisation tool is applied to maximise PHB production while maintaining the total number of cycles with “famine” phase failures minimum.

In this section, BANN models are implemented in the optimisation problem to provide a more reliable platform for optimal operation. Zhang (2004) made use of the BANN model structure to reduce model plant mismatch by introduction of model prediction confidence bounds as a penalty in the optimisation objective function. In an optimisation problem with embedded prediction confidence bounds, the solution is found such that the confidence bounds are forced to tighten up. This method increases reliability of the results derived from solving the optimisation problem. Therefore, in optimisation of a two variable problem, a four-variable objective function is defined as follow

$$\begin{aligned} \min_F J = & -1 \text{ [PHB]} + K_1(\text{FamineFail}) + & (8.2) \\ & K_2(\text{STDerr}_{\text{PHB}}) + K_3(\text{STDerr}_{\text{FamineFail}}) \end{aligned}$$

where standard deviation of prediction errors generated by each individual neural network forming a BANN model is implemented in the objective function. The following definition of the standard deviation of a data vector Er is applied in this study:

$$\text{STD}_{err} = \sqrt{\frac{1}{n-1} \sum_{i=1}^n (Er_i - \overline{Er})^2} \quad (8.3)$$

where (n) is the number of neural network models within a BANN model, Er is the vector of prediction error values and \overline{Er} is the average value of the Er vector. The K_1 , K_2 and K_3 parameters in Equation (8.2) are the weighting factors for the elements defined in the objective function. The optimisation weighting factor K_1 is considered for the total number of cycles with “famine” phase failures in a SBR process (FamineFail) relative to the total PHB concentration ([PHB]). In the objective function, the weighting factors K_2 and K_3 are multiplied to the standard deviations of PHB concentrations

($STDerr_{PHB}$) and the total number of cycles with “famine” phase failure ($STDerr_{FaminFail}$) obtained from single neural network models respectively and relative to the total PHB concentration ([PHB]). Since optimisation algorithm is used to find the minimum value of the objective function by tuning the three recipe variables RF8, RF9 and RF11, -1 is multiplied to the weighting factor associated with total PHB concentration term in Equation (8.2).

In order to specify weighting factors, the range of change in the elements of the objective function should be specified primarily. Different combination of scaled input values for the three recipe variables were introduced to the function and their outputs were recorded for each element. Table 8.2 tabulates the minimum and maximum values recorded for each element.

Table 8.2 Range of outputs from objective function for scaled data

Elements of objective function for optimisation	Minimum	Maximum	Difference	Ratio to minimum difference
PHB	-1.190	0.907	2.097	51.1 \approx 50
FamineFail	-1.127	1.262	2.389	58.2 \approx 60
$STDerr_{PHB}$	0.011	0.052	0.041	1
$STDerr_{FamineFail}$	0.024	0.107	0.083	2

The objective function can be altered to exhibit equivalent weighting factors. The ratio factors in Table 8.2 are obtained by dividing the range of differences to the minimum difference range (0.041 for $STDerr_{PHB}$). Using these ratios and fixing the relative importance factors by the reference of [PHB], Equation (8.2) is transformed to Equation (8.4):

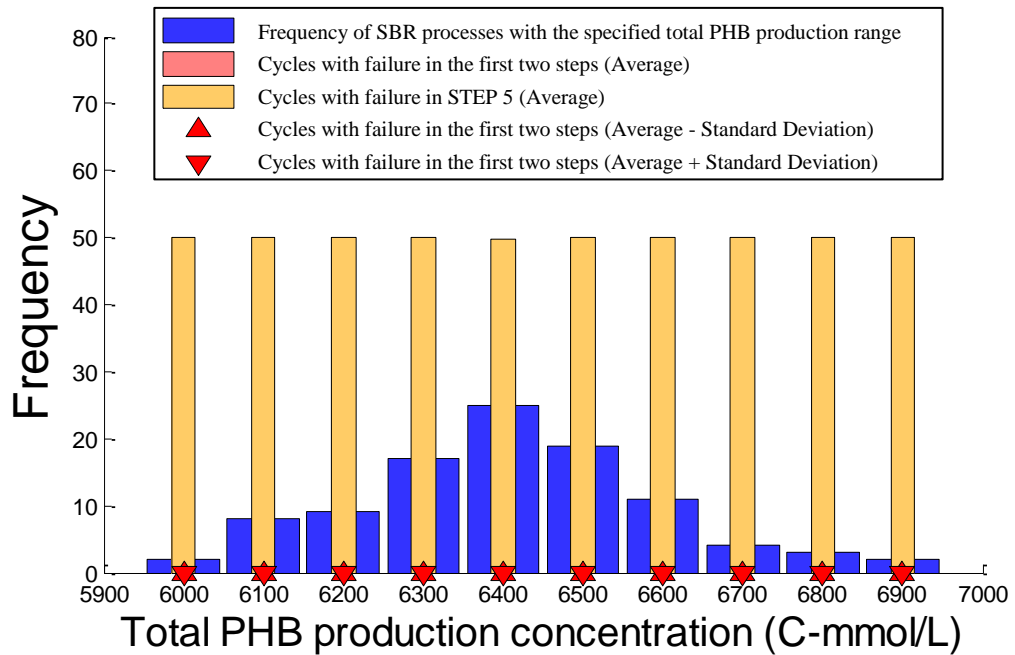
$$\min_F J = -\frac{6}{5} [PHB] + K_1(FamineFail) + 60K_2(STDerr_{PHB}) + 30K_3(STDerr_{FamineFail}) \quad (8.4)$$

Based on the K values assigned to the objective function, the three recipe factors are obtained using the SQP optimisation algorithm. Table 8.3 shows five optimisation solutions for five different combinations of weighting parameters. For each case, a histogram of 100 SBR runs using the reference recipe given in Table 7.4 and updated with optimal values for RF8, RF9 and RF11 tabulated in Table 8.3 is produced. Similar methodology applied to generate histograms in Chapter 7 is used to draw histograms for optimisation results in this section. A maximum deviation of 10% from the recipe specified value is considered in simulation studies of the optimal SBR runs with 50 sequential cycles.

Table 8.3 Optimisation results for different combinations of K values

Run No.	K_1	K_2	K_3	RF8	RF9	RF11	Plot
1	0	0	0	1	0.2	298	Figure 8.6
2	1	0	0	14	3	300	Figure 8.7
3	1	1	1	19	2.4	245	Figure 8.8
4	0.5	0.5	0.5	18	2.8	291	Figure 8.9
5	0.5	1	1	16	1.9	198	Figure 8.10

In the first optimisation solution, the aim is to maximise PHB production regardless of “famine” phase failures ($K_1=0$) or reduction of prediction error between the BANN and their actual results ($K_2=0$, $K_3=0$). The optimisation solution proposed RF8, RF9 and RF11 values of 1, 0.2 and 298 respectively. The histogram generated by the designed SBR recipe is depicted in Figure 8.6.

**Figure 8.6 Histogram of 100 SBR runs for the first run tabulated in Table 8.3**

As shown in Figure 8.6, total PHB production is considerably high with majority of SBR runs producing PHB in a range between 6,200 C-mmol/L and 6,600 C-mmol/L. The high production is obtained at the expense of high “famine” phase failure rate. Absence of “famine” phase occurrence in STEP 5 of each cycle and its replacement with “feast” operations increase PHB production in the simulation. However, as mentioned earlier in this chapter with refer to Dias *et al.* (2005), occurrence of a “famine” phase operation is essential once a “feast” phase operation takes place in a sequential production mode. Therefore, although the optimal recipe defined in the first optimisation solution looks tempting in simulation, in reality it is not practical.

With the aim of reducing failure in the STEP 5 operations, the weighting parameter associated with “famine” phase failure (K_1) is increased to 1 in the second optimisation problem. The solution of the second optimisation problem is used to generate Figure 8.7. This figure demonstrates that average number of cycles with “famine” phase failure decreases from about 50 to less than 5 cycles. The reduction of “famine” phase failure rate increases process sustainability by augmentation of bacterial adaptation. Comparing Figure 8.6 and Figure 8.7 demonstrates PHB production reduction from the 6,000-6,900 range to about 5,200-6,300 range in C-mmo/L. Low “famine” phase failure rate was obtained at expense of less PHB production with higher “feast” phase failure rate.

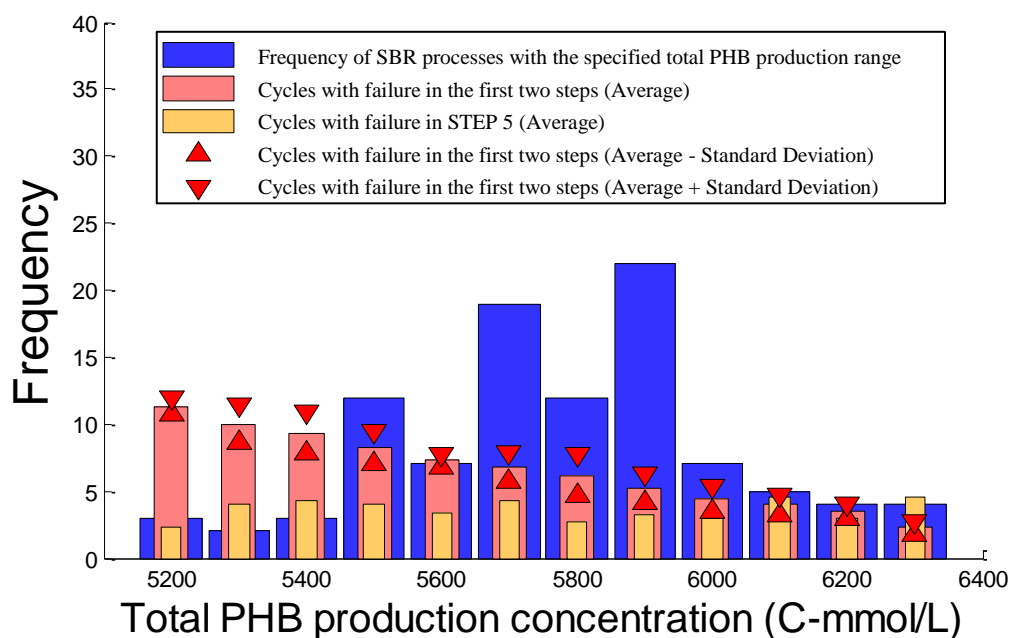


Figure 8.7 Histogram of 100 SBR runs for the second run tabulated in Table 8.3

In the third optimisation problem, weighing parameters associated with the standard deviation of model errors (K_2 and K_3) are increased to the unit value. Figure 8.8 shows that the majority of SBR productions appear in the middle of the bell shape histogram demonstrating less process variation in the simulation studies. In other words, SBR process is directed towards operational regions where model accuracy is higher regarding both PHB production and “famine” phase factors.

Comparing Figure 8.8 with Figure 8.6 and Figure 8.7 demonstrates PHB production in a range higher than the range depicted in Figure 8.7 and lower than the range shown in Figure 8.6 while “famine” phase failure rate remains high. Low process variation was obtained at the expense of lower PHB production in comparison to the first optimisation solution.

In the fourth optimisation solution, PHB production has the highest weighting parameter and the other three parameters share the same weightings of half the highest parameter ($K_1=0.5$, $K_2=0.5$ and $K_3=0.5$). This combination is selected to maximise PHB production while low rate of “famine” phase failure and model mismatch is maintained. Generating a histogram with 100 SBR runs operated with the optimal recipe values shows that high PHB production is achievable while “famine” phase failure rate is kept low. Moreover, the majority of SBR runs appear in the middle of the histogram to demonstrate low level of model mismatch as depicted in Figure 8.9.

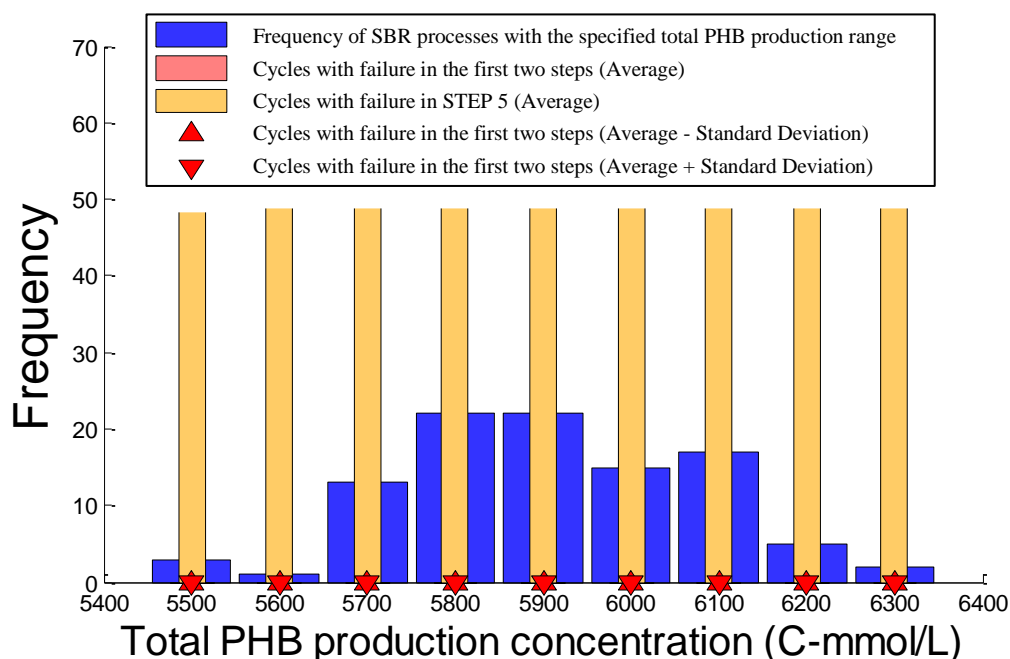


Figure 8.8 Histogram of 100 SBR runs for the third run tabulated in Table 8.3

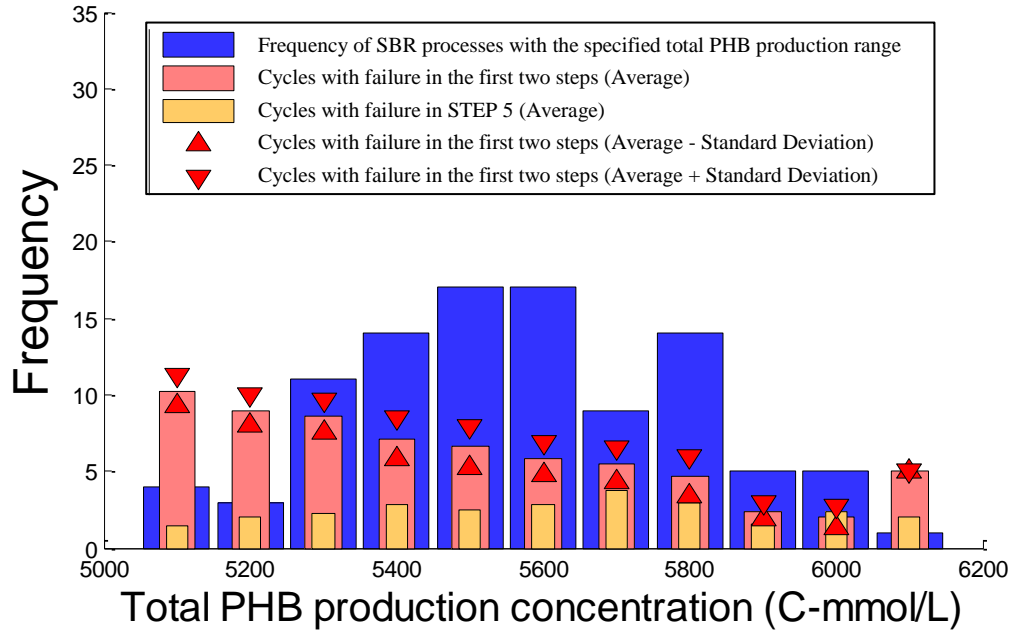


Figure 8.9 Histogram of 100 SBR runs for the fourth run tabulated in Table 8.3

In the last optimisation problem, weighting parameters associated with the standard deviation terms of the objective function are increased to the same magnitude of the PHB production term. Consequently, model prediction mismatch decreases with the cost of reducing total PHB production range as depicted in Figure 8.10.

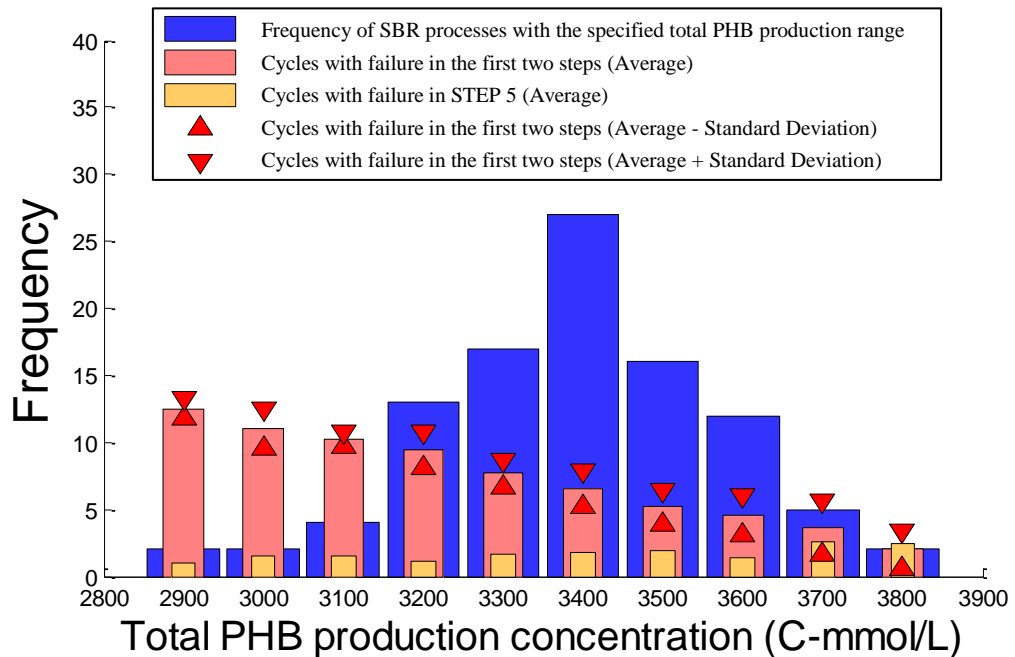


Figure 8.10 Histogram of 100 SBR runs for the fifth run tabulated in Table 8.3

8.6 Conclusions

The two SBR process elements associated with PHB production in cultivation of mixed microbial cultures were defined in this chapter. These two elements were modelled with three operational variables associated with the amount of substances injected/exploited into/from the process during execution of an SBR operating under the recipe established in Chapter 7. It was shown that the BANN technique was able to provide more accurate and reliable prediction results in comparison to the single structured NN models and the non-linear MLR models.

The BANN models were applied in an optimisation problem with an objective function defined to consider the model prediction confidence bounds as penalty. It was also shown that Sequential Quadratic Programming is a powerful tool in optimisation of problems with non-linear behaviour.

The recipe parameters were optimised to address maximum PHB production while “famine” phase failure rate was kept at its minimum and model-process mismatch is forced to minimise. Different optimisation scenarios led to the conclusion that low rate “famine” phase failure can be achieved in price of mitigating PHB production rate. Additionally, implementation of mathematical terms in the objective function with the aim of reducing model-process mismatch can be beneficial if optimisation weighting factors are assigned wisely. Optimisation weightings with rigorous focus on reduction of model-process mismatch leads to SBR operations with unacceptable PHB production rate and consequent loss of resources.

The investigations carried out in this chapter confirmed credibility of the BANN modelling and SQP optimisation algorithm to define SBR recipes that govern optimal SBR processes.

Chapter 9

Conclusions and Recommendations for Future Works

9.1 Conclusions

The initial motivation of the research work was to build empirical models predicting PHB batch operation critical process attributes for optimisation studies and generation of production recipes. Failure to provide empirical models predicting PHB concentration at the end of the production batch in the first attempts led to the conclusion that sophisticated process understanding is required.

It was shown that application of analytical methods to obtain operational enhancement for complex behaviour systems such as the PHB batch production is essential adjunct to the experimental techniques. In this research work, an analytical tool was successfully developed and applied to generate superior process understanding using a computer-based process simulator. PHB production process investigated in this study exhibits complex biological behaviour that requires a sophisticated analytical method to classify its operational routine. Classification of the operational pathways enabled accurate modelling of the process critical attributes when empirical models were trained on classified process data.

It was demonstrated that the acetate and ammonia batch profiles have dominant effects on the total PHB concentration profile. Mathematical algorithms were successfully developed with the aim of generating meaningful code values describing most significant occurrences in the process profiles. The code values were implemented to generate graphics that visualised operational progression with regards to feeding concentrations and operational duration. Observation of the operational graphics led to the following conclusions for PHB batch process using Mixed Microbial Cultures:

- Application of the process feeding profiles including carbon and nitrogen sources can perform process classification
- There are three different operational pathways considering variations of feeding concentrations
- Two operational pathways lead to “famine” phase operations while the third pathway performs a “feast” phase operation.

- In order to perform a more efficient “famine” phase operation, the operational pathway with initial acetate depletion is more favourable than the other “famine” phase operation pathway with initial ammonia depletion.
- For “feast” phase operation occurrence, initial ammonia depletion is followed by acetate stability in the final stage of the operation.
- In the case of “feast” phase operation pathway, there is a window of optimal operational termination period. A “feast” phase operation can fail if batch operation is conducted for a prolonged period leading to acetate exhaustion and PHB lost.
- The “feast” and “famine” phase operational areas can be segregated by a linear border.
- The mathematical equations using initial acetate, ammonia, biomass and PHB concentrations can estimate the linear border differentiating the “feast” and “famine” phase areas. The predictions are reliable even if mathematical terms associated with randomness in biological behaviour of the simulated process are accentuated.
- Process classification enables process data classification for target modelling of process critical attributes

The “Phase Differentiating Equation” proved to be a useful tool for segregation of the process data into two sub-sets of “feast” and “famine” phase data. Target modelling for process data on each sub-set provided more reliable models which could not be obtained without data segregation. The outcomes of the modelling investigations are:

- more accurate prediction is obtained using non-linear models (BANN) when compared to their linear counterparts (MLR) due to nonlinearity associated with biological behaviour of the PHB production operation.
- more reliable models are developed by aggregating neural networks models using bootstrapping method compared to single structured neural networks.
- optimal number of neurons in the hidden layer of a neural network varies for initial training parameters. The high number of hidden neurons does not guarantee a more accurate model.
- generation of a number of models to be aggregated can be applied in calculation of prediction variance. A factor of standard deviation of the prediction error can be used to demonstrate estimation confidence bounds.

- in a number of occasions, models with fewer input variables can provide more accurate predictions and additional input variables prevent sophisticated model training process.
- in “feast” phase operations, empirical models can provide acceptable predictions for final biomass and PHB concentrations using initial biomass and ammonia concentration values.
- in “famine” phase operations, final biomass concentration is best modelled with initial biomass and ammonia concentrations while final PHB concentration is best modelled with initial PHB and acetate concentration values.
- segregation of “famine” phase process data into the two sub-sets of “famine” phase operational pathway is not recommended since model predictions for final biomass and PHB concentrations do not improve significantly by data segregation.

In Chapter 7, Sequential Batch Reactor (SBR) approach which is a common method of bacterial cultivation using Mixed Microbial Culture (MMC) was implemented to develop a production recipe structure. The key element of innovation in the SBR recipe is application of the “Phase Differentiating Equation” to direct the process into either of the “feast” or “famine” phase operation to ensure occurrence of the both phases within each process sequence/cycle. Along with the general recipe structure, a procedure for appropriate assignment of the recipe parameter values was introduced using empirical models developed in this study. A series of simulated test runs were carried out on the SBR process to confirm capability of the generated recipe for disturbance mitigation and performing a robust and reliable. The simulation results demonstrated promising operational outcome using the production recipe proposed in this study. Further investigations should be carried out using real process experiments. The analytical method developed in Chapter 4 proved to be a powerful tool for encapsulation of the process information into the form of meaningful code numbers.

At the end, the SBR process was modelled for optimisation purposes. Two elements of the process associated with successful occurrence of “feast” and “famine” operations within each SBR sequence were quantified and modelled using MLR, ANN and BANN techniques. Since BANN models proved to be more reliable and accurate, they were implemented in Sequential Quadratic Programming optimisation algorithm. The objective function was defined such that the model prediction confidence bounds were considered as penalty. It was shown the optimisation algorithm was capable of

providing sound results if appropriate weight factors in the objective function were assigned based on good knowledge about the PHB production process using MMC.

Using the optimal values, a series of SBR operation runs were performed to generate histograms presenting the overall recipe performance based on the quantitative attributes to the successful “feast” and “famine” phase operations. It was shown that implementation of the model prediction confidence bounds as penalty factors in the objective function of the optimisation problem can increase accuracy of the prediction estimations in price of reducing volumetric production of the PHB product. In the other words, distribution of the production concentration around the average value is narrow when penalty factor is capitalised. However this distribution is wider around a smaller average value when this factor is paralysed.

In the next section, application of Principal Component Analysis (PCA) along with the characterisation method developed in Chapter 4 will be discussed for classification of operational regimen of batch processes with different operational profile.

9.2 Recommendation for future works

9.2.1 Application of PCA in the “Characterisation Method”

The “Characterisation Method” developed in Chapter 4 can also be applied on different simulation processes with similar operational specifications in order to provide valuable analytical results. Application of this method enables formation of illustrations that relate process elements of high significance (usually the process production amount) to the most dominant process variables.

In the case of the PHB production process, the two feeding concentrations were considered as the process variables and total PHB product was the operational output. However, more than two dominant variables can be identified to affect the process output in a process. In that case, Principal Component Analysis (PCA) can be used to summarise information within a large set of original variables into a new set of variables with few number of components.

PCA is a well-known mathematical technique in multivariate analysis. Like many other multivariate methods, application of PCA gained attention with the advent of electronic computers and has effectively entrenched in virtually every statistical computer package. Reduction of data dimensionality is the central idea of this technique when interrelated variables form the major body of the process information. Dimensionality

reduction is achieved by transforming correlated process data variables to a new set of uncorrelated variables, the principal components (PCs). Different mathematical methods have been introduced in literatures to perform PCA analysis on a set of data. In general, principal components are generated so that the first few PCs can present most of the variations present in the original data. Therefore, computation of eigenvalues and eigenvectors can be found in the core of almost of the PCA development techniques. Jolliffe (2005) has mentioned history, development procedures and application of PCA in detail. In brief, the following procedure is known to generate principal components of a number of variables.

1. Data should be scaled and mean centred in respect to each variable
2. The covariance of the data matrix is calculated
3. The eigenvectors and eigenvalues are obtained for the covariance matrix
4. Eigenvector associated with the highest eigenvalue is PC1, the second highest eigenvalue presents PC2 and the other PCs are followed as such.

If a set of data with many variables lies close to a two-dimensional subspace, this data can be plotted with respect to these two dimensions with much more visual clarity. In this case, PCA provides a representation of data to enable best fitting of each observation to the first two PCs and thus drawing a two-dimensional plot of the data. The question of whether or not two PCs are adequate to present most of the variation in the data depends on the amount of variation they can capture. The cumulative percentage of total variation obtained from the eigenvalues is the most obvious criterion in identification of the amount of variation captured by selected number of PCs.

The biplot of PC1 versus PC2 provides valuable graphical information about the relationship between variables of the process provided that these two PCs can capture most of the data variance. In the case of “Characterisation Method” analysis, each PC is treated as an individual process variable and should be considered as such in the analysis. The validity of the “Characterisation Method” explained in this study highly depends on the amount of total variation captured by the first two PCs.

The PC profiles are scrutinised along with the main product profile or any other profile that contributes to the critical quality attributes of the process. Depending on the type and nature of the process being simulated, different occurrences gain attention in the profile analysis. A combination of mathematical and logical algorithms coded in adjunct to the simulation program enables detection of the critical process attributes. For a

specific simulated process, a precise algorithm is required to be developed and be tuned to detect important process occurrences. The outcome of the profile analysis step will be used to generate “Code Values”. These “Code Values” would be used to generate code vectors similar to the description given in Chapter 4.

A code vector consists of code values that enable qualitative interpretation of the process profiles. In fact, a set of identical code values can provide a rapport between the process profiles that present similar qualitative characteristics. This property of identical code vectors builds up the foundation of the “Characterisation Method” in order to find clusters of process profiles with the same qualitative descriptions.

Similar to the procedure explained in Chapter 4, a bank of code vectors is formed by the code vectors that appear in process simulations for different combinations of process variables. In this context, PC1 and PC2 that capture most of the process variations are used as the process variables to enable process screening in different process conditions. With proper classification of the code vectors, foundation for characterisation plot generation is obtained. A characterisation plot can provide a general insight to the process behaviour regarding the two PCs effacing the process. Visualisation of the process qualitative behaviour can potentially lead to obtaining valuable information about the process and can open a window to improve process monitoring and control.

9.2.2 Realisation of the simulated research work

This research study was performed to provide a tool for classification of PHB production process using MMC in simulations. Application of the “Phase Differentiating Equation” developed based on simulation studies should be validated on real batch operations as the final step of confirmation.

The empirical modelling methods applied in this study demonstrated high performance of non-linear methods in comparison to the linear techniques for the simulated process data. It is also expected to observe better estimation capability of the non-linear models than the linear counterparts when using real batch process data. Biological batch processes are known to be highly non-linear and the supremacy of non-linear modelling techniques for PHB batch operation should also be confirmed by real operational data.

The “Phase Differentiating Equation” obtained from the simulation studies should be coupled with the empirical models developed using real PHB batch operation data to assign appropriate recipe factors in the SBR recipe structure established in this study. SBR execution for a real process under the proposed recipe structure is the final stage of

the recipe validation procedure. Execution of the SBR process with variation of the recipe factors can provide an operability window for SBR optimisation. Using the modelling techniques and optimisation algorithm discussed in this study, the SBR process can be optimised as defined by the objective function.

References

- ACCINELLI, C., SACCÀ, M. L., MENCARELLI, M. & VICARI, A. (2012) Deterioration of bioplastic carrier bags in the environment and assessment of a new recycling alternative. *Chemosphere*, 89, 136-143.
- ACUÑA, J. M., BIELECKA, A., HÄUSSLER, S., SCHOBERT, M., JAHN, M., WITTMANN, C., JAHN, D. & POBLETE-CASTRO, I. (2014) Production of medium chain length polyhydroxyalkanoate in metabolic flux optimized *Pseudomonas putida*. *Microbial cell factories*, 13, 88.
- ALBUQUERQUE, M. D. G. E. (2009) *Production of polyhydroxyalkanoates (PHA) from sugar cane molasses by Mixed Microbial Cultures*. PhD, Universidade de Lisboa.
- ALBUQUERQUE, M. G. E., EIROA, M., TORRES, C., NUNES, B. R. & REIS, M. A. M. (2007) Strategies for the development of a side stream process for polyhydroxyalkanoate (PHA) production from sugar cane molasses. *Journal of biotechnology*, 130, 411-421.
- ANDERSON, A. J. & DAWES, E. A. (1990) Occurrence, metabolism, metabolic role, and industrial uses of bacterial polyhydroxyalkanoates. *Microbiological reviews*, 54, 450-472.
- ANIS, S. N. S., MD IQBAL, N., KUMAR, S. & AMIRUL, A.-A. (2013) Effect of different recovery strategies of P (3HB-co-3HHx) copolymer from *Cupriavidus necator* recombinant harboring the PHA synthase of *Chromobacterium* sp. USM2. *Separation and Purification Technology*, 102, 111-117.
- ANIS, S. N. S., NURHEZREEN, M. I., SUDESH, K. & AMIRUL, A. A. (2012) Enhanced recovery and purification of P (3HB-co-3HHx) from recombinant *Cupriavidus necator* using alkaline digestion method. *Applied biochemistry and biotechnology*, 167, 524-535.
- AVELLA, M. & MARTUSCELLI, E. (1988) Poly-d-(3-hydroxybutyrate)/poly (ethylene oxide) blends: phase diagram, thermal and crystallization behaviour. *Polymer*, 29, 1731-1737.
- BAFGHI, M. K. & FAZAEIPOOR, M. H. (2012) Application of rhamnolipid in the formulation of a detergent. *Journal of Surfactants and Detergents*, 15, 679-684.
- BANERJEE, A., CHATTERJEE, K. & MADRAS, G. (2014) Enzymatic degradation of polymers: a brief review. *Materials Science and Technology*, 30, 567-573.
- BARNES, D.K.A., GALGANI, F., THOMPSON, R.C. & BARLAZ, M. (2009) Accumulation and fragmentation of plastic debris in global environment. *Philosophical Transactions of the Royal Society B: Biological Sciences*, 364(1526), pp. 11985-1998
- BARHAM, P. J., KELLER, A., OTUN, E. L. & HOLMES, P. A. (1984) Crystallization and morphology of a bacterial thermoplastic: poly-3-hydroxybutyrate. *Journal of Materials Science*, 19, 2781-2794.

- BEREKAA, M. M. & AL THAWADI, A. M. (2012) Biosynthesis of polyhydroxybutyrate (PHB) biopolymer by *Bacillus megaterium* SW1-2: Application of Box-Behnken design for optimization of process parameters. *African Journal of Microbiology Research*, 6, 2101-2108.
- BERNARD, M. (2014) Industrial Potential of Polyhydroxyalkanoate Bioplastic: A Brief Review. *USURJ: University of Saskatchewan Undergraduate Research Journal*, 1.
- BEUN, J.J., DIRCKS, K., VAN LOOSDRECHT, M.C.M. & HEIJNEN, J.J. (2002) poly- β -hydroxybutyrate metabolism in dynamically fed mixed microbial cultures, *Water Research*, 36(5), pp. 1167-1180
- BEUN, J. J., PALETTA, F., VAN LOOSDRECHT, M. C. & HEIJNEN, J. J. (2000) Stoichiometry and kinetics of poly- β -hydroxybutyrate metabolism in aerobic, slow growing, activated sludge cultures. *Biotechnology and Bioengineering*, 67, 379-389.
- BIBY, G. D. (2013) *Degradable Polymers* [Online]. Available: <http://www.icma.com/info/polymers.htm> [Accessed July 11 2013].
- BIRD, A. (2004) Thomas Kuhn.
- BOON, N., DEFOIRDT, T., DE WINDT, W., VAN DE WIELE, T. & VERSTRAETE, W. (2013) Hydroxybutyrate and poly-hydroxybutyrate as components of animal feed or feed additives. Google Patents.
- BRANDRUP, J., IMMERGUT, E. H., GRULKE, E. A., ABE, A. & BLOCH, D. R. (1999) *Polymer handbook*, Wiley New York.
- BYROM, D. (1987) Polymer synthesis by microorganisms: technology and economics. *Trends in Biotechnology*, 5, 246-250.
- CARRIGLIO, M., CLARICH, A., RUSSO, R., NOBILE, E. & RANUT, P. (2014) modeFRONTIER for Virtual Design and Optimization of Compact Heat Exchangers. SAE Technical Paper.
- CARTA, F., BEUN, J. J., VAN LOOSDRECHT, M. C. M. & HEIJNEN, J. J. (2001) Simultaneous storage and degradation of PHB and glycogen in activated sludge cultures. *Water research*, 35, 2693-2701.
- CARUCCI, A., DIONISI, D., MAJONE, M., ROLLE, E. & SMURRA, P. (2001) Aerobic storage by activated sludge on real wastewater, *Water Research*, 35(16), pp. 3833-3844
- CHEN, D., CHEN, Y., OUYANG, X., ZUO, J. & YE, X. (2014) Influence of MicroPCMs on thermal and dynamic mechanical properties of a biodegradable P3HB4HB composite. *Composites Part B: Engineering*, 56, 245-248.
- CHEN, G.-Q. (2009) A microbial polyhydroxyalkanoates (PHA) based bio-and materials industry. *Chemical Society Reviews*, 38, 2434-2446.
- CHEN, G.-Q. (2010) Industrial production of PHA. *Plastics from Bacteria*. Springer.

- CHEN, G., ZHANG, G., PARK, S. & LEE, S. (2001) Industrial scale production of poly (3-hydroxybutyrate-co-3-hydroxyhexanoate). *Applied Microbiology and Biotechnology*, 57, 50-55.
- CHEN, J. & DAVIS, S. S. (2002) The release of diazepam from poly (hydroxybutyrate-hydroxyvalerate) microspheres. *Journal of microencapsulation*, 19, 191-201.
- CHEN, W. & TONG, Y. W. (2012) PHBV microspheres as neural tissue engineering scaffold support neuronal cell growth and axon–dendrite polarization. *Acta biomaterialia*, 8, 540-548.
- CLINT, J. H. (1975) Micellization of mixed nonionic surface active agents. *Journal of the Chemical Society, Faraday Transactions 1: Physical Chemistry in Condensed Phases*, 71, 1327-1334.
- CRANK, M. & PATEL, M. (2005) Techno-economic feasibility of large scale production of Bio-based polymers in Europe. *European commission joint research centre*
- DAWES, E. A. & SENIOR, P. J. (1973) The role and regulation of energy reserve polymers in micro-organisms. *Advances in microbial physiology*, 10, 135-266.
- DEDKOVA, E. N. & BLATTER, L. A. (2014) Role of β -hydroxybutyrate, its polymer poly- β -hydroxybutyrate and inorganic polyphosphate in mammalian health and disease. *Name: Frontiers in Physiology*, 5, 260.
- DEMIRBAS, A. (2008) The importance of bioethanol and biodiesel from biomass. *Energy Sources, Part B*, 3, 177-185.
- DI VENTURA, B., LEMERLE, C., MICHALODIMITRAKIS, K. & SERRANO, L. (2006) From in vivo to in silico biology and back. *Nature*, 443, 527-533.
- DIAS, J.M.L. (2008) Metabolic Modelling and Optimisation of Polyhydroxyalkanoates Production by Mixed Microbial Cultures. PhD of Chemical Engineering, Universidade Nova de Lisboa
- DIAS, J.M.L., LEMOS, P.C., SERAFIM, L.S., OLIVEIRA, C., EIROA, M., ALBUQUERQUE, M.G.E., RAMOS, A.M., OLIVEIRA, R. & REIS, M.A.M. (2006) Recent advances in polyhydroxyalkanoate production by mixed aerobic cultures: from the substrate to the final product, *Macromolecular bioscience*, 6(11), pp. 885-906.
- DIAS, J. M. L., SERAFIM, L. S., LEMOS, P. C., REIS, M. A. M. & OLIVEIRA, R. (2005) Mathematical modelling of a mixed culture cultivation process for the production of polyhydroxybutyrate. *Biotechnology and Bioengineering*, 92, 209-222.
- DIONISI, D., BECCARI, M., DI GREGORIO, S., MAJONE, M., PAPINI, M. P. & VALLINI, G. (2005) Storage of biodegradable polymers by an enriched microbial community in a sequencing batch reactor operated at high organic load rate. *Journal of Chemical Technology and Biotechnology*, 80, 1306-1318.

- DIONISI, D., MAJONE, M., PAPA, V. & BECCARI, M. (2004) Biodegradable polymers from organic acids by using activated sludge enriched by aerobic periodic feeding. *Biotechnology and Bioengineering*, 85, 569-579.
- DIRCKS, K., HENZE, M., VAN LOOSDRECHT, M., MOSBÆK, H. & ASPEGREN, H. (2001) Storage and degradation of poly- β -hydroxybutyrate in activated sludge under aerobic conditions. *Water research*, 35, 2277-2285.
- DOI, Y. (1990) Microbial polyesters. *VCH Publishers*.
- EDGAR, T. F., HIMMELBLAU, D. M. & LASDON, L. S. (2001) Optimization of Chemical Processes. 2001. McGraw Hill, New York.
- ESCAPA, I. F., GARCÍA, J. L., BÜHLER, B., BLANK, L. M. & PRIETO, M. A. (2012) The polyhydroxyalkanoate metabolism controls carbon and energy spillage in *Pseudomonas putida*. *Environmental microbiology*, 14, 1049-1063.
- EUROPEAN-BIOPLASTICS. (2013) *European Science and technology observatory*, EUR 22103 EN. Available: <http://en.european-bioplastics.org/> [Accessed June 5 2014].
- FABRA, M. J., BUSOLO, M. A., LOPEZ-RUBIO, A. & LAGARON, J. M. (2013a) Nanostructured bilayers in food packaging. *Trends in Food Science & Technology*, 31, 79-87.
- FABRA, M. J., LOPEZ-RUBIO, A. & LAGARON, J. M. (2013b) High barrier polyhydroxyalkanoate food packaging film by means of nanostructured electrospun interlayers of zein. *Food Hydrocolloids*, 32, 106-114.
- FABRA, M. J., LÓPEZ-RUBIO, A. & LAGARON, J. M. (2014) On the use of different hydrocolloids as electrospun adhesive interlayers to enhance the barrier properties of polyhydroxyalkanoates of interest in fully renewable food packaging concepts. *Food Hydrocolloids*, 39, 77-84.
- FIEBACH, K. & GRIMM, D. (2000) Resins, Natural. *Ullmann's Encyclopedia of Industrial Chemistry*. Wiley-VCH Verlag GmbH & Co. KGaA.
- FURRER, P., PANKE, S. & ZINN, M. (2007) Efficient recovery of low endotoxin medium-chain-length poly ([R]-3-hydroxyalkanoate) from bacterial biomass. *Journal of microbiological methods*, 69, 206-213.
- GHARAEI-FATHABAD, E. (2011) Biosurfactants in pharmaceutical industry: A mini-review. *American Journal of Drug Discovery and Development*, 1, 58-69.
- GILL, P. E., MURRAY, W. & SAUNDERS, M. A. (2002) SNOPT: An SQP algorithm for large-scale constrained optimization. *SIAM journal on optimization*, 12, 979-1006.
- GOH, L.-K., PURAMA, R. K. & SUDESH, K. (2014) Enhancement of Stress Tolerance in the Polyhydroxyalkanoate Producers without Mobilization of the Accumulated Granules. *Applied biochemistry and biotechnology*, 172, 1585-1598.

- GREDES, T., GEDRANGE, T., HINÜBER, C., GELINSKY, M. & KUNERT-KEIL, C. (2014) Histological and molecular-biological analyses of poly (3-hydroxybutyrate)(PHB) patches for enhancement of bone regeneration. *Annals of Anatomy-Anatomischer Anzeiger*.
- GRÖTSCHHEL, M. & MATHEMATIKER-VEREINIGUNG, D. (2012) *Optimization Stories*, Dt. Mathematiker-Vereinigung.
- GUJER, W., HENZE, M., MINO, T. & LOOSDRECHT, M. V. (1999) Activated sludge model no. 3. *Water Science and Technology*, 39, 183-193.
- GURIEFF, N. (2007) Production of biodegradable polyhydroxyalkanoate polymers using advanced biological wastewater treatment process technology.
- HACKING, I. (1983) *Representing and intervening: Introductory topics in the philosophy of natural science*, Cambridge Univ Press.
- HANKERMAYER, C. R. & TJEERDEMA, R. S. (1999) Polyhydroxybutyrate: plastic made and degraded by microorganisms. *Reviews of environmental contamination and toxicology*. Springer.
- HAZER, B. & STEINBÜCHEL, A. (2007) Increased diversification of polyhydroxyalkanoates by modification reactions for industrial and medical applications. *Applied Microbiology and Biotechnology*, 74, 1-12.
- HEY, A.J.G., TANSLEY, S. & TOLLE, K.M. (2009) The fourth paradigm: data-intensive scientific discovery.
- HOUMIEL, K. L., SLATER, S., BROYLES, D., CASAGRANDE, L., COLBURN, S., GONZALEZ, K., MITSKY, T. A., REISER, S. E., SHAH, D. & TAYLOR, N. B. (1999) Poly (β -hydroxybutyrate) production in oilseed leukoplasts of *Brassica napus*. *Planta*, 209, 547-550.
- HRABAK, O. (1992) Industrial production of poly- β -hydroxybutyrate. *FEMS Microbiology Letters*, 103, 251-255.
- HUTMACHER, D. W. (2000) Scaffolds in tissue engineering bone and cartilage. *Biomaterials*, 21, 2529-2543.
- IRVINE, R. L. & BUSCH, A. W. (1979) Sequencing batch biological reactors: an overview. *Journal (Water Pollution Control Federation)*, 235-243.
- JONES, D.P. (2013) Going for Growth - A practical route to a circular economy. Available at : <http://www.esauk.org/> (Accessed: 12 September 2014).
- KADOURI, D., JURKEVITCH, E., OKON, Y. & CASTRO-SOWINSKI, S. (2005) Ecological and agricultural significance of bacterial polyhydroxyalkanoates. *Critical reviews in microbiology*, 31, 55-67.
- KASHIWAYA, Y., TAKESHIMA, T., MORI, N., NAKASHIMA, K., CLARKE, K. & VEECH, R. L. (2000) d- β -Hydroxybutyrate protects neurons in models of Alzheimer's and Parkinson's disease. *Proceedings of the National Academy of Sciences*, 97, 5440-5444.

- KATOH, T., YUGUCHI, D., YOSHII, H., SHI, H. & SHIMIZU, K. (1999) Dynamics and modeling on fermentative production of poly (β -hydroxybutyric acid) from sugars via lactate by a mixed culture of *Lactobacillus delbrueckii* and *Alcaligenes eutrophus*. *Journal of biotechnology*, 67, 113-134.
- KHANNA, S. & SRIVASTAVA, A. K. (2005) Statistical media optimization studies for growth and PHB production by *Ralstonia eutropha*. *Process Biochemistry*, 40, 2173-2182.
- KHOO, H.H. & TAN, R.B.H. (2010) Statistical media optimisation studies for growth and PHB production by *Ralstonia eutropha*. *Process Biochemistry* 40(6): 2173-2182
- KIM, B. S. (2000) Production of poly (3-hydroxybutyrate) from inexpensive substrates. *Enzyme and microbial technology*, 27, 774-777.
- KULKARNI, A. R., SOPPIMATH, K. S., AMINABHAVI, T. M., DAVE, A. M. & MEHTA, M. H. (2000) Glutaraldehyde crosslinked sodium alginate beads containing liquid pesticide for soil application. *Journal of Controlled Release*, 63, 97-105.
- LEE, S. Y. (1996a) Bacterial polyhydroxyalkanoates. *Biotechnology and Bioengineering*, 49, 1-14.
- LEE, S. Y. (1996b) Plastic bacteria? Progress and prospects for polyhydroxyalkanoate production in bacteria. *Trends in Biotechnology*, 14, 431-438.
- LEMOIGNE, M. (1926) Produit de déshydratation et de polymérisation de l'acide β -oxybutyrique. *Bull Soc Chim Biol*, 8, 770-782.
- LEMONS, P. C., SERAFIM, L. S. & REIS, M. A. M. (2006) Synthesis of polyhydroxyalkanoates from different short-chain fatty acids by mixed cultures submitted to aerobic dynamic feeding. *Journal of biotechnology*, 122, 226-238.
- Leonidou, L.C. and Katsikeas, C.S. (1996) The export development process: an integrative review of empirical models, *Journal of international business studies*, pp. 517-551.
- LI, Z.-J., SHI, Z.-Y., JIAN, J., GUO, Y.-Y., WU, Q. & CHEN, G.-Q. (2010) Production of poly (3-hydroxybutyrate- co-4-hydroxybutyrate) from unrelated carbon sources by metabolically engineered *Escherichia coli*. *Metabolic engineering*, 12, 352-359.
- LIU, Q., LUO, G., ZHOU, X. R. & CHEN, G.-Q. (2011) Biosynthesis of poly (3-hydroxydecanoate) and 3-hydroxydodecanoate dominating polyhydroxyalkanoates by β -oxidation pathway inhibited *Pseudomonas putida*. *Metabolic engineering*, 13, 11-17.
- LOFBERG, J. Y. (2004) A toolbox for modeling and optimization in MATLAB. *Computer Aided Control Systems Design*, IEEE International Symposium on, 2004. IEEE, 284-289.

- LOPEZ-VAZQUEZ, C. M., OEHMEN, A., HOOIJMANS, C. M., BRDJANOVIC, D., GIJZEN, H. J., YUAN, Z. & VAN LOOSDRECHT, M. (2009) Modeling the PAO–GAO competition: effects of carbon source, pH and temperature. *Water research*, 43, 450-462.
- LOU, X.F. & NAIR, J. (2009) The impact of landfilling and composting on greenhouse gas emissions- a review, *Bioresource technology*, 100(16), pp. 3792-3798.
- LOVE, J. (2007) *Process Automation Handbook: A guide to theory and practice*, Springer.
- MACDONALD, L. J. (1997) *Process to recover polyesters from transgenic plants*. PCT/US1996/017757.
- MADBOULY, S. A., SCHRADER, J. A., SRINIVASAN, G., LIU, K., MCCABE, K. G., GREWELL, D., GRAVES, W. R. & KESSLER, M. R. (2014) Biodegradation behavior of bacterial-based polyhydroxyalkanoate (PHA) and DDGS composites. *Green Chemistry*, 16, 1911-1920.
- MADISON, L. L. & HUISMAN, G. W. (1999) Metabolic engineering of poly (3-hydroxyalkanoates): from DNA to plastic. *Microbiology and molecular biology reviews*, 63, 21-53.
- MAKKAR, R. & CAMEOTRA, S. (2002) An update on the use of unconventional substrates for biosurfactant production and their new applications. *Applied Microbiology and Biotechnology*, 58, 428-434.
- MARCHANT, R. & BANAT, I. M. (2012) Microbial biosurfactants: challenges and opportunities for future exploitation. *Trends in Biotechnology*, 30, 558-565.
- MARTIN, D. P. & WILLIAMS, S. F. (2003) Medical applications of poly-4-hydroxybutyrate: a strong flexible absorbable biomaterial. *Biochemical Engineering Journal*, 16, 97-105.
- MASON, A. J. (2013) SolverStudio: A New Tool for Better Optimisation and Simulation Modelling in Excel. *INFORMS Transactions on Education*, 14, 45-52.
- MASOOD, M. A., JABBAR, R. A., MASOUM, M. A. S., JUNAID, M. & AMMAR, M. (2012) An innovative technique for design optimization of core type 3-phase distribution transformer using mathematica. *Global Journal of Technology & Optimization*, 3.
- METABOLIX. (2014) Available: <http://www.metabolix.com/> [Accessed June 5 2014].
- MITTENDORF, V., ROBERTSON, E. J., LEECH, R. M., KRÜGER, N., STEINBÜCHEL, A. & POIRIER, Y. (1998) Synthesis of medium-chain-length polyhydroxyalkanoates in *Arabidopsis thaliana* using intermediates of peroxisomal fatty acid β -oxidation. *Proceedings of the National Academy of Sciences*, 95, 13397-13402.
- MOORE, R., BARU, C., MARCIANO, R., RAJASEKAR, A. & WAN, M. (1999) Data-intensive computing, *The Grid: Blueprint for a New Computing Infrastructure*, Morgan Kaufmann, pp. 105-129.

- MORA-HUERTAS, C. E., FESSI, H. & ELAISSARI, A. (2010) Polymer-based nanocapsules for drug delivery. *International Journal of Pharmaceutics*, 385, 113-142.
- MUKHERJEE, A. & ZHANG, J. (2008) A reliable multi-objective control strategy for batch processes based on bootstrap aggregated neural network models. *Journal of Process Control*, 18, 720-734.
- MÜLLER, M. M., KÜGLER, J. H., HENKEL, M., GERLITZKI, M., HÖRMANN, B., PÖHNLEIN, M., SYLDATK, C. & HAUSMANN, R. (2012) Rhamnolipids—Next generation surfactants? *Journal of biotechnology*, 162, 366-380.
- MURNLEITNER, E., KUBA, T., VAN LOOSDRECHT, M. C. M. & HEIJNEN, J. J. (1997) An integrated metabolic model for the aerobic and denitrifying biological phosphorus removal. *Biotechnology and Bioengineering*, 54, 434-450.
- NEWSRX. (2013) "Chemically inducible expression of biosynthetic pathways" in patent application approval process [Online]. Available: <http://www.highbeam.com/doc/1G1-323547527.html> [Accessed July 07 2014].
- NITSCHKE, M. & COSTA, S. (2007) Biosurfactants in food industry. *Trends in Food Science & Technology*, 18, 252-259.
- NONATO, R., MANTELATTO, P. & ROSSELL, C. (2001) Integrated production of biodegradable plastic, sugar and ethanol. *Applied Microbiology and Biotechnology*, 57, 1-5.
- OLIVER, D.S., REYNOLDS, A.C. & LIU, N. (2008) Inverse theory for petroleum reservoir characterisation and history matching.
- PACHEKOSKI, W.M., AGNELLI, J.A.M. & BELEM, L.P. (2009) Thermal, mechanical and morphological properties of poly (hydroxybutyrate) and polypropylene blends after processing. *Materials research*, 12(2), pp. 159-164.
- PASSANHA, P., ESTEVES, S. R., KEDIA, G., DINSDALE, R. M. & GUWY, A. J. (2013) Increasing polyhydroxyalkanoate (PHA) yields from *Cupriavidus necator* by using filtered digestate liquors. *Bioresource technology*, 147, 345-352.
- PATNAIK, P. R. (2005) Perspectives in the modeling and optimization of PHB production by pure and mixed cultures. *Critical reviews in biotechnology*, 25, 153-171.
- PÉREZ-MARTÍNEZ, J. I., MORILLO, E., MAQUEDA, C. & GINES, J. M. (2001) Ethyl cellulose polymer microspheres for controlled release of norfluzon. *Pest management science*, 57, 688-694.
- PHUKON, P., SAIKIA, J. P. & KONWAR, B. K. (2012) Bio-plastic (P-3HB-co-3HV) from *Bacillus circulans* (MTCC 8167) and its biodegradation. *Colloids and Surfaces B: Biointerfaces*, 92, 30-34.
- PILETSKA, E. V., TURNER, N. W., TURNER, A. P. F. & PILETSKY, S. A. (2005) Controlled release of the herbicide simazine from computationally designed molecularly imprinted polymers. *Journal of Controlled Release*, 108, 132-139.

- PINTÉR, J. D., LINDER, D. & CHIN, P. (2006) Global Optimization Toolbox for Maple: An introduction with illustrative applications. *Optimisation Methods and Software*, 21, 565-582.
- POIRIER, Y. (2001) Production of polyesters in transgenic plants. *Biopolyesters*. Springer.
- POIRIER, Y., DENNIS, D. E., KLOMPARENS, K. & SOMERVILLE, C. (1992) Polyhydroxybutyrate, a biodegradable thermoplastic, produced in transgenic plants. *Science*, 256, 520-523.
- QASIM, S.R. & CHIANG, W. (1994) Sanitary landfill leachate: generation, control and treatment. *CRC Press*.
- REDDY, C. S. K., GHAI, R. & KALIA, V. C. (2003) Polyhydroxyalkanoates: an overview. *Bioresource technology*, 87, 137-146.
- REIS, M. A. M., SERAFIM, L. S., LEMOS, P. C., RAMOS, A. M., AGUIAR, F. R. & VAN LOOSDRECHT, M. C. M. (2003) Production of polyhydroxyalkanoates by mixed microbial cultures. *Bioprocess and Biosystems Engineering*, 25, 377-385.
- REUSCH, R. N. (1995) Low molecular weight complexed poly (3-hydroxybutyrate): a dynamic and versatile molecule in vivo. *Canadian journal of microbiology*, 41, 50-54.
- ROSEN, M. J. & KUNJAPPU, J. T. (2012) *Surfactants and interfacial phenomena*, John Wiley & Sons.
- RUTH, K., GRUBELNIK, A., HARTMANN, R., EGLI, T., ZINN, M. & REN, Q. (2007) Efficient production of (R)-3-hydroxycarboxylic acids by biotechnological conversion of polyhydroxyalkanoates and their purification. *Biomacromolecules*, 8, 279-286.
- SAHINIDIS, N. V. (1996) BARON: A general purpose global optimization software package. *Journal of Global Optimization*, 8, 201-205.
- SALAMANCA-CARDONA, L., ASHE, C. S., STIPANOVIC, A. J. & NOMURA, C. T. (2014) Enhanced production of polyhydroxyalkanoates (PHAs) from beechwood xylan by recombinant *Escherichia coli*. *Applied Microbiology and Biotechnology*, 98, 831-842.
- SALEHIZADEH, H. & VAN LOOSDRECHT, M. C. M. (2004) Production of polyhydroxyalkanoates by mixed culture: recent trends and biotechnological importance. *Biotechnology advances*, 22, 261-279.
- SAMY, S. M., SILVA, N., PINTO, L. A. M., CASTRO, A. C. T. D., ALMEIDA, H. L., ALMEIDA, A., SOUSA, N., SALGADO, A. J., GIMBLE, J. M. & REIS, R. L. (2013) Development and characterization of PHB-HV based 3D scaffolds for a tissue engineering and cell-therapy combinatorial approach for spinal cord Injury regeneration.

- SATOH, H., RAMEY, W., KOCH, F., OLDHAM, W., MINO, T. & MATSUO, T. (1996) Anaerobic substrate uptake by the enhanced biological phosphorus removal activated sludge treating real sewage. *Water Science and Technology*, 34, 9-16.
- SEEBACH, D., BECK, A. K., BREITSCHUH, R. & JOB, K. (1992) Direct Degradation of the Biopolymer Poly [(R)-3-Hydroxybutyric Acid] to (R)-3-Hydroxybutanoic Acid and its Methyl Ester. *Organic Syntheses*, 39-39.
- SENDIL, D., GÜRSEL, I., L WISE, D. & HASIRCI, V. (1999) Antibiotic release from biodegradable PHBV microparticles. *Journal of Controlled Release*, 59, 207-217.
- SERAFIM, L. S., LEMOS, P. C., ALBUQUERQUE, M. G. E. & REIS, M. A. M. (2008) Strategies for PHA production by mixed cultures and renewable waste materials. *Applied Microbiology and Biotechnology*, 81, 615-628.
- SERAFIM, L. S., LEMOS, P. C., OLIVEIRA, R. & REIS, M. A. M. (2004) Optimization of polyhydroxybutyrate production by mixed cultures submitted to aerobic dynamic feeding conditions. *Biotechnology and Bioengineering*, 87, 145-160.
- SHAH, A.A., HASAN, F., HAMEED, A. & AHMED, S. (2008) Biological degradation of plastics: a comprehensive review, *Biotechnology advances*, 26(3), pp. 246-265.
- SHAHHOSSEINI, S. (2004) Simulation and optimisation of PHB production in fed-batch culture of *Ralstonia eutropha*. *Process Biochemistry*, 39, 963-969.
- SHRIVASTAV, A., KIM, H.-Y. & KIM, Y.-R. (2013) Advances in the applications of polyhydroxyalkanoate nanoparticles for novel drug delivery system. *BioMed Research International*, 2013.
- SHUBHRASEKHAR, C., SUPRIYA, M., KARTHIK, L., GAURAV, K. & BHASKARA RAO, K. V. (2013) Isolation, characterization and application of biosurfactant produced by Marine actinobacteria isolated from Saltpan Soil from costal area of Andhra Pradesh, India. *Research Journal of Biotechnology Vol*, 8, 1.
- SHUKLA, P. G., KALIDHASS, B., SHAH, A. & PALASKAR, D. V. (2002) Preparation and characterization of microcapsules of water-soluble pesticide monocrotophos using polyurethane as carrier material. *Journal of microencapsulation*, 19, 293-304.
- SNELL, K. D. & PEOPLES, O. P. (2009) PHA bioplastic: A value-added coproduct for biomass biorefineries. *Biofuels, Bioproducts and Biorefining*, 3, 456-467.
- SOMERVILLE, C. R. & BONETTA, D. (2001) Plants as factories for technical materials. *Plant Physiology*, 125, 168-171.

- SOMLEVA, M. N., SNELL, K. D., BEAULIEU, J. J., PEOPLES, O. P., GARRISON, B. R. & PATTERSON, N. A. (2008) Production of polyhydroxybutyrate in switchgrass, a value-added co-product in an important lignocellulosic biomass crop. *Plant Biotechnology Journal*, 6, 663-678.
- STEINBÜCHEL, A. (1992) Biodegradable plastics. *Current Opinion in Biotechnology*, 3, 291-297.
- STEINBÜCHEL, A. & FÜCHTENBUSCH, B. (1998) Bacterial and other biological systems for polyester production. *Trends in Biotechnology*, 16, 419-427.
- STEINBÜCHEL, A. & VALENTIN, H. E. (1995) Diversity of bacterial polyhydroxyalkanoic acids. *FEMS Microbiology Letters*, 128, 219-228.
- STEVENS, E. S. (2002) *Green plastics: an introduction to the new science of biodegradable plastics*, Princeton University Press.
- SUDESH, K. (2013) Potential Applications of PHA. *Polyhydroxyalkanoates from Palm Oil: Biodegradable Plastics*. Springer.
- SUDESH, K., ABE, H. & DOI, Y. (2000) Synthesis, structure and properties of polyhydroxyalkanoates: biological polyesters. *Progress in polymer science*, 25, 1503-1555.
- SUDESH, K., BHUBALAN, K., CHUAH, J.-A., KEK, Y.-K., KAMILAH, H., SRIDEWI, N. & LEE, Y.-F. (2011) Synthesis of polyhydroxyalkanoate from palm oil and some new applications. *Applied Microbiology and Biotechnology*, 89, 1373-1386.
- SUDESH, K., LOO, C. Y., GOH, L. K., IWATA, T. & MAEDA, M. (2007) The Oil-Absorbing Property of Polyhydroxyalkanoate Films and its Practical Application: A Refreshing New Outlook for an Old Degrading Material. *Macromolecular bioscience*, 7, 1199-1205.
- SURIYAMONGKOL, P., WESELAKE, R., NARINE, S., MOLONEY, M. & SHAH, S. (2007) Biotechnological approaches for the production of polyhydroxyalkanoates in microorganisms and plants—a review. *Biotechnology advances*, 25, 148-175.
- THOMPSON, R., MOORE, C., ANDRADY, A., GREGORY, M., TAKADA, H. & WEISBERG, S. (2005) New directions in plastic debris, *Science (New York, NY)*, 310(5751), pp. 1117-1117.
- THOMPSON, R.C., MOORE, C.J., VOM SAAL, F.S. & SWAN, S.H. (2009) Plastics, the environment and human health: current consensus and future trends, *Philosophical Transactions of the Royal Society B: Biological Sciences*, 364(1526), pp. 2153-2166.
- THIRD, K. A., NEWLAND, M. & CORD-RUWISCH, R. (2003) The effect of dissolved oxygen on PHB accumulation in activated sludge cultures. *Biotechnology and Bioengineering*, 82, 238-250.

- TIAN, F., ZHAO, Y.-L., LIU, C.-J., LI, F. & XING, N. (2008) The vitro and vivo study of Poly (3-hydroxybutyrate) microspheres. 7th Asian-Pacific Conference on Medical and Biological Engineering, Springer, 615-622.
- TIANJINGREENBIO. (2014) Available: <http://www.tjgreenbio.com/en/> [Accessed June 5 2014].
- TOKIWA, Y., CALABIA, B. P., UGWU, C. U. & AIBA, S. (2009) Biodegradability of plastics. *International journal of molecular sciences*, 10, 3722-3742.
- TRIPATHI, A. D., SRIVASTAVA, S. K. & SINGH, R. P. (2013) Statistical optimization of physical process variables for bio-plastic (PHB) production by *Alcaligenes sp.* *biomass and bioenergy*, 55, 243-250.
- ULRICH, W. (1988) Systems thinking, systems practice, and practical philosophy: A program of research. *Systems Practice*, 1, 137-163.
- VAEZIPOUR, A., MOSAVI, A. & SEIGERROTH, U. (2013) Visual analytics and informed decisions in health and life sciences. Paper in Proceedings of International CAE Conference, Verona, Italy, 2013.
- VALENTIN, H. E., BROYLES, D. L., CASAGRANDE, L. A., COLBURN, S. M., CREELY, W. L., DELAQUIL, P. A., FELTON, H. M., GONZALEZ, K. A., HOUMIEL, K. L. & LUTKE, K. (1999) PHA production, from bacteria to plants. *International journal of biological macromolecules*, 25, 303-306.
- VAN AALST-VAN LEEUWEN, M. A., POT, M. A., VAN LOOSDRECHT, M. C. M. & HEIJNEN, J. J. (1997) Kinetic Modeling of Poly (3-hydroxybutyrate) Production and Consumption by *Paracoccus pantotrophus* under Dynamic Substrate Supply. *Biotechnology and Bioengineering*, 55, 773-782.
- VAN LOOSDRECHT, M.C.M. & HEIJNEN, J.J. (2002) Modelling of activated sludge processes with structured biomass, *Water Science and Technology*, 45(6), p. 10.
- VAN LOOSDRECHT, M. C. M., POT, M. A. & HEIJNEN, J. J. (1997) Importance of bacterial storage polymers in bioprocesses. *Water Science and Technology*, 35, 41-47.
- VENKATA MOHAN, S. & VENKATESWAR REDDY, M. (2013) Optimization of critical factors to enhance polyhydroxyalkanoates (PHA) synthesis by mixed culture using Taguchi design of experimental methodology. *Bioresource technology*, 128, 409-416.
- VILOS, C., GUTIÉRREZ, M., ESCOBAR, R. A., MORALES, F., DENARDIN, J. C., VELASQUEZ, L. & ALTBIR, D. (2013a) Superparamagnetic Poly (3-hydroxybutyrate-co-3 hydroxyvalerate)(PHBV) nanoparticles for biomedical applications. *Electronic Journal of Biotechnology*, 16, 8-8.
- VILOS, C., MORALES, F. A., SOLAR, P. A., HERRERA, N. S., GONZALEZ-NILO, F. D., AGUAYO, D. A., MENDOZA, H. L., COMER, J., BRAVO, M. L. & GONZALEZ, P. A. (2013b) Paclitaxel-PHBV nanoparticles and their toxicity to endometrial and primary ovarian cancer cells. *Biomaterials*, 34, 4098-4108.

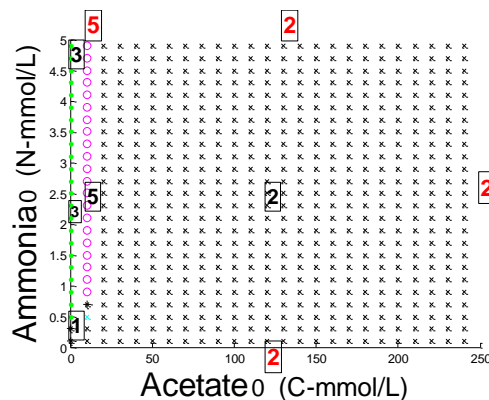
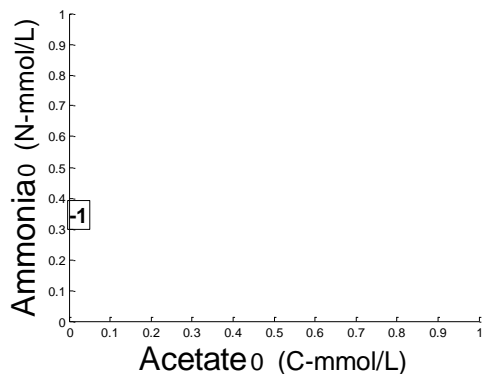
- VILOS, C. & VELASQUEZ, L. A. (2012) Therapeutic strategies based on polymeric microparticles. *BioMed Research International*, 2012.
- VOINOVA, O. N., KALACHEVA, G. S., GRODNITSKAYA, I. D. & VOLOVA, T. G. (2009) Microbial polymers as a degradable carrier for pesticide delivery. *Applied Biochemistry and Microbiology*, 45, 384-388.
- WANG, B., SHARMA-SHIVAPPA, R. R., OLSON, J. W. & KHAN, S. A. (2012a) Upstream process optimization of polyhydroxybutyrate (PHB) by *Alcaligenes latus* using two-stage batch and fed-batch fermentation strategies. *Bioprocess and biosystems engineering*, 35, 1591-1602.
- WANG, B., SHARMA-SHIVAPPA, R. R., OLSON, J. W. & KHAN, S. A. (2013) Production of polyhydroxybutyrate (PHB) by *Alcaligenes latus* using sugarbeet juice. *Industrial Crops and Products*, 43, 802-811.
- WANG, Q., TAPPEL, R. C., ZHU, C. & NOMURA, C. T. (2012b) Development of a new strategy for production of medium-chain-length polyhydroxyalkanoates by recombinant *Escherichia coli* via inexpensive non-fatty acid feedstocks. *Applied and environmental microbiology*, 78, 519-527.
- WELLES, L., LOPEZ-VAZQUEZ, C. M., HOOIJMANS, C. M., VAN LOOSDRECHT, M. C. M. & BRDJANOVIC, D. (2014) Impact of salinity on the anaerobic metabolism of phosphate-accumulating organisms (PAO) and glycogen-accumulating organisms (GAO). *Applied Microbiology and Biotechnology*, 1-14.
- WILLIAMS, S. F. & MARTIN, D. P. (2003) Therapeutic uses of polymers and oligomers comprising gamma-hydroxybutyrate. Google Patents.
- WOLLNY, V., DEHOUST, G., FRITSCH, U. R. & WEINEM, P. (2001) Comparison of plastic packaging waste management options: feedstock recycling versus energy recovery in Germany, *Journal of Industrial Ecology*, 5(3), pp. 49-63.
- YAGCI, N., ARTAN, N., ÇOKGÖR, E. U., RANDALL, C. W. & ORHON, D. (2003) Metabolic model for acetate uptake by a mixed culture of phosphate- and glycogen-accumulating organisms under anaerobic conditions. *Biotechnology and Bioengineering*, 84, 359-373.
- YAMASHITA, F. & HASHIDA, M. (2003) Mechanistic and empirical modeling of skin permeation of drugs, *Advanced drug delivery reviews*, 55(9), pp. 1185-1199.
- YU, J. & CHEN, L. X. L. (2006) Cost-Effective Recovery and Purification of Polyhydroxyalkanoates by Selective Dissolution of Cell Mass. *Biotechnology progress*, 22, 547-553.
- ZAFAR, M., KUMAR, S., KUMAR, S. & DHIMAN, A. K. (2012) Optimization of polyhydroxybutyrate (PHB) production by *Azohydromonas lata* MTCC 2311 by using genetic algorithm based on artificial neural network and response surface methodology. *Biocatalysis and Agricultural Biotechnology*, 1, 70-79.

- ZHANG, J. (1999) Developing robust non-linear models through bootstrap aggregated neural networks. *Neurocomputing*, 25, 93-113.
- ZHANG, J. (2004) A reliable neural network model based optimal control strategy for a batch polymerization reactor. *Industrial & engineering chemistry research*, 43, 1030-1038.
- ZHANG, X., LUO, R., WANG, Z., DENG, Y. & CHEN, G.-Q. (2009) Application of (R)-3-hydroxyalkanoate methyl esters derived from microbial polyhydroxyalkanoates as novel biofuels. *Biomacromolecules*, 10, 707-711.
- ZOU, X.-H., LI, H.-M., WANG, S., LESKI, M., YAO, Y.-C., YANG, X.-D., HUANG, Q.-J. & CHEN, G.-Q. (2009) The effect of 3-hydroxybutyrate methyl ester on learning and memory in mice. *Biomaterials*, 30, 1532-1541.
- ZUÑIGA, C., MORALES, M. & REVAH, S. (2013) Polyhydroxyalkanoates accumulation by *Methylobacterium organophilum* CZ-2 during methane degradation using citrate or propionate as cosubstrates. *Bioresource technology*, 129, 686-689.

Appendix-A

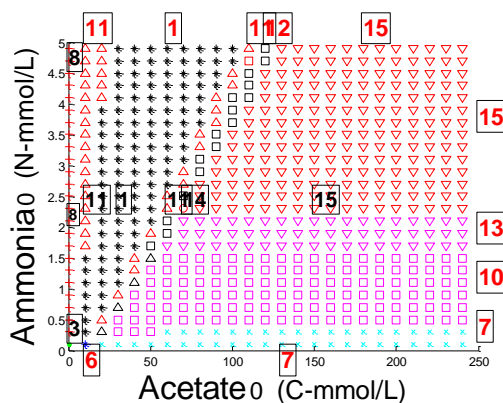
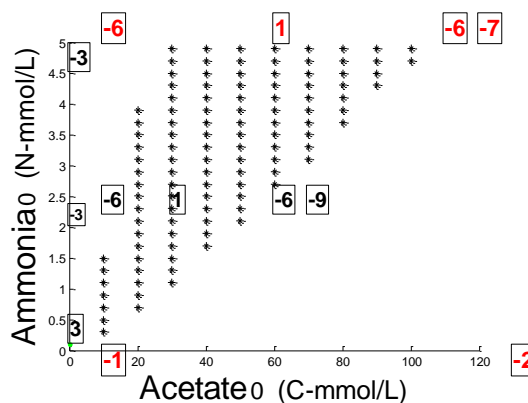
Run No.1

	CV(1)	CV(2)	CV(3)	CV(4)	CV(5)	CV(6)	CV(7)
CV1	1	0	1	1	0	3	0
CV2	1	0	0	0	0	0	0
CV3	1	0	1	1	0	1	0
CV4	1	0	0	0	0	2	0
CV5	1	0	1	1	0	3	1

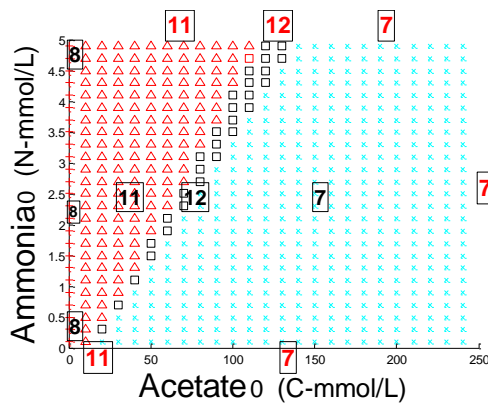


Run No.2

	CV(1)	CV(2)	CV(3)	CV(4)	CV(5)	CV(6)	CV(7)
CV6	1	1	1	1	2	3	1
CV7	1	1	1	0	1	2	1
CV8	1	1	1	1	2	1	0
CV9	1	1	1	1	1	3	1
CV10	1	1	0	0	0	2	1
CV11	1	1	1	1	2	3	0
CV12	1	1	1	1	1	3	0
CV13	1	1	0	0	0	2	0
CV14	1	1	1	0	1	3	0
CV15	1	1	0	0	0	0	0
CV16	1	1	1	1	0	3	0

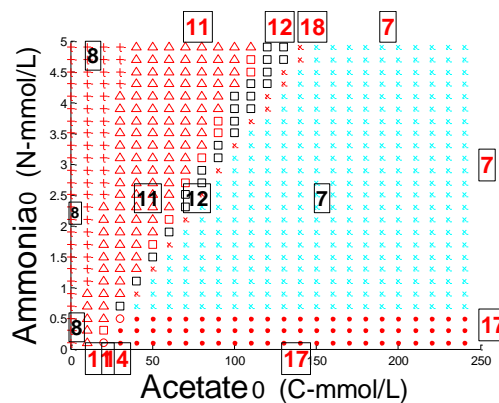
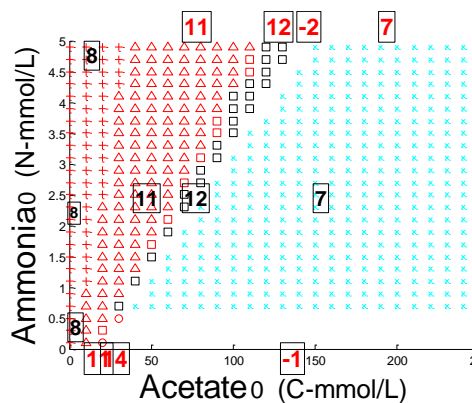


Run No.3



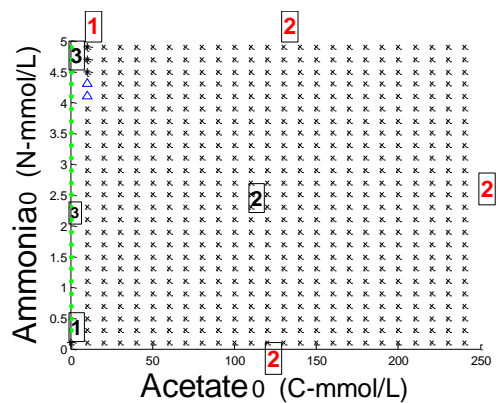
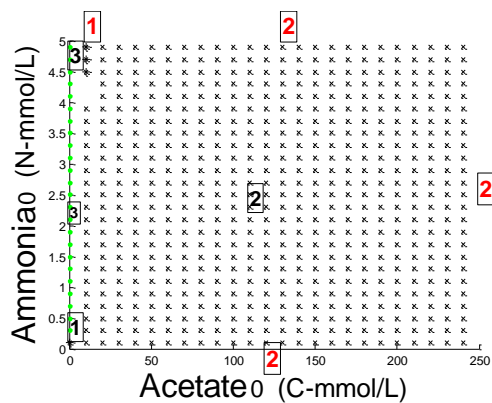
Run No.4

	CV(1)	CV(2)	CV(3)	CV(4)	CV(5)	CV(6)	CV(7)
CV17	1	1	1	0	1	2	0
CV18	1	1	1	0	1	3	1

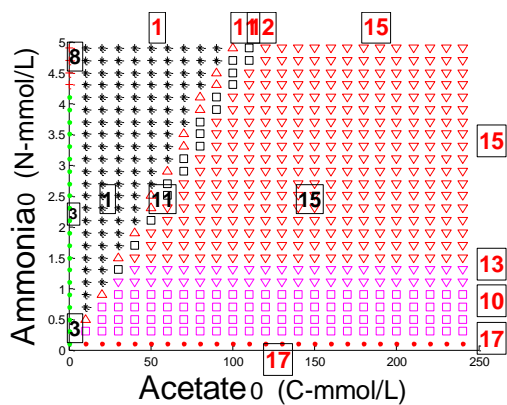


Run No.5

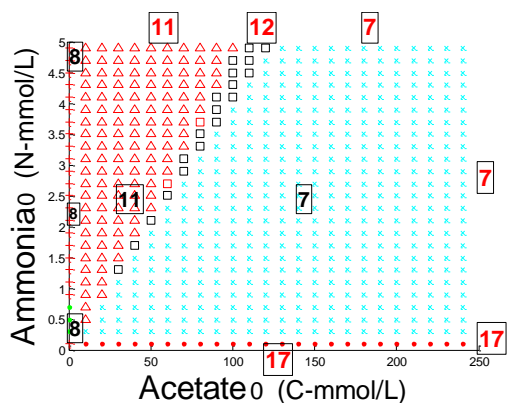
	CV(1)	CV(2)	CV(3)	CV(4)	CV(5)	CV(6)	CV(7)
CV19	1	0	0	1	0	3	0



Run No.6

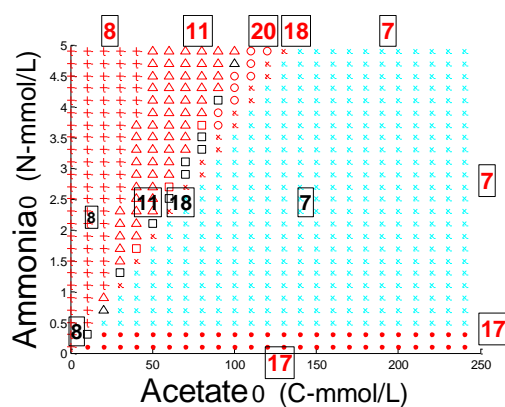
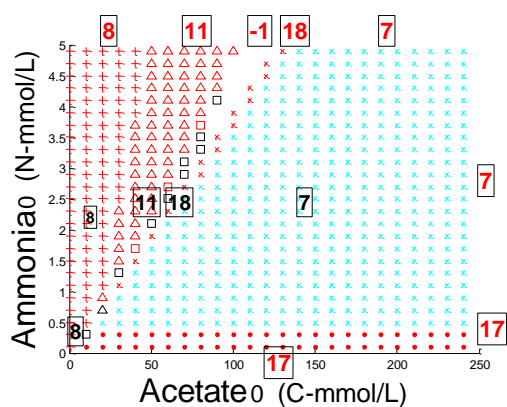


Run No.7



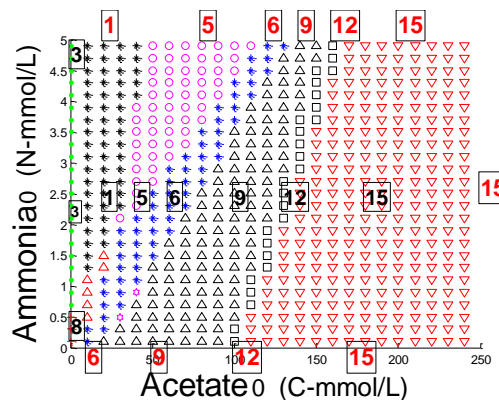
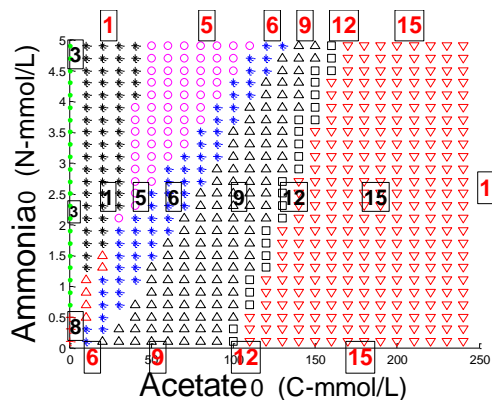
Run No.8

	CV(1)	CV(2)	CV(3)	CV(4)	CV(5)	CV(6)	CV(7)
CV20	1	1	1	1	1	1	0
CV21	1	1	1	1	0	1	0

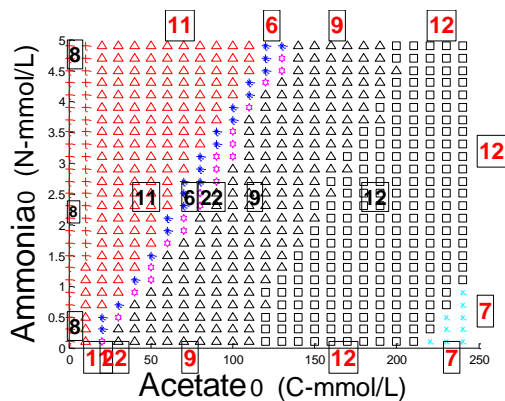


Run No.9

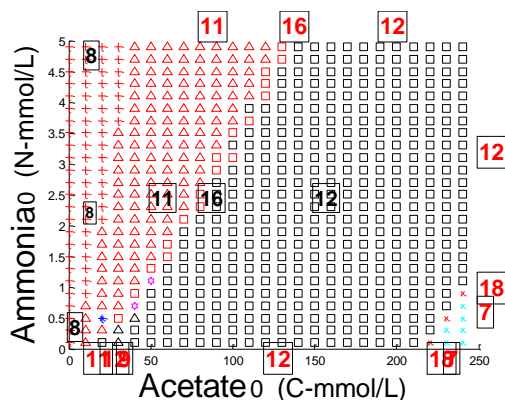
	CV(1)	CV(2)	CV(3)	CV(4)	CV(5)	CV(6)	CV(7)
CV22	1	1	1	1	0	3	1



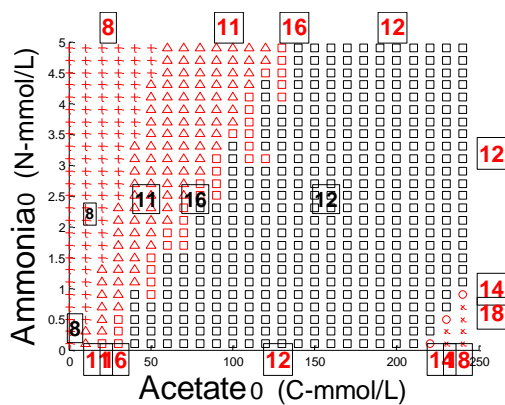
Run No.10



Run No.11

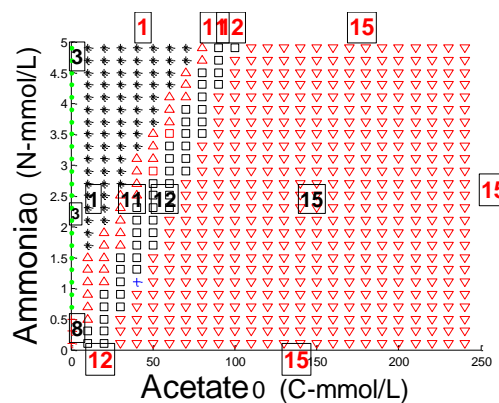
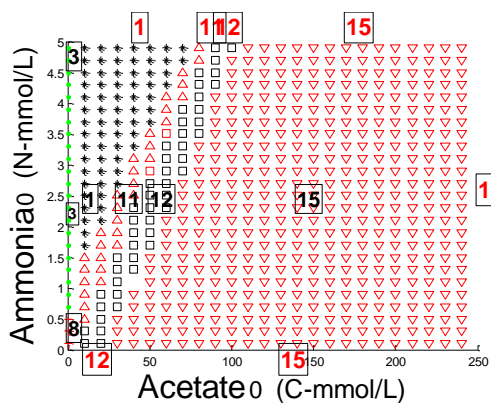


Run No.12

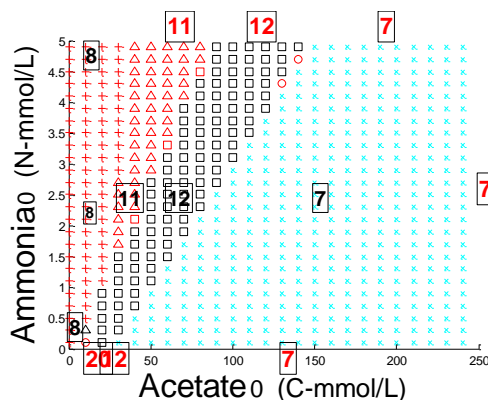


Run No.13

	CV(1)	CV(2)	CV(3)	CV(4)	CV(5)	CV(6)	CV(7)
CV23	1	1	0	1	0	3	0

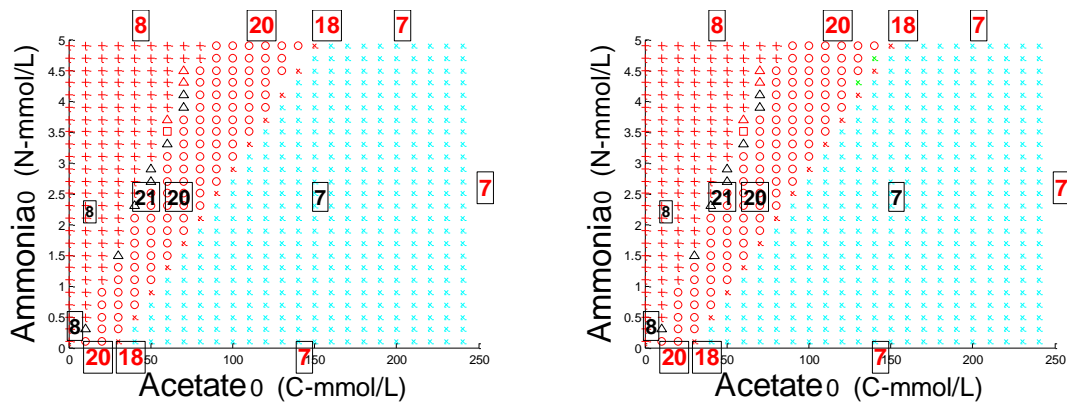


Run No.14

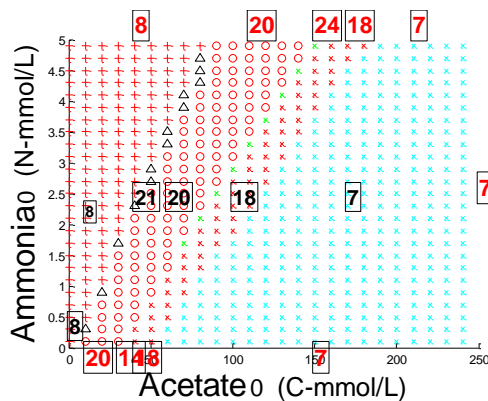


Run No.15

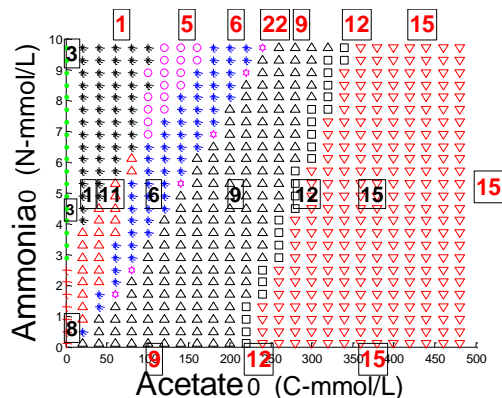
	CV(1)	CV(2)	CV(3)	CV(4)	CV(5)	CV(6)	CV(7)
CV24	1	1	1	0	1	1	0



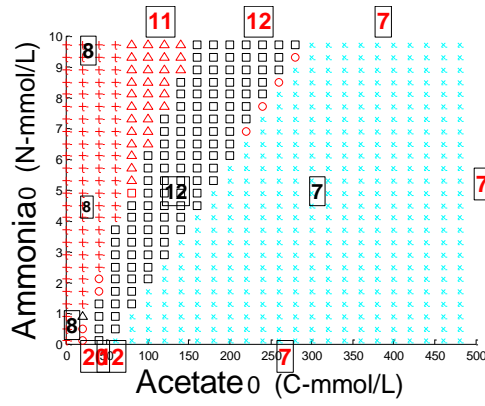
Run No.16



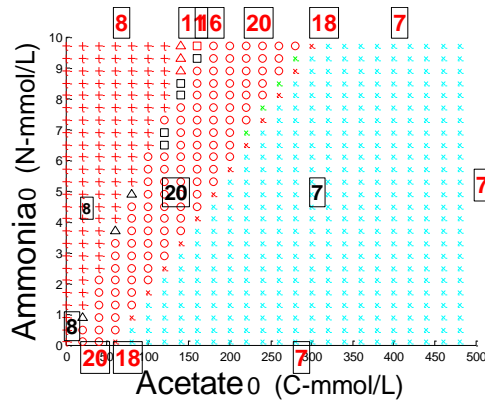
Run No.17



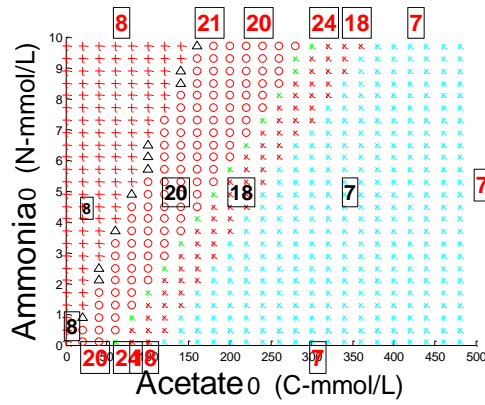
Run No.22



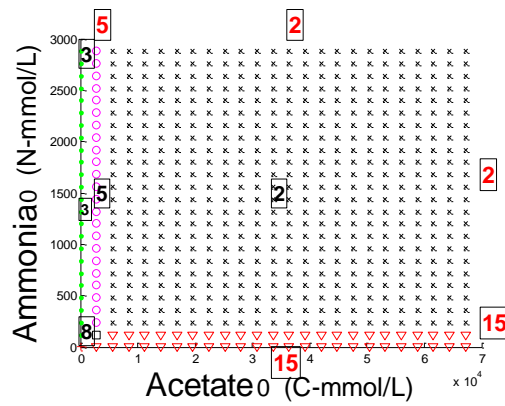
Run No.23



Run No.24

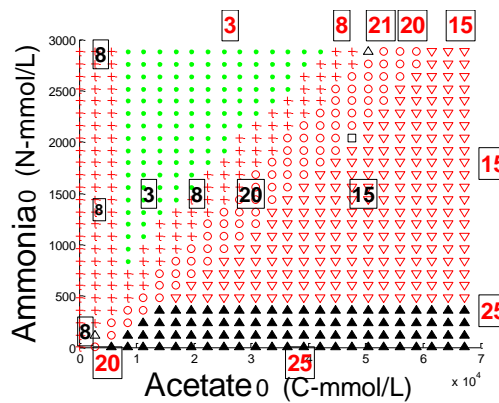
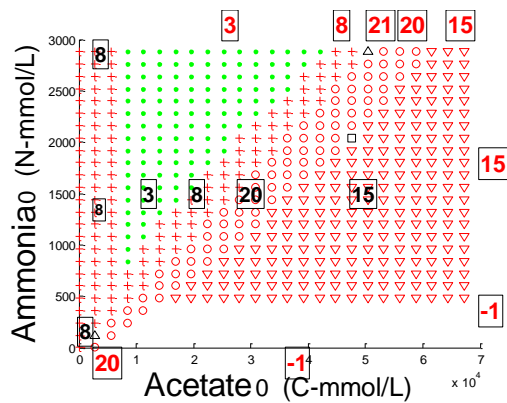


Run No.25

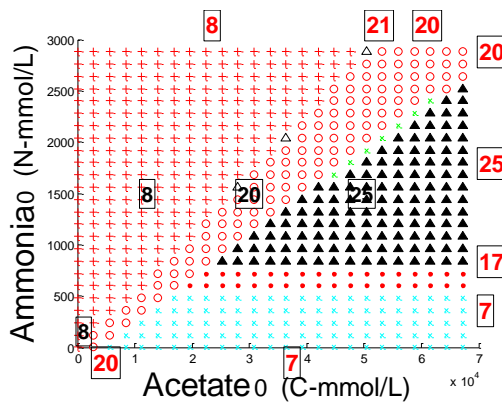


Run No.26

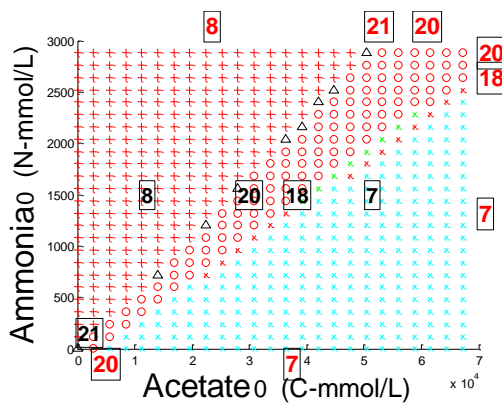
	CV(1)	CV(2)	CV(3)	CV(4)	CV(5)	CV(6)	CV(7)
CV25	1	1	1	0	1	0	0



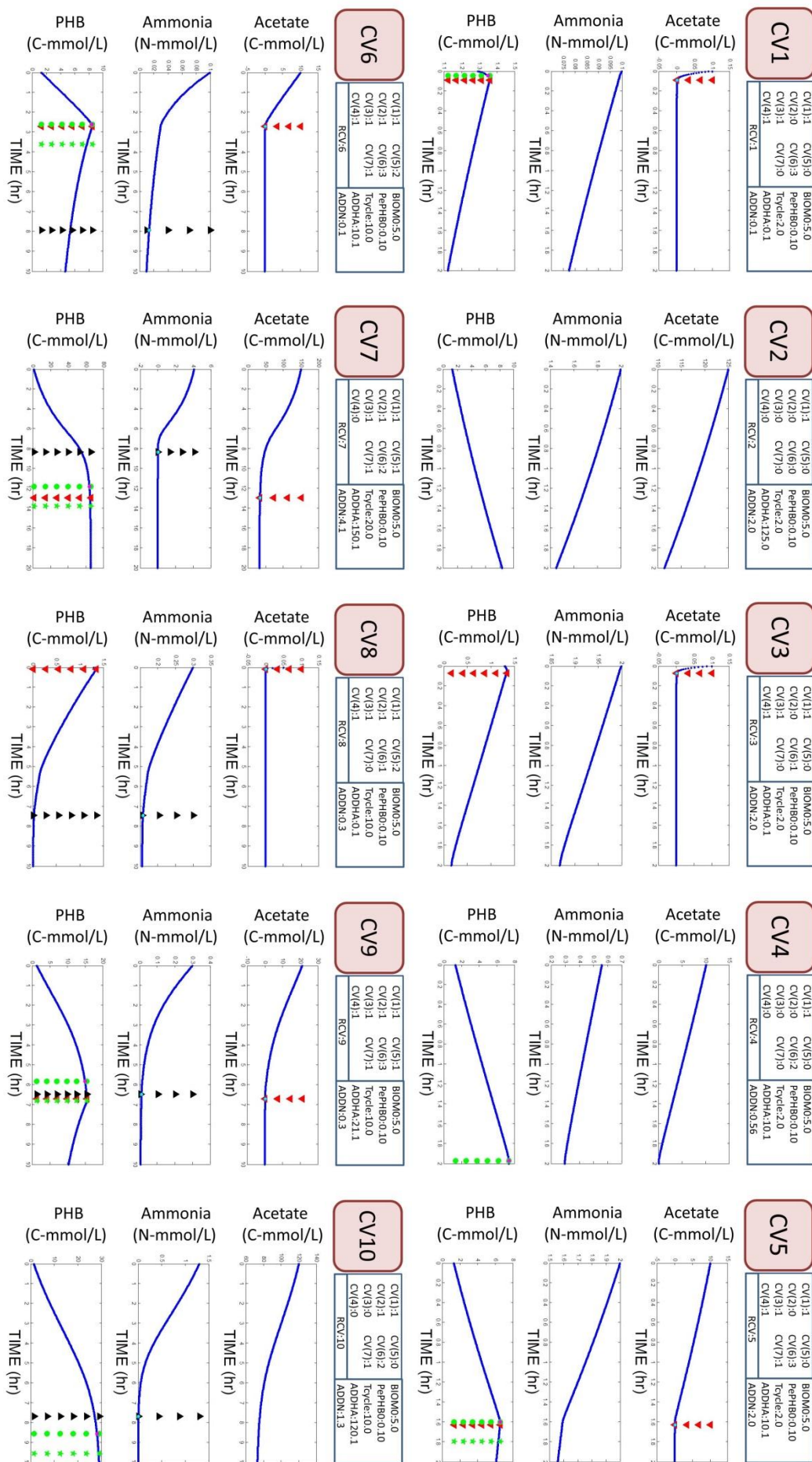
Run No.27

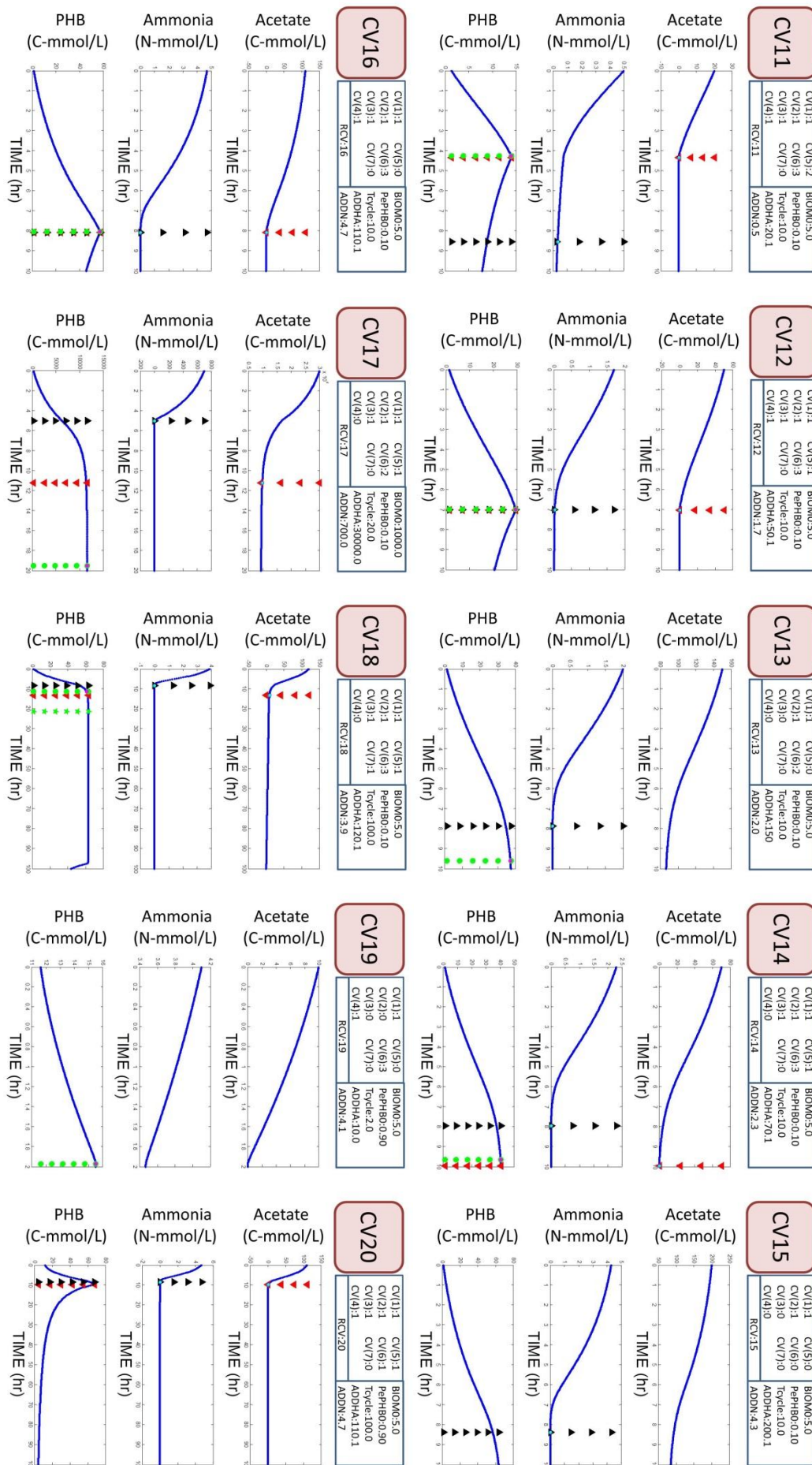


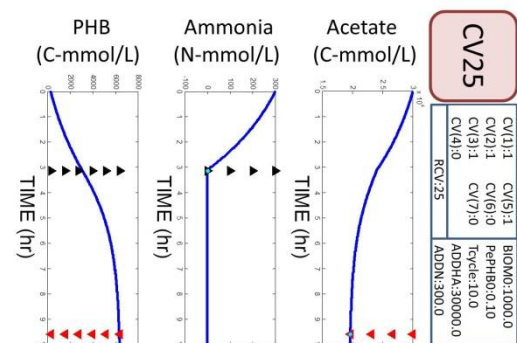
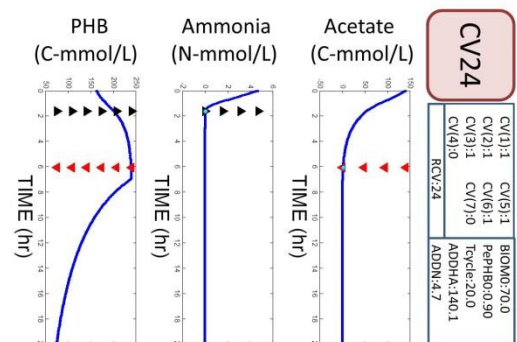
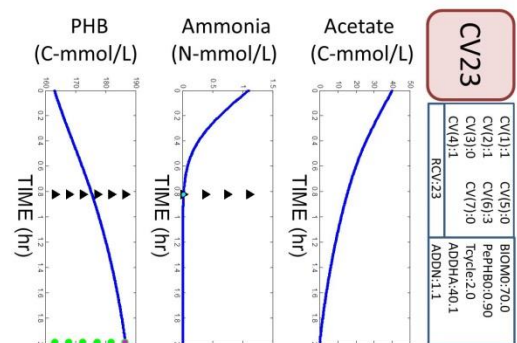
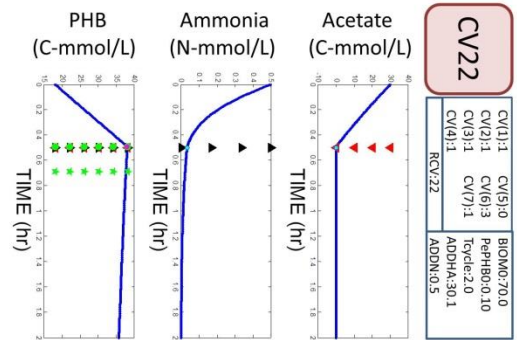
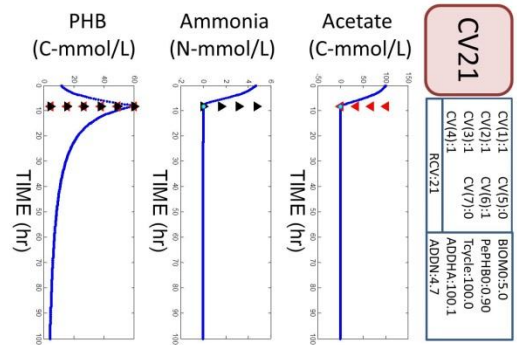
Run No.28



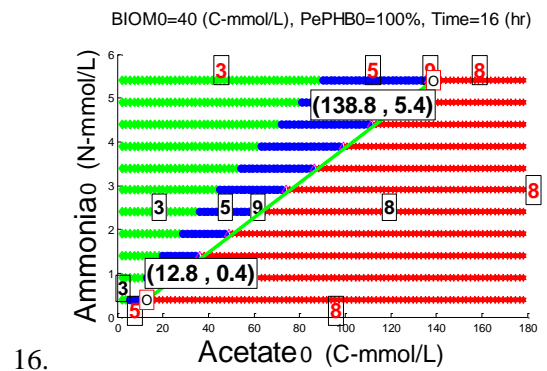
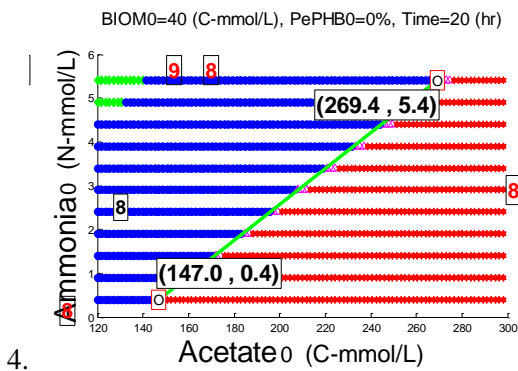
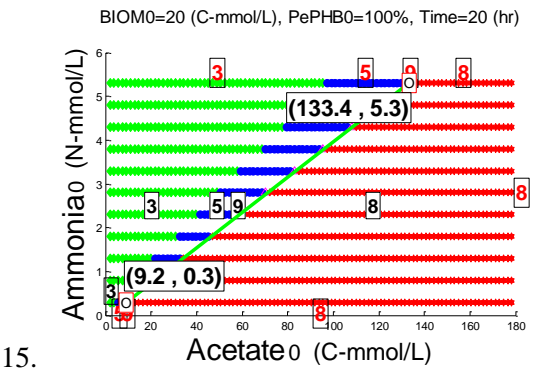
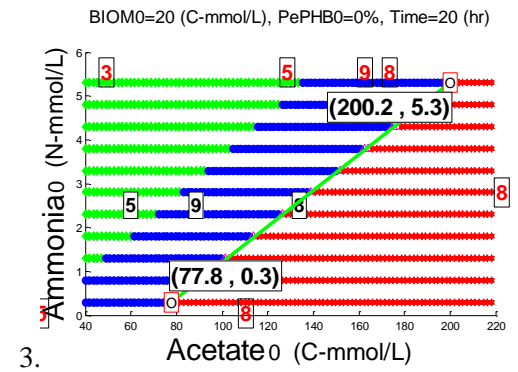
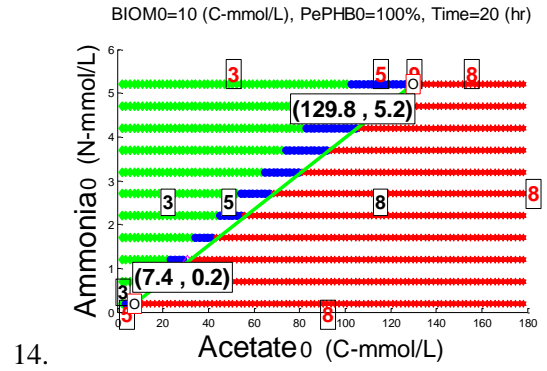
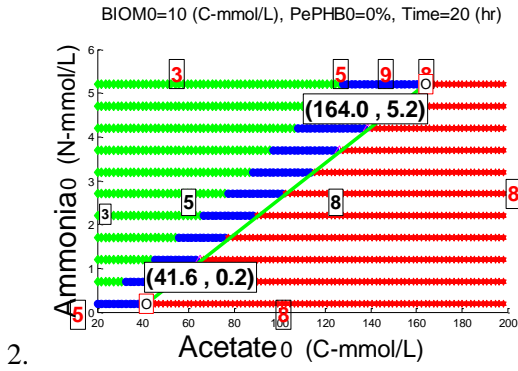
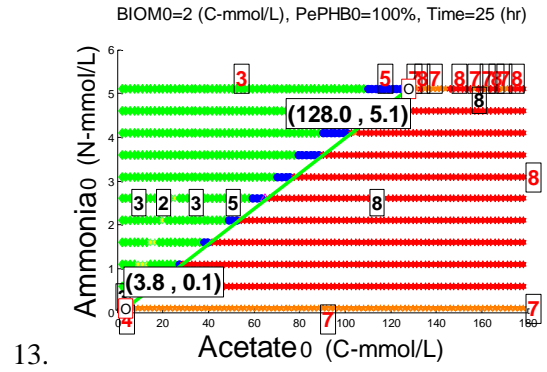
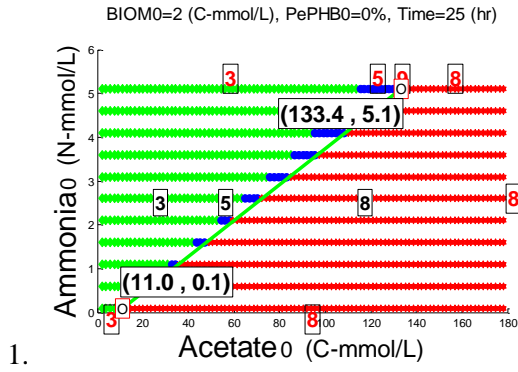
Appendix-B

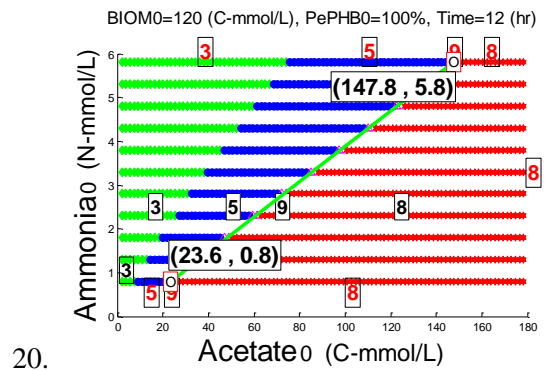
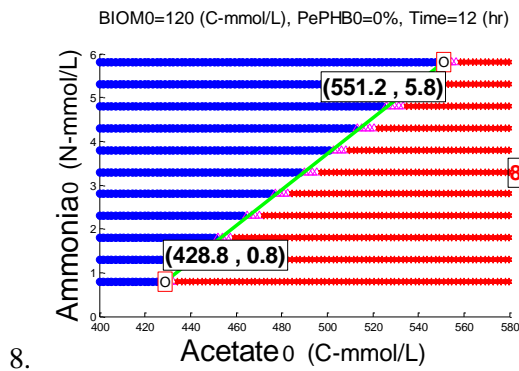
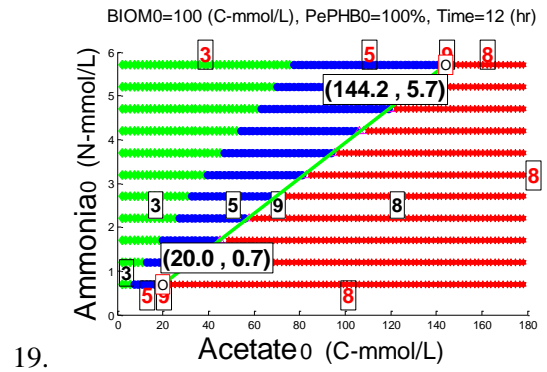
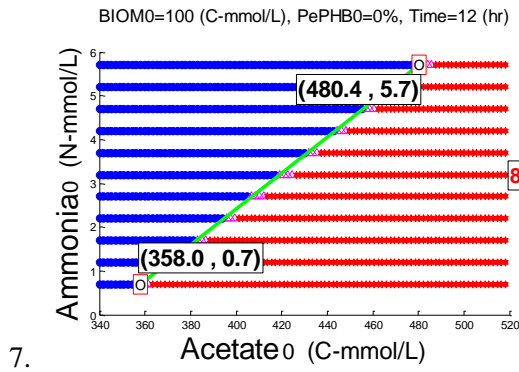
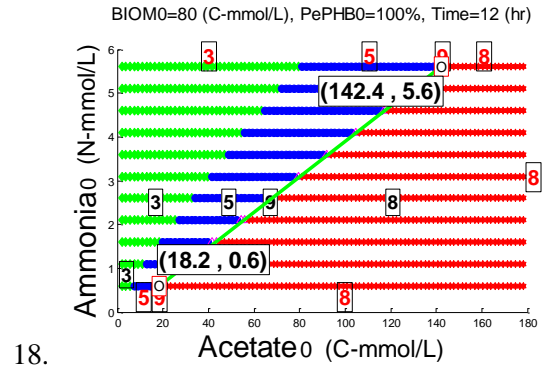
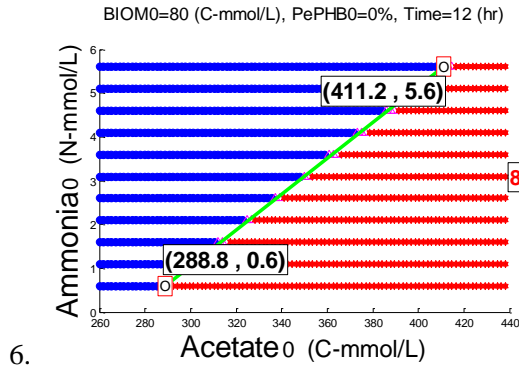
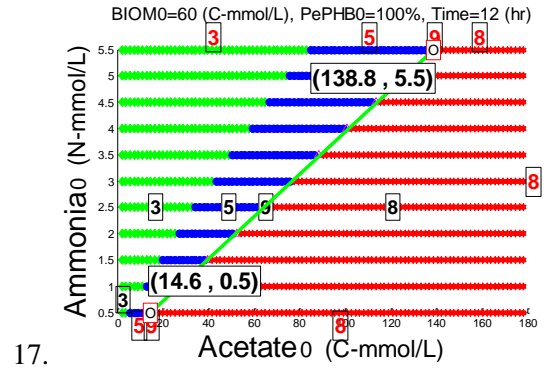
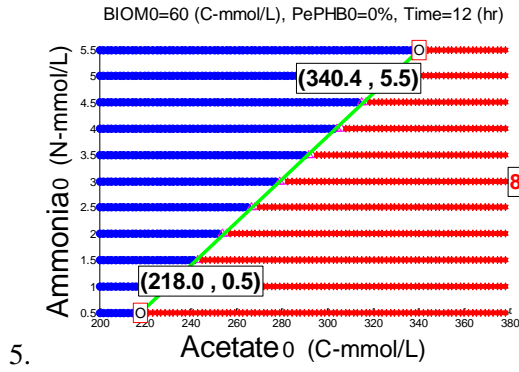


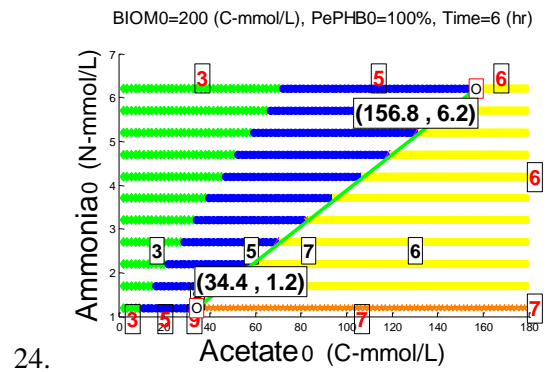
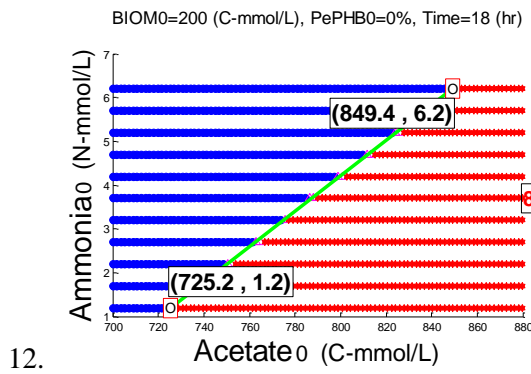
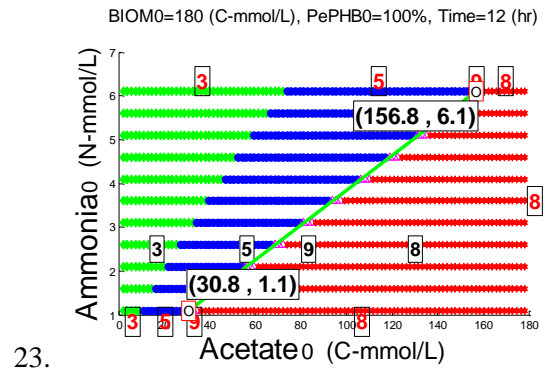
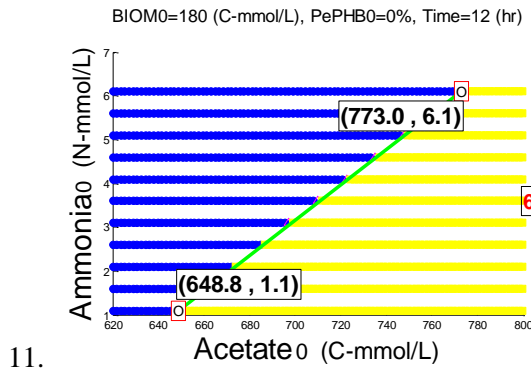
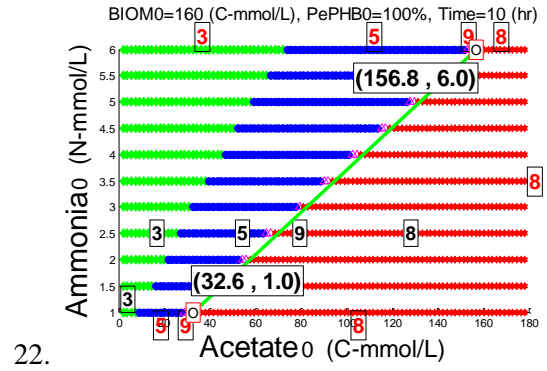
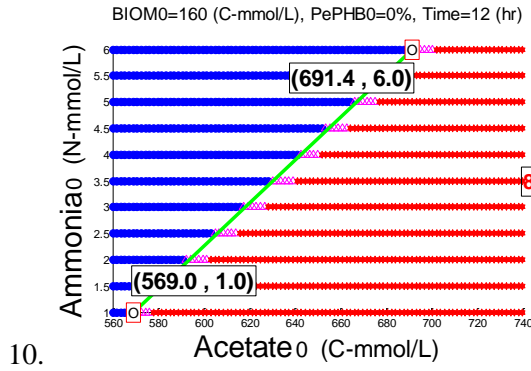
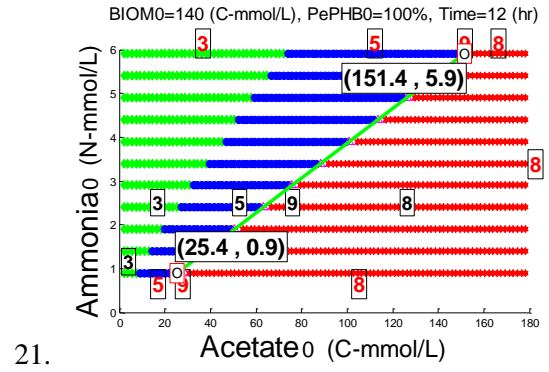
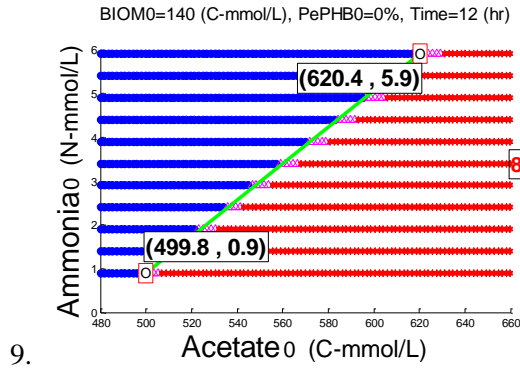




Appendix-C



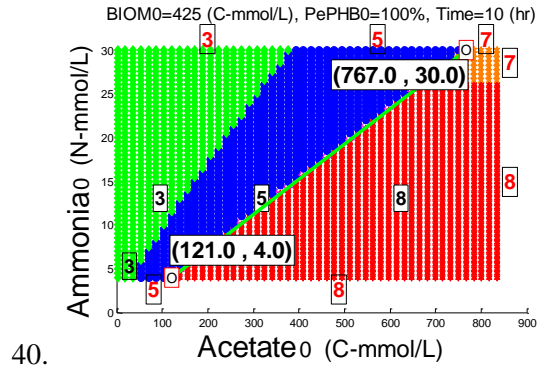
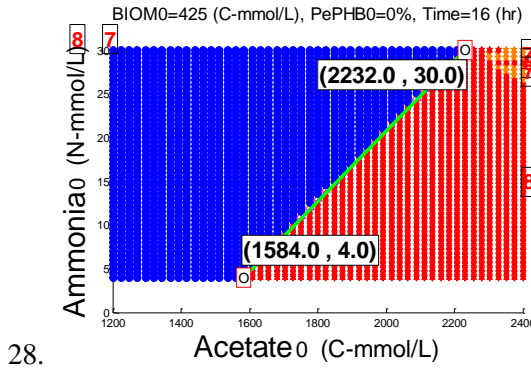
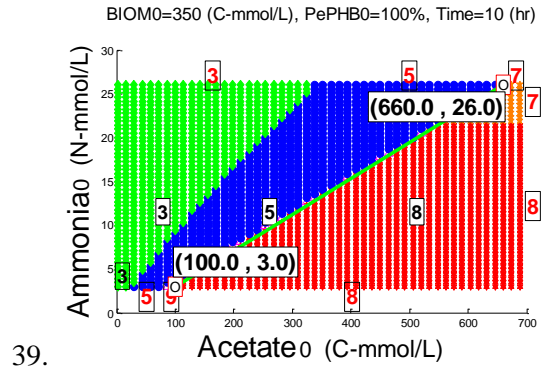
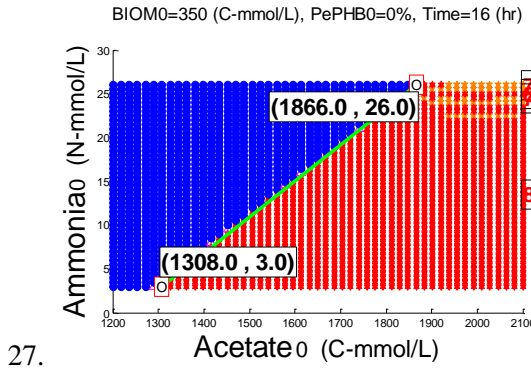
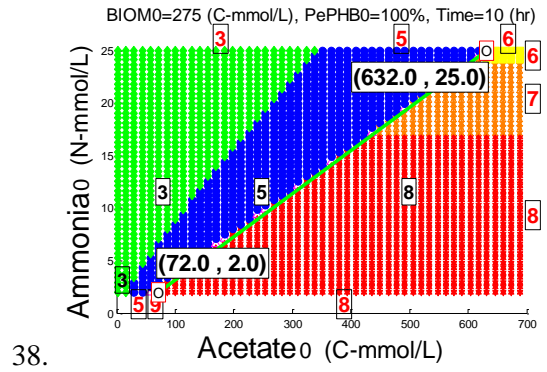
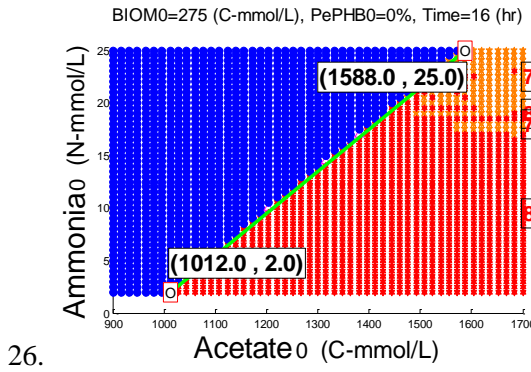
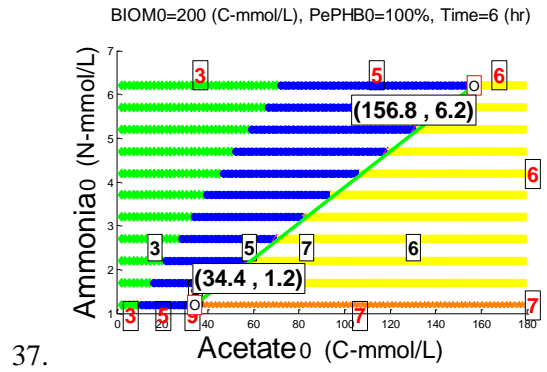
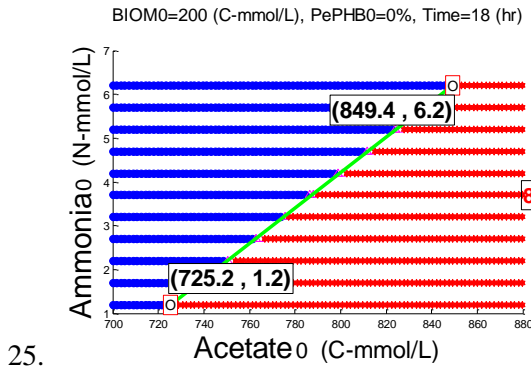


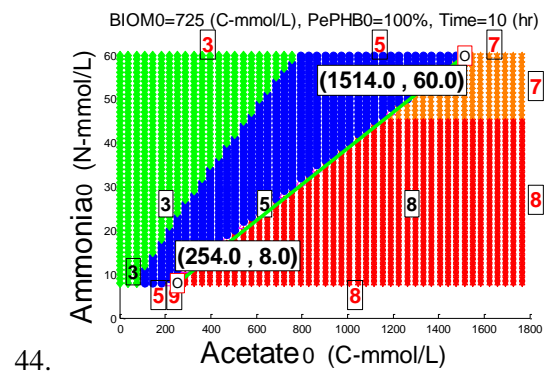
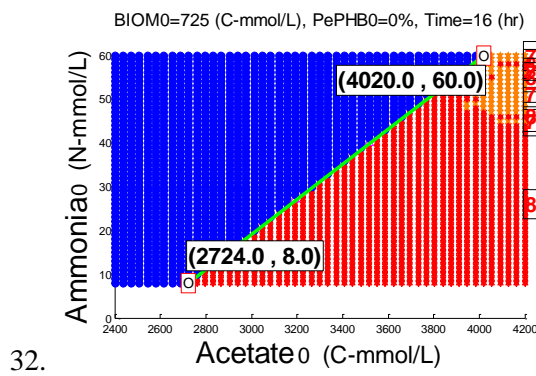
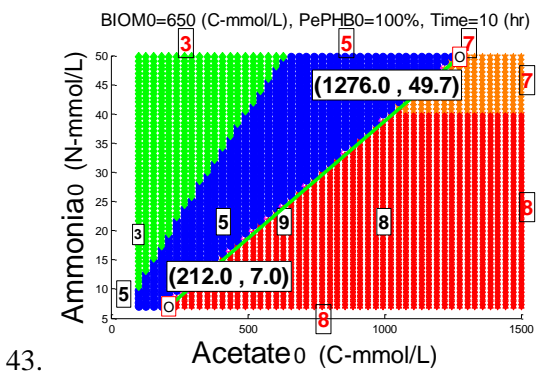
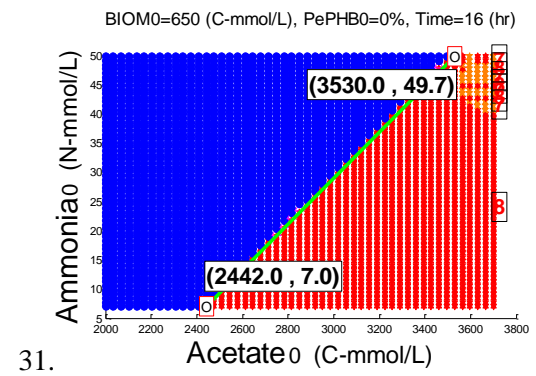
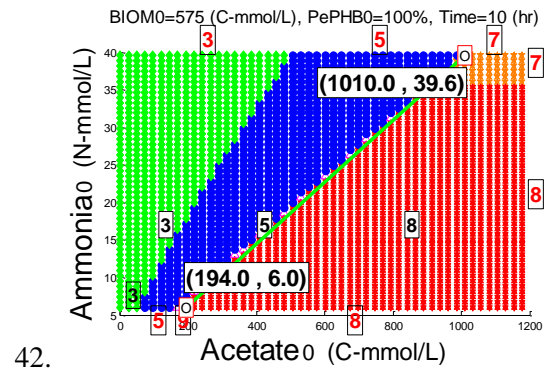
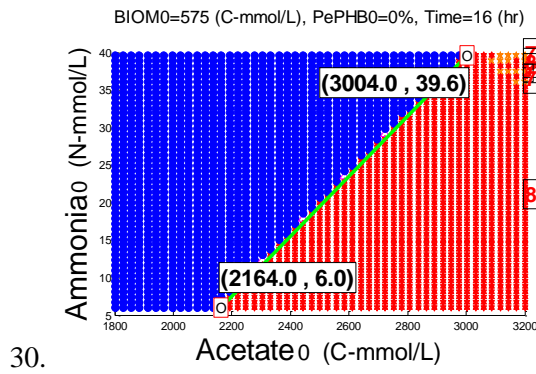
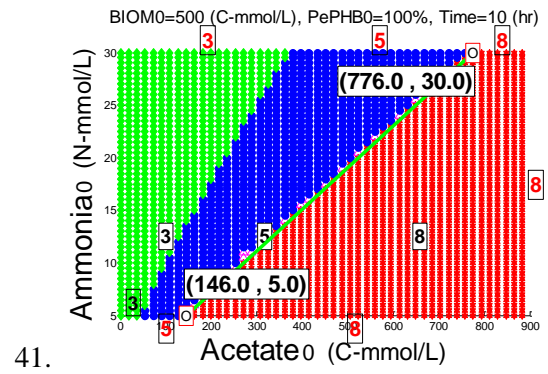
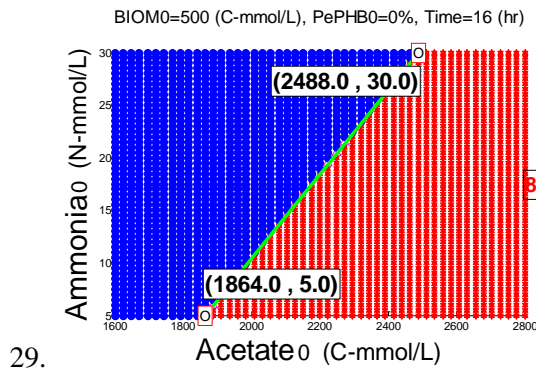


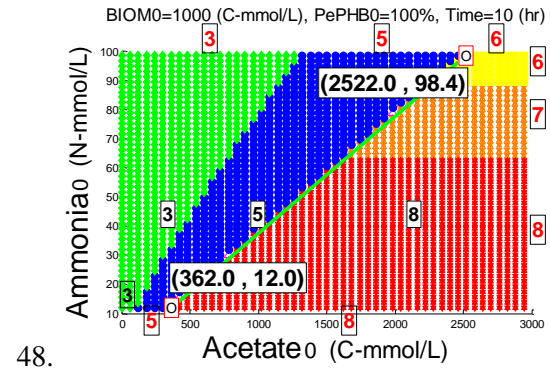
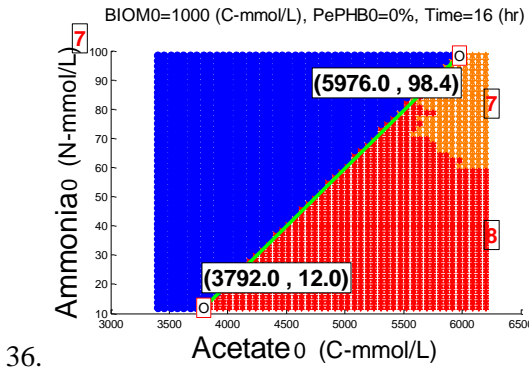
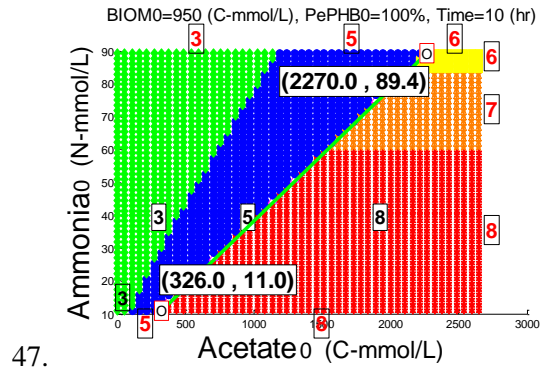
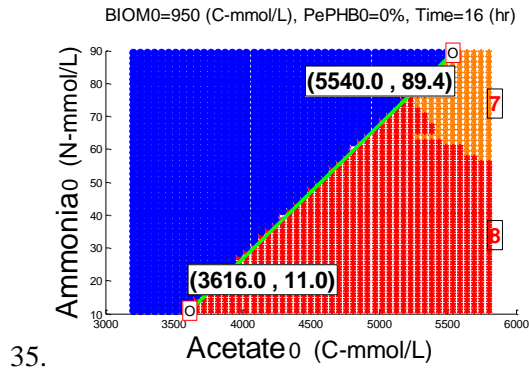
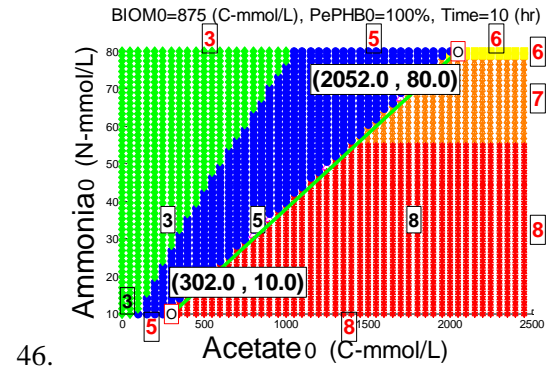
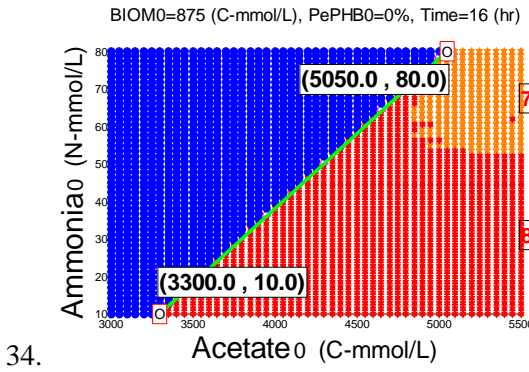
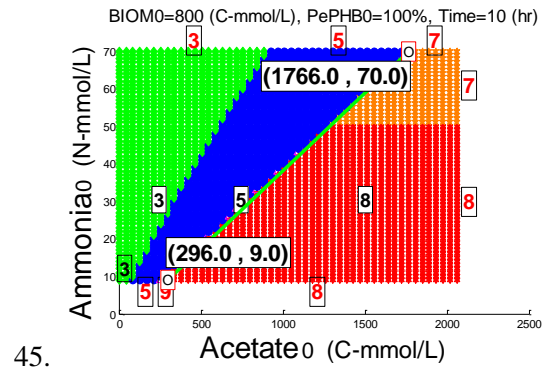
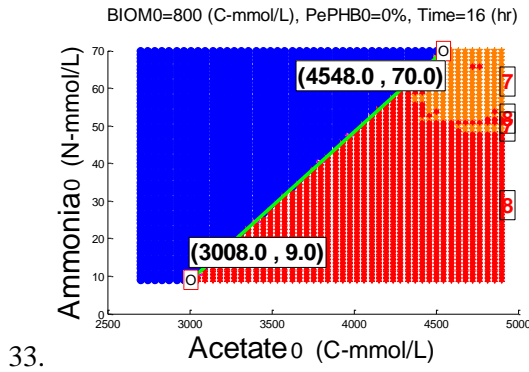
PePHB0=0%							
Simulation run number	Initial Biomass (C-mmol/L)	Point1 Acetate ₀ (C-mmol/L)	Point1 Ammonia ₀ (N-mmol/L)	Point2 Acetate ₀ (C-mmol/L)	Point2 Ammonia ₀ (N-mmol/L)	LG_{α} $(\frac{N\text{-mmol}}{C\text{-mmol}})$	$acetate_{Intercept}$ (C-mmol/L)
1	2	11	0.1	133.4	5.1	0.04084	8.552
2	10	41.6	0.2	154	5.2	0.04448	37.104
3	20	77.8	0.3	200.2	5.3	0.04084	70.456
4	40	147	0.4	269.4	5.4	0.04084	137.20
5	60	218	0.5	340.4	5.5	0.04084	205.76
6	80	288.8	0.6	411.2	5.6	0.04084	274.11
7	100	358	0.7	480.4	5.7	0.04084	340.86
8	120	428.8	0.8	551.2	5.8	0.04084	409.21
9	140	499.8	0.9	620.4	5.9	0.04145	478.09
10	160	569	1	691.4	6	0.04084	544.52
11	180	648.8	1.1	773	6.1	0.04025	621.47
12	200	725.2	1.2	849.4	6.2	0.04025	695.39

PePHB0=100%							
Simulation run number	Initial Biomass (C-mmol/L)	Point1 Acetate ₀ (C-mmol/L)	Point1 Ammonia ₀ (N-mmol/L)	Point2 Acetate ₀ (C-mmol/L)	Point2 Ammonia ₀ (N-mmol/L)	LG_{α} $(\frac{N-mmol}{C-mmol})$	$acetate_{Intercept}$ (C-mmol/L)
13	2	3.8	0.1	128	5.1	0.04025	1.316
14	10	7.4	0.2	129.8	5.2	0.04084	2.504
15	20	9.2	0.3	133.4	5.3	0.04025	1.748
16	40	12.8	0.4	138.8	5.4	0.03968	2.72
17	60	14.6	0.5	138.8	5.5	0.04025	2.18
18	80	18.2	0.6	142.4	5.6	0.04025	3.296
19	100	20	0.7	144.2	5.7	0.04025	2.612
20	120	23.6	0.8	147.8	5.8	0.04025	3.728
21	140	25.4	0.9	151.4	5.9	0.03968	2.72
22	160	32.6	1	156.8	6	0.04025	7.76
23	180	30.8	1.1	156.8	6.1	0.03968	3.08
24	200	34.4	1.2	156.8	6.2	0.04084	5.024

Appendix-C

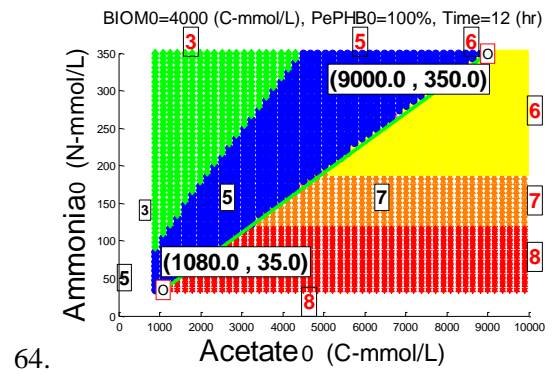
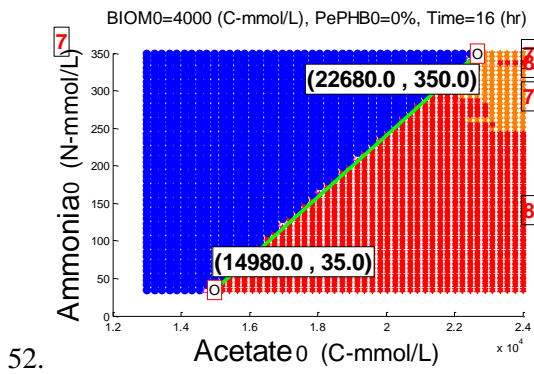
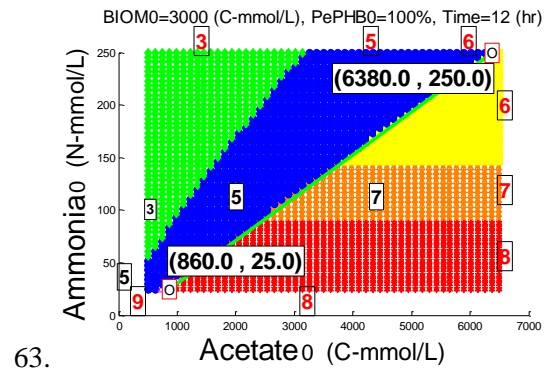
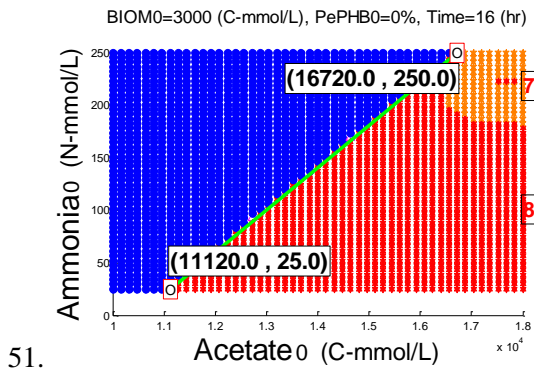
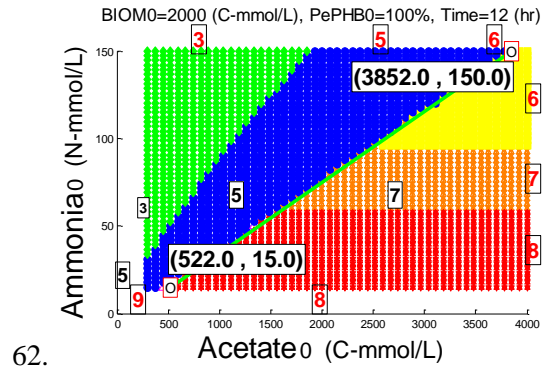
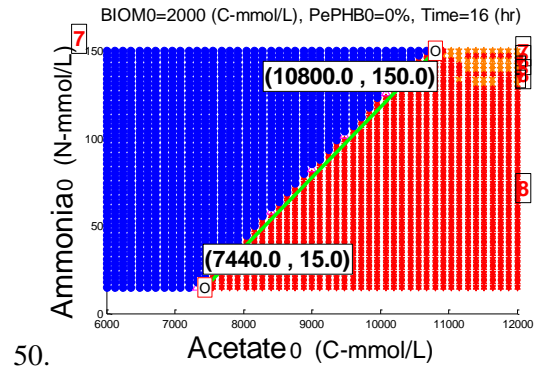
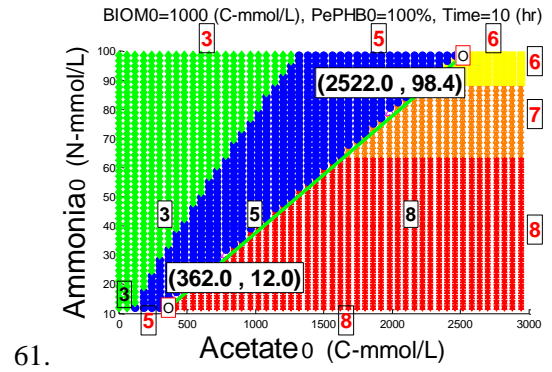
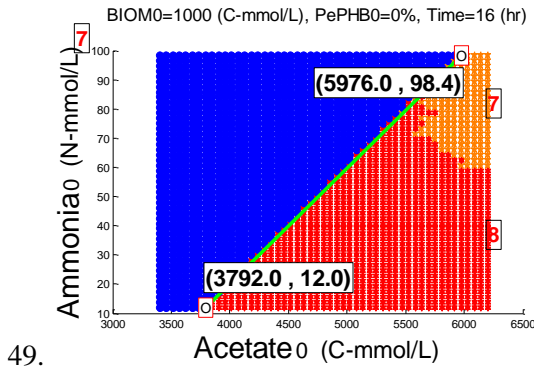


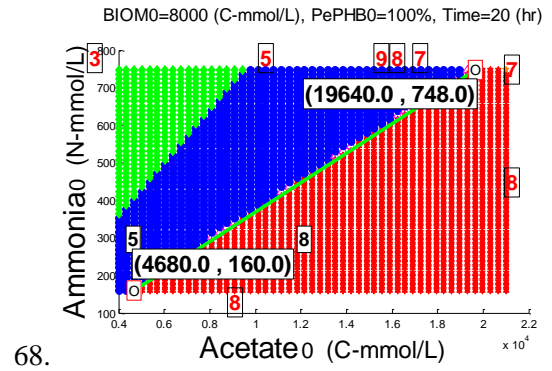
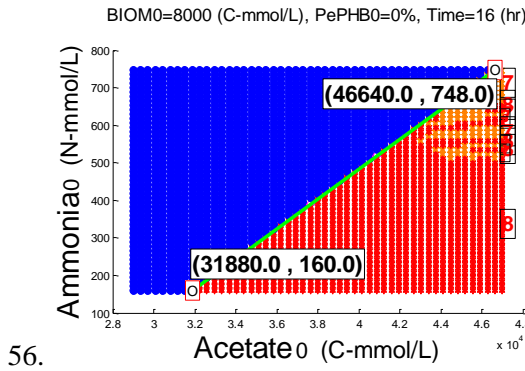
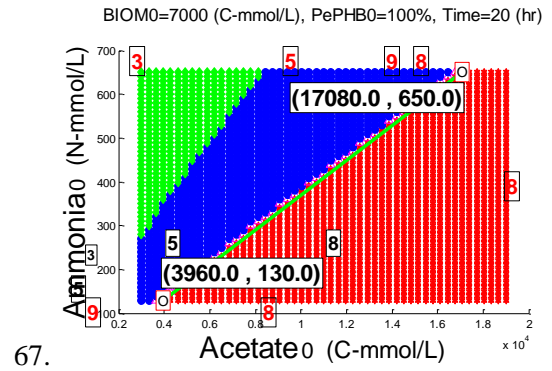
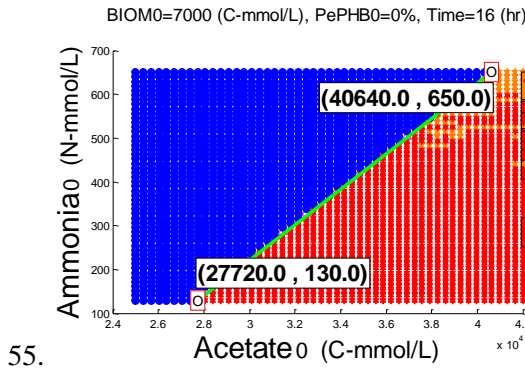
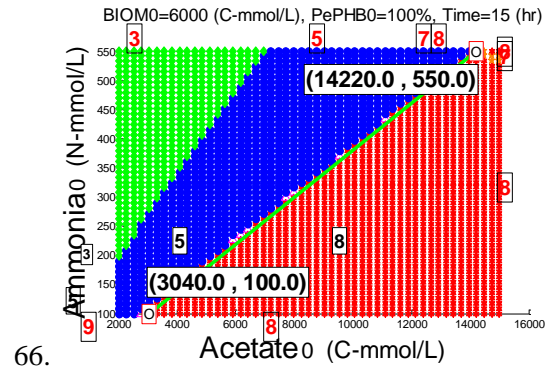
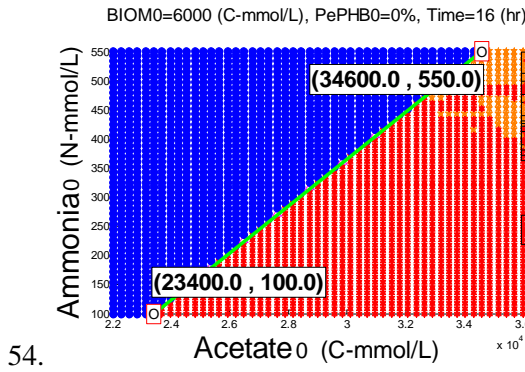
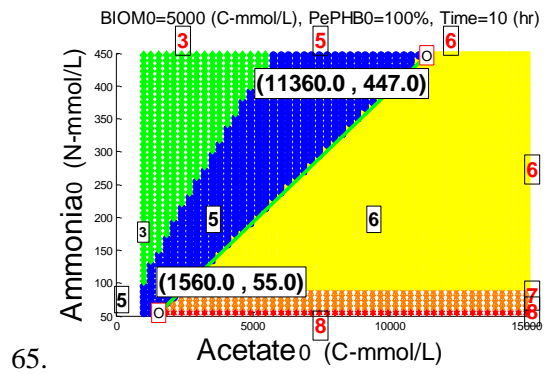
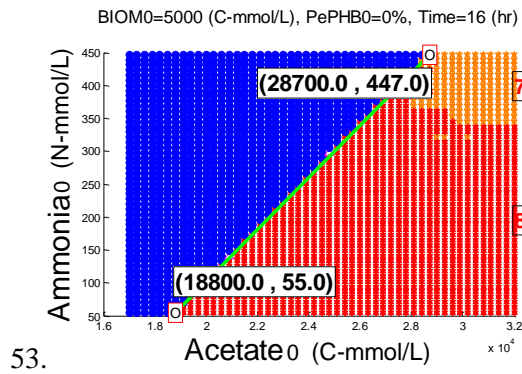




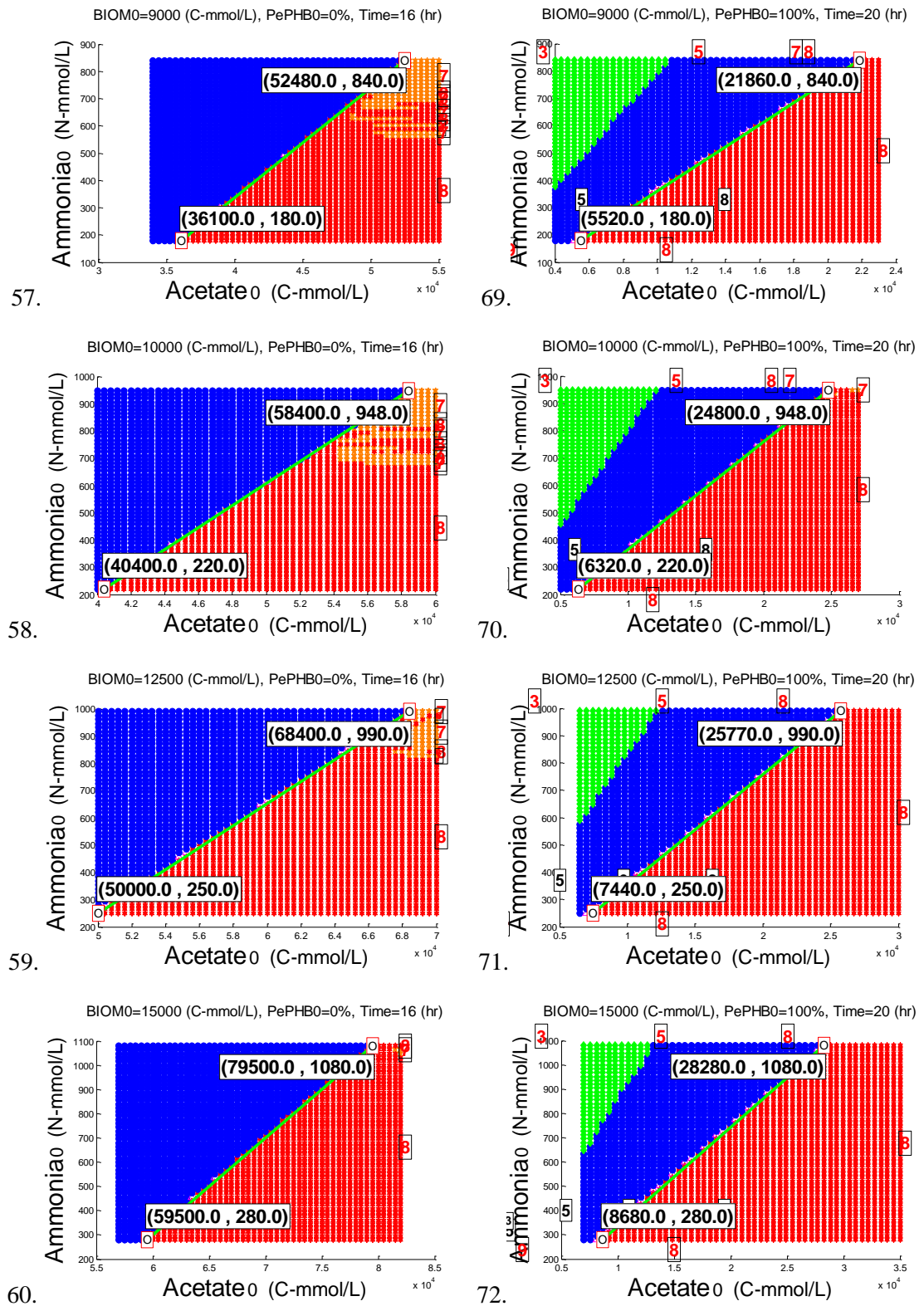
PePHB0=0%							
Simulation run number	Initial Biomass (C-mmol/L)	Point1 Acetate ₀ (C-mmol/L)	Point1 Ammonia ₀ (N-mmol/L)	Point2 Acetate ₀ (C-mmol/L)	Point2 Ammonia ₀ (N-mmol/L)	LG_{α} $(\frac{N-mmol}{C-mmol})$	$acetate_{Intercept}$ (C-mmol/L)
25	200	725.2	1.2	849.4	6.2	0.04025	695.39
26	275	1012	2	1588	25	0.03993	961.9130
27	350	1308	3	1866	26	0.04121	1235.217
28	425	1584	4	2232	30	0.04012	1484.307
29	500	1864	5	2488	30	0.04006	1739.2
30	575	2164	6	3004	39.6	0.04	2014
31	650	2442	7	3530	49.7	0.03924	2263.639
32	725	2724	8	4020	60	0.04012	2524.615
33	800	3008	9	4548	70	0.03961	2780.786
34	875	3300	10	5050	80	0.04	3050
35	950	3616	11	5540	89.4	0.04074	3346.051
36	1000	3792	12	5976	98.4	0.03956	3488.666

PePHB0=100%							
Simulation run number	Initial Biomass (C-mmol/L)	Point1 Acetate ₀ (C-mmol/L)	Point1 Ammonia ₀ (N-mmol/L)	Point2 Acetate ₀ (C-mmol/L)	Point2 Ammonia ₀ (N-mmol/L)	LG_{α} $(\frac{N-mmol}{C-mmol})$	$acetate_{Intercept}$ (C-mmol/L)
37	200	34.4	1.2	156.8	6.2	0.0408	5.024
38	275	72	2	632	25	0.04107	23.3043
39	350	100	3	660	26	0.04107	26.9565
40	425	121	4	767	30	0.04024	21.6153
41	500	146	5	776	30	0.03968	20
42	575	194	6	1010	39.6	0.04117	48.2857
43	650	212	7	1276	49.7	0.04013	37.5737
44	725	254	8	1514	60	0.04126	60.1538
45	800	296	9	1766	70	0.04149	79.1147
46	875	302	10	2052	80	0.04	52
47	950	326	11	2270	89.4	0.04032	53.2448
48	1000	362	12	2522	98.4	0.04	62





Appendix-C



PePHB0=0%							
Simulation run number	Initial Biomass (C-mmol/L)	Point1 Acetate ₀ (C-mmol/L)	Point1 Ammonia ₀ (N-mmol/L)	Point2 Acetate ₀ (C-mmol/L)	Point2 Ammonia ₀ (N-mmol/L)	LG_{α} $(\frac{N-mmol}{C-mmol})$	$acetate_{Intercept}$ (C-mmol/L)
49	1000	3792	12	5976	98.4	0.03956	3488.666
50	2000	7440	15	10800	150	0.04017	7066.666
51	3000	11120	25	16720	250	0.04017	10497.77
52	4000	14980	35	22680	350	0.04090	14124.44
53	5000	18800	55	28700	447	0.03959	17410.96
54	6000	23400	100	34600	550	0.04017	20911.11
55	7000	27720	130	40640	650	0.04024	24490
56	8000	31880	160	46640	748	0.03983	27863.67
57	9000	36100	180	52480	840	0.040	31632.72
58	10000	40400	220	58400	948	0.04044	34960.43
59	12500	50000	250	68400	990	0.04021	43783.78
60	15000	59500	280	79500	1080	0.04	52500

PePHB0=100%							
Simulation run number	Initial Biomass (C-mmol/L)	Point1 Acetate ₀ (C-mmol/L)	Point1 Ammonia ₀ (N-mmol/L)	Point2 Acetate ₀ (C-mmol/L)	Point2 Ammonia ₀ (N-mmol/L)	LG_{α} $(\frac{N-mmol}{C-mmol})$	$acetate_{Intercept}$ (C-mmol/L)
61	1000	362	12	2522	98.4	0.04	62
62	2000	522	15	3852	150	0.04054	152
63	3000	860	25	6380	250	0.04076	246.666
64	4000	1080	35	9000	350	0.03977	200
65	5000	1560	55	11360	447	0.04	385
66	6000	3040	100	14220	550	0.04025	555.5555
67	7000	3960	130	17080	650	0.03963	680
68	8000	4680	160	19640	748	0.03930	809.2517
69	9000	5520	180	21860	840	0.0439	1063.63
70	10000	6320	220	24800	948	0.03939	1035.38
71	12500	7440	250	25770	990	0.04037	1247.43
72	15000	8680	280	28280	1080	0.04081	1820

Appendix-D

“famine” phase modelling (RT3 and RT5)

Table D.1 Scaling parameters for “famine” phase data sets

	T_0		Point-P		Point-T	
	Min	Max	Min	Max	Min	Max
Time (h)	-	-	0.15	5	4.5	14.55
Biomass (C-mmol/L)	15.5	197.3	40.4	243.7	41.7	243.7
PHB (C-mmol/L)	34.6	497.1	50.7	552.4	17.2	212.3
Acetate (C-mmol/L)	5.9	268.5	0	0	0	0
Ammonia (N-mmol/L)	0.3	9.9	0	7.5	0	2

Table D.2 MLR model parameters for the “famine” phase data sets

$y = f(x_1, x_2, x_3, x_4)$		θ_0	θ_1	θ_2	θ_3	θ_4
Model outputs						
Point-P	Time	-0.1207	-0.4518	0.1677	0.8779	-0.2056
	Biomass	0.0883	0.7236	0.1891	0.1743	-0.1463
	PHB	0.0499	0.0830	0.8204	0.3081	0.0687
Point-T	Time	0.7082	-0.2147	0.4275	0.7820	-0.5287
	Biomass	0.2345	0.7204	0.2061	0.0826	-0.2817
	PHB	0.0863	0.0921	0.9175	0.2286	0.0419

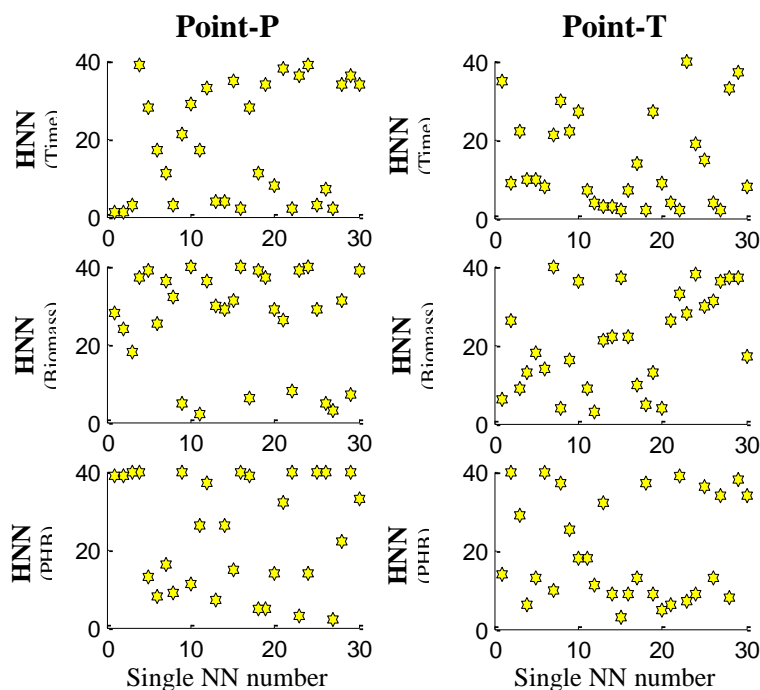


Figure D.1 Number of hidden neurons in single NN structure for the “famine” phase data sets

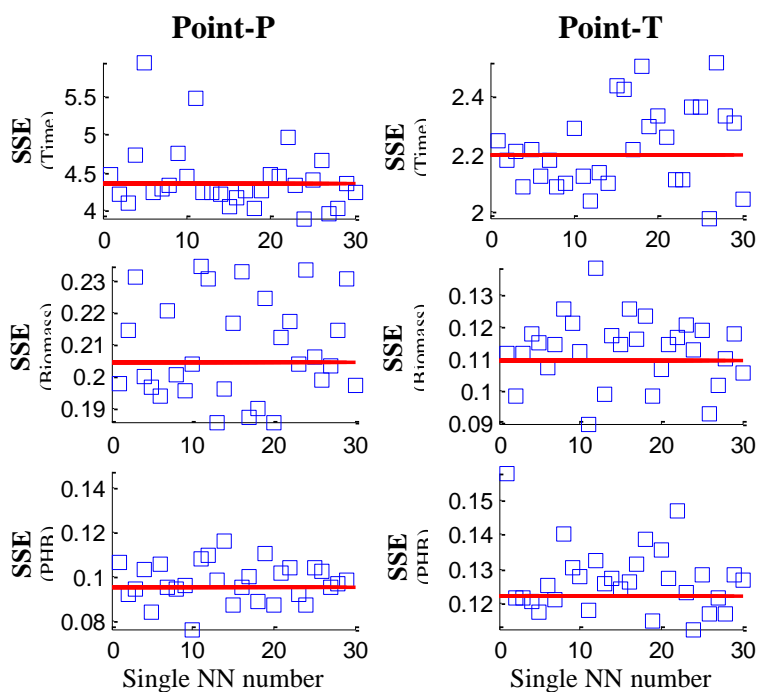


Figure D.2 Sum of squared errors of single and aggregated model predictions for “famine” phase scaled data

Table D.3 RMSE values for different model structures developed using BANN technique for “famine” phase profile

RMSE (Scaled validation)		$y=f(x_1, x_4)$	$y=f(x_2, x_3)$	$y=f(x_1, x_2, x_3)$	$y=f(x_1, x_2, x_4)$
		BANN	BANN	BANN	BANN
Point-P	Time	0.68	0.39	0.38	0.67
	Biomass	0.09	0.14	0.09	0.10
	PHB	0.18	0.04	0.05	0.17
Point-T	Time	0.56	0.41	0.40	0.56
	Biomass	0.03	0.16	0.12	0.05
	PHB	0.14	0.06	0.06	0.13

RMSE (Scaled validation)		$y=f(x_1, x_3, x_4)$	$y=f(x_2, x_3, x_4)$	$y=f(x_1, x_2, x_3, x_4)$		$y=f(x_1, x_2, x_3, x_4, x_5)$
		BANN	BANN	BANN	MLR	BANN
Point-P	Time	0.34	0.35	0.34	0.35	---
	Biomass	0.06	0.13	0.07	0.18	---
	PHB	0.11	0.06	0.05	0.08	---
Point-T	Time	0.25	0.25	0.24	0.33	0.22
	Biomass	0.03	0.13	0.05	0.33	0.05
	PHB	0.09	0.06	0.06	0.11	0.05

“famine” phase modelling (RT3)

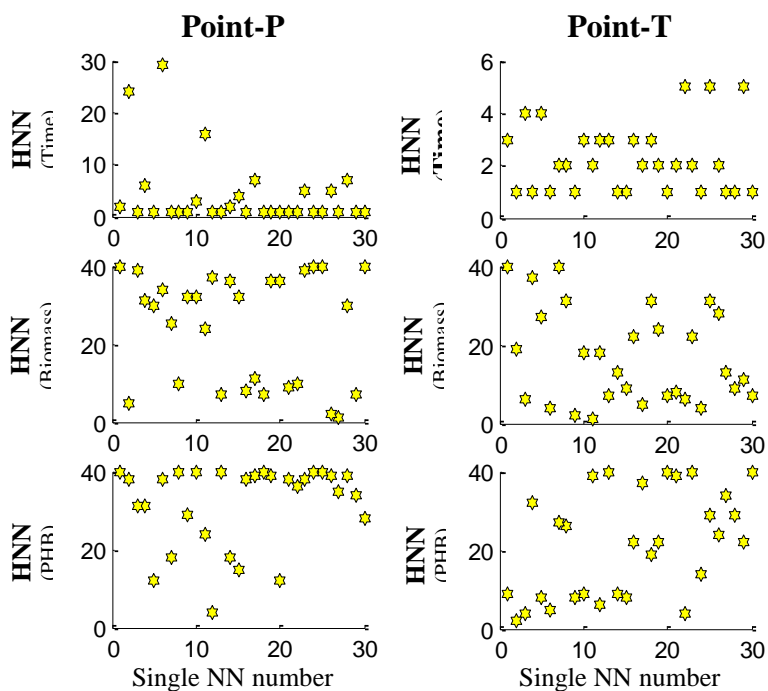


Figure D.3 Number of hidden neurons for each single NN structure for the RT3 data sets

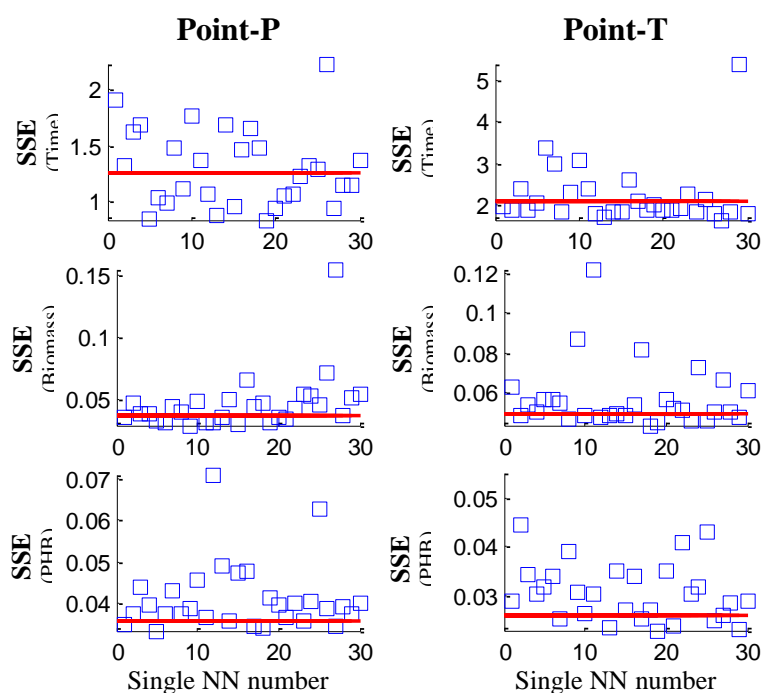


Figure D.4 Sum of squared errors of single and aggregated model predictions for RT3 scaled data sets

Table D.4 RMSE values for different model structures developed using BANN technique for RT3 data sets

RMSE (Scaled validation)		$y=f(x_3, x_4)$	$y=f(x_1, x_2, x_3)$	$y=f(x_1, x_2, x_4)$	$y=f(x_1, x_3, x_4)$
		BANN	BANN	BANN	BANN
Point-P	Time	0.46	0.26	0.42	0.28
	Biomass	0.60	0.05	0.09	0.02
	PHB	0.52	0.05	0.05	0.10
Point-T	Time	0.31	0.50	0.57	0.35
	Biomass	0.60	0.08	0.06	0.03
	PHB	0.52	0.04	0.06	0.09

RMSE (Scaled validation)		$y=f(x_2, x_3, x_4)$	$y=f(x_1, x_2, x_3, x_4)$	$y=f(x_1, x_2, x_3, x_4, x_5)$
		BANN	BANN	BANN
Point-P	Time	0.29	0.28	---
	Biomass	0.11	0.05	---
	PHB	0.01	0.05	---
Point-T	Time	0.35	0.36	0.35
	Biomass	0.11	0.06	0.05
	PHB	0.03	0.04	0.04

“famine” phase modelling (RT5)

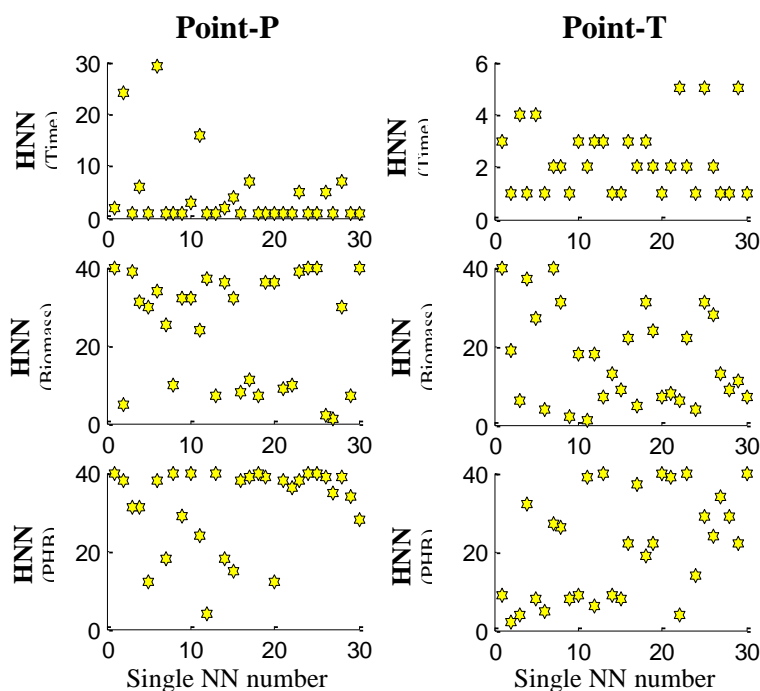


Figure D.5 Number of hidden neurons for each single NN structure for the RT5 data sets

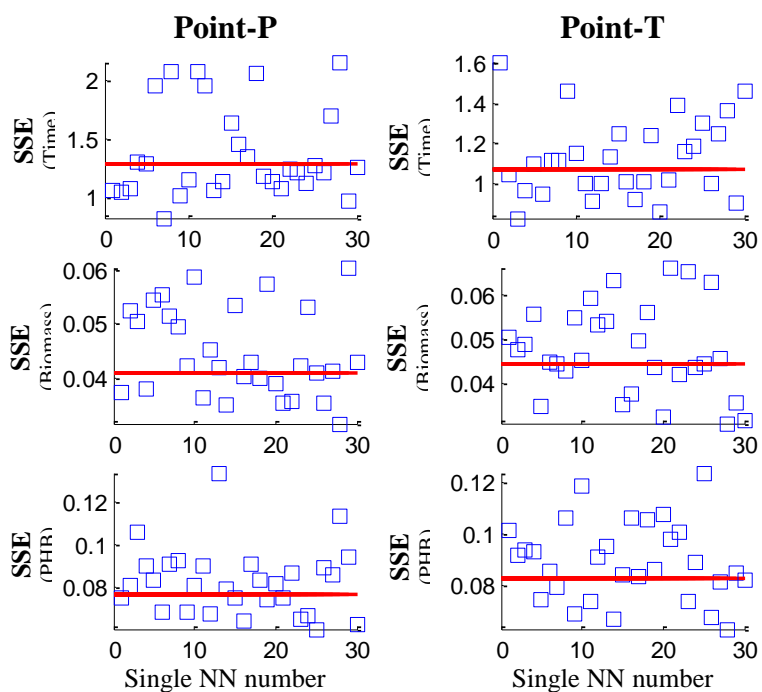


Figure D.6 Sum of squared errors of single and aggregated model predictions for RT5 scaled data sets

Table D.5 RMSE values for different model structures developed using BANN technique for RT5 batch profiles

RMSE (Scaled validation)		$y=f(x_2, x_3)$	$y=f(x_1, x_2, x_3)$	$y=f(x_1, x_2, x_4)$	$y=f(x_1, x_3, x_4)$
		BANN	BANN	BANN	BANN
Point-P	Time	0.39	0.25	0.39	0.23
	Biomass	0.14	0.09	0.05	0.01
	PHB	0.04	0.06	0.16	0.11
Point-T	Time	0.41	0.22	0.32	0.22
	Biomass	0.16	0.09	0.05	0.01
	PHB	0.06	0.05	0.14	0.09

RMSE (Scaled validation)		$y=f(x_2, x_3, x_4)$	$y=f(x_1, x_2, x_3, x_4)$	$y=f(x_1, x_2, x_3, x_4, x_5)$
		BANN	BANN	BANN
Point-P	Time	0.22	0.24	---
	Biomass	0.11	0.04	---
	PHB	0.06	0.06	---
Point-T	Time	0.21	0.22	0.14
	Biomass	0.11	0.04	0.05
	PHB	0.06	0.06	0.06